University of Alberta

Differential Gene Expression in Light-induced Retinal Degeneration in Rats

Focus on the Crystallins

by

Benjamin John Donald McDonald

A thesis submitted to the Faculty of Graduate Studies and Research in partial fulfillment of the requirements for the degree of Master of Science

in

Molecular Biology and Genetics

Department of Biological Sciences

Edmonton, Alberta

Spring 2003

National Library of Canada
Acquisitions and Bibliographic Services
395 Wellington Street
Ottawa ON K1A 0N4
Canada

Bibliothèque nationale du Canada
Acquisitions et services bibliographiques
395, rue Wellington
Ottawa ON K1A 0N4
Canada

Your file Votre référence

Our file Notre référence

The author has granted a non-exclusive licence allowing the National Library of Canada to reproduce, loan, distribute or sell copies of this thesis in microform, paper or electronic formats.

L'auteur a accordé une licence non exclusive permettant à la Bibliothèque nationale du Canada de reproduire, prêter, distribuer ou vendre des copies de cette thèse sous la forme de microfiche/film, de reproduction sur papier ou sur format électronique.

The author retains ownership of the copyright in this thesis. Neither the thesis nor substantial extracts from it may be printed or otherwise reproduced without the author's permission.

L'auteur conserve la propriété du droit d'auteur qui protège cette thèse. Ni la thèse ni des extraits substantiels de celle-ci ne doivent être imprimés ou autrement reproduits sans son autorisation.

0-612-82308-3

Canada

University of Alberta

Library Release Form

Name of Author: Benjamin John Donald M^{c}Donald

Title of Thesis: Differential Gene Expression in Light-induced Retinal Degeneration in Rats: Focus on the Crystallins

Degree: Master of Science

Year this Degree Granted: 2003

Permission is hereby granted to the University of Alberta Library to reproduce single copies of this thesis and to lend or sell such copies for private, scholarly or scientific research purposes only.

The author reserves all other publication and other rights in association with the copyright in the thesis, and except as herein before provided, neither the thesis nor any substantial portion thereof may be printed or otherwise reproduced in any material form whatever without the author's prior written permission.

Ben M^{c}Donald

Ben M^{c}Donald
Box 1553
High Prairie, Alberta
Canada
T0G 1E0

08/04/03.

University of Alberta

Faculty of Graduate Studies and Research

The undersigned certify that they have read, and recommend to the Faculty of Graduate Studies and Research for acceptance, a thesis entitled Differential Gene Expression in Light-induced Retinal Degeneration in Rats: Focus on the Crystallins submitted by Benjamin John Donald M^{c}Donald in partial fulfillment of the requirements for the degree of Master of Science in Molecular Biology and Genetics.

Paul Wong

Paul Wong

John Bell

John Bell

Ross Hodgetts

Roseline Godbout

07/04/03

Abstract

Retinal degeneration can be induced in dark-reared rats (*Rattus norvegicus* Sprague-Dawley) by exposing them to intense green light (490-590 nm). The degeneration is known to be effected through the apoptotic death of rod photoreceptor cells, which contain the chromophore rhodopsin, (Absorption λ_{Max} = 500 nm). The stress generated in the photoreceptor cells is known to be oxidative in nature. A differential cross screen of a dark-reared rat retina cDNA library with cDNA derived from light-treated and untreated rat retinae identified genes for members of the crystallin family of proteins. This is a novel observation, since most crystallin proteins are not known to be expressed outside the lens. Northern, Western and immunohistochemical analysis confirmed the results of the screen. The possible role of the crystallin proteins in the context of light-induced retinal degeneration is discussed.

Table of Contents

Chapter 1 Introduction 1
A Physiology 2
1 Retinal Morphology 4
2 Phototransduction 7
3 Lens Biology and the Crystallins 10
B Light-induced Retinal Degeneration 12
1 Studying Human Retinal Degeneration 12
2 Retinal Degeneration in Rats 13
3 Oxidative Stress in Retinal Degeneration 16
4 Apoptosis in Retinal Degeneration 19
C Hypothesis 22

Chapter 2 Materials and Methods 23
A Experimental Animals 24
B Experimental Treatments 24
C Retina Dissection 26
D Rat Retina RNA Isolation 26
E Northern Transfer 29
1 RNA Gel System 29
2 RNA Sample Treatment 30
3 RNA Sample Electrophoresis 30
4 RNA Sample Visualization 31
5 Northern Transfer 31
F mRNA Isolation 34
G cDNA Synthesis 35
H cDNA Library Synthesis 36
I Differential Cross Screening of 4 Hour Library 38
1 Plaque Lifts 38
2 Radioactive Labelling of cDNA 41
3 Probe Hybridization 42
4 Hybridization Washes 43
5 Autoradiography 43
6 Primary Screen 43
7 Secondary Screen 44
8 Tertiary Screen 44
A Polymerase Chain Reaction 44
B Gel Electrophoresis 45
C Ethidium bromide Visualization 45
D Southern Transfer 45
E Radioactive Hybridization 46

J cDNA Insert Sequencing 46
1 Plaque Purification 46
2 cDNA Purification 46
3 cDNA Insert Sequencing 47
4 BLAST Analysis 50
K Northern Blot Hybridization 50
1 Radioactive Labelling of Clone Inserts 52
2 Probe Hybridization 52
3 Hybridization Washes 52
4 Autoradiography 53
5 Densitometry 53
L Rat Retina Protein Isolation 54
M Western Blotting 55
1 Gel Preparation 56
2 Sample Preparation and Electrophoresis 56
3 Western Transfer 57
4 Immunodetection 59
N Fluorescent Immunohistochemistry 61
1 Tissue Fixation 61
2 Tissue Sectioning 61
3 Immunohistochemistry 62
4 Fluorescence Microscopy 63

Chapter 3 Differential Cross Screen 64
A Primary Screen 66
1 Comparing Signal Intensity 68
2 Primary Screen of the 4 Hour Library 69
B Secondary and Tertiary Screens 69
1 Secondary Screen of the 4 Hour Library 71
2 Tertiary Screen 71
C Confirmation by Northern Analysis 72
D Discussion 75

Chapter 4 Sequence Analysis 77
A Sequence Analysis 78
1 Photoreceptor Cell Sequences 78
2 Novel and Unidentified Clones 78
3 Orthologous Sequences 79
B Classification of Identified Clones 79
C Stress-related Sequences 79
D Energy Metabolism Sequences 83
E RNA Synthesis 84
1 Transcription Sequences 84
2 Pre-mRNA Processing Sequences 85
F Translation 86
1 Ribosomal Sequences 86
2 Post-translational Modification Sequences 87

G Signalling Sequences 88
H Membrane Sequences 89
I Photoreceptor Cell Protein Sequences 91
J Cytoskeleton Sequences 92
K Apoptosis-related Sequences 92
L Protein Degradation Sequences 93
M Cell Interaction Sequences 94
N Other Sequences 95
O Gene Expression in Light-induced Retinal Degeneration 95

Chapter 5 Bioinformatics: Chromosomal Localization 100
A LIRD as a Model for Human Disease 101
B Determining Gene Location 102
C Human Retinopathy Genes 103
D Potential Human Retinopathy Genes 106
1 Senior-Løken Syndrome Type 4 108
2 Cone-rod dystrophy 8 109
3 Senior-Løken Syndrome Type 3 111
4 Stargardt disease 4 111
5 Cystoid macular edema 112
6 Joubert Syndrome Type 1 112
7 Vitreoretinopathy neovascular inflammatory disease 112
8 Leber congenital amaurosis type III 113
E Conserved Synteny 113
F Bioinformatic Analysis and the Laboratory 114

Chapter 6 Bioinformatics: *In silico* Northern Analysis 118
A Northern Analysis 119
B UniGene Database 119
C Testing the Predictions of the *In silico* Analysis 121
1 Atp1a2 Expression 131
2 Fdps Expression 131
3 Pak1 Expression 131
4 Pea15 Expression 131
5 Gene Expression in the Eye 131
D Conclusion 133

Chapter 7 Crystallin Gene Expression 136
A Crystallin Superfamily 137
1 α-Crystallins 139
2 βγ-Crystallin Superfamily 141
B Stress Proteins 144
C Experimental Outline 145

D Northern Analysis 146
1 Cryaa 146
2 Cryab 146
3 Crybal 146
4 Crybb2 148
5 Crygs 148
6 Hspa1a 148
7 Hspca 148
8 Sod1 148
E Western Analysis 148
1 αA-Crystallin (Cryaa) 148
2 αB-Crystallin (Cryab) 150
3 β-Crystallin 150
4 γS-Crystallin (Crygs) 150
5 Hsp70 (Hspa1a) 151
F Immunohistochemistry 151
1 αB-Crystallin (Cryab) 151
2 γS-Crystallin (Crygs) 153
G Discussion 155

Chapter 8 Conclusion 168

References 175

Appendix 1. Reagent Recipes 188

Appendix 2. Gene Symbols and Names for *Homo sapiens*, *Rattus norvegicus*, and *Mus musculus* 191

Appendix 3. *Homo sapiens* Gene Expression in Normal Tissues as Determined by Bioinformatics 198

Appendix 4. *Homo sapiens* Gene Expression in Representative Cancerous Tissues as Determined by Bioinformatics, with Accompanying *In Silico* Northern Analysis of Various Genes 202

Appendix 5. Comparison of Mouse and Rat Protein Sequence Identity by Alignment of Sequence 205

List of Tables

2-1. Antibodies Used for Western Immunodetection 60
2-2. Antibodies Used for Immunohistochemistry 62
4-1. Sequence Identities of Stress-related Clones 82
4-2. Sequence Identities of Energy Metabolism Clones 83
4-3. Sequence Identities of Transcription-related Clones 85
4-4. Sequence Identities of Pre-mRNA Processing Clones 86
4-5. Sequence Identities of Ribosomal Clones 87
4-6. Sequence Identities of Post-translational Modification Clones 87
4-7. Sequence Identities of Signalling Clones 88
4-8. Sequence Identities of Membrane Clones 90
4-9. Sequence Identities of Photoreceptor Cell Clones 91
4-10. Sequence Identities of Cytoskeleton Clones 92
4-11. Sequence Identities of Apoptosis-related Clones 93
4-12. Sequence Identities of Protein Degradation Clones 94
4-13. Sequence Identities of Cell Interaction Clones 94
4-14. Sequence Identities of Other Clones 95
5-1. Gene Localizations in Rat, Mouse, and Human 104,105
5-2. Known Human Retinal Disease Genes Identified in Rat LIRD Differential Cross-screen 106
5-3. Retinal Disease Loci and Disease Genes 107
5-4. Retinal Disease Regions and LIRD-identified Orthologues in the Same Region 108
6-1. Genes with No UniGene Retina-derived Sequences 133
7-1. Crystallin Gene Locations in Rat, Mouse and Human 143
7-2. Gene and Protein Expression Analyses Performed 145
IIII-1. Human Gene Expression in Cancerous Tissues 202

List of Figures

1-1. Diagram of the Eye. **3**
1-2. Retinal Morphology. **5**
1-3. Rhodopsin and Retinal. **6**
1-4. Signal Transduction by Rhodopsin. **8**
1-5. Light Absorption by Rhodopsin and Transmission by Plexiglass Filters. **14**
1-6. Reactions Involving Reactive Oxygen Species (ROS). **18**
1-7. Protective Effect of Dimethylthiourea in Light-induced Retinal Degeneration. **21**
2-1. Light Chambers. **25**
2-2. Rat Retina Dissection. **27**
2-3. Northern Transfer. **32**
2-4. Outline of cDNA Library Synthesis. **37**
2-5. Insertion Site of Multiple Cloning Site (MCS) of λ Uni-ZAP. **39**
2-6. Volume of Purified PCR Product for Sequencing Reaction. **48**
2-7. Anatomy of a BLAST Search. **51**
2-8. Western Transfer Cassette. **58**
3-1. Screening the 4 Hour cDNA Library for Differentially Expressed Messages. ... **67**
3-2. Primary and Tertiary Screens. **70**
3-3. Normalized Relative Intensity of Autoradiograph Bands of LIRD Northern Blots Probed with Clones Identified in the Differential Cross Screen of the 4 Hour Library. **73**
4-1. Class Distribution of Sequenced Clones. **80**
4-2. Orthology. **81**
5-1. Human Retinal Dystrophy Regions. **110**
5-2. Evolutionary Divergence. **115**
5-3. Ideogram of Gross Rat, Mouse and Human Conserved Synteny. **116**
6-1. Tissue Distribution in the UniGene Database of Rat Sequences **122**
6-2. Tissue Distribution in the UniGene Database of Human Sequences.. **123-126**
6-3. Eye Tissue Distribution in the UniGene Database of Human Sequences. **127-130**
6-4. Multi-tissue Northern Analysis of Rat Gene Expression. **132**
7-1. The Crystallin Proteins. **138**
7-2. α-Crystallin Acts as a Chaperone. **140**
7-3. Normalized Relative Intensity of Autoradiograph Bands of LIRD Northern Blots. **147**
7-4. Electrochemoluminescence Detection of Peroxidase-conjugated Secondary Antibodies. **149**
7-5. Fluorescent Microscopy of αB-Crystallin Immunohistochemistry. **152**
7-6. Fluorescent Microscopy of γS-Crystallin Immunohistochemistry. **154**
7-7. Change in mRNA Levels of Crystallins and Stress Proteins During Light-induced Retinal Degeneration. **156**
7-8. Sulfur Containing Amino Acids in the Crystallins. **160**
7-9. Glutathione and Thioredoxin Peroxidase Reactions. **163**
7-10. Proposed Role of the Crystallins in the Response of Rat Retinae to Light Exposure. **166**
IIII-1. Cancer Tissue Distribution in the UniGene Database of Human Sequences **203,204**

Abbreviations

Species Names

Bos taurus (cow)
Drosophila melanogaster (fruit fly)
Escherichia coli XL1 Blue MRF' (*E. coli*)
Gallus gallus (chicken)
Homo sapiens (human)
Moloney Murine Leukemia Virus (MMLV)
Mus musculus (mouse)
Rattus rattus (black rat)
Rattus norvegicus (Norway rat)
Saccharomyces cerevisiae (yeast)

Retina Physiology

inner nuclear layer (INL)
inner plexiform layer (IPL)
inner segment layer (IS)
outer segment layer (OS)
outer nuclear layer (ONL)
outer plexiform layer (OPL)
retinal pigment epithelium (RPE)

Retinal Degeneration

light-induced retinal degeneration (LIRD)
macular degeneration (MD)
retinal degeneration slow (rds)
retinitis pigmentosa (RP)

Light-induced Retinal Degeneration

derived from mRNA from dark-reared rat retinae untreated with light (Dark)
derived from mRNA from dark-reared rat retinae treated with 4 hours of intense green light (4 Hour)
derived from mRNA from dark-reared rat retinae treated with 8 hours of intense green light (8 Hour)
Northern/Western blot containing the RNA/Protein from all three treatments: Dark, 4 Hour, 8 Hour (LIRD Profile)
unamplified λ Uni-ZAP cDNA library derived from mRNA from dark-reared rat retinae treated with 4 hours of intense green light (4 Hour Library)

General

deoxyribonucleic acid (DNA)
complementary DNA (cDNA)
ribonucleic acid (RNA)
messenger RNA (mRNA)
ribosomal RNA (rRNA)
reactive oxygen species (ROS)

---

standard deviation (s.d.)
absorbance at 260 nm (A_{260})
absorbance at 280 nm (A_{280})
absorbance at 595 nm (A_{595})
optical density at 600 nm (OD_{600})
mass per volume (w/v)
volume per volume (v/v)
counts per minute (cpm)

---

denaturing polyacrylamide gel electrophoresis (SDS-PAGE)
electrochemoluminescence (ECL)
outside diameter (o.d.)
polymerase chain reaction (PCR)
plaque forming units (pfu)

Agencies

Association for the Assessment and Accreditation of Laboratory Animal Care International (AAALAC)
Animal and Plant Health Inspection Service (APHIS)
Basic Local Alignment Search Tool (BLAST)
DNA Data Bank of Japan (DDBJ)
European Molecular Biology Laboratory (EMBL)
Institute for Laboratory Animal Resources (ILAR)
National Centre for Biotechnology Information (NCBI)
National Institute of Health (NIH)
Protein Data Bank (PDB)
U.S. Department of Agriculture (USDA)

Chemical

2-Amino-2-(hydroxymethyl)-1,3-propanediol•HCl (Tris)
3', 5'-cyclic guanosine monophosphate phosphodiesterase (cGMP-PDE)
3', 5'-cyclic guanosine monophosphate (cGMP)
3-keto-gulofuranolactone (Synonyms: ascorbic acid, Vitamin C)
4-morpholine propanesulfonicacid (MOPS)
4',6-diamidinophenyl-indole (DAPI)
(N,N,N',N')-tetramethylethylene diamine (TEMED)
chloroform ($CHCl_3$)
deionized and distilled H_2O (ddH_2O)
diethylpyrocarbonate (DEPC)
dimethylthiourea [DMTU, $SC(NHCH_3)_2$]
docosahexaenoic acid (DHA)
dry ice ($CO_{2(s)}$)
ethanol (EtOH)
ethidium bromide (EtBr)
ethylene diamine tetraceteic acid (EDTA)
guanosine 5' monophosphate (GMP)
guanosine 5' diphosphate (GDP)
guanosine 5' triphosphate (GTP)
isopropanol (iPrOH)
methanol (MeOH)
paraformaldehyde (*p*-CHO)
reactive oxygen species (ROS: H_2O_2, O_2^-, HO•)
sodium dodecyl sulfate (SDS)

Solutions

0.1 % Triton X-100 (v/v) in TBS (TBS/T)
DEPC-treated ddH_2O (DEPC•H_2O)
Luria-Bertani Broth/Agar (LB Broth/Agar)
paraformaldehyde in PBS (*p*-CHO•PBS)
phosphate buffered saline (PBS)
sodium chloride, sodium citrate buffer (SSC)
Tris acetate EDTA (TAE)
Tris borate EDTA (TBE)
Tris buffered saline (TBS)
Optimal Cutting Temperature Compound (OCT)
Storage Media (SM)

Chapter 1 Introduction

Chapter 1 Introduction

The mammalian eye has evolved into an intricate system for capturing light and transferring the total collected light input to the brain where it can be processed to form an image. Light enters the eye through the cornea, the amount controlled by the muscular circle of the iris, and is focused by the lens onto the retina. The photoreceptor cells of the retina capture light photons and transmit a neural signal to the neurons of the retina which lead to a total signal being transferred through the optic nerve. Behind the retina the retinal pigment epithelium absorbs the remainder of the light energy which is not absorbed by the photoreceptor cells, preventing reflective signalling. The entire system is enclosed in a strong, collagenous tissue called the sclera, which maintains the correct shape of the eye and is the site of attachment of the ocular muscles (**Figure 1-1.**; Hart, 1992; Oyster, 1999).

The most abundant type of photoreceptor cell in the retina is the rod cell, which detects the quantity of light that reaches the retina by the activity of the chromophore rhodopsin. The less numerous cone cells provide colour and detail vision. These are of three types, which differ in the type of chromophore they contain, and thus in the wavelength of light that activates the visual transduction signal. The neurons which connect to the photoreceptor cells transmit the information through a network of interacting neurons that, *in totum*, provide the signals necessary for the brain to derive the quantity and wavelength of light, and the spatial distribution of this information in order to translate the received signals into an image (Hart, 1992; Oyster, 1999).

1-A Physiology

The tissues of the eye act as a coordinated whole to provide sight, and all of them are important elements of ocular physiology. Defects in the cornea that prevent the proper organization of the collagen fibres reduce the transparency of the cornea and decrease the light levels entering the eye. Problems with muscular control of the iris impair the ability to respond to changing light levels. Even the seemingly inert aqueous and vitreous humour play important roles in controlling the intraocular pressure of the eye, a pressure that must be homeostatic to avoid distorting the shape of the eye which would, in turn, distort the shape of the retina or the lens (Hart, 1992; Harding, 1997; Oyster, 1999). While this is true, the study presented here deals almost exclusively with

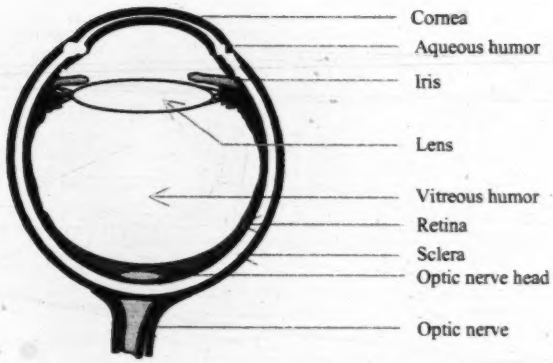

Figure 1-1. Diagram of the Eye. (After Oyster, 1999.)
The retina is an unpigmented layer of neural cells overlying the retinal pigment epithelium and choroid.

the function of the retina, arguably the most important of the functional elements of the eye.

1-A1 Retinal Morphology: The retina is distinctive for its intricately layered network of neuronal cells. This network is established to collect and process the information gathered by the photoreceptor cells, which are unique, and highly specialized, terminally-differentiated neurons. Retinal structure is very similar among the class Mammalia, with the exception that the order Primates has a specialized cone-rich region in the centre of the retina known as the fovea that is responsible for colour differentiation and detail. All mammals have cones interspersed with rods in the retina, but rods are the predominant photoreceptor cell throughout the mammalian retina (Hart, 1992; Oyster, 1999).

The photoreceptor cells are the major components of the three most posterior cell layers of the retina, so that they are actually outer retinal layers from the perspective of the centre of the eye (**Figure 1-2.**). The outer segment layer (OS) contains the chromophore-containing membranes of the photoreceptor cells and is a specialized cellular compartment that contains the membrane-bound chromophore of the photoreceptor cell. In rod cells, the OS contains stacks of lamellae, phospholipid bilayers arranged as flattened, hollow spheres, in which rhodopsin is embedded (**Figure 1-3a.**). In cones, the chromophore is embedded in deep invaginations of the plasma membrane, and it is this structural difference that is the determinant of cell type between rods and cones—despite the names (Hart, 1992; Oyster, 1999). The OS has interesting biology in that it is being continually digested at the outermost tip by the overlying retinal pigment epithelium (RPE). In rods, this phagocytosis is thought to be the means by which the photoreceptor cells regenerate rhodopsin and lamellae. The rhodopsin-containing lamellae have been shown to migrate towards the RPE, and new lamellae are added at the anterior face of the OS (Young, 1971, 1972, 1978). In this fashion, the retina ensures that the rhodopsin present in the OS is continuously renewed, presumably to prevent the accumulation of potentially damaged proteins or toxic products derived from lipid metabolism.

The inner segment layer (IS) contains the mitochondria and endoplasmic reticulum of the photoreceptor cells, and a cilium that connects the OS to the IS through a

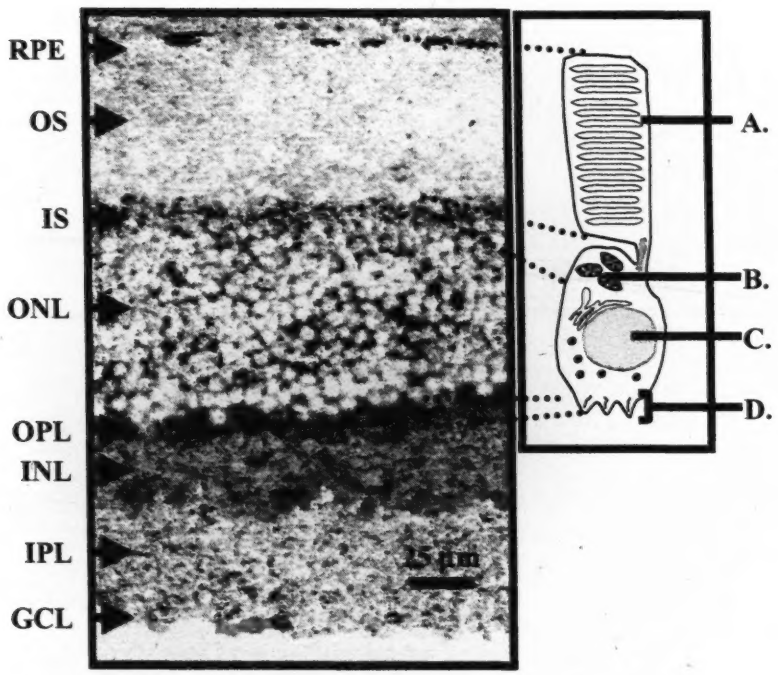

Figure 1-2. Retinal Morphology. (Modified reflective dark-field micrograph; Photoreceptor cell: After Oyster, 1999)
Tissue structure showing rat retina cell layers, with accompanying schematic of photoreceptor cell morphology. The rhodopsin-containing lamellae (**A.**) of the rod photoreceptor cells are found in the outer segment (**OS**), the inner segment (**IS**) contains the mitochondria (**B.**) and endoplasmic reticulum, and the outer nuclear layer (**ONL**) contains the nuclei (**C.**). The outer plexiform layer (**OPL**) contains the synaptic junctions of the photoreceptor cells (**D.**) and the retinal neurons. The nuclei of the retinal neurons are found in the inner nuclear layer (**INL**), and their processes are found in the inner plexiform layer (**IPL**). The **OS** is the most posterior layer of the retina, and posterior to it is the Retinal Pigment Epithelium (**RPE**; Top). The Ganglion Cell Layer (**GCL**; Bottom) is the most anterior layer of the retina, and borders the vitreous humour. Light would enter the retina from the bottom of this figure.

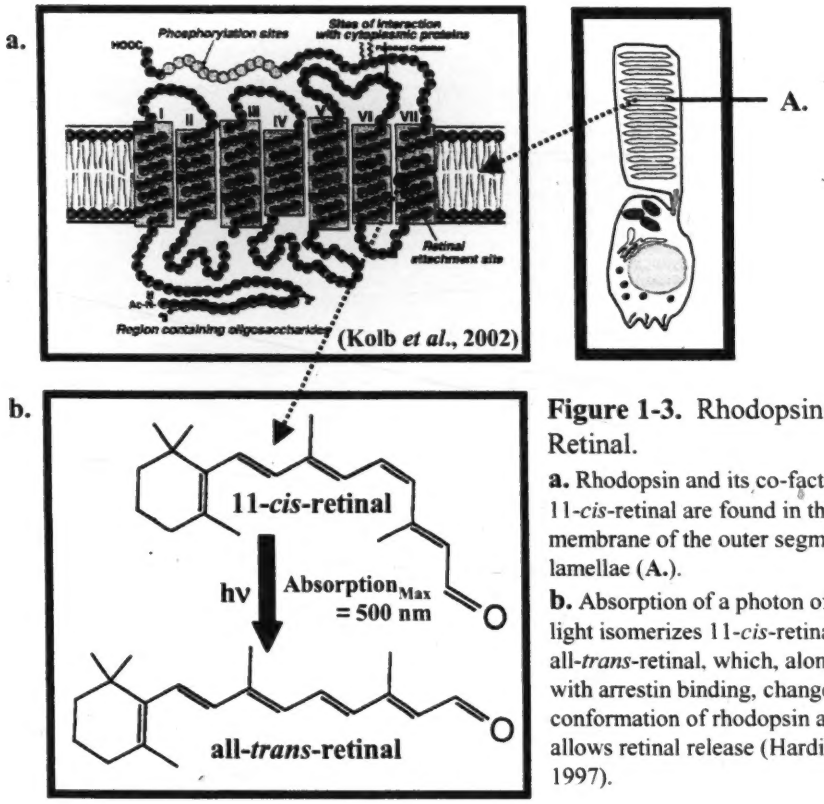

Figure 1-3. Rhodopsin and Retinal.

a. Rhodopsin and its co-factor 11-*cis*-retinal are found in the membrane of the outer segment lamellae (**A.**).

b. Absorption of a photon of light isomerizes 11-*cis*-retinal to all-*trans*-retinal, which, along with arrestin binding, changes the conformation of rhodopsin and allows retinal release (Harding, 1997).

narrow cytoplasmic channel. The nuclei of the photoreceptor cells are found in the outer nuclear layer (ONL). At the interior base of the photoreceptor cell is found the synaptic terminus, which is distinguished by an electron-rich structure termed the synaptic ribbon. The synaptic ribbon is proposed to be a means of delivering large quantities of neurotransmitter to the synapse by docking neurotransmitter-containing vesicles, and promoting their movement towards the plasma membrane. The photoreceptor cell synaptic terminus makes up part of the outer plexiform layer (OPL; Hart, 1992; Oyster, 1999; Kolb *et al.*, 2002).

The other part of the OPL is the other half of the photoreceptor cell synapse, the bi-polar neuron. These neurons are the first connection of the rod photoreceptor cells to the neural network. These neurons then connect to horizontal, and amacrine cells, from where the signal is relayed to the retinal ganglion cells, which in turn relay the signals through the optic nerve to the optic lobe. The nuclei of the bipolar, horizontal, and amacrine neurons are found in the inner nuclear layer (INL), and their processes, connections to the retinal ganglion cells and each other, make up the inner plexiform layer (IPL). The nuclei of the retinal glial cells, Müller cells, are also found in the INL. The ganglion cell layer is the innermost of the retinal layers, bordering directly on the vitreous humour, just below the IPL. The INL occurs just below the OPL, and the IPL is just below the INL (Hart, 1992; Oyster, 1999; Kolb *et al.*, 2002).

1-A2 Phototransduction: The absorption of light by the retina and transmission of the message to the brain is effected by a signalling pathway referred to as phototransduction (**Figure 1-4.**). The model organism used in this study is *Rattus norvegicus*, which lack a fovea, so the cascade described in the following paragraphs is specific to rod photoreceptor cells, the predominant photoreceptor in rat retinae (Noell, 1980; Oyster, 1999).

In rod photoreceptor cells, the cascade begins with the absorption of light by rhodopsin (Rho)[1] and its co-factor 11-*cis* retinal. Rhodopsin associated with 11-*cis*-retinal is the active form of rhodopsin, and is considered unbleached. When 11-*cis*-retinal absorbs a photon of the appropriate wavelength, it is isomerized to all-*trans*-retinal (**Figure 1-3b.**). This causes a conformational change in rhodopsin, and the

[1] Where known, the names of the rat genes that produce these products are provided in brackets.

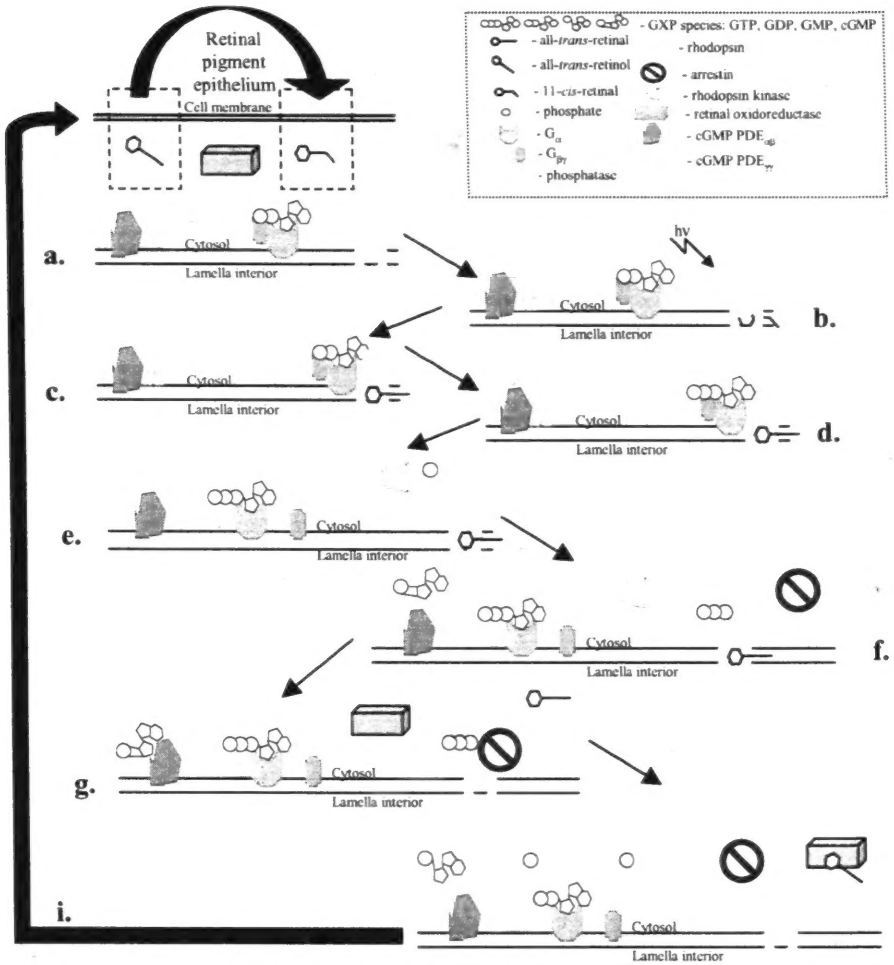

Figure 1-4. Signal Transduction by Rhodopsin. (After: Oyster, 1999. pp. 565-583.)
a. All-*trans*-retinol is exported from the outer segment of the photoreceptor to the retinal pigment epithelium where it is converted to 11-*cis*-retinal and imported into the photoreceptor. **b.** 11-*cis*-retinal is bound by rhodopsin in the membrane of the photoreceptor lamella. **c.** Absorption of a photon of the appropriate wavelength converts 11-*cis*-retinal into all-*trans*-retinal, and $G_{\alpha\beta\gamma}$, with bound GDP, associates with the activated rhodopsin. **d.** GDP bound by $G_{\alpha\beta\gamma}$ is exchanged for GTP when the $G_{\alpha\beta\gamma}$-activated rhodopsin complex is formed. **e.** The GDP-GTP exchange causes the $G_{\alpha\beta\gamma}$-activated rhodopsin complex to dissociate, and $G_{\beta\gamma}$ to dissociate from G_α. **f.** G_α-GTP associates with cGMP phosphodiesterase (cGMP PDE) and inactivates cGMP $PDE_{\gamma\gamma}$'s inhibition of the phophodiesterase activity of CGMP $PDE_{\alpha\beta}$. The activated rhodopsin is phosphorylated at the C-terminus by rhodopsin kinase. **g.** cGMP $PDE_{\alpha\beta}$ cleaves the cyclic bond of cGMP to form GMP. Arrestin binds the phosphorylated, activated rhodopsin and prevents further $G_{\alpha\beta\gamma}$ association, as well as causing the release, or bleaching, of all-*trans*-retinal. **h.** GTP bound by G_α is cleaved to form GDP, inactivating G_α and allowing $PDE_{\gamma\gamma}$ to inhibit $PDE_{\alpha\beta}$ once again. A phosphatase removes the phosphate groups from rhodopsin. Retinal oxidoreductase converts all-*trans*-retinal to all-*trans*-retinol. **i.** $G_{\alpha\beta\gamma}$ is reformed, and the cycle continues. Lowering the concentration of cGMP in the cell closes membrane channels, and changes the current entering the photoreceptor, a difference interpreted by ganglion cells as a neural signal.

G-protein transducin associates with the activated rhodopsin. Transducin is a heterotrimeric protein made of G_α (Gnat1), G_β[2], and G_γ[2], subunits. The G-proteins exist as $G_{\alpha\beta\gamma}$ proteins when guanosine 5' diphosphate (GDP) is bound to them, and they dissociate to form G_α and $G_{\beta\gamma}$ when GDP is exchanged for guanosine 5' triphosphate (GTP). The Gα-GTP subunit associates with an inactive 3', 5'-cyclic guanosine monophosphate (cGMP) phosphodiesterase (cGMP-PDE), and this activates the cGMP-PDE by displacing one of the two cGMP-PDE_γ subunits, exposing the active centre of the holoenzyme, cGMP-$PDE_{\alpha\beta}$ (cGMP-PDE_β: Pde6b). cGMP-PDE then breaks the 3'-5' bond of the cGMP to produce guanosine 5' monophosphate (GMP). These steps are the activation steps of phototransduction, and all of them occur at the membrane of the OS lamellae (Hart, 1992; Harding, 1997; Oyster, 1999).

In order to deactivate phototransduction, rhodopsin kinase (Rhok) phosphorylates rhodopsin at the C-terminus of the protein. An arrestin protein, S-antigen (Sag), binds the phosphorylated rhodopsin and prevents association of transducin with the activated rhodopsin. This binding also causes the release of all-*trans*-retinal by rhodopsin, and the rhodopsin is considered to be bleached. The Gα-GTP subunit of transducin that activated the cGMP-PDE hydrolyzes GTP to GDP, and this promotes the reformation of the inactive transducin holoenzyme and the inactive conformation of the cGMP-PDE holoenzyme. A protein phosphatase[3] removes the phosphate groups from the C-terminus of rhodopsin. A retinal oxidoreductase, short-chain reductase 1 (Sdr1) in humans, converts all-*trans*-retinal to all-*trans*-retinol, which is then transported from the photoreceptor to the RPE, where it is oxdized to 11-*cis*-retinal. From the RPE, 11-*cis*-retinal is returned to the OS where it reassociates with unbound rhodopsin to regenerate unbleached rhodopsin (Hart, 1992; Harding, 1997; Oyster, 1999).

The key element of phototransduction is the generation of GMP from cGMP. Lowering the concentration of cGMP in the cell closes cGMP-gated cation membrane channels in the OS, and decreases the rate of Na^+ entering the OS. This change results in a hyperpolarization of the entire cell since cations from the synaptic terminus of the

[2] There are multiple G_β and G_γ proteins as products of multiple genes, and the specific $G_{\beta\gamma}$, if one exists, used in rod phototransduction is not clear. In human cones, Gngt2 is suspected to be the gene for the G_γ protein.

photoreceptor cell move towards the more negative OS, reducing the total potential of the cell. The neurotransmitter released at the photoreceptor terminus is glutamate, which is carried to the synapse in vesicles that associate with the synaptic ribbon. The release of glutamate occurs through exocytosis as these vesicles fuse with the cell membrane, and vesicle fusion is increased in the presence of high concentrations of Ca^{2+}. When hyperpolarization occurs, the local concentration of Ca^{2+} decreases and slows vesicle fusion. Counter-intuitively, photoreceptor synaptic signalling is maximal when no light is absorbed by the retina and minimal when the photoreceptor cell is maximally stimulated. The signalling is not a binary switch, but rather it is the relative rate of glutamate release from the photoreceptor cell at the synapse that signals the bipolar cells and, from them, the rest of the retinal neurons. This means that there is a constant signal travelling to the optic lobe that contains information about the relative intensity of the light, the location of the light source relative to the photoreceptors that are signalling, and, because of the constant signal, the temporal distribution of the signal (Hart, 1992; Harding, 1997; Oyster, 1999).

1-A3 Lens Biology and the Crystallins: While this study examines the retina, the major part of the study focused on the expression of supposedly lens-specific proteins, the crystallins, in the retina. These proteins, with two exceptions, were considered to have no role of significance outside the lens. This study has shown that the crystallins are expressed in the rat retina. Based on the data obtained, this study suggests a likely reason for their expression in this tissue.

Two aspects of lens biology impact on this study: the clarity of the lens, and its longevity. In terms of clarity, it is essential that the lens has a minimal impact on the path of light to the retina. Light-scattering by the lens will impair vision, so this tissue must be uniform in optical density. The lens must therefore maintain a uniform intracellular environment and prevent the formation of large intracellular bodies that will scatter the incident light (Bloemendal and de Jong,1991; Harding, 1997; Hejtmancik, 1998; Oyster, 1999).

The problem of maintaining clarity is compounded by the fact that the lens is formed early in development—5 to 6 weeks after gestation in *Homo sapiens* (Oyster,

[3] In humans, this protein is protein phosphatase 2, which contains many regulatory and catalytic subunits.

1999). The lens forms from an invagination, called the lens placode, of the surface ectoderm above the forming optic cup. The lens placode separates from the epithelium as a hollow sphere, the lens vesicle, which is then filled by the expansion of the epithelial cells that border the cavity. The cells that fill the lens vesicle then lose their mitochondria and nuclei. The cells remain as discrete membrane bound entities, but are not actively involved in transcription or aerobic metabolism. The consequence of this is that these embryonic lens cells cannot replace their proteins, and so the proteins in them must be exceptionally stable and long-lived. Some cells and proteins within the lens are almost as old as the organism. Lens growth continues throughout the life of the organism, and is accomplished by mitosis and differentiation of cells on the anterior face of the lens. The differentiating cells elongate, and they also lose their nuclei and mitochondria as they form a layer of lens fibres over previously formed lens fibres (Harding, 1997; Oyster, 1999).

The crystallin (α-, β-, and γ-) proteins meet the criteria of ideal lens proteins, clarity and longevity, and make up 90% of the dry-weight of the lens. Despite the name of the crystallins, the lens cells are not crystalline. The crystallins are all water soluble proteins that form a relatively dense and uniform aqueous structure within the lens. γ-Crystallins are monomeric proteins, while the α- and β-crystallins form heteromeric aggregates (Wistow and Piatigorsky, 1988; Graw, 1997; Horwitz *et al.*, 1998, 1999; Slingsby and Clout, 1999)

α-Crystallin is the protein formed from the aggregation of 30-40 α-crystallin subunits in the ratio of three αA-crystallins to one αB-crystallin (Horwitz *et al.*, 1998, 1999). α-Crystallin is noted as a systemic heat shock protein, acting as a chaperone to misfolded proteins. α-Crystallin's role as a chaperone is to prevent molten globule proteins from denaturing further, which allows refolding chaperones the chance to repair damaged proteins, and increases the longevity of the lens proteins. As well, the chaperone activity also prevents the denaturation of proteins to the point that they serve as the nucleus of hydrophobic interactions. Hydrophobic interaction with other proteins could result in protein precipitation that would create large, dense aggregates that would scatter light. The β-crystallin aggregates range from dimers to octomers, that are formed from all seven of the β-crystallin proteins (Wistow and Piatigorsky, 1988; Bloemendal

and de Jong, 1991; Graw, 1997; Slingsby and Clout, 1999). Except for their general role as structural proteins, no function has been assigned to the βγ-crystallins.

While α-crystallin provides obvious means of maintaining lens longevity and clarity, it is likely that the βγ-crystallins have a significant role as well. The βγ-crystallins provide a malleable cytoplasmic stability that allows the lens cells to respond to the extralenticular environment, *e.g.* changes in intraocular pressure. This study will suggest another possible role for the βγ-crystallins.

1-B Light-induced Retinal Degeneration

Retinal degeneration is a condition that results in the apoptotic death of the photoreceptor cells, resulting in blindness. In humans, retinal degeneration is often the result of hereditary diseases such as retinitis pigmentosa (RP) and macular degeneration (MD). While standard genetic analysis can identify genes that are the cause of the disease, the identification does not explain the process of retinal degeneration. (Wong, 1994; Maw *et al.*, 1997; Rattner *et al.*, 1999; Hafezi *et al.*, 2000; Daiger, 2002). The process by which the cells are switched from functioning, fully differentiated, post-mitotic cells to apoptotic cells is not explained by identifying the cause of the switch. This study is an attempt to describe one aspect of the degeneration process, crystallin expression in the retina and its role in retinal degeneration.

1-B1 Studying Human Retinal Degeneration: It is not possible to examine the process of retinal degeneration in humans at the level of its molecular biology because of the extreme difficulty in determining the exact factors that lead to retinal degeneration in humans. Genetic mutation and polymorphisms in a range of genes could result in the net effect of retinal degeneration, especially since retinal degeneration is also the end result of multiple environmental factors, including diet and light exposure. As well, retinal degeneration could also be considered to have occurred with defects in tissues outside the retina, *e.g.* defects in iris control could result in a decrease in the ability of the eye to respond normally to intense light, and defects in blood supply to the whole eye could result in impaired metabolism in the retina (Hart, 1992; Oyster, 1999). Dissecting the exact contributions of the myriad factors to retinal degeneration would be an immense task.

The complexity of contributing factors to retinal degeneration is compounded by the fact that while retinal degeneration in humans has an adverse impact on the quality of the affected individual's life, it is not a lethal disease. In many cases retinal degeneration is a progressive process, affected individuals can survive long past the point of complete retinal degeneration. Should the affected individual be willing to donate their retinae to research after their death, the tissue will not be useful in determining the active degeneration process, only the end result. The likelihood of obtaining retinae from an individual who is actively undergoing retinal degeneration is exceedingly low, and is also attended by moral and ethical questions as to its appropriateness. An image of the ghoulish vivisectionists of the Renaissance, "Give me your eyes!", is an exceptionally negative response to suggestions that living, or accidentally deceased, individuals donate their eyes for research. These factors make human retinae for research a rare resource.

While molecular biology studies of the human retina are difficult, studies in humans can focus on the changes of living retinae, by photography of the retina, fundus photography, or by changes in response to light stimuli as measured by electroretinography. These studies can then be examined with regard to distinguishable changes that can be associated by family studies to particular mutations or, as far as possible, environmental conditions (*e.g.* Morimura *et al.*, 1999; Lagali *et al.*, 2000; Zhang *et al.*, 2001). These studies identify genes which have roles in the phenotype of retinal degeneration, and these genes can then be examined in model systems that can account for the variability of contributing factors in human disease (*e.g.* Portera-Cailliau *et al.*, 1994; Organisciak *et al.*, 1998, 1999a). The converse is also true, in that genes and proteins identified in model systems can be examined for their contribution to retinal degeneration in humans.

1-B2 Retinal Degeneration in Rats: Retinal degeneration in Sprague-Dawley rats can be induced by exposing dark-reared rats to intense green light for fixed lengths of time. Green light (490-580 nm) is used because this wavelength of light matches the activation wavelength of rhodopsin, the primary chromophore in the rod cells of the retina (Section **1-A2**, **Figure 1-5.**). The activation of rhodopsin leads to over-bleaching since the regeneration of active rhodopsin cannot match the levels of rhodopsin bleaching

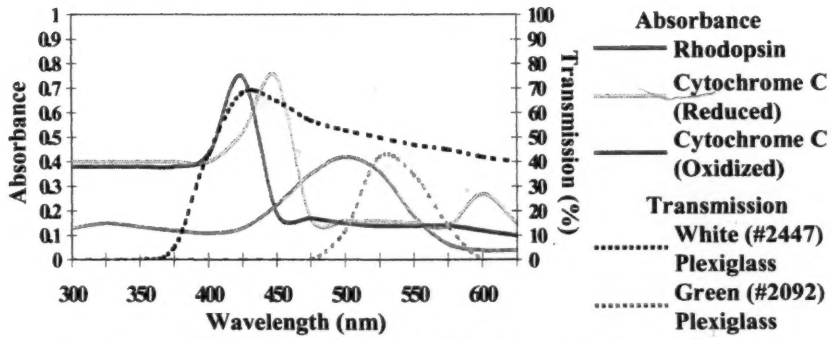

Figure 1-5. Light Absorption by Rhodopsin and Transmission by Plexiglass Filters. (After: Organisciak and Winkler, 1994)

Absorption (left axis, arbitrary units)

Rhodopsin light absorption is maximal at 500 nm (green).

Reduced cytochrome C light absorption is maximal at 420 nm (blue).

Oxidized cytochrome C light absorption is maximal at 444 nm (blue), another peak occurs at 605 nm (orange).

Transmission (right axis, %)

White plexiglass (#2447), a common light filter, transmits light with wavelengths 370-650 nm. Note the transmission peak of 400-470 nm (blue).

Green plexiglass (#2092) transmits light with wavelengths 490-580 nm. This transmission overlaps rhodopsin's absorbance very well.

when the light intensity is 1500 lux[4] (Noell *et al.*, 1966; Noell, 1980; Organisciak and Winkler, 1994). A signal advantage of the use of green light is that the retinal degeneration induced by the light exposure is attributable to a single cause (Noell *et al.*, 1966; Noell, 1980; Williams and Howell, 1983; Organisciak and Winkler, 1994; Tan *et al.*, 2001). The rats used are an inbred wild-type colony, so that polymorphisms or mutations are unlikely in the treated animals, and are an albino strain, which means that the effect of melanin light absorption in the iris and RPE is minimized and that light absorption by the retina is maximized (Noell, 1980; Rapp and Williams, 1980; Organisciak and Winkler, 1994).

As well, the rats are all cared for and raised in the dark, with identical light exposure and diet. This means that retinal degeneration in the rats is the result of exposure to intense green light, a wavelength of light which activates the major chromophore in the rat retina, rod photoreceptor cell rhodopsin. Retinal degeneration in this system is likely the direct result of changes in rhodopsin metabolism (Noell, 1980; Organisciak and Winkler, 1994; Tan *et al.*, 2001).

Retinal degeneration can also be induced in rats by exposure to other wavelengths of light. White light (370-650 nm, **Figure 1-5.**) is composed of all the visible wavelengths of light, and causes retinal degeneration in rats (Lerman, 1980; Waxler and Hitchins, 1986; Remé *et al.*, 1995). The strength of white light irradiance is that the light exposure mimics the light exposure that animals, and humans, are regularly exposed to. This means that changes in rat retinae represent the *in totum* response of the retina and RPE to light exposure and absorption. Blue light (<480 nm) is also used to expose rat retinae, since blue light is a major fraction of white light (**Figure 1-5.**). Early research suggests that blue light damage has two effects, damage to photoreceptor cells, and damage to the RPE, which can be separated depending on the length of light exposure: short exposure leads to photoreceptor cell damage, and long exposure leads to photoreceptor cell and RPE damage (Ham *et al.*, 1976; Sperling, 1980, 1986; Sperling *et al.*, 1980; Ham *et al.*, 1982, 1984).

---

[4] One lux is the equivalent of 1.46 milliwatt of radiant electromagnetic power at a frequency of 540 terahertz, impinging at a right angle on a surface whose area is one square meter. A frequency of 540 THz corresponds to a wavelength of about 555 nm, which is in the middle of the visible-light spectrum. An equivalent non-SI (Système International d'Unités) unit is the foot-candle which is equal to 10.764 lux.

The current study uses green light to induce retinal degeneration because the drawbacks of white and blue light exposure seem insuperable with regards to a molecular biological dissection of the process of retinal degeneration. Since white light-induced retinal degeneration is the *in totum* response of the retina and RPE, determining the changes inherent to only the retina is not possible. Blue light exposure results in damage to both the RPE, and to photoreceptor cells. RPE damage might result in retinal degeneration, but the degeneration is not a specific malfunction of photoreceptor cell metabolism, rather it is a secondary cellular response to the creation of a deficiency in RPE metabolism. Blue light that damages photoreceptor cells directly is likely targetting some other chromophore in the photoreceptor cells, since most of the wavelengths absorbed by rhodopsin (425-550 nm) are greater than 480 nm (**Figure 1-5.**). Likely candidates for this absorption are mitochondrial cytochromes (**Figure 1-5.**), and heme- and riboflavin-containing proteins (Organisciak and Winkler, 1994). This means that the mechanism of blue light-induced retinal degeneration is likely to be different than that induced by green light. As well, since cytochromes, and heme and riboflavin proteins are found in all tissues, the response is not necessarily a photoreceptor-specific response. Green light avoids these drawbacks because it targets rhodopsin, and therefore rod photoreceptor cells, and the retinal degeneration can then be reasonably considered to be a rod photoreceptor cell-specific response that is the direct result of a change in rod photoreceptor cell metabolism.

1-B3 Oxidative Stress in Retinal Degeneration: Rats that are pretreated with an antioxidant, *e.g.* dimethylthiourea [DMTU, $SC(NHCH_3)_2$; Lam *et al.*, 1990; Organisciak *et al.*, 1991, 1992b, 1999b; Kutty *et al.*, 1995] or 3-keto-gulofuranolactone (Synonyms: ascorbic acid, Vitamin C; Organisiciak *et al.*, 1984, 1985, 1987, 1990, 1991, 1992a; Li *et al.*, 1985; Noell *et al.*, 1987), prior to light exposure show a significant degree of protection from light-induced retinal degeneration (LIRD). Both compounds are free radical scavengers, and the protective effect of Vitamin C was shown to be directly antioxidant rather than due to induction of enzymatic activity by showing a similar protective effect of both the L- and D- stereoisomers (Organisciak *et al.*, 1992a). This suggests that LIRD has an oxidative stress component which is the main effector of the LIRD phenotype (Organisciak *et al.*, 1992a, 1992b, 1995, 1999b; Kutty *et al*, 1995;

Specht *et al.*, 1999). In addition, after light exposure of rats that are not treated with DMTU, a steady up-regulation of heme oxygenase-1, an oxidative stress-inducible gene, correlates with increasing amounts of light-exposure (Kutty *et al.*, 1995; Organisciak *et al.*, 1995; Ossola and Tomaro, 1998; Wong *et al.*, 2001). Lack of another antioxidant protein, superoxide dismutase 1 (SOD1), results in increased light-induced retinal damage in *Mus musculus* (Mittag *et al.*, 1999). These observations support the inference that a key component of the retinal response to LIRD will be a stress response. The element of the oxidative stress environment that the retina is responding to is the high concentration of reactive oxygen species (ROS) and other radicals generated as a consequence of intense light exposure

Molecules with extensive conjugated double bonds, like retinal, rhodopsin's cofactor (**Figure 1-3b.**), are a potential source of radicals because they have stable resonance structures that allow relatively easy electron movement within the system of conjugated double bonds (**Figure 1-6b.**). It is the stability of retinal's resonance structures that allow isomerization from 11-*cis*-retinal to all-*trans*-retinal. Abstraction of an electron from this system would be possible for molecular oxygen, and a superoxide anion would be generated, or the resonance structure could abstract an electron from a close neighbour such as docosahexaenoic acid (DHA) in the membrane of the lamella, and generate a fatty acid radical (Brunori and Rotilio, 1984; Green and Hill, 1984; Halliwell, 1991; Jones, Jr., 1997; Winkler *et al.*, 1999). The important consideration in the generation of radicals and ROS is that the process continuously generates radicals from non-radicals in a chain reaction until two radicals extinguish each other in a chain termination reaction.

There are other secondary sources of oxidative stress in the retina. The mitochondria of the IS are a possible source of ROS because the light exposure results in a continuous activation of the visual transduction cascade, which requires an increase in available energy. This means that the mitochondria are more active, and there is more possibility of an escape of electrons from the electron transport chain that could react with molecular oxygen to produce a superoxide anion (**Figure 1-6a.**; Brunori and Rotilio, 1984; Green and Hill, 1984; Ham *et al.*, 1984; Halliwell, 1991; Winkler *et al.*, 1999; Boulton *et al.*, 2001; Roberts, 2001).

a. electron (e^-) transport chain → 'free' [e^-] + O_2 → [$O_2^{\bullet}$]

b. conjugated double bond (R–C=C–C=C–R) + energy (hv)
→ [R–C•–C=C–C•–R] + O_2 → [R–C–C=C–C–R]$^{\bullet}$ + [$O_2^{\bullet}$]

c. Superoxide dismutase (Cu/Zn): 2 [$O_2^{\bullet}$] + 2 H_2O → 2 H_2O_2 + O_2

d. Iron oxidation: H_2O_2 + Fe^{2+} → Fe^{3+} + [$HO^{\bullet}$] + HO^-

e. polyunsaturated fatty acid (R–HC=HC–H_2C–HC=HC–R–COOH) + [$HO^{\bullet}$] + O_2
→ [R–HC=HC–H_2C–C($O_2^{\bullet}$)=HC–R–COOH] + fatty acid
→ lipid peroxide (R–HC=HC–H_2C–C(OOH)=HC–R–COOH)
→ alkyl radical, dialdehyde, carboxylic acid, *etc.*
and → fatty acid radical [R–HC=HC–H_2C–C•=HC–R–COOH]
+ fatty acid → fatty acid radical (Chain Reaction)
or, → lipid cross-linking (Chain Termination)

f. Catalase: 2 H_2O_2 → 2 H_2O + O_2

g. Glutathione peroxidase: 2 glutathione (G–SH) + H_2O_2 → 2 H_2O + G–S–S–G

h. Heme oxygenase 1: heme + [e^-] → bilirubin

Figure 1-6. Reactions Involving Reactive Oxygen Species (ROS).
Commonly occurring ROS reactions that occur within mammalian tissues. **b.** An example of a retinal molecule that contains conjugated double bonds is 11-*cis* retinal, rhodopsin's co-factor (Oyster, 1999). **e.** A retinal polyunsaturated fatty acid is docosahexaenoic acid, a major component of the lamellae of the outer segment (Organisciak *et al.*, 1996, 1998). **c.** Superoxide dismutase (Cu/Zn), **f.** catalase, **g.** glutathione peroxidase, and **h.** heme oxygenase 1 are known to be expressed in the rat retina (Kutty *et al.*,1995; Organisciak *et al.*, 1998).

As well, the OS of the rod photoreceptor cells are excellent potential sources of ROS and radicals. This is because of two essential components of the rod photoreceptor cell OS, retinal and DHA, which are integral components of the lamellae of the OS and occur there in high concentrations. DHA generation of radicals or damaged lipids is a result of increasing oxidative stress. The chain begins with SOD1, an enzyme which causes a dismutation of the ROS superoxide anion and water to form molecular oxygen and the ROS hydrogen peroxide (**Figure 1-6c.**; Brunori and Rotilio, 1984; Green and Hill, 1984; Halliwell, 1991; Fridovitch, 1995; Mittag *et al.*, 1999; Winkler *et al.*, 1999; Boulton *et al.*, 2001; Roberts, 2001). Enzymes for oxidizing hydrogen peroxide exist, but high concentrations of hydrogen peroxide mean that it can spontaneously oxidize iron (II) to iron (III), generating the extremely reactive ROS hydroxyl radical and a hydroxyl ion. Polyunsaturated fatty acids, like DHA—a major component of the lamellae (Organisciak *et al.*, 1996, 1998; Rodriguez de Turco *et al.*, 1997), are potential source of radicals because they are subject to peroxidation by hydroxyl radicals and molecular oxygen. The resultant lipid peroxide can abstract hydrogen from another fatty acid and then degrade to generate an alkyl radical and other reactive products, *e.g.* dialdehydes and carboxylic acids. The alkyl radicals produced from the degradation, or the fatty acid radical generated by the abstraction, can then propagate a chain reaction of radical generation and lipid degradation, or can react with another radical, alkyl or fatty acid, to result in covalent modification and cross-linking of fatty acids (Esterbauer and Cheeseman, 1990; Halliwell, 1991; Boulton *et al.*, 2001).

1-B4 Apoptosis in Retinal Degeneration: High intensity green light induces retinal degeneration in rats by an apoptotic mechanism, and it is thought that it causes such a significant stress to the photoreceptor cells that the molecular balance between cell survival and apoptosis is tilted toward apoptosis (Organisciak and Winkler, 1994; Portera-Cailliau *et al.*, 1994; Wong, 1994; Remé *et al.*, 1995; Colley *et al.*, 1995; Rattner *et al.*, 1999; Specht *et al.*, 1999). That LIRD involves apoptotic death of the photoreceptor cells has been shown by the identification in photoreceptor cells of DNA degradation with the characteristic apoptotic "laddering" of 180 basepair DNA fragments, caused by the internucleosomal cleavage of DNA (Organisciak *et al.*, 1995, 1999b; Remé *et al.*, 1995; Specht *et al.*, 1999). Evidence of apoptosis in LIRD also comes from the

identification of photoreceptor cell nuclei labelled using terminal deoxynucleotidyl transferase (TdT)-mediated dUTP-biotin nick end labelling (TUNEL), which labels the 3' ends of DNA fragments created by degradation of DNA (Remé *et al.*, 1995).

The process of apoptosis is one that is inherent to all eukaryotic cells, and functions to remove superfluous or damaged cells from the organism to avoid endangering the organism as a whole, or the incorrect development of a particular tissue. Wild-type rats do not have a genetic condition that predisposes them to abnormal apoptotic loss of photoreceptor cells. In the LIRD system, the death of photoreceptor cells due to light exposure is caused by the induction of the apoptotic cascade when the photoreceptor cells have incurred irreparable damage (Davidson and Steller, 1998; Alloway *et al.*, 2000; Grimm *et al.*, 2000; Hao *et al.*, 2002). RP and MD photoreceptor cell-loss has been shown to occur through apoptosis (Chang *et al.*, 1993; Lolley *et al.*, 1994; Milam and Li, 1995; Abler *et al.*, 1996; Carmody and Cotter, 2000), thus the wild-type molecular response to intense stress in rodents may be indicative of what occurs in the retinae of rodents with mutations which result in retinal degeneration.

Intense light exposure causes significant stress to the photoreceptor cell, and it is likely that a point is reached where the net effect of cell damage overrides the cell's capacity for survival, and photoreceptor cell death occurs. A light treatment of 4 hours is sufficient to cause photoreceptor cell loss in dark-reared rats that are not immediately sacrificed, but the extent of photoreceptor cell loss is not as extensive over 4 hours as it is in animals exposed to light for longer periods of time, *e.g.* 8 hours or 16 hours (**Figure 1-7.**; Organisciak *et al.*, 1992a, 1992b, 1995, 1999b; Wong *et al.*, 2001) This suggests that the retinae of dark-reared rats treated for 4 hours with intense green light are not as fully committed to apoptotic photoreceptor cell loss. Perhaps a 4 hour of light exposure creates a tissue and cellular environment that is poised between the normal retinal phenotype and committing to the apoptotic cascade in the face of irreversible damage to the cells of the retina.

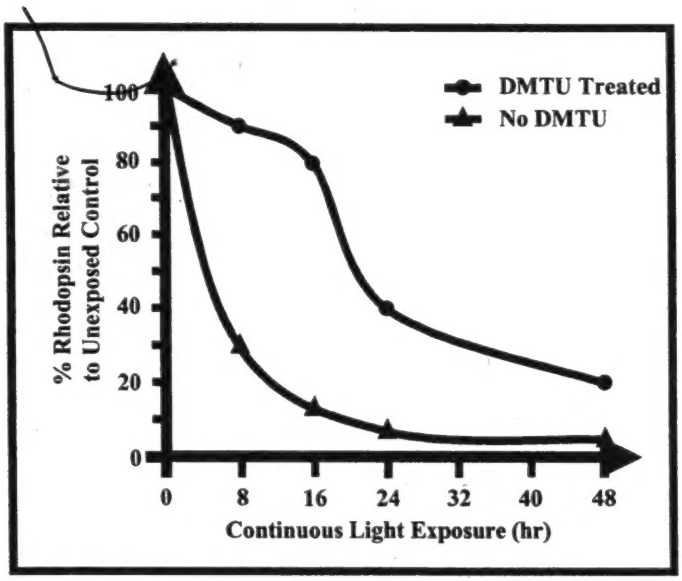

Figure 1-7. Protective Effect of Dimethylthiourea in Light-induced Retinal Degeneration. (After: Organisciak *et al.*, 1992b)

Pretreatment of rats with dimethylthiourea (DMTU) before continuous light exposure results in protection of the retina, as measured by the concentration of rhodopsin protein in DMTU-treated and -untreated samples as a percentage of non-light treated control animals. Rhodopsin is a rod photoreceptor cell-specific protein so decreases in rhodopsin levels are a marker of the loss of rod photoreceptor cells in the retina.

1-C Hypothesis

Retinal degeneration in rats induced by exposure to intense green light (LIRD) will be marked by a particular molecular phenotype which is characteristic of the retinal response to the oxidative stress induced in the retina.

The cells in the retina will express a set of messenger RNAs (mRNAs) which is characteristic of the degeneration of the retina in response to intense green light. The current study was begun with an examination of the differences in gene expression between rat retinae exposed for either 0 or 4 hours of intense green light. The 4 hour light treatment was chosen as the focus because this treatment seems to create a cellular environment that is still able to respond to the light insult. The retina as a whole is not fully committed to apoptosis, and so must still be responding to the stress induced by the light damage.

A major class of retinal-expressed genes that change expression after light exposure will be known stress-response genes. It is likely that other genes will also change expression without having been previously characterized as stress-response genes, and this study will examine previously unidentified aspects of known genes. One set of genes that received particular attention in this study was the crystallin genes. The identification of these putatively lens-specific mRNAs in a rat retina subject to oxidative stress, prompted an investigation of their expression in the rat retina because this is the first time that these genes have been associated with the retinal degeneration process. The results of this investigation have suggested a possible role for the crystallin proteins in the retina.

Hereditary human retinal degenerations, *e.g.* RP and MD, have been linked to specific gene mutations, meaning that the gene product is important in the etiology of retinal degeneration. While the triggering of retinal degeneration is different between hereditary human retinal degeneration and rat LIRD, rat orthologues of some of the human genes should be identified in rat LIRD, since these genes are demonstrably implicated in one form of a mammalian retinal degeneration when mutant. Analysis of the rat mRNAs identified in this study may indirectly implicate other human genes as candidates in hereditary retinal degeneration.

Chapter 2 Materials and Methods

Chapter 2 Materials and Methods

2-A Experimental Animals

Male albino Sprague-Dawley rats (*Rattus norvegicus*) were obtained from Harlan Laboratories (Indianapolis, Indiana) when weaned, *i.e.* 14-20 days after birth. The animals were cared for under the guidelines and regulations of the Association for the Assessment and Accreditation of Laboratory Animal Care International (AAALAC), the Animal and Plant Health Inspection Service (APHIS) of the U.S. Department of Agriculture (USDA), and the National Institute of Health's (NIH) Institute for Laboratory Animal Resources (ILAR) Guide for the Care and Use of Laboratory Animals.

2-B Experimental Treatments

The rats were raised in the dark until 60 days of age with a uniform regimen of feeding (Laboratory Animal Facility, Wright State University, Dayton, Ohio). At 0900 on the sixty-first day after birth the rats were subjected to three different light treatments in a specially designed light chamber (**Figure 2-1.**). The tubular chambers are encircled by seven circular fluorescent 32 W Cool White tubes with an outside diameter (o.d.) of 25 cm (GE FC 12T/CW, General Electric Company, Cleveland, Ohio) such that a light meter at the centre of the 15 cm o.d. plexiglass tube measures 1500 lux. Green Plexiglass 2092 (Dayton Plastics, Dayton, Ohio), used to fashion the chamber, filters out all but light of wavelengths 490-580 nm.

Treatment 1: 5 rats were immediately sacrificed in the dark using carbon dioxide (CO_2).

Treatment 2: 5 rats were treated with 4 hours of intense (1500 lux) green (490-580 nm) light, and sacrificed using CO_2.

Treatment 3: 5 rats were treated with 8 hours of intense (1500 lux) green (490-580 nm) light, and sacrificed using CO_2.

In the course of this study three batches of rats were treated this way, and the eye tissue from these batches was used to obtain rat retina RNA (Sections **2-C** and **2-D**), rat retina protein (Section **2-C** and **2-L**), and whole eyes for immunohistochemistry (Section **2-N**).

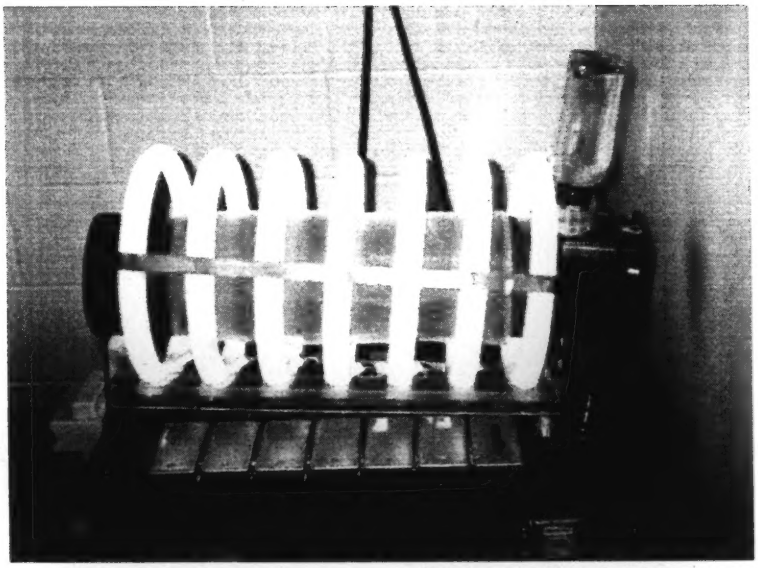

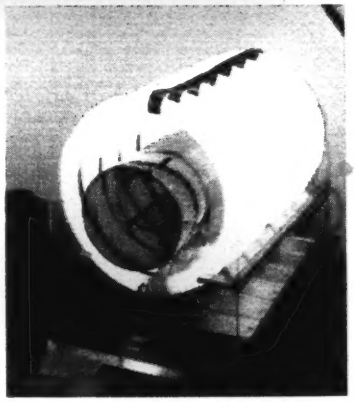

Figure 2-1. Light Chambers. Light intensity and wavelength are controlled by exposing the rats in specially designed plexiglass chambers. The tubular chambers are encircled by seven circular fluorescent 32 W bulbs with an 25 cm (o.d.) such that a light meter at the centre of the 15 cm (o.d.) plexiglass tube measures 1500 lux. Green Plexiglass 2092 filters out all but light of wavelengths 490-580 nm.

2-C Retina Dissection

Immediately after the rats were sacrificed, the retinae were excised in either complete darkness or under low intensity red light for RNA and protein extraction (Sections **2-D** and **2-L**). The small size of the rat eye makes retinal excision a very difficult process, but practice allows for removal of the lens and vitreous humour, and isolation of the retina in less than a minute (**Figure 2-2.**). This was achieved by cupping and raising the eye in a pair of forceps that grasp the optic nerve. The eye is extruded, and a thin razor blade, in a smooth, fast stroke on the anterior face of the eye, was used to cut through the length of the cornea and the anterior chamber into the lens. This cut results in the lens adhering to the razor blade without shattering, and creates a large opening for the vitreous humour and retina to be removed from the eye. The forceps holding the eyecup was then gently pulled up the optic nerve, which presses the eye flat, and ejects, in order: the vitreous humour, and the retina. The vitreous humour is usually so viscous that it remains a single mass discrete from the retina which is a tannish-pink colour. The excised retina was then placed in a tube on ice until all ten retinae were isolated, and the tube was then flash frozen on dry-ice ($CO_{2(S)}$) and ethanol and stored at –70°C to –80°C.

2-D Rat Retina RNA Isolation

RNA isolation was performed using TRIzol (Gibco BRL, Gaithersburg, MD) and a PT3100 Polytron homogenizer (Kinematica, Kriens-Lucerne, Switzerland), with the manufacturer's protocol. TRIzol is a monophasic mixture of phenol and a chaotropic agent, guanidine isothiocyanate. The probe of the Polytron was cleaned and soaked in 0.1% (v/v) aqueous diethylpyrocarbonate (DEPC; ethoxyformic acid anhydride; Sigma-Aldrich, St. Louis, Missouri) for 12 hours prior to use to ensure no RNases contaminate the solutions. As well, all chemicals, lab equipment, and plastics used were RNase-free. DEPC-treated water (DEPC•H_2O) was prepared by treating deionized, distilled water (Milli-Q; Millipore, Etobicoke, Ontario) with 0.1% (v/v) DEPC for 12 hours with stirring and subsequent autoclaving at 121°C for 20 minutes to break down any residual DEPC.

To prepare for the homogenization and subsequent probe cleaning, 50 mL tubes

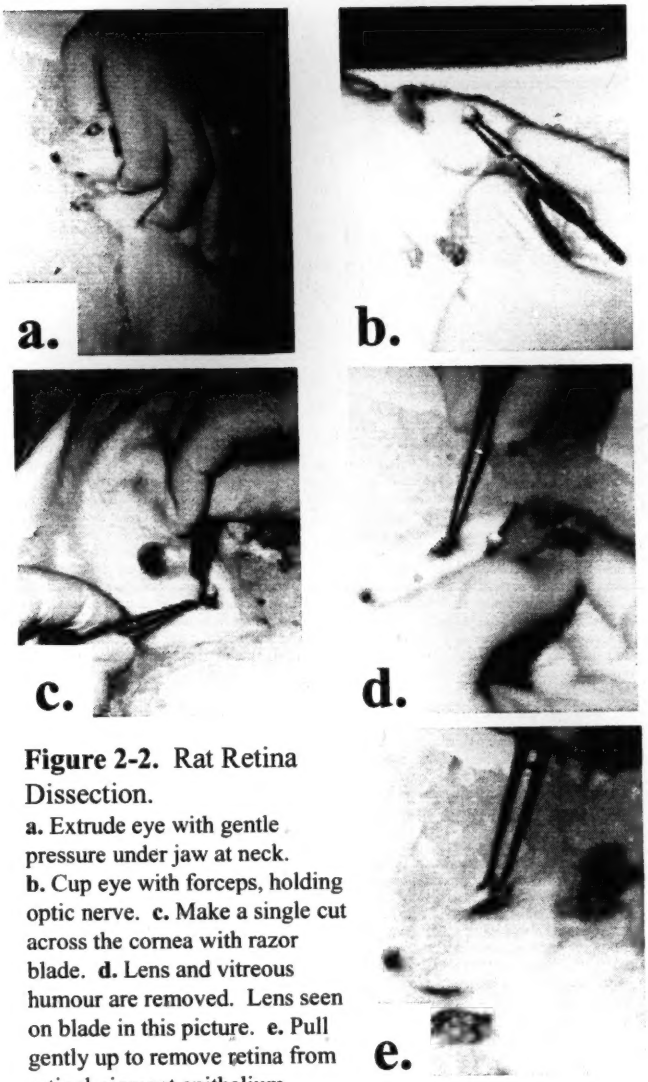

Figure 2-2. Rat Retina Dissection.
a. Extrude eye with gentle pressure under jaw at neck. **b.** Cup eye with forceps, holding optic nerve. **c.** Make a single cut across the cornea with razor blade. **d.** Lens and vitreous humour are removed. Lens seen on blade in this picture. **e.** Pull gently up to remove retina from retinal pigment epithelium.

were prepared ahead of time containing the appropriate volumes of solutions required. For each set of retinae to be homogenized there should be: one 50 mL tube for the homogenization, one 50 mL tube containing 35 mL of absolute ethanol (EtOH; Mallinckrodt Baker Inc., Paris, Kentucky), and three 50 mL tubes containing 35 mL DEPC•H_2O. On the day of RNA extraction, the homogenizer's probe was rinsed thoroughly with EtOH, DEPC•H_2O, and TRIzol before use to remove any DEPC from the 12 hour soaking. For each set of retinae, the retinae were removed from the tube with a sterile scalpel and transferred to the 50 mL homogenization tube. The appropriate amount of TRIzol was added to the tube, usually 2.0 mL for 10 rat retinae, and the mixture was homogenized at high speed using the Polytron homogenizer. Homogenization continued until the magenta TRIzol became cloudy with small particles, *i.e.* no large pieces of tissue remain, this was usually accomplished with 2-3 minutes of homogenization at high speed. This tissue homogenate was then immediately placed on ice to inhibit the activity of native RNases. The probe was then washed thoroughly with the prepared wash solutions, EtOH then DEPC•H_2O, by running the probe in the wash solution to remove any material from the homogenization. It is imperative that each set of retinae be homogenized with a clean, RNase-free probe. After the homogenizations were done, the probe was cleaned and dried thoroughly to avoid having it rust.

To each tissue homogenate on ice, 0.2 mL of chloroform ($CHCl_3$; BDH Inc., Toronto, Ontario) was added. The $CHCl_3$-TRIzol homogenates were then shaken vigorously for 15 seconds to ensure complete miscibility of the $CHCl_3$ and TRIzol, and incubated for 15 minutes on ice. Equal aliquots of each homogenate were transferred to two separate 1.5 mL polypropylene tubes. ($CHCl_3$ degrades polystyrene and other plastics, but not polypropylene.) The tubes were then centrifuged at 12000 g at 4°C for 30 minutes to separate the aqueous phase of the TRIzol mixture, containing the RNA and guanidinum isothiocyanate, from the organic $CHCl_3$ and phenol phase, containing proteins and lipids. DNA is found at the interphase, but not in the aqueous phase. The aqueous phase was removed from both tubes of each set of retinae and transferred to separate, single 1.5 mL conical bottom polypropylene tubes. The conical bottom is necessary to ensure that a pellet is formed on precipitation that will not easily be moved. The organic phase, interphase and remaining aqueous phase of each set of retinae were

retained and stored at -20°C for later isolation of protein. To precipitate the RNA, an equal volume of cold isopropanol (iPrOH; BDH Inc., Toronto, Ontario) was added to each aqueous solution on ice, and the solution was stored at –20°C overnight (12 hours). A stock of 75% EtOH (v/v) was prepared from EtOH and DEPC•H_2O and stored at -20°C.

To pellet the precipitated RNA, the solution was centrifuged at 12000 g at 4°C for 30 minutes after the -20°C incubation. The supernatant was removed by decanting, and the pellet was washed in 1 mL of 75% EtOH on ice to remove any traces of phenol that might have been left from the TRIzol. The tube was centrifuged at 12000 g at 4°C for 15 minutes to ensure that the pellet adhered to the side of the tube. The 75% EtOH was removed, and the pellet was air-dried on a sterile surface with the lid open for 10 minutes. It is imperative that the RNA pellet is not allowed to over-dry. One benchmark to use is the absence of droplets on the inside of the tube, and no obvious pool of liquid surrounding the pellet. On ice, enough DEPC•H_2O was added to each pellet to result in a final RNA concentration of 1μg/μL; 50 μL was the average amount required. Prior to freezing, 2 μL of the final RNA solution obtained from each set of retinae was removed for determination of the concentration by spectroscopy. The pellet was mixed on ice until it was in solution, and the RNA stocks were then flash-frozen on $CO_{2(s)}$-EtOH and stored at -80°C.

The 2 μL of RNA removed from each sample for spectroscopy was diluted appropriately with DEPC•H_2O, and quartz cuvettes were used to take absorbance readings in a spectrophotometer (Pye Unicam Ltd., Cambridge, England) at both 260 and 280 nm (A_{260}, A_{280})—plastic does not transmit light at these wavelengths. An A_{260} of 1.00 is ≅40 μg/mL. The A_{280} reading is used to test the purity of the RNA. Pure aqueous RNA has an A_{260}:A_{280} ratio of very close to 2.00. More definitive qualitative determination of RNA integrity concentration can be obtained by running the sample on an RNA gel (Sections **2-E1-2-E4**).

2-E Northern Transfer (Modified from Sambrook *et al.*, 1989)

2-E1 RNA Gel System: 100 mL of 1% agarose RNA gel is prepared by dissolving 1.0 g of agarose (FMC Bioproducts, Rockland, Maine) in 72 mL of boiling

DEPC•H_2O, allowing it to cool below boiling, and then adding 18 mL of formaldehyde (18% v/v; Anachemia Canada Inc., Montréal Québec), and 10 mL of 10x MOPS buffer (0.5 M 4-morpholine propanesulfonicacid, 10 mM ethylene diamine tetraceteic acid, pH 7.0; Oncor, Gaithersburg, Maryland). An appropriate volume of gel was prepared and poured in the fumehood, *e.g.* a casting tray with dimensions 11.5 cm by 14.5 cm requires 150 mL of 1% RNA gel for a gel that is 0.9 cm thick. A comb with 0.75 cm by 0.2 cm teeth is used to create large wells in the gel since a total of 45 µL of sample will be loaded in each lane.

2-E2 RNA Sample Treatment: While the gel sets, the loading mixture can be prepared. The loading mixture, per sample, contains 4 µL of 10x MOPS buffer, 7 µL of formaldehyde, 20 µL of deionized formamide (VWR International, Edmonton, Alberta), and 1 µL of 1 mg/mL ethidium bromide (EtBr; 3,8-diamino-5-bromo-6-phenyl-phenanthridinium; Sigma-Aldrich, St. Louis, Missouri). MOPS provides the buffering capacity of the system, while the formaldehyde and formamide prevent the formation of RNA secondary structure. Ethidium bromide fluoresces at ultraviolet wavelengths (270-370 nm) and interacts with nucleic acid, allowing detection of RNA by fluorescence. For each RNA sample, RNA and DEPC•H_2O were added to 32 µL of this loading mixture to bring the final volume to 40 µL. To allow the potential detection of rare mRNAs, 5-30 µg of total RNA were loaded per lane. A size and concentration standard should also be run, and a good one for total RNA is one that covers 0.24–9.5 kb, where each of the six bands is of equal concentration (Invitrogen, Burlington, Ontario). The same loading mixture was used to prepare 10 µg of marker RNA. The RNA and loading mixture was incubated at 50°C for 15 minutes to remove any secondary structure, and the samples were then immediately placed on ice, and 5 µL of RNase-free 6x loading dye[5] (eppendorf 5'→3', Boulder, Colorado) was added to each sample. The samples were them immediately loaded into the wells of the buffer-covered gel.

2-E3 RNA Sample Electrophoresis: 1 L of MOPS running buffer consists of 817 mL of DEPC•H_2O, 83 mL (8.3% v/v) formaldehyde, and 100 mL of 10x MOPS buffer. The prepared gel is placed in the electrophoresis apparatus and covered in MOPS running

buffer. The denatured RNA samples were loaded into the wells and electrophoresis was allowed to continue until the bottom band (bromophenol blue) was approximately 2.5 cm from the end of the gel closest to the anode, which takes approximately 480 V•hours.

2-E4 RNA Sample Visualization: After electrophoresis, the gel was rinsed in distilled water for 20 minutes to remove excess formaldehyde, formamide, and EtBr that is not complexed with the RNA. Ultraviolet light of 302 nm was used to cause the fluorescence of the EtBr complexed with the RNA in the gel. This fluorescence was photographed with a Kodak DC120 Digital Camera (Eastman Kodak Company, New Haven, Connecticut), both with and without a fluorescent ruler (Bio-Rad Laboratories Inc., Mississauga, Ontario) so that the photographs contained an internal reference to the size of the gel and the movement of the marker RNA from the wells. (For gels which fluoresce very brightly, it is useful to also have pictures of the fluorescence at 365 nm, with and without a ruler.) These pictures were used to densitometrically (Section **2-K5**) determine the evenness of RNA loading by reference to the ribosomal RNA (rRNA; Correa-Rotter *et al.*, 1992).

2-E5 Northern Transfer: The visualized gel was set up for Northern transfer of the RNA to nylon membrane as shown in **Figure 2-3.** and described here. A piece of nylon membrane (DuPont NEN Research Products, Boston, Massachusetts) that is the exact size of the gel was cut, and soaked in 0.3 M sodium chloride, 0.03 M sodium citrate buffer[6] (2x SSC) for 15 minutes. Also prepared were: four pieces of Whatman filter paper (Whatman, Ann Arbor, Michigan) the exact size of the gel, a piece of Whatman paper that was the exact width of the gel but three times as long as the gel, and a stack of paper towels whose size is as close to the size of the gel as possible and is approximately 16 cm high. The Northern transfer was set up in a shallow tray in which a support rested that was as close to the size of the gel as possible. The long piece of Whatman paper was laid over the support so that equal amounts of the long tails hung on either side of the support. Enough 10x SSC to soak the Whatman paper was poured on it, and a sterile serological

---

[5] 6x loading dye: 0.25% Bromophenol Blue (w/v) and 0.25% (w/v) xylene cyanol [2-(2,2-bis(4-(dimethylamino) phenyl)ethyl)benzenesulfonic acid] in aqueous 30% glycerol (v/v)

[6] 20x SSC: 3 M NaCl (BDH Inc., Toronto, Ontario), and 0.3 M sodium citrate (BDH Inc., Toronto, Ontario), pH 7.0

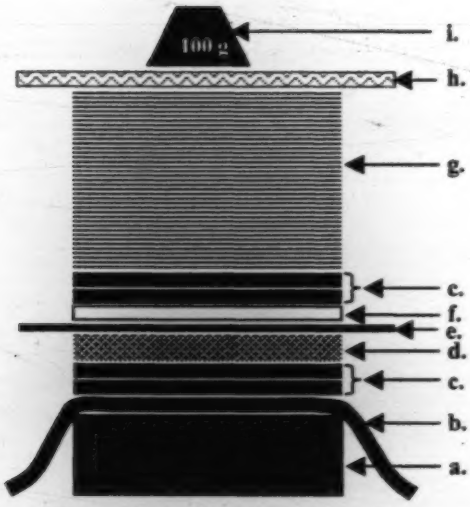

Figure 2-3. Northern Transfer. (After Sambrook *et al.*, 1989)
a. support, **b.** Whatman paper bridge, **c.** Whatman paper for stability, **d.** RNA gel (upside down), **e.** Parafilm (barely overlapping the edges of the gel), **f.** nylon membrane, **g.** paper towel for absorption, **h.** glass plate, **i.** weight (<100 g)

pipette was used to roll the excess SSC off the support. This piece of filter paper is the bridge which delivers the transfer buffer (10x SSC) to the gel from the tray, which is acting as a reservoir of transfer buffer. Then, one by one, the two remaining pieces of Whatman paper were placed on the long piece so that the widths matched exactly, and the pouring and rolling was repeated to remove any bubbles between the layers. The RNA gel was turned so that the bottom face of the gel was uppermost, and the gel was arranged on the Whatman paper, and any bubbles were rolled out. Turning the gel upside down ensures that the membrane is touching the most even side of the gel, and later makes interpreting Northern hybridization results intuitive, since the RNA face of the membrane has the same orientation as the top side of the gel.

Four long pieces of Parafilm (Pechiney Plastic Packaging Inc., Neenah, Wisconsin) were lain over each edge of the gel so that they completely, but just barely, overlap each edge of the gel. The Parafilm is used to ensure that the movement of transfer buffer can only be through the membrane so that RNA is transferred to the membrane. Then the nylon membrane was overlain on the gel and Parafilm to exactly fit the gel. The membrane must not contact the gel unless it is in its final position, as RNA transfer to the membrane is likely. One way to manage this is to hold the edges of the membrane, line up the centre of the membrane with the centre of the gel, and the sides as best as possible, touch the centre to the gel, and then let go of the edges. Very carefully, 10x SSC was poured on the membrane and all air bubbles were rolled out of the gel-membrane interface. The two remaining pieces of Whatman paper were added, with pouring and rolling, and the stack of paper towel was placed on top of the whole setup. The stack of paper towel was covered with a glass plate to keep the stack even, and a small weight (<100 g) was added to the top of the plate. The reservoir was filled to below the top level of the support with 10x SSC so that the only way that transfer buffer could move was to be drawn up the bridge by the absorption of the paper towels.

Northern transfers were allowed to continue for a minimum of 12 hours, as long as there was still buffer in the reservoir and the paper towels were not soaked through. After 12 hours, and before the transfer buffer soaked the entire stack of paper towels or evaporated, the Northern transfer was dismantled to the level of the nylon membrane. Before removing the membrane, the location of the wells was indicated in pencil on the

uppermost face of the membrane. This works to establish that the RNA is on the umarked side, which has the same orientation as the gel, and gives an indication of the distance that detected bands moved from the wells. The date and name of the Northern blot was also be written on the membrane. The membrane was then removed, and care was taken not to allow the membrane to touch any potential source of nucleic acid, including lab benches, the RNA gel, and skin. Before the membrane dried completely, it was treated in a Stratalinker ultraviolet light cross linker (Stratagene, La Jolla, California) which forms bond between the membrane and the RNA. The membrane was then stored flat between two pieces of Whatman paper in a sealed plastic bag until used.

The gel should be collapsed, but intact, after the transfer. To determine if the transfer of RNA to the membrane is complete, the gel was visualized over ultraviolet light (302 nm). If the transfer was complete, no EtBr fluorescence would be seen since the EtBr-RNA complexes would have transferred to the membrane. If transfer was incomplete, then EtBr fluorescence would be detected in the gel after transfer. In all Northern transfers performed, transfer was complete after 12 hours. A photograph of the gel after transfer was taken to indicate the completeness of transfer.

2-F mRNA Isolation

Most messenger RNAs (mRNAs) in eukaryotes have a string of AMP added to the end of the mRNA that is postulated to control the lifetime of the mRNA within the cell (Ross, 1995). This provides a tool to separate mRNA, from structural RNA, *i.e.* rRNA and transfer RNA. Since RNA is capable of base pairing, a poly(T) tract is able to basepair with the poly(A) tail of mRNAs. Oligotex (QIAgen, Mississauga, Ontario) polystyrene beads with poly(T) chains have been developed that allow the isolation of mRNAs in a salt concentration-dependent process. As per the manufacturer's protocol, heat-denatured total RNA was mixed with a high salt buffer and the Oligotex beads. Basepairing between the poly(T) tract on the beads and the mRNA, driven by the high salt concentrations, occurs during incubation at room temperature for 10 minutes. RNA molecules without a poly(A) tail remained in solution. The Oligotex beads were pelleted in the tube by centrifugation and the supernatant was removed. The pellets were washed with a supplied buffer and transferred to the manufacturer's supplied spin columns which contain a frit that prevents precipitated material from flowing through the

column but allows the wash solution to flow through during centrifugation. The column was transferred to a fresh tube, and the precipitate in the column was resuspended in a low volume of hot, low salt concentration elution buffer which disrupts the basepairing of the poly(A)-poly(T) tracts. Centrifugation of the column in this collection tube allows the mRNA in solution in the column to flow through the frit, and maximum yield was gained by another low volume elution of the Oligotex pellets, followed by centrifugation to collect the flowthrough. For this study, mRNA was isolated from the total RNA isolated from the rat retinae treated with no light, and from the total RNA isolated from the rat retinae treated with 4 hours of intense green light. Both samples were eluted in a total of 50 μL of low salt concentration buffer.

2-G cDNA Synthesis

Complementary DNA (cDNA) synthesis is a necessary step for two reasons: RNA is exceptionally labile and DNA is far more stable, and cDNA can be used to generate probes representing the mRNAs expressed in a given condition or tissue and used to generate a cDNA library. Both the latter aspects of cDNA use were an important consideration in this study. The generation of probes representing the untreated rat retinae mRNA population and the 4 hour light-treated rat retinae mRNA population is a necessary step in a screen for differentially expressed mRNAs. These probes were used to differentially screen a cDNA library generated from the 4 hour light-treated rat retinae.

cDNA synthesis for use as probes was done using the methods and material provided by the manufacturer of both the 5' and 3' RACE System for Rapid Amplification of cDNA Ends (GIBCO BRL, Gaithersburg, Maryland). In brief, the manufacturer's cDNA synthesis involved synthesizing a DNA strand complementary to the mRNA using Superscript II Reverse Transcriptase, an engineered Moloney Murine Leukemia Virus (MMLV) RNA-dependent DNA polymerase without RNase H activity. The reaction requires a primer to allow initiation of polymerization, and this is readily provided by a mixture of poly(T) anchor primers complementary to the 3' poly(A) tail of mRNA and the 3 nucleotides immediately preceding the poly(A) tail. The 3' triplet of the mRNA could be matched by 64 individual anchor primer triplets, but the use of the bases uracil and inosine allows the manufacturers to limit the anchor primers to 16 different primers. RNase H was added to the reaction after incubation with the reverse

transcriptase to digest the mRNA from the RNA-DNA hybrid. The first strand cDNA was isolated using the manufacturer's glass milk columns, and eluted in DEPC•H_2O. Terminal deoxynucleotide transferase was used to add a poly(C) tail to the 3' end of the first strand cDNA, which provided a primer site for the manufacturer's Universal Amplification Primer, a poly(G)-inosine oligonucleotide. Complementary priming was provided by an abbreviated poly(T) version of the primers used to prime the first strand synthesis. The polymerase chain reaction (PCR), using *Taq* polymerase, then allowed the generation of double-stranded cDNAs.

The concentration of cDNA generated in each reaction was determined by dotting a series of known amounts of double-stranded DNA, *e.g.* Lambda DNA *Hin*d III Fragments (500 ng/μL; Gibco BRL, Burlington, Ontario), on 1% agarose (w/v) plates containing 1 ng/mL EtBr. From each reaction, 1 μL of the cDNA generated was spotted on the plate, and the ultraviolet (365 nm) fluorescence of each cDNA dot was compared with the fluorescence of the dots in the series of known DNA amounts.

2-H cDNA Library Synthesis

The synthesis of cDNA for preparation of a library is similar to the methodology discussed above with the important exception that the cDNA is engineered to allow ligation into the selected cloning vector. This study chose the λ Uni-ZAP (Stratagene, La Jolla, California) λ phage-derived vector for incorporation of 500-5000 bp cDNAs. A useful element of this cloning system is the uni-directional cloning provided by specifically designed linker-primers and adapters. After library construction was complete, the Uni-ZAP vector contained cDNAs representing the mRNAs expressed in rat retinae after 4 hours of treatment with intense green light, and is referred to as the 4 Hour Library.

The 4 Hour Library was constructed in the lab (Chambers *et al.*, 1998) according to the manufacturer's protocol (**Figure 2-4.**). In short, cDNA was synthesized from the mRNA isolated from rat retinae treated with 4 hours of light using a poly(T) linker-primer which contains a *Xho*I site. *Eco*RI adapters were added to the ends, but a *Xho*I digestion removed the *Eco*RI sites from the sense 3' end. The cDNA was size-

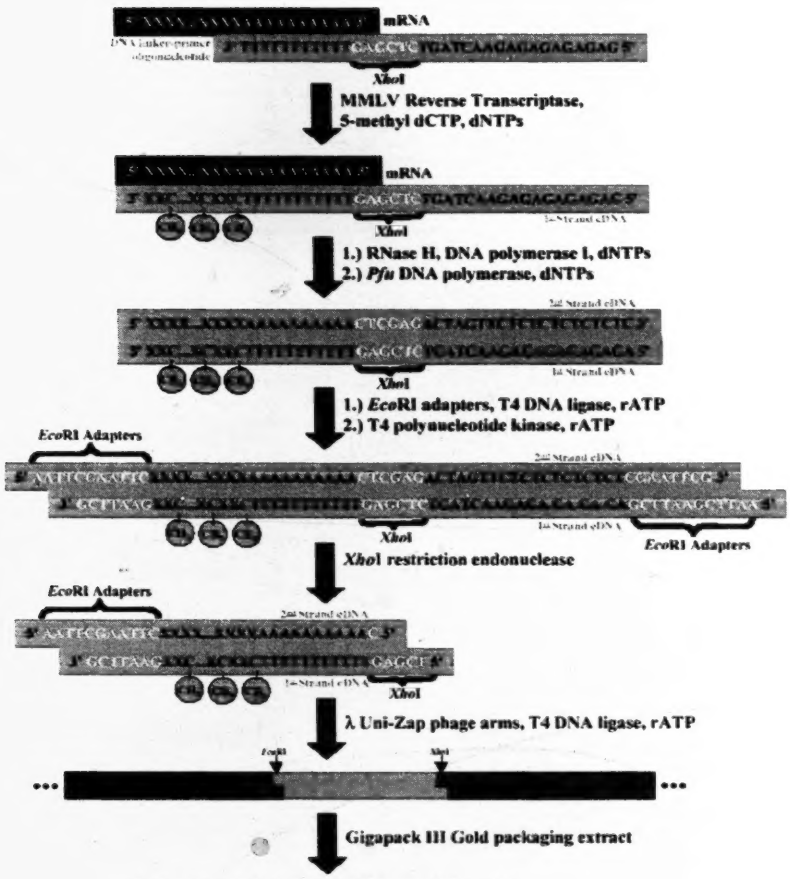

Figure 2-4. Outline of cDNA Library Synthesis. (Stratagene, La Jolla, California)

The mRNA isolated from the rat retinae treated with 4 hours of intense green light was used to make a cDNA library in the λ Uni-ZAP vector. The library was named the 4 Hour Library, and had a titre of 380 pfu/μL with an average insert size of 890 bp (n=14).

fractionated in a size exclusion column to remove unused adapters and nucleotides, and the larger cDNA fractions were collected. The Uni-ZAP phage arms were ligated to the collected cDNA fractions and packaged for infection of *Escherichia coli* XL1 Blue MRF'. During first strand synthesis, the cDNA was made with 5-methyl dCTP to create hemi-methylated double-stranded cDNA which allows the Uni-ZAP with insert to avoid restriction by this host. See **Figure 2-5.** for the sequence of the multiple cloning site of the Uni-ZAP vector.

When the 4 Hour Library was analyzed for this study, it had a titre of 380 plaque forming units (pfu)/μL, and 500 μL of library was obtained. (See Section **2-I1** for instructions on plating a phage library.) T3 and T7 primers (**Figure 2-5.**) in a PCR, followed by agarose gel electrophoresis and EtBr visualization (Section **2-I8**), was used to determine that the average insert size of the library was 890 bp (n=14).

2-I Differential Cross Screening of 4 Hour Library

Rat retinae treated with 4 hours of light are thought to express a different set of genes than rat retinae which have not been exposed to light. A differential cross screen is capable of determining what genes are expressed in one condition versus another. The cDNAs from two different conditions can be radioactively labelled to allow for detection, and used to separately probe two identical nylon membrane representations of a cDNA library. Clones which hybridize to give different intensities with the two probes represent genes that are differently expressed in one condition or the other (After Sambrook *et al.*, 1989).

2-I1 Plaque Lifts: 100 mL of Luria-Bertani (LB) Broth[7], supplemented to a final $MgSO_4$ concentration of 10 mM (BDH Inc., Toronto, Ontario) and a final concentration of 0.2% (w/v) maltose (Sigma-Aldrich, St. Louis, Missouri), was inoculated with a single colony of *E. coli* XL1 Blue MRF' and grown at 37ºC for 12 hours. The bacteria were gently pelleted by centrifugation at 500 g for 10 minutes at room temperature, the supernatant was removed, and the bacteria were resuspended in sufficient (≅50 mL)

[7] LB Broth: 1 L deionized and distilled H_2O (ddH_2O), 10.0 g NaCl, 10.0 g tryptone (Becton Dickinson and Company, Sparks, Maryland), 5.0 g yeast extract (Becton Dickinson and Company, Sparks, Maryland), pH 7.0, autoclaved at 121ºC

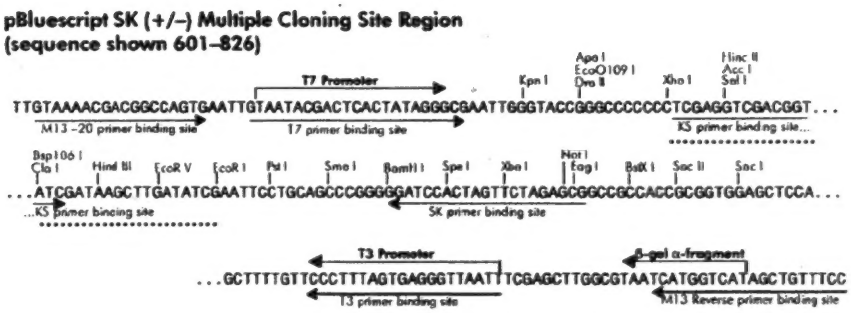

Figure 2-5. Insertion Site of Multiple Cloning Site (MCS) of λ Uni-ZAP. (Stratagene, La Jolla, California)

Based on pBluescript SK (+/-). The underlined (·····) sequence is not present in the MCS after cloning. The T7 and M13 Forward primer sites occur at the sense 3' end, and the SK, T3, and M13 Reverse primer sites occur at the sense 5' end.

10 mM $MgSO_4$ until the bacterial suspension had an optical density at 600 nm of 0.5 (OD_{600}=0.5) as determined by spectroscopy. Ten 200 μL aliquots of this bacterial suspension were prepared in 1.5 mL tubes, and these aliquots were each infected with 2.5 μL (950 pfu) of the 4 Hour Library (380 pfu/μL), mixed, and incubated at 37°C for 15 minutes. The maltose in the initial culture medium causes the bacterial expression of *lam*B, encoding the maltose receptor which is the attachment site of λ phage, and the 15 minute incubation allows for attachment of the phage to the receptor.

After the incubation, the bacteria with attached phage were used to inoculate ten separate 10 mL aliquots of LB Top Agar[8] kept at 42-45°C. These ten inoculated aliquots of top agar were poured evenly on ten 150 mm diameter LB Agar[9] plates labelled A-J. The top agar was allowed to set, the plates were inverted, and incubated at 37°C. The plates are monitored for signs of plaque formation, and when the plaques were visible, but still small, the plates were removed from their 37°C incubation (≅10 hours). Small plaques are desirable because the entire process of the screen can take several days, and large plaques might grow and merge, mixing the phage from each plaque and invalidating the screen. The plates were stored at 4°C to chill the plates so that the top agar remained intact during the process of lifting the plaques. On average (n=3), each plate had 1066 plaques.

Ten 137 mm diameter circular nylon membranes (DuPont NEN Research Products, Boston, Massachusetts) were labelled and notched differently, *i.e.* ten membranes labelled A-J with a single notch and 10 membranes labelled A-J with two notches. Each membrane was laid on its corresponding plate of phage, *e.g.* A membranes on plate A; first, the membrane with one notch is placed on the plate for 1 minute, and then the membrane with two notches is placed on the plate for 2 minutes. When the first membrane was laid on the plate, it was pierced in three close random spots with a sterile needle, and the plate is turned over. The location of the notch in the membrane and the site of the needle stabs was marked on the bottom of the plate with green ink, and the process was repeated for the second membrane in black ink. Later, the markings on the plate were used to orient the location of specific plaques detected by radioactive

[8] LB Top Agar: 1% (w/v) agar (Difco Laboratories, Detroit, Michigan) in LB Broth
[9] LB Agar: 1.5% (w/v) agar in LB Broth

hybridization of the membranes. Some of the phage in the plaques will adhere to the membranes. The phage DNA is released from its capsid and denatured by soaking the membrane in 0.5 M NaOH (BDH Inc., Toronto, Ontario) for 2 minutes, which also kills any bacteria adhering to the membrane. The membrane is then rinsed in 1.5 M Tris•HCl[10] pH 7.5 (ICN Biomedicals Inc., Aurora, Ohio) for 4 minutes, which neutralizes the basic solution and removes contaminating material like bacterial cell walls and traces of agar. The denatured DNA is then crosslinked to the membrane in a Stratalinker and stored flat, covered by a clean piece of Whatman paper. The process is repeated for each plate of phage.

2-I2 Radioactive Labelling of cDNA: cDNA was prepared from the mRNA isolated from the total RNA isolated from the retinae of dark-reared rats treated with no light (Dark cDNA) or 4 hours of light (4 Hour cDNA) in separate reactions (Section **2-G**). These two pools of cDNA were separately radioactively triple-labelled using a Random Primers DNA Labelling System (Gibco BRL, Burlington, Ontario) and the radioactive nucleotides: [α-^{32}P]dCTP, [α-^{32}P]dATP, [α-^{32}P]dGTP all with activities of 3000 Ci/mmol (Amersham Canada Ltd., Oakville, Ontario). From each cDNA pool, 100 ng was heat denatured and immediately cooled on ice. To the denatured cDNA, 30 µL of random hexamers in buffer were added, along with 10 µL of the single non-radioactive nucleotide, dTTP (0.5 mM), and 10 µL of each of the three radioactive nucleotides (0.5 mM). On ice, 2 µL of the Klenow Fragment of *E. coli* DNA polymerase I (3U/µL) was added and mixed thoroughly. The reaction was incubated for 10 hours at room temperature.

After the incubation, 1 µL was removed from each reaction for later use in determining the total radioactivity in the reaction. The remainder of the reaction was applied to the top of a mini Quick Spin DNA Column (Roche Diagnostics, Laval, Quebec) and centrifuged at 1100 g for 4 minutes at room temperature. The flow-through, containing the radio-labelled DNA was collected in a 1.5 mL collection tube, unincorporated nucleotides are retained in the Sephadex G-50 column. After the

[10] 2-Amino-2-(hydroxymethyl)-1,3-propanediol•HCl

centrifugation, 1 μL of the collected volume was removed for determination of the amount of radioactivity in the collected probe. The samples collected from the reaction before and after purification were sampled for ^{32}P radioactivity by counting Cerenkov radiation with a 1600 TR Liquid Scintillation Analyzer (Packard Instrument Company, Meriden, Connecticut). The percent incorporation of nucleotide was determined by dividing the radioactivity of 1 μL of sample after purification in counts per minute (cpm) by the amount of radioactivity of 1 μL of sample before purification in cpm. An acceptable probe was one that had 1.6 million cpm/μL and greater than 75% incorporation.

2-I3 Probe Hybridization: The nylon membrane plaque lifts were placed, five in each bottle, separated by fine nylon mesh (PGC Scientific, Frederick, Maryland), in 30 cm glass hybridization bottles (Wheaton, Millville, New Jersey). The plaque lifts were grouped: 1. First lift A-E, 2. First lift F-J, 3. Second lift A-E, and 4. Second lift F-J. The bottles were filled with approximately 190 mL of 65°C 2x SSC, and rotated at medium speed at 65°C in a rotary incubator (Hybaid Limited, Ashford, United Kingdom) for 20 minutes. After this initial wash of the blots, the 2x SSC was removed, and 50 mL of 65°C Hybrisol II (Intergen Company, Purchase, New York) was added to each bottle. The blots were prehybridized in Hybrisol II for 4 hours in the rotary incubator at medium speed at 65°C.

After 4 hours of prehybridization, 160 million total cpm of each radioactive cDNA probe was boiled separately for 5 minutes in a water bath with 200 μL of 10 μg/μL salmon sperm DNA (Digene Diagnostics Inc., Beltsville, Maryland) to denature the probe, and were immediately placed on ice. The denatured probes, with salmon sperm DNA as a competitor DNA, were then separately added to 80 mL of 65°C Hybrisol II. The prehybridization Hybrisol II was removed from each bottle. The radioactive 4 Hour cDNA probe in Hybrisol II was split into two equal aliquots which were added to bottles 1. and 2. The radioactive Dark cDNA probe in Hybrisol II was also split into two equal aliquots which were added to bottles 3. and 4. The plaque lifts were hybridized with radioactive cDNA probe in the rotary incubator at medium speed at 65°C for 12 hours.

2-I4 Hybridization Washes: After the 12 hour hybridization of the blots, the radioactive cDNA probe in Hybrisol II was removed from each hybridization bottle, and the blots were washed in 190 mL of 65°C 2x SSC for 15 minutes in the rotary incubator at medium speed at 65°C. This wash was repeated after removing the initial wash solution. After the second 2x SSC wash, the blots were washed in 150 mL of 65°C 2x SSC and 0.1% (w/v) sodium dodecyl sulfate (SDS) in the rotary incubator at medium speed at 65°C for 20 minutes. This wash was also repeated, as it has been noted that blots that omit a second 2x SSC/0.1% SDS wash have significantly more background than those that do undergo the second wash. The last wash, the critical one, consisted of 150 mL of 65°C 0.1x SSC/0.1% SDS in the rotary incubator at medium speed at 65°C for 10 minutes. After the 0.1x SSC/0.1% SDS wash, the blots were immediately removed from the hybridization bottles and immersed in 2x SSC. The blots were then placed on Whatman paper soaked in 2x SSC, and wrapped flat in plastic film.

2-I5 Autoradiography: The wrapped blots were then placed in large (35 cm x 43 cm) film cassettes (Eastman Kodak Company, New Haven, Connecticut) with Kodak TransScreen HE intensifying screens (Eastman Kodak Company, New Haven, Connecticut), and the radioactive blots were used to expose Kodak X-Omat AR film (Eastman Kodak Company, New Haven, Connecticut) for 16 hours. The film was developed in a Kodak X-Omat Processor (Eastman Kodak Company, New Haven, Connecticut). The autoradiographs were clearly marked to indicate the blot name, the number and location of notches, and the location of the puncture marks in the blot. Additional exposures of the blots were made if needed.

2-I6 Primary Screen: The signals present on the autoradiographs were then lined up with the plaques on the plates by orienting the plate and autoradiograph by virtue of the notches and puncture marks. Comparison of the intensity of hybridization of each probe to particular plaques was done by orienting one autoradiograph on the other by transferring the notch marks for one probe from the plate to the other probe's autoradiograph, *e.g.* Dark probe notches from the plate to the Normal probe autoradiograph (**Figure 3-2.**). These plaques were isolated using sterile small bore glass pipettes to core out a plug of LB Agar containing the plaque from the plate. The plug

containing the plaque was transferred to 500 µL of Storage Media (SM) buffer[11] in 1.5 mL polypropylene tubes, and labelled with a clone number. To each clone in SM buffer, 30 µL of $CHCl_3$ was added to kill any bacteria in the tube, and the tubes were shaken to dislodge the phage from the agar plug. The phage clones in SM buffer were stored at 4°C for 24 hours before further manipulation.

2-I7 Secondary Screen: The 1229 clones identified as putatively differentially expressed were further screened to ensure that the identification was accurate. Two 20 cm x 20 cm square LB Agar plates were each spread with 35 mL of LB Top Agar inoculated with 600 µL of bacteria prepared as in Section **2-I1**. The top agar was allowed to set, and the plates were inverted and incubated for 80 minutes at 37°C. After the incubation, 1 µL of each of the 1229 clones was dotted onto the top agar in order of clone number. The phage dots were allowed to be absorbed into the top agar, the plates were inverted and then incubated at 37°C for 12 hours. Enough space was allowed between each phage dot that the plaques would not grow together. Duplicate plaque lifts were again performed, using 20 cm x 20 cm nylon membrane, as in Section **2-I1**. Radioactive probes were generated from the 4 Hour and Dark cDNA and used to probe the square duplicate plaque lifts at 65°C (Sections **2-I2-2-I4**). Again, the hybridized and washed blots were used expose film (Section **2-I5**), and the developed film was oriented relative to the blot, screened with the other probe, to indicate which clones were differentially expressed.

2-I8 Tertiary Screen: As a tertiary screen, PCR, and Southern transfer of the PCR products, was further used to confirm the differential status of the group of clones identified as differentially expressed by the secondary screen. The end result was strong confirmation of the results of the secondary screen, as 173 of the 205 clones from the secondary screen were confirmed as differential in the tertiary screen.

2-I8A Polymerase Chain Reaction: The 205 clones identified were used as templates in PCR reactions using the T3 and T7 primers sites which flank the cDNA insert (**Figure 2-5.**). Each 100 µL reaction consisted of 0.5 mM T3 primer, 0.5 mM T7 primer, 2 µL of phage in SM buffer as template, 2 units of *Pyrococcus*

[11] SM buffer: 0.01 M $MgSO_4$, 0.1 M NaCl, 50 mM Tris•HCl (pH 7.5), 0.01% (w/v) gelatin (Sigma-Aldrich, St. Louis, Missouri)

furiosus (*Pfu*) DNA polymerase, and 1x *Pfu* PCR buffer[12]. The PCR consisted of: one phage denaturing step of 95°C for 5 minutes, 30 cycles of: a 1 minute DNA denaturing step at 95°C, a 1 minute primer annealing step at 50°C, and a 3 minute elongation step at 72°C, and a final elongation step of 7 minutes at 72°C.

2-I8B Gel Electrophoresis: The products of the 205 PCRs were subjected to 1% agarose (w/v) gel electrophoresis in 1x TAE buffer[13]. From each reaction, 9 μL of PCR product was mixed with 1 μL of 10x loading dye[14]. As a size and mass standard for the PCR products, 10 μL of Lambda DNA *Hind* III Fragments (50 ng/μL; Gibco BRL, Burlington, Ontario) mixed with 1 μL of 10x loading dye was used. The samples were then loaded in order into the wells of the gel and subjected to gel electrophoresis until the bottom dye band (Bromophenol blue) was either 2 cm from the next set of lanes or from the bottom of the gel. Duplicate gels were run for each set of samples.

2-I8C Ethidium bromide Visualization: These gels were visualized by staining in EtBr (1 μg/mL) for 15 minutes and then rinsing the gel in H_2O for 30 minutes. The EtBr-stained gels were then photographed over ultraviolet (365 nm) light using the Kodak DC120 digital camera.

2-I8D Southern Transfer: The DNA in the 1% agarose (w/v) TAE gels was Southern transferred to nylon membrane in a process very similar to that in Section **2-E5**. The exceptions are that the acidic gel must be neutralized and the double-stranded DNA denatured. This is achieved by bathing the gel in the alkaline transfer buffer (0.5 M NaOH, 1.5 M NaCl) for 20 minutes, and replacing the 10x SSC buffer used in the Northern transfer with this alkaline transfer buffer. In all other respects the Southern transfer is identical.

---

[12] 10x *Pfu* PCR buffer: 0.1 M KCl (BDH Inc., Toronto, Ontario), 0.1 M NH_4SO_4 (BDH Inc., Toronto, Ontario), 0.2 M Tris•HCl (pH 8.75), 0.02 M $MgSO_4$, 1% (v/v) Triton X-100 [poly(oxy-1,2-ethanediyl), alpha-(octylphenyl)-omega-hydroxy-; Sigma-Aldrich, St. Louis, Missouri]

[13] 50x Tris Acetate Ethylene diamine tetraacetic acid (EDTA) buffer: 1 L ddH_2O, 50 mM EDTA (BDH Inc., Toronto, Ontario), 2.0 M Tris, 1 M glacial acetic acid (≅57.1 mL; BDH Inc., Toronto, Ontario), pH 7.0

[14] 10x Loading Dye: 0.25% (w/v) Bromophenol Blue (Sigma-Aldrich, St. Louis, Missouri) and 0.25% (w/v) xylene cyanol (Sigma-Aldrich, St. Louis, Missouri) in aqueous 30% (v/v) glycerol (BDH Inc., Toronto, Ontario)

2-I8E Radioactive Hybridization: Radioactive probes were prepared from the 4 Hour and Dark cDNAs, and these probes were used to hybridize to the Southern blots of the PCR products of the 205 clones (Sections **2-I2-2-I5,** and **2-I8D**). The intensity of signal on the autoradiographs generated was used to further verify the differential status of the 205 clones (**Figure 3-2.**).

2-J cDNA Insert Sequencing (Modified from Sambrook *et al.*, 1989)

Clones identified as putatively differential were sequenced. The cDNA inserts used for sequencing must be pure and concentrated because sequencing reactions are done in very small volumes, which is also compounded by the sensitivity of the DNA polymerases to contaminants in the solution.

2-J1 Plaque Purification: Some of the clones identified as differentially expressed appeared to have multiple PCR products when visualized (Section **2-I8B** and **2-I8C**; **Figure 3-2.**). The most likely explanation for this was that the isolated plaque had inadvertently become contaminated with phage from another plaque. This was easily remedied by inoculating 50 µL of *E. coli* XL1 Blue with 5 µL of the contaminated phage, inoculating 5 mL of LB Top Agar with the attached phage and bacteria, and allowing plaque formation (Section **2-I1**). Ten to fifteen of the resulting plaques were then isolated (Section **2-I6**), used as templates in PCR, and subjected to gel electrophoresis (Section **2-I8A-2-I8C**). One of the subclones that produced a band that matched the size of the band hybridized to by the cDNA probes (Sections **2-I8B** and **2-I8E**) was then chosen to replace the master clone.

2-J2 cDNA Purification: The remaining PCR product (82 µL) from Sections **2-I8A** or **2-J1** of the clones identified as differentially expressed was mixed with 8 µL of 10x loading dye. A thick 1.2% agarose (w/v) 1xTAE gel[15] was prepared using a comb with large teeth that would hold 75 µL of PCR product, and 75 µL of the PCR product of the clones to be sequenced was loaded in each well. As a size and mass standard for the PCR product, 10 µL of Lambda DNA *Hin*d III Fragments (50 ng/µL) mixed with 1 µL of 10x loading dye was used. The gel was subjected to electrophoresis, and visualized as in

[15] One factor influencing the choice of the TAE buffer for electrophoresis is that DNA yield from the QIAquick Gel Extraction Protocol is higher than when Tris Borate EDTA (TBE) buffer is used for electrophoresis.

Sections **2-I8B** and **2-I8C**. After the gel was photographed, the bands in the gel were excised with a clean razor blade and placed in 2.0 mL tubes. In cases where the plaque purification described in Section **2-J1** continually produced more than one PCR product, the band that was the correct size was excised.

The excised band was weighed, and then gel-purified using a QIAquick Gel Extraction Kit (QIAgen,, Mississauga, Ontario) according to the manufacturer's protocol. The gel purification process consists of dissolving the agarose gel slice in a chaotropic solution, QG Buffer, and centrifuging the solution through a QIAgen spin column. The spin column retains the cDNA on the frit while allowing the solution to flow through. To use the amplified cDNA inserts for sequencing purposes the cDNA was washed with QG Buffer again to remove any agarose that may be complexed with the cDNA, and centrifuged. The cDNA was then washed with another solution, PE Buffer, which acts to remove excess ions from the cDNA. The cDNA was incubated in PE Buffer for 2-5 minutes since sequencing is a salt-sensitive application, and was then centrifuged through the frit. PE Buffer contains EtOH, and to ensure that this was completely removed, the dry column was centrifuged again. The cDNA was eluted in a minimum (30 μL) volume of ddH_2O. To ensure that the purified cDNA was recovered from the column, that it was pure, and to determine the concentration of the cDNA through reference to the mass standard of the gel, 5 μL of the eluted cDNA was removed for gel electrophoresis and visualization (Sections **2-I8B** and **2-I8C**).

2-J3 cDNA Insert Sequencing: Determination of the concentration of the purified PCR product is necessary because the cycle sequencing reaction of the DYEnamic ET Terminator Cycle Sequencing Kit (Amersham Pharmacia Biotech Inc., Piscataway, New Jersey) used is very sensitive to the amount of template used. It is necessary to use 0.05-0.1 pmol of template in the 10 μL reaction. It is important to note that this is a molar quantity, not a mass. The number of moles of a given PCR product is determined from the gel used to check the purification recovery (Section **2-J2**) which provides the apparent mass and the size, in basepairs (bp), of the 5 μL of purified PCR product loaded. With this information it is relatively easy to judge the volume of template to be used in the cycle sequencing reaction from the gel, using the formula in **Figure 2-6**. The volume

$$V_T = \frac{n_T V_L M_{Av} l}{m_O}$$

$$= \frac{l\ (0.1 \times 10^{-12}\ \text{mol})\ (5\ \mu\text{L})\ (649.90\ \text{g/mol•bp})}{m_O}$$

$$= \left(\frac{l}{m_O}\right) 5.2495 \times 10^{-10}\ \mu\text{L•g/bp}$$

n = moles of template required = 0.1 pmol
V_L = volume of DNA in gel = 5 µL
M_{Av} = average molar mass of a base pair = 649.90 g/mol
m_O = observed mass (g) of DNA in gel
l = observed size (bp) of DNA in gel
V_T = volume (µL) of template required

Figure 2-6. Volume of Purified PCR Product for Sequencing Reaction.
The amount of template to be used can be determined by the mass of DNA in the gel and its size in bp.

of template used cannot exceed 5 μL in any case as 5 μL of sequencing reagent premix and primer is required for the 10 μL reaction.

The isolated cDNA insert was PCR-amplified using the T3 and T7 primer sites. This means that three primer sites are available for sequencing reactions (**Figure 2-5.**). The T3 and T7 primer sites are terminal sites of the purified PCR product, and use of the T7 primer site would result in sequencing the poly(A) tail of the cDNA. Instead, the internal sense 5' SK primer site is the one used to sequence the purified PCR product. The reaction mixture is completed by adding 1 μL of SK primer (2.5 μM), and 4 μL of the sequencing reagent premix, containing heat stable DNA polymerase and fluorescently-labelled chain terminator dideoxy NTPs. The small volume of the sequencing reaction means that the reactions need to be thoroughly mixed to ensure good results.

The reaction consists of 25 cycles of: 20 seconds denaturation at 95°C, 15 seconds of primer annealing at 50°C, and 60 seconds of extension at 60°C. An eppendorf Mastercycler Personal PCR machine (Brinkmann Instruments Inc., Mississauga, Ontario) was used to achieve these short incubations. While the reactions were cycled, one 1.5 mL tube per reaction was prepared by labelling the tube and adding 1 μL of the supplied sodium acetate (1.5 M, pH>8.0)/EDTA buffer (250 mM) to each tube. Solutions of 75% EtOH and 95% EtOH were prepared and stored at -20°C. When the reactions were finished the entire reaction volume was transferred to the appropriate tube, and 40 μL of 95% EtOH was added to each tube. The reactions were then precipitated for 12 hours at -20°C.

After precipitation, the tubes were centrifuged at 12000 g at 4°C for 1 hour. The supernatant was removed by aspiration, and the pellet was then washed with 75% EtOH and centrifuged at 12000 g at 4°C for 15 minutes. The supernatant was removed by aspiration, and the pellets were dried in a vacuum centrifuge for 5 minutes to remove any traces of EtOH from the pellets.

The precipitated reactions were then subjected to electrophoresis in the PE ABI 373 Stretch sequencer (PE Corporation, Foster City, California) of the Molecular Biology Service Unit (MBSU; Department of Biological Sciences, University of Alberta, Edmonton, Alberta) by the staff of the MBSU. This involved dissolving the pellet in the

formamide loading dye provided with the kit, and injecting samples in the appropriate lanes of the polyacrylamide gel of the PE ABI 373 sequencer.

The collected sequence data for each clone were analyzed by comparing the raw sequence text with the sequence chromatogram to ensure that the raw text was an accurate reflection of the detected fluorescence of the sample. Any necessary corrections were made to the sequence, and the 38 nucleotides of sequence representing the vector sequence before the *Eco*RI insertion site were removed.

2-J4 BLAST Analysis: The sequence obtained was analyzed using the NIH Basic Local Alignment Search Tool (BLAST; Altschul *et al.*, 1990, 1997; Madden *et al.*, 1996) available at: www.ncbi.nlm.nih.gov/BLAST/. These programs take submitted sequence data and attempt to find sequences that match the submitted sequence in the GenBank (NIH), European Molecular Biology Laboratory (EMBL), DNA Data Bank of Japan (DDBJ), and Protein Data Bank (PDB) nucleotide databases. The identity of any sequences in the databases that match the submitted sequence is given to the submitter by either e-mail or as a results page on the Internet (**Figure 2-7.**). The matching sequences are ranked from top to bottom in the order of decreasing likelihood of an exact match. The parameter used to determine whether a match is exact is the Expect-value (E-value) which is the likelihood of the submitted sequence matching the identified database sequence solely by chance, as determined by statistical evaluation of the size of the database as a whole, the size of the submitted sequence, and the size of the identified sequence. An E-value of 0.00 indicates that the identified sequence is an exact match over a significant length of nucleotides for the submitted sequence, and any identity assigned to the identified sequenced can with confidence be applied to the submitted sequence. E-values greater than 0.00 indicate that less confidence can be assigned to the match identified by BLAST.

2-K Northern Blot Hybridization

Multiple Northern blots were prepared as described in Section **2-E**. These Northern blots allow the determination of gene expression in rat retinae over the course of increasing exposure to intense green light (Section **2-B**). Sequenced clones (Section **2-J**) provide a ready source of PCR template to produce PCR product (Sections **2-I8A-**

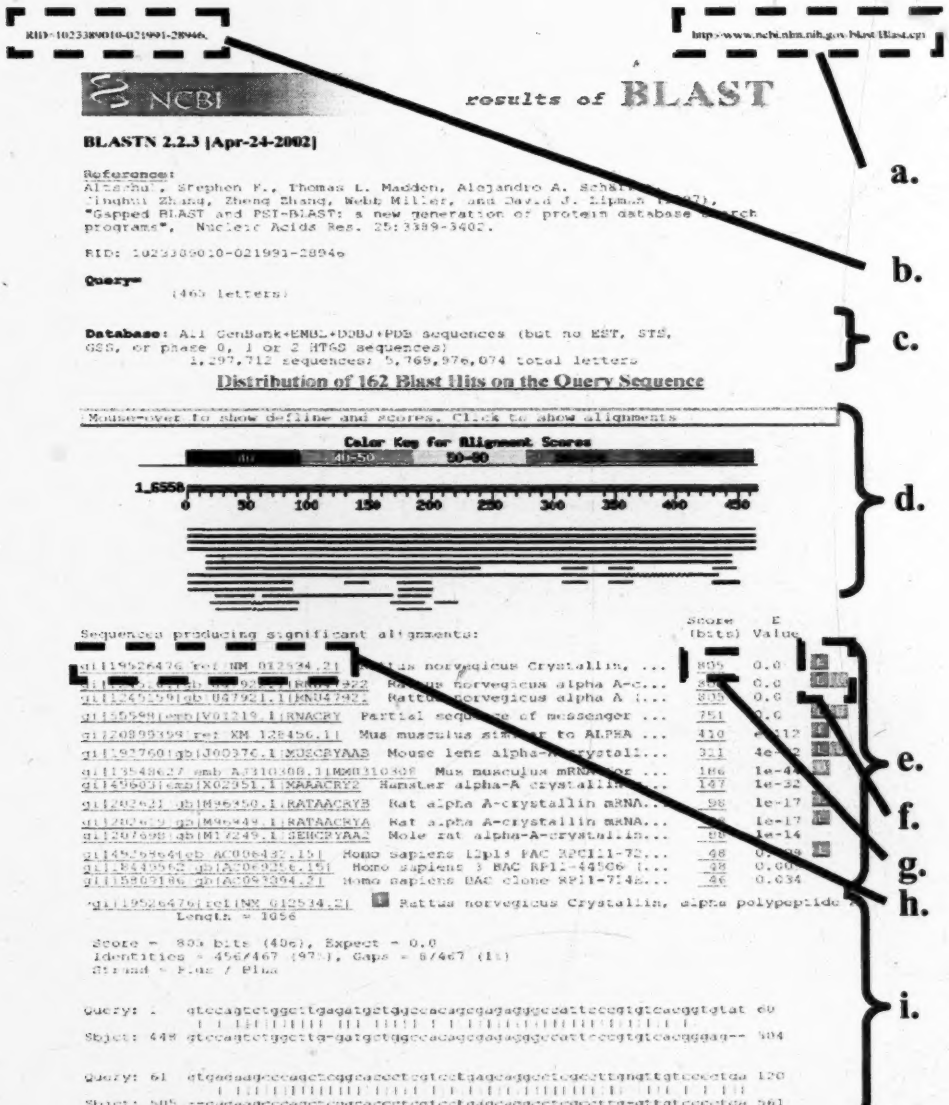

Figure 2-7. Anatomy of a BLAST Search. (Altschul *et al.*, 1990, 1997)
a. Web address. **b.** Request ID (RID) number for later retrieval of the search. **c.** Databases searched and their total size. **d**. Graphic representation of the identified matches. **e.** List of identified matches in order of decreasing identity. E-values are given in scientific notation, *i.e.* e-112 is 10^{-112}. **f.** These links lead to additional information about the clone entry. **g.** The link in the score column leads to the individual entry match where the target and query alignment is shown. **h.** The link beside the match name leads to that entry in the databases. The "L" and "U" links lead to additional information about the clone entry in the LocusLink and UniGene databases, respectively. **i.** The individual entry for each match where the target and query alignment is shown, including gaps in the alignment.

2-I8C) which can be purified (Section **2-J2**), radioactively labelled, and used to probe these Northern blots (Thomas, 1980; Sambrook *et al.*, 1989).

2-K1 Radioactive Labelling of Clone Inserts: The purified PCR products were each radioactively labelled using a Random Primers DNA Labelling System and the radioactive nucleotide [α-^{32}P]dCTP, with an activity of 3000 Ci/mmol. For each labelling reaction, 25 ng of each purified PCR product was heat denatured and immediately cooled on ice. Each labelling reaction consisted of: the 25 ng of denatured PCR product, 15 µL of random hexamers in buffer, 5 µL of each of the non-radioactive nucleotides (dTTP, dATP, dGTP; 0.5 mM), and 5 µL of [α-^{32}P]dCTP (0.5 mM). On ice, 1 µL of the Klenow Fragment of *E. coli* DNA polymerase I (3U/µL) was added and mixed thoroughly. The reaction was incubated for 10 hours at room temperature. Probe purification and determination of percent incorporation was performed as in Section **2-I2**.

2-K2 Probe Hybridization: The Northern blots were individually placed in 15 cm glass hybridization bottles (Wheaton, Millville, New Jersey), and the bottles were filled with approximately 80 mL of 65°C 2x SSC, and rotated at medium speed at 65°C in a rotary incubator for 20 minutes. After this initial wash of the blots, the 2x SSC was removed, and 25 mL of 65°C Hybrisol II was added to each bottle. The blots were prehybridized in Hybrisol II for 4 hours in the rotary incubator at medium speed at 65°C. After 4 hours of prehybridization, 20 million total cpm of each radioactive probe was boiled separately for 5 minutes in a water bath with 100 µL of 10 µg/µL salmon sperm DNA to denature the probe, and were immediately placed on ice. The denatured probes, with salmon sperm DNA as a competitor DNA, were then separately added to 20 mL of 65°C Hybrisol II to give 1 000 000 cpm/mL for each probe. The prehybridization Hybrisol II was removed from each bottle. Each probe in Hybrisol II was then added to the appropriate Northern blot and the blots were hybridized in the rotary incubator at medium speed at 65°C for 12 hours.

2-K3 Hybridization Washes: After the 12 hour hybridization of the blots, the radioactive probe in Hybrisol II was removed from each hybridization bottle, and the blots were washed in 90 mL of 65°C 2x SSC for 15 minutes in the rotary incubator at medium speed at 65°C. This wash was repeated after removing the initial wash solution. After the second 2x SSC wash, the blots were washed in 70 mL of 65°C 2x SSC/0.1%

SDS in the rotary incubator at medium speed at 65°C for 20 minutes, and this wash was also repeated. The critical wash is the last one, and it must not be allowed to continue past 10 minutes. The last wash consisted of 70 mL of 65°C 0.1x SSC/0.1% SDS in the rotary incubator at medium speed at 65°C for 10 minutes. After the 0.1x SSC/0.1% SDS wash, the blots were immediately removed from the hybridization bottles and immersed in 2x SSC. The blots were then placed RNA side up on Whatman paper soaked in 2x SSC, and wrapped in plastic film with no bubbles.

2-K4 Autoradiography: The wrapped blots were then placed in film cassettes with intensifying screens, and the radioactive blots were used to expose Kodak X-Omat AR film for 24 hours. The film was developed, and the location of the wells and an outline of the blot was marked on each exposure, along with the name of the PCR product used as a probe, and the length of the exposure. In cases where the signal intensity on the film was not strong enough, or was too strong, the blots were used to expose film for an appropriate length of time, as judged from the 24 hour exposure. The 14.26 day half life of ^{32}P was taken into account for very long exposures.

2-K5 Densitometry: When appropriate film exposures were obtained, the film was photographed using the Kodak DC120 digital camera. Each Northern blot was prepared from a RNA gel that was photographed before the transfer. The software accompanying the digital camera, Kodak: Digital Science 1D Image Analysis Software (Version 1.0, Eastman Kodak Company, New Haven, Connecticut), is designed to measure the intensity of signal from digital images. By counting individual pixels and assigning an intensity value to each pixel, the software determines the average signal intensity of the image, and then identifies areas of high signal intensity, such as an EtBr-stained rRNA band in a gel or silver crystals deposited in a band on a piece of film exposed by radioactive probe hybridized to a specific RNA on the blot derived from the gel. So, for each blot, the intensity of the visible EtBr-stained 18S rRNA band in each lane of the RNA gel can be determined. Since 18S rRNA levels are constant, the evenness of RNA loading can be determined and used as a correction factor for signal intensities measured in the image of the exposure (Correa-Rotter *et al.*, 1992).

e.g. *If the EtBr signal intensity of the 18S rRNA band in lane 1 has a value of 1000 while the intensity in lane 2 is 800, lane 2 must have only 80% of the RNA that lane 1 does. On the film exposure of a radioactively probed blot*

made from this gel, the same sized band is identified in both lanes 1 and 2. In both lanes, the signal intensity of the band is 100. Without correction, it would seem that the mRNA detected by the probe occurs at equal levels in the RNA loaded in both lanes, but since there is less RNA in lane 2, the mRNA is actually more prevalent in the RNA loaded in lane 2. With correction (Lane 1: 100/1.00=100; Lane 2: 100/0.80=125), it is evident that the mRNA is present at 25% increased levels in lane 2.

Using the Kodak software, the signal intensities, and hence levels of mRNA that the probe hybridizes to, can be determined, and the mRNA levels in the RNA from the rat retinae subjected to each treatment (Section **2-B**) can be determined. The software is also capable of determining the mobility of the size standard in the RNA gel, and so can be used to determine the size of bands detected on the exposures. The size, in nucleotides, of each visible band of the standard is entered, and the software measures the distance that these bands have travelled from the wells. From this, a mobility curve can be prepared by plotting the Mobility (cm) on the x-axis and the $\log_{10}$(Band Size) on the y-axis. The size of a particular band on the exposure can then be interpolated by finding the distance the band is from the wells, which were marked on the exposure from their location on the Northern blot.

2-L Rat Retina Protein Isolation

Protein from each set of retinae was extracted from the organic $CHCl_3$ and phenol phase retained from the RNA extraction (Section **2-D**) according to the manufacturer's protocol (Gibco BRL, Gaithersburg, MD). The volumes in the protein extraction tend to be larger so the organic phase was separated from the interphase and remaining aqueous phase and placed in 15 mL polypropylene tubes—since $CHCl_3$ is present in the organic phase. For each 1 mL of TRIzol used in the homogenate, 1.5 mL of iPrOH was added to each tube. The tubes were then lightly mixed by inverting and allowed to sit at room temperature for 10 minutes to allow a miscible iPrOH, $CHCl_3$ and phenol solution to form which precipitates the proteins. This solution was then centrifuged at 12000 g at 4°C for 10 minutes. The supernatant was removed, and 2 mL of 0.3 M guanidine•HCl (Sigma-Aldrich, St. Louis, Missouri) in 95% EtOH for each mL of TRIzol used for the homogenization was added to each tube to wash the pellet and remove all solvents and chaotropic agents from the pellet. The washes were incubated with occasional gentle agitation for 20 minutes at room temperature. The solutions were then centrifuged at

7500 g at 4°C for 5 minutes, and the supernatant was removed. The wash and centrifugation were done three times in total. After the third wash, 1.5 mL of EtOH was added to the each tube, and the pellets were resuspended by vortexing at moderate speed. The resulting mixture was then incubated with occasional gentle agitation for 20 minutes at room temperature. The solutions were then centrifuged at 7500 g at 4°C for 15 minutes, and the supernatant was gently removed. The pellets were dried in a vacuum centrifuge for 5 minutes, and were then dissolved in 250 μL of 1% SDS (w/v), which required gentle heating at no greater than 50°C for complete solubilization. The proteins in 1% SDS were then centrifuged at 10000 g at 4°C for 10 minutes to remove insoluble proteins and membrane remnants. The supernatant was transferred to a new tube and stored at -20°C.

Protein concentration was spectroscopically determined using the Bradford Assay of protein concentration. A_{280} readings, which could also be used, will likely be incorrect due to trace amounts of phenol in the protein solution. Bradford Reagent contains 5% methanol (v/v), 9% phosphoric acid (v/v), 0.1% Coomasie Brilliant Blue (w/v)[16], and 0.5% sodium lactate (w/v). The A_{595}, which represents the absorbance maximum of the protein-bound form of Coomassie Brillant Blue, was measured for a series of dilutions of a protein of known concentration dissolved in 1% SDS and mixed with equal volumes of Bradford Reagent. A standard curve was prepared, and protein from the sets of rat retinae was added to the same volume of Bradford Reagent, the A_{595} was measured and protein concentration was interpolated from the standard curve.

2-M Western Blotting (After Sambrook *et al.*, 1989)

Changes in gene expression are detected at both the RNA and protein level, so it is necessary to have some means of detecting the level of both. Northern blots have been described in Section **2-K**, and their analysis allows the determination of steady state levels of mRNA. Western analysis allows the detection of specific proteins by antibody detection on Western blots prepared from proteins subjected to denaturing polyacrylamide gel electrophoresis (SDS-PAGE).

---

[16] Benzenemethanaminium, N-(4-((4-((4-ethoxyphenyl)amino)phenyl) (4-(ethyl((3-sulfophenyl) methyl) amino)-2-methylphenyl)methylene)-3-methyl-2,5-cyclohexadien-1-ylidene)-N-ethyl-3-sulfo-, hydroxide, inner salt, monosodium salt (9CI)

2-M1 Gel Preparation: The SDS-PAGE gel used to separate proteins is an upright, bipartite polyacrylamide gel with two different polyacrylamide concentrations in each part. The lower, separating gel, is 12-13% polyacrylamide, and serves to separate the proteins based on their mass-determined mobility. The upper, stacking gel, is 5% polyacrylamide, and serves to ensure that all the proteins in the sample enter the separating gel at the same time. The mini-gels used were poured 1mm thick between two glass plates. In a 10 cm mini-gel, the separating gel was poured without bubbles to a level height of 6-7 cm from the table top. After the separating gel was set, the stacking gel was poured on top of the separating gel without bubbles to fill the space between the plates, and a comb was inserted at the top of the gel. For four mini-gels, 60 mL of the separating gel[17] and 30 mL of the stacking gel[18] is required. The gels set by the polymerization of acrylamide into polyacrylamide, and the cross linking of polyacrylamides occurs because of the presence of 5% branched bisacrylamide. The polymerization reaction is catalyzed by the addition of ammonium persulfate (APS; Sigma-Aldrich, St. Louis, Missouri) and (N,N,N',N')-tetramethylethylene diamine (TEMED; Sigma-Aldrich, St. Louis, Missouri). Separating gels were polymerized by 300 μL of 10% (w/v) APS and 30 μL of TEMED, while stacking gels were polymerized by 150 μL of 10% (w/v) APS and 30 μL of TEMED. Polymerization of the acrylamide is impeded in the presence of oxygen, so the gels were covered to prevent exposure to the air. The separating gel was protected by covering the gel solution in the plates with iPrOH while it set, and the stacking gel was protected by covering it with the comb and plastic wrap. When the stacking gel was set, the comb was removed and the wells were washed out with ddH_2O and dried with strips of Whatman paper. The gels were placed in the buffer reservoir of the electrophoresis apparatus and covered with running buffer[19].

2-M2 Sample Preparation and Electrophoresis: 950 μL of Laemmli buffer[20] was placed in a 1.5 mL tube and 50 μL of β-mercaptoethanol (BDH Inc., Toronto, Ontario)

---

[17] Separating gel: 0.375 M Tris•HCl pH 8.8, 0.1% SDS (w/v), 13% (v/v) [19 acrylamide:1 bisacrylamide] (Bio-Rad Laboratories Inc., Hercules, California)

[18] Stacking gel: 0.125 M Tris•HCl pH 6.8, 0.1% SDS (w/v), 5% [19 acrylamide:1 bisacrylamide] (v/v)

[19] Running buffer: 1 L dd H_2O, 0.025 M Tris, 0.2 M glycine (Bio-Rad Laboratories Inc., Hercules, California), 0.02% SDS (w/v), pH 8.5

[20] Laemmli buffer: 0.375 M Tris•HCl pH 6.8, 0.1% SDS (w/v), 0.25% Bromophenol blue (w/v), 13.2% glycerol (v/v)

was added. The same mass (10 μg) of protein from each treatment (Sections **2-B** and **2-L**) was put in separate 1.5 mL tubes, and enough Laemmli buffer was added to each tube so that the tubes all contained 20 μL. The size standard, 5 μL of Kaleidoscope Prestained Standards (Bio-Rad Laboratories Inc., Mississauga, Ontario) was also prepared in 15 μL Laemmli buffer. The proteins were heat-denatured by boiling for 3 minutes in the presence of the disulfide-reducing agent β-mercaptoethanol. The samples were then loaded in the wells of the stacking gels. There were usually empty wells, and these were loaded with the same volume of only Laemmli buffer to ensure an even distribution of current through the gel. The gels were run at a constant voltage of 80 V until the Bromophenol blue band entered the separating gel when the voltage was increased to 150 V. Electrophoresis was stopped when the Bromophenol blue reached the bottom of the separating gel.

2-M3 Western Transfer: Two pieces of Whatman paper were cut to provide a 1 cm margin around the gel, and a piece of polyvinylidene fluoride membrane (Bio-Rad Laboratories Inc., Mississauga, Ontario) was cut the same size as the gel. The membrane was soaked in methanol (MeOH; Caledon Laboratories Inc., Georgetown, Ontario) for 15 seconds, ddH_2O for 2 minutes and Transfer buffer[21] for 5 minutes. Two sponges and the Whatman paper were soaked in Transfer buffer until the transfer apparatus was assembled. The gel was removed from the glass plates, and the corner nearest the size standard was notched. The gel was placed on a piece of Whatman paper, which was placed on a sponge, the membrane was carefully laid on the gel and not moved after it was laid down. The remaining Whatman paper and sponge completed the sandwich, and the whole construction was clamped into the transfer cassette (**Figure 2-8.**). The transfer cassette was then placed in the electrophoresis apparatus with the membrane side closest to the anode. A constant current of 100 mA for 12 hours was applied through the transfer cassette. When the transfer was complete the apparatus was dismantled and the gel was stained in Coomassie blue[22] for 30 minutes and then destained in destaining solution[23] for

[21] Transfer buffer: 1 L dd H_2O, 0.025 M Tris, 0.2 M glycine, 0.05% SDS (w/v), pH 8.3
[22] Coomassie blue: 0.1% Coomassie Brilliant Blue (w/v), 45% MeOH (v/v), 10% glacial acetic acid (v/v)
[23] Destaining solution: 40% MeOH (v/v), 10% glacial acetic acid (v/v)

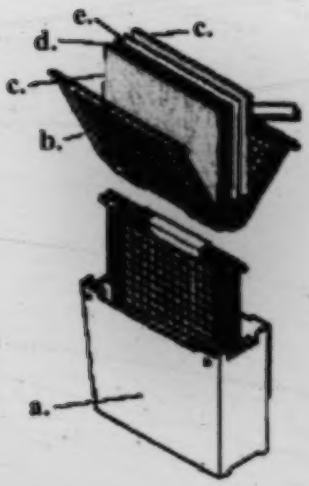

Figure 2-8. Western Transfer Cassette.

a. Buffer tank.

b. Transfer cassette. The black face should be oriented towards the anode (+) and the red face oriented towards the cathode (-).

c. Sponge and Whatman paper hold gel and membrane immobile when transfer cassette is closed.

d. Polyacrylamide gel.

e. Membrane.

(Bio-Rad Gel Holder, 170-3913)

30 minutes. A photograph of the stained gel was taken with the Kodak DC120 digital camera. The membrane was stained with Ponceau S[24] for 30 minutes, rinsed in ddH_2O, and photographed with the Kodak DC120 digital camera. The Western blots were stored in ddH_2O at 4°C until used for immunodetection.

2-M4 Immunodetection: The Western blots were incubated in Blocking buffer[25] at room temperature for 1 hour. Primary antibodies to proteins of interest were obtained and diluted in Antibody buffer[26] to the concentration given in the supplier's data sheet. The blocked blots were rinsed with ddH_2O, and then incubated in the primary antibody for 12 hours at 4°C with slight agitation. After the incubation, the blots were rinsed with ddH_2O, and then washed three times in excess Antibody buffer at room temperature for 20 minutes. The appropriate secondary antibody for each primary antibody was diluted in Antibody buffer to the correct concentration. Each Western blot was incubated in the appropriate secondary antibody for 1 hour at room temperature with slight agitation. The blots were rinsed with ddH_2O, and then washed three times in excess Antibody buffer at room temperature for 20 minutes. Antibodies used are listed in Table 2-1., along with the concentrations or dilutions used.

The secondary antibodies used for Western analysis in this study were conjugated to horseradish peroxidase, which is oxidized in the presence of peroxides and cleaves 3-aminophthalhydrazide (luminol) to generate electrochemoluminescence (ECL) in a reaction which is enhanced by 4-iodophenol. The ECL RPN 2106 kit (Amersham Pharmacia Biotech Inc., Piscataway, New Jersey) provides the luminol and 4-iodophenol in two separate solutions. These solutions were mixed in equal volumes, 0.0625 mL of each solution per cm^2 of blot, and spread on the Western blots. The blots were then wrapped in plastic wrap and used to expose film. The film was developed and the size and orientation of the Western blots was indicated on the film. Since an equal mass

---

[24] Ponceau S: 0.5% (w/v) 3-hydroxy-4-(2-sulfo-4-[4-sulfophenylazo]-phenylazo)-2,7-napthalenedisulfonic acid (Amersham Biosciences Inc., Piscataway, New Jersey), 10% glacial acetic acid (v/v)

[25] Blocking buffer: 10 mM Tris, 0.05% (v/v) IGEPAL CA-630 (NP-40) [(octylphenoxy)polyethoxyethanol; Sigma-Aldrich, St. Louis, Missouri], 140 mM NaCl, 10% (w/v) Bovine Serum Albumin Fraction V (Boehringer Mannheim Corporation, Indianapolis, Indiana), pH 7.4

[26] Antibody buffer: 140 mM NaCl, 10 mM Tris, 0.03% Polyoxyethylenesorbitan monolaurate (Tween 20; Caledon Laboratories, Georgetown, Ontario), pH 7.4

Table 2-1. Antibodies Used for Western Immunodetection

Antibody	Catalog Number	Supplier	Isotype	Immunogen	Concentration/ Dilution Used
Anti-αA Crystallin Peptide	SPA-221 Lot 701430	StressGen Biotechnologies Corporation	rabbit polyclonal	Peptide: *Homo sapiens* αA Crystallin C-terminus	1:1000 dilution of whole serum
Anti-αB Crystallin Peptide	SPA-223 Lot 811407	StressGen Biotechnologies Corporation	rabbit polyclonal	Peptide: REEKPAVTAAPKK	1:2000 dilution of whole serum
Anti-β Crystallin	SPA-230 Lot 602408	StressGen Biotechnologies Corporation	mouse monoclonal IgG_1	*B. taurus* β_H Crystallin	1 μg/mL
Anti-γS Crystallin Peptide 1	Dr. G. Wistow, National Eye Institute, National Institutes of Health, Bethesda, Maryland		rabbit polyclonal	Peptide: DKKEYRKPVD	1:1000 dilution of whole serum
Anti-Heat Shock Protein 70 (HSP72)	SPA-760 Lot 00249	StressGen Biotechnologies Corporation	rabbit polyclonal	Peptide: *R. norvegicus* HSP72 (residues 446-641)	1:40 000 dilution of whole serum
Anti-Heat Shock Protein 90 (HSP90)	SPA-830 Lot 002417	StressGen Biotechnologies Corporation	mouse monoclonal IgG_1	*Achlya ambisexualis* HSP90	1 μg/mL
Anti-Rabbit IgG Horseradish Peroxidase Conjugate (HRP)	SAB-300 Lot 004429	StressGen Biotechnologies Corporation	goat polyclonal	*Oryctolagus cuniculus* immunoglobulin G (IgG)	1:10 000 dilution of whole serum
Anti-Mouse IgG Fab-specific Horseradish Peroxidase Conjugate (HRP)	SAB-100 Lot 911440	StressGen Biotechnologies Corporation	goat polyclonal	*Mus musculus* immunoglobulin G Fab fragments(IgG Fab)	1:10 000 dilution of whole serum

(10 μg) of protein was loaded in each lane (Section **2-M2**), the change in protein levels between the different treatments of rat retinae (Section **2-B**) was determined by densitometry (Section **2-K5**).

2-N Fluorescent Immunohistochemistry (Modified from Ausubel *et al.*, 1994)

2-N1 Tissue Fixation: Whole rat eyes were obtained after light treatment by lifting the eye and cutting the optic nerve. An incision was made at the junction of the cornea and sclera in the superior region of the eye. The eye was then immersed in 10 mL of 4% (w/v) paraformaldehyde (*p*-CHO; Sigma-Aldrich, St. Louis, Missouri) in phosphate buffered saline [27] for 15 minutes at 4°C. After the initial fixation the lens was removed by cutting around the cornea, although the corneal flap is left attached at the inferior of the eye to allow orientation of the eye. The tissue was then fixed again in 20 mL of 4% *p*-CHO•PBS for 4 hours with gentle shaking. The eye was then rinsed three times in 20 mL of PBS for 10 minutes at room temperature. The tissue was cryopreserved in 30% sucrose (w/v) •PBS for at room temperature until the eye sinks to the bottom of the container. The cryopreservation is intended to prevent the tissue from fracturing during freezing and sectioning. The eye was then frozen in $CO_{2(s)}$ in Optimal Cutting Temperature (OCT) Compound[28] (Sakura Finetek USA, Torrance, California) in a tissue holder with the corneal flap oriented up. Care was taken to avoid introducing bubbles into the OCT Compound. The frozen eye was covered in foil and stored at -70°C.

2-N2 Tissue Sectioning: The frozen tissue was placed at -20°C for two hours so that it would be at the same temperature as the TissueTek II Microtome/Cryostat 4551 (Lab-Tek Division Miles Laboratories Inc., Naperville, Illinois). Sections of the eye were cut 6 μm thick and transferred to SuperFrost Plus microscope slides (Fisher Scientific Ltd., Nepean, Ontario). The slides were fixed in 4% *p*-CHO•PBS for 5 minutes and then dehydrated by immersing the slides sequentially for 2 minutes in 30%, 80% and 100% EtOH. The slides were then wrapped in foil and stored at -70°C.

---

[27] Phosphate Buffered Saline (PBS): 140 mM NaCl, 2.7 mM KCl, 8 mM Na_2HPO_4 (Sigma-Aldrich, St. Louis, Missouri), 1.5 mM KH_2PO_4 (Sigma-Aldrich, St. Louis, Missouri), pH 7.4

[28] Optimal Cutting Temperature (OCT) Compound: 10.24% (w/w) polyvinyl alcohol, 4.26% (w/w) polyethylene glycol, 85.50% (w/w) nonreactive ingredients

2-N3 Immunohistochemistry: A steam bath was prepared ahead of time to lightly denature the proteins in the sections. The frozen sections were immersed in hot (≅95°C) citrate buffer[29] and then placed in the steam bath for 15 minutes. They were allowed to cool to room temperature, and then blocked with 500 µL of 0.1% Triton X-100 (v/v) and 5% skim milk (w/v) in Tris-buffered saline[30] for 1 hour at room temperature. The blocking solution was washed off the slides by immersing the slides three times for 5 minutes each time in 0.1% Triton X-100 (v/v) in TBS (TBS/T). The primary antibody was diluted with 5% skim milk (w/v) in TBS/T to the appropriate concentration for immunohistochemistry, approximately five times the concentration used for Western analysis. The section was covered with 200 µL of the primary antibody and incubated for 12 hours at 4°C.

Table 2-2. Antibodies Used for Immunohistochemistry

Antibody	Catalog Number	Supplier	Isotype	Immunogen	Concentration/ Dilution Used
Anti-αB Crystallin Peptide	SPA-223 Lot 811407	StressGen Biotechnologies Corporation	rabbit polyclonal	Peptide: REEKPAVTAA PKK	1:200 dilution of whole serum
Anti-γS Crystallin Peptide 1	Dr. G. Wistow, National Eye Institute, National Institutes of Health, Bethesda, Maryland		rabbit polyclonal	Peptide: DKKEYRKPVD	1:200 dilution of whole serum
Anti-Rabbit IgG $F(ab')_2$ Cy3 Conjugate	111-166-006 Lot45725	Jackson Immunoresearch Laboratories, Incorporated	goat IgG $F(ab')_2$ fragments	*Oryctolagus. cuniculus* immunoglobulin G $F(ab')_2$ Fragments	2 µg/mL

After the incubation the slide was washed three times for 5 minutes each time in TBS/T at 4°C. The secondary antibody was diluted to the appropriate concentration in 5% skim milk (w/v) in TBS/T. The section was covered with 200 µL of the secondary antibody and incubated for 1 hour at 4°C in the dark. The secondary antibody is labelled with the Cy3 fluorophore (Table I-2.; Amersham Biosciences Inc., Piscataway, New Jersey) which is light-sensitive, and must be kept in the dark. In the dark, the slides were washed three times for 5 minutes each time in TBS/T at 4°C. A solution of 1 µg/mL 4',6-diamidinophenyl-indole (DAPI; Sigma-Aldrich, St. Louis, Missouri) was prepared in 5% skim milk (w/v) in TBS/T. The sections were covered with 200 µL of this solution

[29] Citrate Buffer: 10 mM citric acid monohydrate, pH 6.5
[30] Tris-Buffered Saline (TBS): 140 mM NaCl, 2.7 mM KCl, 12.4 mM Tris, pH 7.4

and incubated for 10 minutes at 4°C. The slides were then again washed three times for 5 minutes each time in TBS/T at 4°C. Three separate sections of three separate retinae subjected to either: 0, 4 or 8 hours of light treatment were analyzed this way (Section **2-B**).

M-N4 Fluorescence Microscopy: The fluorescence of the Cy3-DAPI labelled sections was excited and digitally microphotographed using a 40x oil immersion objective with a Leica DM R multiphoton microscope and the accompanying software (Leica Microsystems, Wetzlar, Germany). Bright field micrographs were also taken of each tissue section. The Cy3 fluorophore is excited at 550 nm and emits at 615 nm, while the DAPI fluorophore is excited at 350 nm and emits at 470 nm. The multichannel capacity of the microscope allowed exactly overlapping Cy3, DAPI and bright field images to be taken.

Chapter 3 Differential Cross Screen

Chapter 3 Differential Cross Screen

This study was initiated with a differential cross screen of an unamplified rat retina cDNA library derived from the mRNA of rats treated with 4 hours of intense green light, the 4 Hour Library (Sections **2-B-2-I**). The basis of this technique is that the individual cDNAs in a cDNA population made from a single source of mRNA should exist in close proportion to the individual mRNA molecules that make up the mRNA pool because the mRNA molecules serve as the templates for synthesis of the cDNA. The cDNAs from two different conditions can be radioactively labelled so that they are easily detectable, and used to separately probe two identical representations, *i.e.* nylon membrane plaque lifts, of a cDNA library. Radioactive probe will hybridize to complementary sequences on the membranes, and the intensity of the signal detected by autoradiography is an indication of the amount of cDNA present in the cDNA pool from which the probe was made. The unamplified 4 Hour cDNA library is also derived from a single source of mRNA, and it too should contain a true reflection of all the mRNA species present in the retinae of rats treated with 4 hours of light.

Each detected signal corresponds to an individual mRNA represented by the cDNA insert in a clone from the phage cDNA library. The intensity of signal for one particular plaque can be compared when the two membranes are probed with one radioactive cDNA probe *versus* the other, *i.e.* 4 Hour cDNA derived from rat retinae treated with 4 hours of intense green light *versus* Dark cDNA derived from mRNA of untreated rat retinae (Section **2-B**). If different signal intensities are seen from one autoradiograph to the other when the probes as a whole have the same level of labelling, it means that the mRNA represented by the cDNA insert in the plaque is hybridized to less frequently by one cDNA probe than the other. This indicates that there is less cDNA for the specific expressed gene in the radioactive probe that is capable of hybridization to the specific cDNA inserted in the clone under consideration, which, by extension, indicates that there are fewer mRNA copies of that gene in the tissue that gave rise to the cDNA probe that resulted in the lower autoradiographic signal intensity. Since the plaques that are transferred to the membranes are the result of a single phage infection, the phage in the plaque that shows differential hybridization, and hence differential expression, are clones that should be isolated for determination of the identity of the

cDNA insert that they contain. Further screening of the clones identified in the first phase of the screen can increase confidence in the results, and reduce large numbers of initially identified clones. In this study, the end result of the differential cross screen of the 4 Hour Library and sequencing of the resultant clones was that 167 clones represented mRNAs that were identified as differentially expressed between no light treatment and 4 hours of light treatment of dark-reared rat retinae (**Figure 3-1.**).

3-A Primary Screen

The unamplified λ Uni-ZAP 4 Hour Library was used to infect *Escherichia coli* XL1 Blue MRF' and the infected bacteria were plated, in top agar, on ten separate plates at an average density of 1066 plaques per plate (Section **2-11**). The differential cross screen of the 4 Hour cDNA Library started with a pool of 10660 plaques representing 10660 mRNAs present in the mRNA pool of dark-treated rat retinae after 4 hours of treatment with intense green light.

This is far too large a pool to examine. As well, the majority of the cDNA inserts in the 10660 plaques will represent mRNAs that are common to both untreated and 4 hour light-treated retinae. These will be the mRNAs for the "housekeeping" genes that maintain the basic functions of the cells in the retina. While these mRNAs are important, their ubiquitous presence does not help determine, at the molecular level, how a 4 hour light-treated retina is different from an untreated retina. After 4 hours of light treatment, the rat retinal photoreceptor cells are still alive, and not all of the photoreceptor cells die if the rats are allowed to recover from the light insult in the dark (Organisciak *et al.*, 1992). This means that the majority of the photoreceptor cells in the rat retina after 4 hours of light treatment must be continuing the basic metabolic processes that were occurring in photoreceptor cells of untreated rat retinae, and so must have many of the same mRNA requirements as untreated rat retinae. These mRNAs do not provide significant insight into what differences exist at the mRNA level between the two states.

At the same time, there must be a difference in gene expression because the cellular environment of 4 hour light-treated rat retinae becomes far more oxidative than the cellular environment of untreated rat retinae (Organisciak *et al.*, 1992, 1995, 1999b; Kutty *et al.*, 1995). This means that a fundamental component of metabolism, reduction

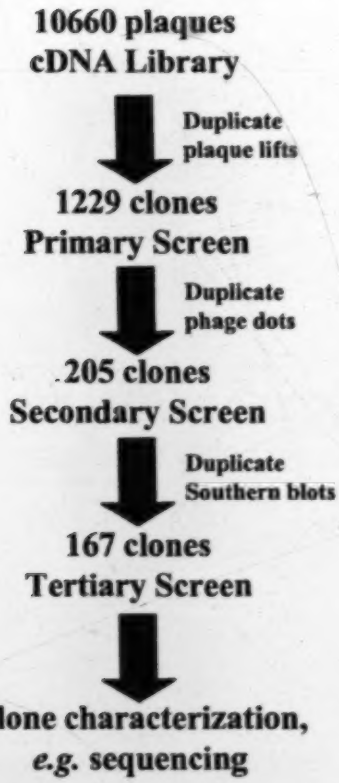

Figure 3-1. Screening the 4 Hour cDNA Library for Differentially Expressed Messages.
At each step, duplicate nylon membranes are prepared containing the phage that survive the previous screen. Each set of membranes is probed with a radioactively labelled probe derived from either 4 Hour cDNA or Dark cDNA. Clones which continuously indicate a difference in signal intensity between the two probes are selected to carry on to the next step.

and oxidation balance, has changed, and requires different metabolic activities to maintain homeostasis. This means that the levels of mRNA transcripts for some proteins will increase, and the mRNA levels for others will decrease as the cells adjust to their changing environment.

3-A1 Comparing Signal Intensity: The level of hybridization signal intensity on one autoradiograph *versus* the other allows the identification of mRNAs that are differentially expressed, and also allows the exclusion of mRNAs that are commonly expressed in the two tissues at high levels and are likely to be housekeeping genes. For example, in one condition, untreated rat retinae, there are *e.g.* 500 000 copies of a particular mRNA that is reverse-transcribed into cDNA. In another related condition, 4 hours of light-treated rat retinae, there are *e.g.* 400 000 copies of the same mRNA that is reverse-transcribed into cDNA. The untreated (Dark) cDNA is radioactively labelled, and the 4 hour light-treated (4 Hour) cDNA is radioactively labelled to the same extent, meaning that there should be 125% as much radioactive probe for the mRNA in the Dark probe as there is in the 4 Hour probe. Nevertheless, if both probes are used to probe separate duplicate blots of a 4 Hour Library it will be very difficult to see a difference in hybridization intensity on the resulting autoradiographs, because of the relative abundance of complementary sequence present in both probes for the cDNA in the library that represents that mRNA. In the entire retina, this is the most likely case for the relatively abundant housekeeping genes, no matter the treatment. When there are high levels of a particular radioactive cDNA in a probe it means that it is easier to reach the maximum detectable level of radioactivity of that film. In the case of mRNAs for housekeeping genes this maximum will not reflect the true levels of the cDNA in either condition, but this is acceptable since more pronounced changes are likely more significant than the relatively small changes of housekeeping genes.

An example of an easily detectable change would be a change in one condition from no, or extremely low, expression of a given gene across the entire retina to increased expression, at any detectable level, in the other condition. At the level of radioactive labelling and hybridization it would mean that in one cDNA pool there is no or little cDNA to make radioactive probe complementary to that gene's mRNA. In cases where there is no hybridization signal at a particular plaque it may mean that there is no

complementary radioactive signal, or it may mean that there is not enough radioactivity to provide a signal that is detectable with that film—the minimum detectable radioactivity of the film has not been reached, indicating that the cDNA insert found in the library is not found in the cDNA pool and therefore the mRNA is not found, or is not abundant, in the mRNA pool used to make the cDNA.

Many cases will be intermediate between the previous two examples. That is, the level of expression of a gene will not be as high as a housekeeping gene, but it is present at all times at some level, and this expression increases in untreated *versus* 4 hour light-treated rat retinae or *vice versa*. The key to the ability to detect the change in these mRNAs is that the abundance of the mRNA in either condition is far lower than the expression of a housekeeping gene. There is cDNA in both cDNA pools that can be radioactively labelled, but there is far less of it than there is cDNA representing the mRNA of a housekeeping gene. The radioactivity for a particular cDNA of intermediate number should fall within the range of detection of the film used, and it will be possible to detect the relative levels of hybridization of each separate probe.

3-A2 Primary Screen of the 4 Hour Library: Comparison of the two autoradiographs for each plate (Sections **2-I1-2-I7**) resulted in the identification of 1229 plaques representing mRNAs that were putatively differentially expressed between an untreated and a 4 hour light-treated rat retinae (**Figure 3-2a.**). These 1229 clones were then screened again for confirmation of their differential status (Section **3-B**).

3-B Secondary and Tertiary Screens

The secondary and tertiary screens of the 1229 clones selected in the primary screen reduced this initial pool to 205 phage clones. The secondary and tertiary screens were of great value because they were performed on a larger scale, *i.e.* phage dots or PCR bands, than the primary screen. The primary screen analyzed very small (0.5-1 mm diameter) plaques, which means that the signal seen on an autoradiograph is tiny, and differences between signals representing a single plaque could well be obscured by the miniscule size. The phage dots generated plaques that were 5-6 mm in diameter, while the PCR bands were 4 mm wide. This increase in size meant that autoradiograph signals were of commensurately increased size, and were thus more easily comparable from

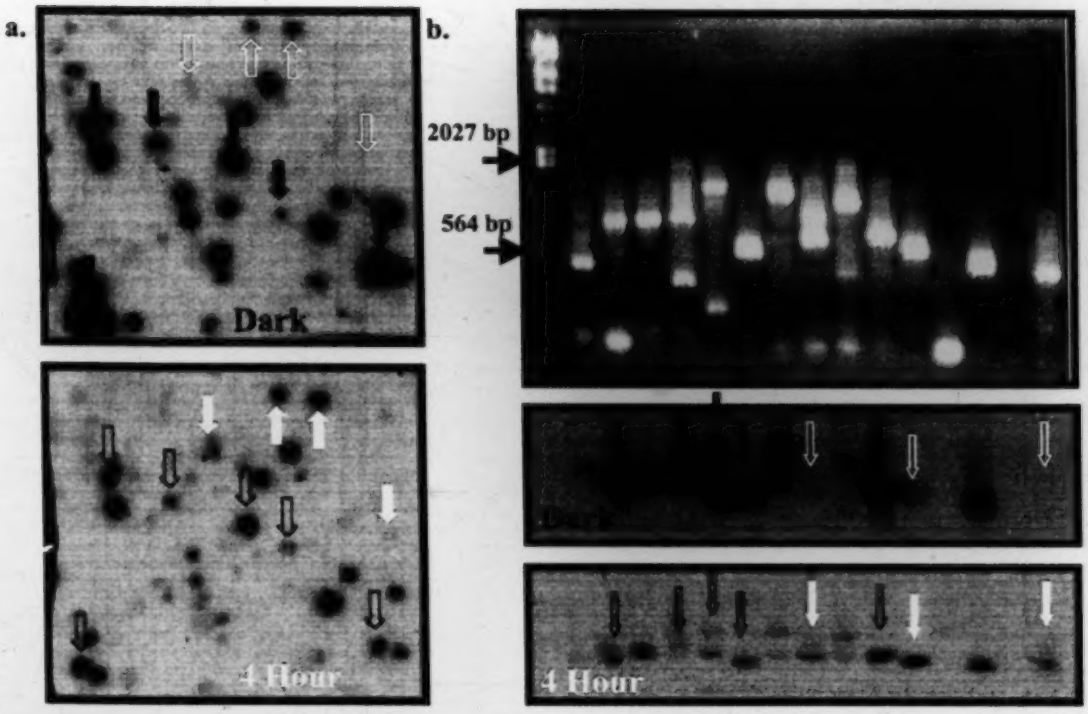

Figure 3-2. Primary and Tertiary Screens.

a. Primary screen using duplicate plaque lifts of the the plated 4 Hour library.

b. Tertiary screen of PCR product of clones isolated in the primary and secondary screens. Duplicate agarose gels were made and Southern transferred to separate membranes.
Each set of membranes is probed with a radioactively labelled probe derived from either Dark cDNA (derived from mRNA of untreated dark-reared rat retinae) or 4 Hour cDNA (derived from mRNA of 4 Hour light-treated dark-reared rat retinae). Clones which continuously indicate a difference in signal intensity between the two probes are selected to carry on to the next step. Black and black-outlined arrows indicate clones or PCR product which have a stronger signal intensity when probed with Dark cDNA. White and white-outlined arrows indicate clones or PCR product which have a stronger signal intensity when probed with 4 Hour cDNA.

autoradiograph to autoradiograph. Since the autoradiographs were more easily comparable, the differences between them were more discernible, and allowed a more confident determination of their differential status. As well, since the number of clones considered was reduced to 12% (1229/10660) of the original number examined it was easier to impose some lower limit of signal intensity difference that would be classed as differential.

3-B1 Secondary Screen of the 4 Hour Library: The phage dots prepared for the secondary screen could be grown to larger sizes than the plaques on the ten initial plates. As well, the orderly array of clones allowed for easier identification of hybridization signals as belonging to a particular clone (Section **2-I7**). The secondary screen confirmed 205 clones of the 1229 identified in the primary screen as differential. This was an 83% reduction in the number of clones to consider, and made subsequent analysis far easier.

3-B2 Tertiary Screen: This screen was intended as the definitive screen that would reduce the 205 clones selected as differential to an even more manageable number for sequencing. Interestingly, this PCR-based screen (Section **2-I8**) actually increased the number of potential clones. This occurred because multiple PCR bands were obtained from some phage stocks, which were originally considered to be single clones. An example of the tertiary screen is given in **Figure 3-2b**. The tertiary screen confirmed 173 of the 205 clones as differentially expressed mRNAs. Unfortunately, the tertiary screen was not useful in further reducing the number of clones identified as differential. This is because this process revealed 19 phage stocks that were considered to contain multiple clones. Rather than continue an indefinite screening process that was considered to be largely successful, the unconfirmed clones (32), and the additional clones from the unpurified stocks (23 clones) were treated as differential clones. This meant that while 173 of the 205 clones were confirmed as differential by the tertiary screen, the total number of putatively differential clones rose to 228 clones. Eventually plaque purification (Section **2-J1**) and comparison of the band sizes obtained from PCR of the purified clones with the hybridized bands on the tertiary screen autoradiographs reduced this number to 210 clones[31].

[31] A calamitous and unplanned loss of clones occurred when unnoticed breakdowns of a 4°C storage unit caused the evaporation of the SM buffer from 100 clones before they were sequenced. 43 of the dried-out clones were unrecoverable.

3-C Confirmation by Northern Analysis

The screening process seemed to work very well, but any potential flaw in the process could bias the identification of differential clones. While it was hoped that this was not the case, a reasonable test of the differential nature of the clones was to use the cDNA inserts from a representative sample of the 167 putatively differential phage clones and radioactively label them to create probes that could be used to probe Northern blots prepared from the RNA extracted from the retinae of dark-reared rats subjected to the three different treatments: untreated, and 4 and 8 hour light-treated (Sections **2-B-2-E**). In this study, a Northern blot containing the RNA from all three treatments (Section **2-B**) is named a Light-induced Retinal Degeneration (LIRD) Profile. The selected phage clone inserts should hybridize differently to the RNA in the untreated and 4 hour light-treated samples because the level of mRNA that the insert represents is different in each sample.

Northern analysis of nine clone inserts has confirmed that the differential cross screen was effective in identifying mRNAs that are differentially expressed in dark-reared rat retinae treated with either no light (Dark) or 4 hours of intense green light (4 Hour). **Figure 3-3.** shows the results of densitometry performed on the most intense band on autoradiographs of LIRD Profiles probed with radiolabelled clone inserts from these nine clones (Section **2-K**). For the nine clone inserts, twenty-five LIRD Profiles were probed in total. The autoradiograph signal intensity for each treatment (Section **2-B**) was determined, as were the signal intensities of the 18S rRNA bands for each treatment on the ethidium bromide-stained RNA gels (Sections **2-E** and **2-D**). The signal intensities of the autoradiographs were normalized using the 18S rRNA band intensity. The figures indicate the amount of autoradiograph signal intensity relative to the untreated rat retinae (Dark).

Clone 22.07, shows the greatest difference in autoradiograph signal between the Dark and 4 Hour treatments (**Figure 3-3a.**). The 720 nucleotide (nt) mRNA represented by this clone's insert is expressed at levels 5.27 times higher after 4 hours of light treatment than it is expressed with no light treatment. The standard deviation (s.d.) of the signal intensities from 3 different LIRD Profiles (n=3) was ±1.18.

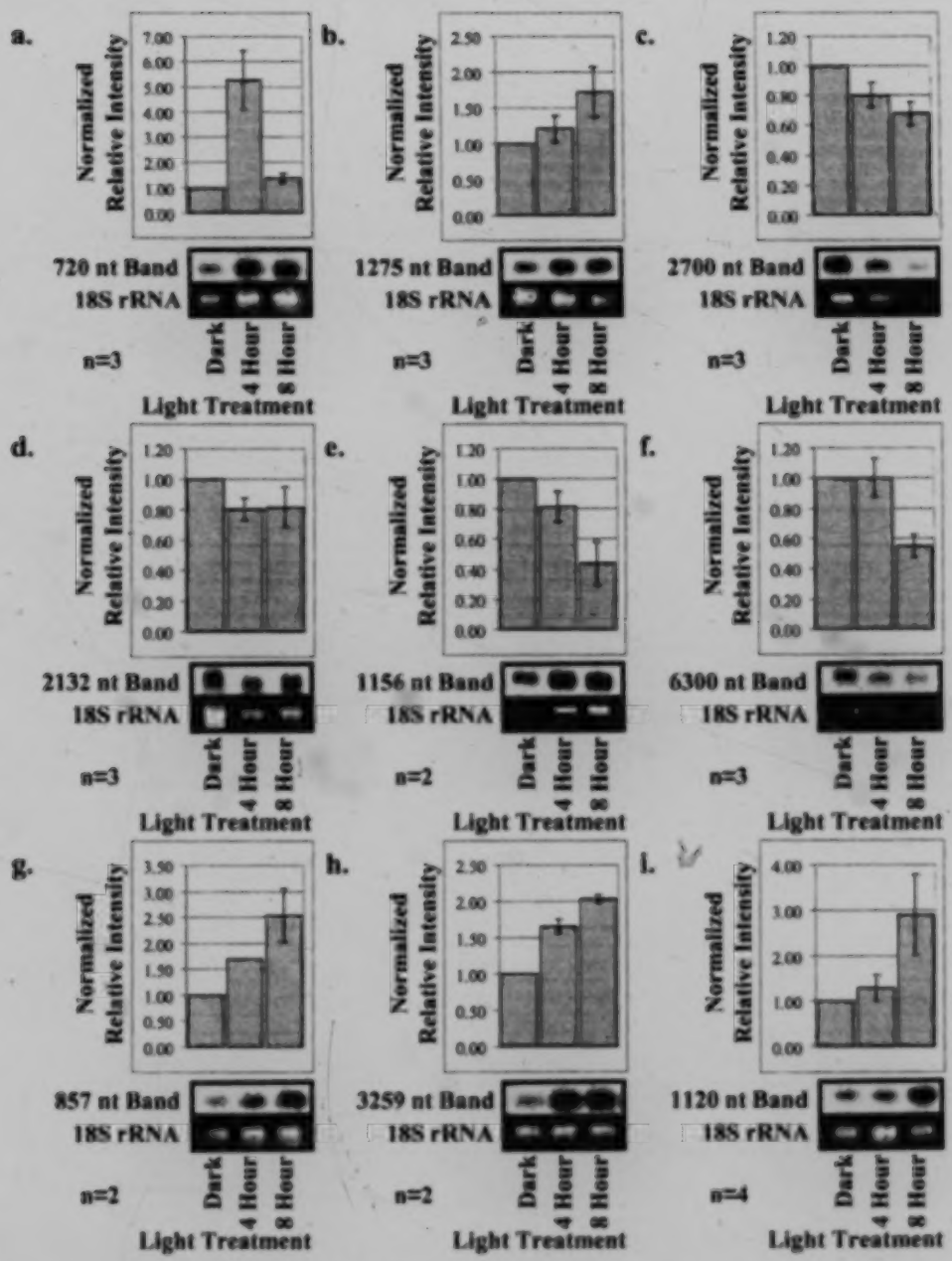

Figure 3-3. Normalized Relative Intensity of Autoradiograph Bands of LIRD Northern Blots Probed with Clones Identified in the Differential Cross Screen of the 4 Hour Library.

a. Clone 22.07, **b.** Clone 113.02, **c.** Clone 38-3, **d.** Clone G151, **e.** Clone 44-5, **f.** Clone 226-1, **g.** Clone 4-3, **h.** Clone 56:66-3, **i.** Clone 40-4

Error Bars indicate the standard deviation of the sample set where n>2, and the mean difference between blots where n=2. Autoradiograph band intensity determined by densitometry is normalized to the intensity of the ethidium bromide stained 18S rRNA band of the gel from which the Northern blot was made. A representative autoradiograph is shown for each clone.

Clone 113.02 has also been confirmed as being differentially expressed , though the difference in expression is far less pronounced than that of clone 22.07 (**Figure 3-3b.**). The 1275 nt mRNA represented by this clone's insert is expressed at levels 1.21 times higher (±0.18 s.d., n=3) in 4 Hour retinae than in Dark retinae. The standard deviation suggests that the expression could be very close to Dark levels, but given the pronounced increase in signal intensity to 1.72 times (±0.35 s.d., n=3) Dark levels after 8 hours of light treatment (8 Hour), it is more likely that the levels of this mRNA are elevated with the 4 Hour treatment rather than depressed.

Clone 38-3 is confirmed as being differentially expressed (**Figure 3-3c.**). Levels of the 2700 nt mRNA represented by this clone's insert with the 4 Hour treatment are 0.80 (±0.09 s.d., n=3) times those of the Dark treatment, and this decrease continues with the 8 Hour treatment to 0.68 (±0.08 s.d., n=3).

Clone G151 is confirmed as being differentially expressed. The 2132 nt mRNA represented by this insert with the 4 Hour treatment is 0.80 (±0.07 s.d., n=3) times the level found with the Dark treatment (**Figure 3-3d.**).

Clone 44-5 is confirmed as differentially expressed. The 1156 nt mRNA represented by this clone's insert shows a decrease in levels from the Dark treatment to 0.81 (±0.10 s.d., n=2) with the 4 Hour treatment, and the decrease in levels to 0.44 (±0.14 s.d., n=2) with the 8 Hour treatment is pronounced (**Figure 3-3e.**).

The mRNA represented by clone 226-1 is differentially expressed over the course of treatments represented by the LIRD profile (**Figure 3-3f.**). The most marked change is the decrease seen with the 8 Hour treatment to 0.55 (±0.07 s.d., n=3) times the Dark levels. There is no apparent change in the levels of the 6300 nt mRNA, 1.00 (±0.13 s.d., n=3) with the 4 Hour treatment. The most likely reason that this clone survived three separate screens with Dark and 4 Hour cDNA is that the clone's insert contains sequence that is hybridized to by more than one cDNA species, *i.e.* the insert of clone 226-1 represents a gene from a well-conserved gene family. When the radioactive cDNA probes hybridize to the plaque lifts or PCR Southern blots (Section **2-I**), all the cDNA species that are complementary to portions of the insert compete in binding to the inserts. When the insert of clone 226-1 is used as a radioactive probe of a Northern blot (Sections **2-E** and **2-K**), only a single radioactive cDNA species is present, and the kinetics of the

reaction drive the hybridization of the probe to its best match (Young and Anderson, 1985). A long exposure (16 days) of one of the 3 Northern blots probed reveals two other bands detected by the probe derived from the insert of clone 226-1.

The 4 Hour treatment increases the levels of expression of the 857 nt mRNA represented by clone 4-3 to 1.70 (±0.01 s.d., n=2) times the levels of the Dark treatment. This trend continues with the 8 hour treatment which increases the levels to 2.54 (±0.50 s.d., n=2) times (**Figure 3-3g.**).

Clone 56:66-3 has an insert representing a 3259 nt mRNA that is differentially expressed in the LIRD profile (**Figure 3-3h.**). With the 4 Hour treatment, the levels of this mRNA increase from Dark levels to 1.65 (±0.10 s.d., n=2) times, and with the 8 Hour treatment the increase is even more pronounced to 2.04 (±0.05 s.d., n=2).

The 1120 nt mRNA represented by clone 40-4 is differentially expressed in the LIRD profile (**Figure 3-3i.**). The level of expression is higher with the 4 Hour treatment, 1.28 (±0.28 s.d., n=4) times, and this level actually rises steeply to high levels with the 8 Hour treatment 2.89 (±0.88 s.d., n=4) times Dark levels.

3-D Discussion

The differential cross screen of the 4 Hour library successfully identified clones with mRNAs that are differentially expressed between the Dark treatment and the 4 Hour treatment (Section **2-B**) of rat retinae. Northern analysis, using LIRD Profiles, of a representative sample (9/167 = 5%) of the sequenced clones identified as differential by the secondary and tertiary screens confirms that all 9 of the clones are differentially expressed after treatment with light for either 4 or 8 hours. Of the 9 clones, 8 (89%) of them represent mRNAs that are differentially expressed after 4 hours of light treatment. This is important since it establishes confidence that the majority of the other clones identified in the screen will also be differentially expressed.

The differential cross screen of this study identified 167 clones that were putatively differentially expressed in untreated and 4 hour light-treated rat retinae. This is a sizeable pool of clones from which to begin an analysis of the molecular biology of rat retinae after 4 hours of light treatment. While the differential screen is considered to be successful, its success is based on the confirmation of the differential status of 5% of the 167 mRNAs by Northern analysis. Northern analysis is the definitive determinant of

differential gene expression because the hybridization of one probe to the blot representing the RNA present in a given condition is specific. The kinetics of a multi-species probe hybridization, as in the screens, are more complicated and prone to error (Britten and Davidson, 1985; Young and Anderson, 1985). In the case of the present study, the differential cross screen seems to have been at least 89% successful, as determined by Northern analysis.

The end result of this phase of the study is that 167 clones were considered suitable candidates for further characterization including sequencing. Their suitability was based on the fact that they could be considered with confidence to largely consist of clones representing mRNAs differentially expressed between the two conditions: dark-reared rat retinae exposed to either no light or 4 hours of intense green light.

Chapter 4 Sequence Analysis

Chapter 4 Sequence Analysis

4-A Sequence Analysis

Differential cross screening of a cDNA library derived from mRNA isolated from the retinae of dark-reared rats treated with 4 hours of intense green light (4 Hour library) resulted in the isolation of 210 clones (**Chapter 3**). To date, 167 clone inserts have been sequenced[32] (Section **2-J**). The average length of quality sequence per insert was 405 nucleotides (n=167). Only 1% of the clones had the poly(A) tail cloned incorrectly at the SK/T3/*Eco*RI sites, indicating that the ligation of the phage arms to the inserts occurred as expected. Of these 167, 121 (72%) have been assigned a gene identity. The remaining 46 (28%) clone sequences do not correspond to anything in the National Institute of Health's (NIH) National Centre for Biotechnology Information (NCBI) GenBank database (Altschul *et al.*, 1990, 1997) and therefore represent novel rat gene sequences.

4-A1 Photoreceptor Cell Sequences: Rod photoreceptor function is impaired in light-treated rat retinae (Organisciak *et al.*, 1992b, 1995, 1999b), so it is expected that there will be a change in expression of mRNAs for visual transduction and rod outer segment (OS) proteins. Some of the sequenced clone inserts (8/121, 7%; Section **4-I**, Table 4-9.) represent mRNAs for photoreceptor proteins, and provide further evidence, beside the confirming Northern analysis (Section **3-C**), that the differential cross screen identified mRNAs that should be differentially expressed between untreated (Dark) and 4 hour intense green light-treated (4 Hour) retinae of dark-reared rats.

4-A2 Novel and Unidentified Clones: Of the 46 unidentified clones, there are 15 clones (33%) that are considered to represent novel mRNAs because they have been sequenced and exhaustively analyzed with only hints as to their identity, despite good sequence data. The remaining 31 clones (67%) that are considered to be unidentified because no significant identity can be assigned to them, but the sequence data are poorer[33], arguing another explanation for the lack of identification beside novelty.

---

[32] 43 clones of the 210 which were to be sequenced did not survive a refrigerator's malfunctions.
[33] These sequences were either less than 130 nt in length, or had a significant proportion (>5%) of undistinguishable nucleotides in repeated sequencing attempts.

4-A3 Orthologous Sequences: Among the 121 sequenced clones with known or putative identities are 86 (71%) mRNAs that have *Rattus* spp. identities. The other 35 (29%) mRNAs have strong sequence identity to 31 (26%) mouse and 4 (3%) human sequences (**Figure 4-1.**). The 35 non-rat sequences were taken to represent mRNAs that are orthologous, *i.e.* derived from the same ancestral gene (**Figure 4-2.**), to mRNAs from currently uncharacterized rat genes. When the comparison is between two closely related species like rat and mouse (33 million year separation), or rat and human (96 million year separation; Section **5-E**, **Figure 5-1.**, Nei *et al.*, 2000), strong sequence identity is a good indication that the genes are orthologous and that the gene products share similar functions in both species. The identification of these 35 putative orthologues represents the first time that these genes have been identified in rats.

4-B Classification of Identified Clones

The 121 clones with known or putative identities have been classified into 12 divisions depending on the reported function of the gene product that each clone's mRNA encodes. The classifications are (**Figure 4-1.**): Stress-related (22, 18%), Energy Metabolism (18, 15%), RNA Synthesis [16, 13%; Transcription (9, 7%); Pre-mRNA Processing (7, 6%)], Translation [14, 12%; Ribosomal Protein (10, 8%); Post-translational Modification (4, 3%)], Signalling (13, 11%), Membrane (10, 8%), Photoreceptor Cell (8, 7%), Cytoskeleton (6, 5%), Apoptosis-related (4, 3%), Protein Degradation (4, 3%), Cell Interaction (3, 2%), and Other (3, 2%). In Tables 4-1.-4-14. gene identities are indicated by gene symbol. When the sequence correspondence is to another species it is followed by an abbreviation of the species name. A descriptive name for the gene product is given in **Appendix 2**.

4-C Stress-related Sequences (22, 18%)

The clones classed as Stress-related (Table 4-1.) are almost all representative of crystallin genes. In mammals there are three crystallin families: α-, β-, and γ-crystallins. The α- and β-crystallins are divided into acidic (A) and basic (B) groups. The classification Stress-*related* is significant since the crystallins identified in this screen have not been unequivocally identified as stress proteins. The only crystallin to be normally classed as a stress response protein, αB-crystallin (Cryab), is absent from the

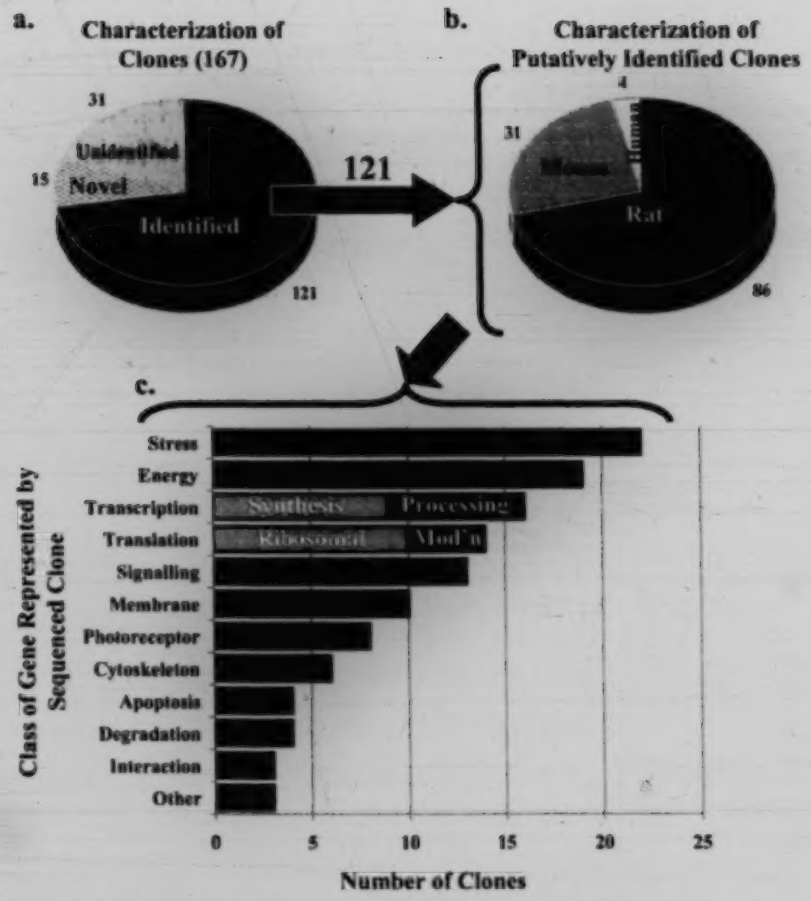

Figure 4-1. Class Distribution of Sequenced Clones.

a. Of 167 sequenced clones, 15 are considered novel, 31 are considered unidentified, and 121 are putatively identified.

b. Of the 121 putatively identified clones, 86 have sequence identity with rat genes, 31 have identity with mouse genes, and 4 have identity with human genes.

c. The 121 putatively identified clones were divided into 12 groups based on the known function of the gene product.

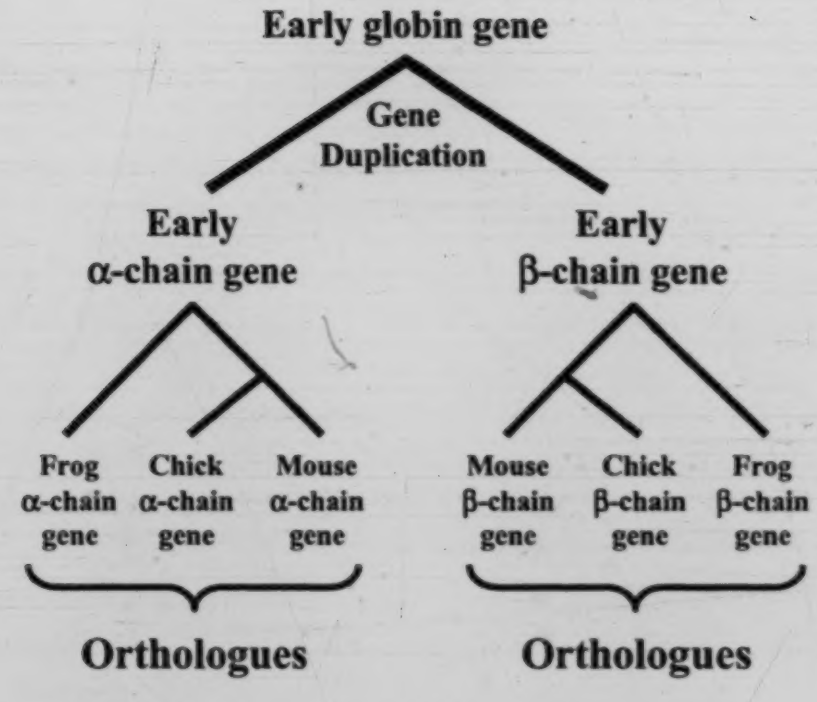

Figure 4-2. Orthology. (After Fassler *et al.*, 2000)
Orthologous genes are genes from different species that are derived from a single common ancestor.

long list of crystallins identified in this study[34]. The other crystallins are all suspected of being involved in a cellular response to stress, but are not positively confirmed as being induced by stress. In fact, the only confirmed biological role of crystallin proteins is their role as the major structural protein of the lens where they function to maintain lens clarity (Wistow and Piatigorsky, 1988; Horwitz *et al.*, 1993, 1998, 1999). The overlap between their suspected role and their confirmed role comes from the likelihood that the crystallins function to maintain clarity in the lens by preventing the aggregation of proteins in the lens that result in opaque inclusion bodies that develop into cataracts (Hejtmancik, 1998).

Table 4-1. Sequence Identities of Stress-related Clones (*Mm - Mus musculus*)

Clone	Sequence Length	Gene Symbol	Accession	Accession Match	E-value
70G80.09	465	Cryaa	NM_012534	1-465/663-1123(97%)	0.00E+00
22G29-8	875	Cryaa	U47922	22-720/137-839(96%)	0.00E+00
287	477	Cryaa	NM_012534	7-467/589-1049(99%)	0.00E+00
270	743	Cryaa	NM_012534	4-731/188-910(98%)	0.00E+00
6	877	Cryaa	NM_012534	14-737/190-904(97%)	0.00E+00
113.02	316	Cryaa	NM_012534	1-316/810-1125(100%)	1.00E-177
567T	412	Cryaa	NM_012534	6-353/141-484(86%)	2.00E-86
629.05	107	Cryaa	NM_012534	1-95/955-1049(93%)	6.00E-35
279.01	156	Cryaa	U47922	23-94/174-248(96%)	2.00E-19
22.07	177	Cryba1	AJ239052	1-160/20-182(94%)	1.00E-160
375T	237	Cryba2 (*Mm*)	NM_021541	1-237/322-558(95%)	1.00E-105
122	728	Cryba4	AF013247	66-701/654-18(97%)	0.00E+00
74G84-3	462	Crybb1	X05900	1-460/186-646(98%)	0.00E+00
567M	470	Crybb1	AF286652	31-470/1-440(100%)	0.00E+00
4-3	414	Crybb2	NM_012937	1-410/102-511(97%)	0.00E+00
193-3	607	Crybb2	NM_012937	1-590/65-651(98%)	0.00E+00
133.10	288	Crybb3	AF287304	12-249/181-416(94%)	4.00E-99
491M2	115	Crybb3	NM_031690	14-106/655-747(98%)	7.00E-43
226	630	Crygb	M19359	273-679/19098-19452(99%)	0.00E+00
38G48.03	580	Crygs (*Mm*)	NM_009967	{1-523/108-631(91%} {511-578/632-699(94%)}	0.00E+00
40-4	615	Crygs (*Mm*)	NM_009967	{39-541/127-631(91%)} {529-593/632-696(95%)}	1.00E-179
56G66-3	133	Hspca	AJ428213	1-66/1796-1861(96%)	1.00E-23

In this class, the exception to the crystallins is Hsp90 (Hspca), which is a known stress-response protein. Hsp90 is an ATP-dependent chaperone that promotes the correct folding of unfolded proteins. Hsp90 is expressed at all times, but transcription and

[34] However, Northern analysis (Section **7-B**, **Figure 7-3b.**) does show that Cryab is present in rat retina.

translation increases in the face of stress of many sorts, including oxidative stress (Fink, 1999; Frydman, 2001).

This study suggests very strongly that an examination of the role of the entire crystallin protein family in stress is necessary. Prior to this work it was not generally accepted that the majority of the crystallins had a significant function outside the lens. As well, the lack of identification of well-characterized stress response proteins may indicate that stress response in the retina is a very distinct process that makes use of cellular pools of stress response proteins supplemented by the recruitment of the crystallins.

4-D Energy Metabolism Sequences (18, 15%)

Table 4-2. Sequence Identities of Energy Metabolism Clones (*Mm* - *Mus musculus*)

Clone	Sequence Length	Gene Symbol	Accession	Accession Match	E-value
5.06	414	Aldh2	X14977	1-196/1448-1647(95%)	4.00E-75
115-3	527	Aldoc	NM_012497	1-522/1061-1581(98%)	0.00E+00
20:27	717	Aldr1	X05884	2-568/109-672(98%)	0.00E+00
134-5	494	Atp5g2	D13124	5-494/1-490 (93%)	0.00E+00
50G60.04	152	Eno1	NM_012554	7-140/662-799 (96%)	7.00E-50
110B	200	Eno2	AF019973	19-200/1443-1623(96%)	3.00E-77
51.08	514	Fdps	M34477	1-514/176-689(99%)	0.00E+00
51.07	690	Fdps	M34477	1-890/139-822(97%)	0.00E+00
120.14	504	Gapdh	X02231	1-504/17-520(99%)	0.00E+00
38G48.02	296	Glb1 (*Mm*)	NM_009752	1-191/1510-1700(86%)	1.00E-40
249-5	334	Mipp65	AB000098	2-168/24-191(96%)	1.00E-81
130.11	538	Mtcyb	J01436	3-531/526-1075(95%)	0.00E+00
33G43.10	274	Mtcyb	J01436	1-270/1179-1455 (97%)	1.00E-126
4G10.02	207	Mtcyb	AF295545	24-149/39-172(91%)	2.00E-29
35G45.03	532	Mtco2	NC_001665	1-461/7028-7498(96%)	0.00E+00
129	398	Ndufa5	D86215	1-393/160-552(99%)	0.00E+00
276.09	146	Pkm2	NM_053297	18-57/771-809(97%)	4.00E-08
134-1	700	Pyp (*Mm*)	AK008575	40-672/105-742(91%)	0.00E+00

Energy production is an important element of normal cellular processes and the stress response. A significant proportion (4 clones; Mtcyb and Mtco2) of the identified clones represent mitochondrial encoded mRNAs, and many of the rest are elements of normal sugar metabolism in the cytosol (Table 4-2.). Two clones have been included in this class which are only peripherally involved in energy production. They both represent mRNA encoding farnesyl pyrophosphate synthetase (Fdps) which is involved in producing the 15 carbon farnesyl pyrophosphate. Farnesyl pyrophosphate is used to

modify proteins and is also further processed into important cofactors like sterol, the carotenoids, coenzyme Q, and heme a. As coenzyme Q is involved in energy production, the two clones were included in this class. With respect to the biology of the retina, farnesyl pyrophosphate is significant because it is a precursor to the carotenoids, some of which are in turn precursors to vitamin A, also known as retinol, which is converted into rhodopsin's cofactor, 11-*cis*-retinal (Voet and Voet, 1995). Further significance also comes from its connection to heme a, which is the substrate of the antioxidant proteins heme oxygenase 1 and 2 (Kutty *et al.*, 1995).

4-E RNA Synthesis (16, 13%)

4-E1 Transcription Sequences (9, 7%): This class of clones is defined by a direct involvement in the process of transcription, or at most one remove from transcription. This group of genes (Table 4-3.) includes four different transcription factors, three of which have not been previously characterized in rat, but have very good sequence identities with known mouse genes. The identification of transcription factors involved in a response to light treatment is intriguing since it is reasonable to suspect that at least one of the factors regulates several genes and so may orchestrate a specific gene program involved in retinal degeneration.

Two clones included in this class represent mRNAs for proteins that control the activity of transcription factors, *i.e.* they are once removed from the process of transcription and actually control the activity of transcription factors. One of these mRNAs is for the α subunit of the transcriptional regulator, IκB (Nfkbia), which sequesters the transcription factor nuclear factor κB (NFκB) in the cytosol until IκB is proteolytically cleaved. Significantly, IκB gene expression is controlled by NFκB, so the upregulation of the IκBα transcript indicates that some gene expression in light-induced retinal degeneration (LIRD) is mediated by NFκB (Lewin, 1997).

The mRNA for another very important regulator of a transcription factor in mice was also identified using the rat sequence of one of the isolated clones. This regulator is the protein cryptochrome 2 (CRY2, Cry2) which is involved in the regulation of the circadian rhythm in mice. CRY2 is a nuclear protein that controls the levels of the PERIOD protein in the nucleus. Together CRY2 and PERIOD control the ability of the heteromeric CLOCK-BMAL1 transcription factor to initiate transcription (Sancar, 2000).

Since other investigators have noted a circadian component to LIRD (Organisciak *et al.*, 2000; Vaughan *et al.*, 2002), the identification of this mRNA may be of some significance.

One of the clones placed in this class represents a mRNA whose sequence has good correspondence[35] to a mouse sequence that encodes a subunit of mouse RNA polymerase II (Polr2h). This is interesting at a general level, because it points out the fact that RNA polymerase II has not yet been characterized fully in rats.

Table 4-3. Sequence Identities of Transcription-related Clones (*Mm* - *Mus musculus*)

Clone	Sequence Length	Gene Symbol	Accession	Accession Match	E-value
51.09	161	Cntf (*Mm*)	U05342	2-161/90-252(96%)	4.00E-73
226-1	488	Cry2 (*Mm*)	AF156987	1-320/151-470(96%)	1.00E-152
2G8-4(T)	151	Ctbp1	AF067795	1-147/1780-1926(95%)	5.00E-60
48G58-4	682	Ctbp1	AF067795	0-666/1770-2425 (98%)	0.00E+00
119-5	937	Lztr1 (*Mm*)	NM_025808	{1-393/750-1142(96%)} {392-789/1348-1745(89%)}	0.00E+00
169.04	141	Nfkbia (*Mm*)	U57524	22-125/78-186(89%)	7.00E-22
58.04	165	Polr2h (*Mm*)	BC002306	15-165/71-221(97%)	2.00E-69
185-2B	385	Tceb2	L42855	1-343/15-357(99%)	0.00E+00
89-2	432	Tcfl4 (*Mm*)	NM_011550	{3-375/208-577(94%)} {403-429/602-628(92%)}	1.00E-160

4-E2 Pre-mRNA Processing Sequences (7, 6%): This class of mRNAs is represented largely (6 clones; Table 4-4.) by pre-mRNA splicing factors that generate mature mRNA by removing introns (Kim *et al.*, 2001), suggesting that LIRD is characterized by a change in the tempo of transcription. This study is the first time that five of the splicing factors have been putatively identified in rat. The sequences of these five clones have good correspondence to mouse or human gene sequences. Three have identity to mouse transcripts, and two have identity with transcripts that encode human proteins that are homologous to the *Saccharomyces cerevisiae* protein Upf3 (Upf3b).

The last clone identified in this class has excellent sequence correspondence to the mRNA for the mouse DEAD-box 6 protein (DDX6, Ddx6), which has not yet been identified in rat. The function of this protein is unclear, but DDX6 in mice is considered to be an RNA helicase involved in RNA splicing, translation initiation and assembly of active ribosomes. Its name derives from the aspartate-glutamate-alanine-aspartate

(DEAD) motif that it contains (Akao and Matsuda, 1996; Smillie and Sommerville, 2002).

Table 4-4. Sequence Identities of Pre-mRNA Processing Clones
(*Mm* - *Mus musculus*, *Hs* - *Homo sapiens*)

Clone	Sequence Length	Gene Symbol	Accession	Accession Match	E-value
25	661	Ddx6 (*Mm*)	NM_007841	25-425/1-406(91%)	1.00E-155
16G23.05	526	Hnrpc (*Mm*)	AK019958	1-179/104-283(94%)	3.00E-70
16G23.11	297	Hnrpc (*Mm*)	AK019958	2-157/77-233(93%)	1.00E-52
223-1	388	Rrp41 (*Mm*)	BC012277	1-257/354-613(92%)	3.00E-91
49G59-1	819	Sfrs5	L13635	16-762/325-1075 (98%)	0.00E+00
373T	520	Upf3b (*Hs*)	NM_080632	26-388/843-1205(87%)	7.00E-96
353.06	438	Upf3b (*Hs*)	NM_080632	1-308/898-1205(86%)	1.00E-72

4-F Translation (14, 12%)

4-F1 Ribosomal Sequences (10, 8%): The majority of the mRNAs in this class are for ribosomal proteins (Table 4-5.). This signifies that there is a potential change in the translation activity of retinal ribosomes. This change in expression has been investigated by another researcher in the lab, so mentioning this study's results is intended only as confirmation that we see similar changes (Stepczynski, 2001). The mRNAs for ribosomal proteins L7a (Rpl7a), L10a (Rpl10a), L19 (Rpl19), L34 (Rpl34), L41 (Rpl41), P1 (Rplp1) and S3 (Rps3) were identified in this screen. The most interesting of these proteins is RPS3, a component of the small (40S) ribosomal subunit, which is implicated in repair of UV damage to DNA (Kim *et al.*, 1995a) and in the active domain of translation in the ribosome. Another significant point about RPS3 is that RNA processing of the RPS3 mRNA generates a small nucleolar RNA (snoRNA) of unknown function, although snoRNAs are found in the nucleolus where pre-mRNA processing occurs (Tycowski *et al.*, 1993; Kiss, 2002). The other proteins are components of the large (60S) ribosomal subunit.

One clone in this class represents the mRNA for a non-ribosomal protein, ATP-Binding Cassette protein (ABC50, Abcf1), which is a modulator of the activity of eukaryotic initiation factor2 (eIF2). Although ABC50 is not a ribosomal protein, it is included in this class because of its intimate association with eIF, an important element

[35] This study considers a match to be excellent if the E-value obtained is between 0 and 10^{-150}, while a match is considered good if the E-value is between 10^{-150} and 10^{-50}.

for translation initiation. The activity of ABC50 is to increase eIF2's affinity for charged methionyl-tRNA. This increase in affinity is linked to the concentration of ATP available for ABC50 to bind, which provides another link to increased energy requirements in a light treated rat retina (Richard *et al.*, 1998).

Table 4-5. Sequence Identities of Ribosomal Clones (*Rr* - *Rattus rattus*)

Clone	Sequence Length	Gene Symbol	Accession	Accession Match	E-value
373B	400	Abcf1	AF293383	30-397/2612-2980(98%)	0.00E+00
53-1	244	Rnr(1-5)	X03838	65-204/1960-1821(94%)	3.00E-53
69-1	607	Rpl7a	X15013	1-607/55-657(98%)	0.00E+00
69-2	732	Rpl7a	X15013	11-628/107-725(97%)	0.00E+00
69G79	337	Rpl10a	NM_031065	1-172/14-188(98%)	1.00E-84
190-5	118	Rpl19	NM_031103	5-114/576-689(95%)	1.00E-38
22G29-5	566	Rpl34 (*Rr*)	X14401	157-552/21-410(99%)	0.00E+00
27-5(B)	323	Rpl41	X82550	7-295/69-357(98%)	1.00E-155
407M	474	Rplp1 (*Rr*)	X15097	21-465/22-467(99%)	0.00E+00
100.10	601	Rps3	X51536	1-601/40-642(98%)	0.00E+00

4-F2 Post-translational Modification Sequences (4, 3%): The sequences of the clones in this class generally have good correspondence to (Table 4-6.) mouse (3 clones), or human (1 clone) mRNAs that code for proteins that modify other proteins either through direct covalent modification, like the transfer of a SO_4^{2-} group by the mouse sulfotransferase (Chst1; Hemmerich *et al.*, 2001), through cellular localization, like the endoplasmic reticulum proteins mouse Sec3 (Sec3; Brymora *et al.*, 2001) and human Sec62 (Tloc1; Daimon *et al.*, 1997), or through protein folding, like the mouse peptidylprolyl isomerase, forkhead binding protein2 (FKBP2, Fkbp2; Patterson *et al.*, 2002).

Table 4-6. Sequence Identities of Post-translational Modification Clones (*Mm* - *Mus musculus*, *Hs* - *Homo sapiens*)

Clone	Sequence Length	Gene Symbol	Accession	Accession Match	E-value
46.13	534	Chst1 (*Mm*)	NM_023850	{20-244/129-353(93%)} {242-531/1706-1992(90%)}	7.00E-90
32-2	258	Fkbp2 (*Mm*)	NM_008020	1-258/32-289(96%)	1.00E-119
186-4	570	Sec3 (*Mm*)	BC024678	82-555/1230-1699(92%)	0.00E+00
60G70-2	825	Tloc1 (*Hs*)	U93239	{220-296/1933-2009(98%)} {448-546/2178-2277(91%)} {343-423/2064-2147(91%)}	3.00E-32

Changes in expression of the rat protein clusterin have been associated with retinal degeneration (Wong *et al.*, 1994a,b, 2001), so it is significant that three of these

proteins fulfill roles related to proteins implicated in rat clusterin biogenesis. Clusterin is translated in and transported through the endoplasmic reticulum in a process dependent on at least one Sec protein. When clusterin reaches the Golgi apparatus, it is modified by the addition of an amino modified sugar (Kapron *et al.*, 1997). Sulfotransferase has been identified as localized to the Golgi apparatus where it acts to transfer SO_4^{2-} to galactose residues (Hemmerich *et al.*, 2001).

4-G Signalling Sequences (13, 11%)

Table 4-7. Sequence Identities of Signalling Clones (*Mm* - *Mus musculus*)

Clone	Sequence Length	Gene Symbol	Accession	Accession Match	E-value
102-3	161	Gnai2	NM_031035	1-161/901-1062(96%)	2.00E-71
18G25-5	783	Gnai2	M12672	1-730/877-1610 (97%)	0.00E+00
16G23.09	553	Gpr19 (*Mm*)	BC021648	1-549/164-700(89%)	1.00E-145
46.11	661	Hspc121 (*Mm*)	Z97207	125-661/1-535(96%)	0.00E+00
45.05	607	Hspc121 (*Mm*)	Z97207	19-500/1-494(92%)	1.00E-172
108-4	827	Il6st	M92340	1-745/2083-2833(95%)	0.00E+00
68.03	353	Itpr2	X61677	2-352/3017-3367(99%)	0.00E+00
611.02	921	Pak1	NM_017198	122-276/646-800(83%)	9.00E-29
639.09	144	Pld3 (*Mm*)	NM_011116	1-106/188-296(89%)	4.00E-14
88-2	523	Rala (*Mm*)	BE311008	117-459/1-350(89%)	1.00E-108
162-2	277	Stmn1	M27876	24-183/646-488(98%)	5.00E-77
326.02	499	Ywhab	NM_019377	12-499/25-510(99%)	0.00E+00
110T	570	Ywhag	NM_019376	1-558/2424-2979(98%)	0.00E+00

While it is hard to separate signalling from all other elements of the cell, especially the cytoskeleton and the membrane, the clones in this class (Table 4-7.) represent genes that code for proteins that are apparently involved in the initial steps of the pathways of various signal cascades. The number of clones included in this class of genes suggests that retinal cells actively respond to light-induced changes in the tissue environment. Signalling pathways implicated by these clones include those activated by G-protein coupled receptors, interleukin-dependent signalling, and inositol triphosphate-mediated signalling. A novel rat transcript with high similarities to the expressed sequence of mouse butyrate-induced 1 (B-IND1, Hspc121; Courilleau *et al.*, 2000) was identified twice in the current study. In mice, this protein is implicated in the modulation of the activity of the GTPase Rac1 activity which in turn acts to activate c-Jun N-terminal kinase (JNK) which is a pro-apoptotic event, but may be anti-apoptotic in its interaction with phosphoinositol-3 kinase (PI3K). Rac1 also interacts with the transcription factor

NFκB. B-IND1 may be an important regulator of the retinal response to light damage, and has not previously been characterized in rat.

4-H Membrane Sequences (10, 8%)

This class of genes (Table 4-8.) encodes proteins that are involved with vacuolar or cell membrane function which have been associated with protein function at neural synapses. This is significant because photoreceptor cells contain a relatively unique structure at the synaptic end of the photoreceptor cell, the ribbon synapse (Oyster, 1999). The ribbon synapse is a structure unique to synapses, like photoreceptor cells and cochlear hair cells, that are providing constant signals to their connecting neurons. The constant traffic of neurotransmitter means that the neurotransmitter must be delivered to the cell membrane for exocytosis at a very fast pace, and the ribbon of the ribbon synapse is postulated to localize and guide neurotransmitter-containing vacuoles to the cell membrane (Lenzi and von Gersdorff, 2001). In a degenerating retina, it is reasonable to assume that there will be a change in the volume of neurotransmitter release, and therefore a change in the requirement for the proteins that modulate this release.

Ca2+-dependent activator protein (CAPS, Caps) is an essential protein found in neuroendrocrine cells as a dimer. It acts to stimulate secretion of hormones on receipt of a neural signal in the form of an increase in concentration of Ca^{2+} (Ann *et al.*, 1997). Complexin II is a protein involved in neurotransmitter release. In conjunction with complexin I it interacts with SNARE[36] complexes to allow the release of neurotransmitters. Complexin I and complexin II (Cplx2) are redundant, but the double knockout mutation is lethal in mice (McMahon *et al.*, 1995; Reim *et al.*, 2001). SNAREs work by binding SNAPs on intracellular vesicles, which results in disruption of the SNARE and subsequent membrane fusion allowing exocytosis. This is generally effected by a change in Ca^{2+} concentration. The rat SNAP25 interacting protein 30 (Sip30; Lee *et al.*, 2002) was also identified in this study and has been specifically implicated in the transfer of neural information from photoreceptor cells to the neurons, as has the rat orthologue of Human Retinal Gene 4 (HRG4), Rat Retinal Gene 4 (RRG4, Unc119; Higashide *et al.*, 1998).

[36] SNAP [soluble NSF (N-ethylmaleimide-sensitive factor) attachment protein] receptor.

The mRNA for the mouse VAMP-associated protein B[37] has good correspondence with the sequence of one of the clones included here, and VAP-B (Vapb) is also connected to vesicular activity through SNAREs (Nishimura *et al.*, 1999). As well, the mouse gene, Schwannomin interacting protein (SchIP1, Schip1; Goutebroze *et al.*, 2000), has excellent correspondence with another clone sequence included in this class, and may be significant because in mice it interacts with neurofibromatosis type 2 protein, which has been characterized as a tumour suppressor that acts as the bridge between membrane-bound proteins and the cytoskeleton.

Table 4-8. Sequence Identities of Membrane Clones (*Mm* - *Mus musculus*)

Clone	Sequence Length	Gene Symbol	Accession	Accession Match	E-value
41-4	647	Atp1a2	NM_012505	29-647/4057-4675(98%)	0.00E+00
39-4	479	Atp6n1a	M58758	58-471/3286-3700(99%)	0.00E+00
96-2	793	Caps	NM_013219	237-700/4126-4589(94%)	0.00E+00
652.05	309	Cplx2	U35099	1-309/414-722(98%)	1.00E-160
42G52	478	Mel (*Mm*)	NM_023126	13-478/36-501(97%)	0.00E+00
407T	598	Prph	NM_013021	19-594/884-1456(97%)	0.00E+00
67G77.02	531	Schip1 (*Mm*)	AK021361	53-531/2-479(94%)	0.00E+00
44-5	611	Sip30	AF439397	9-593/22-605(99%)	0.00E+00
45.02	344	Unc119	NM_017188	1-217/587-807(96%)	2.00E-95
4-4	578	Vapb (*Mm*)	BI455979	184-539/180-536(88%)	4.00E-79

The mRNAs for the Na^+, K^+ ATPase (Atp1a2) and the proton pump (Atp6n1a) could be related to mitochondria and so might need to be reclassified as Energy Metabolism mRNAs, but the initial literature consulted implied that they were cell membrane proteins (Shull *et al.*, 1986; Perin *et al.* 1991).

Vacuolar and plasma membrane interactions at the synaptic terminal are of definite importance in a photoreceptor cell, but an equally important vacuolar and plasma membrane interaction occurs at the other end of the cell body at the junction of the cell body with the OS (**Figure 1-2.**). Rhodopsin translated in the cell body is transported through the endoplasmic reticulum to the Golgi apparatus where vacuoles containing the membrane-bound rhodopsin are pinched off and flattened for transport to the OS where they replace aging OS lamellae, which are the platform for phototransduction. The lamellae are transported from the cell body to the OS along the cilium that connects the inner and outer segment of the photoreceptor (**Figure 1-2.**) in some unknown fashion

[37] VAMP (vesicle associated membrane protein)-associated protein B (VAP-B).

(Oyster, 1999; Moritz *et al.*, 2001). While the exact mechanism of transport is not known, it has been shown in *Xenopus laevis* that impairment of Rab8 (Mel) function by mutation impairs this process and results in retinal degeneration in the frog (Moritz *et al.*, 2001). The exact role of Rab8 is not yet known, so it is unclear whether it functions at the synaptic terminal, at the connecting cilium, or at both. It is also possible that SchIP1, Sip30, and VAP-B are involved in both the release of neurotransmitter and the transportation of new OS lamellae.

4-I Photoreceptor Cell Protein Sequences (8, 7%)

Table 4-9. Sequence Identities of Photoreceptor Cell Clones (*Mm* - *Mus musculus*)

Clone	Sequence Length	Gene Symbol	Accession	Accession Match	E-value
7	740	Gnat1 (*Mm*)	BC022793	31-650/1475-2093(89%)	0.00E+00
249-3	441	Prph2 (*Mm*)	BC026484	173-202/2313-2342(96%)	5.00E-04
721	751	Rho (*Mm*)	BC013125	20-687/1882-2544(88%)	0.00E+00
151	452	Rho	Z46957	6-452/7-453(97%)	0.00E+00
597.02	125	Rho	Z46957	4-106/14-118(95%)	5.00E-35
293	787	Sag	X51781	3-785/532-1306(97%)	0.00E+00
67G77.08	411	Sag	X51781	1-411/789-1206(96%)	0.00E+00
33G43.05	493	Sag	X51781	{208-479/1091-1362(100%)} {1-149/690-838(100%)}	1.00E-158

Some of the sequences of the clones in this class (Table 4-9.) were identical to the mRNAs of the rat genes: rhodopsin (Rho; 2 clones), and S-antigen (Sag; 3 clones). The mRNAs for the mouse genes transducin 1 (Gnat1), peripherin 2 (Prph2), and rhodopsin (Rho) had identity to the sequence of three separate clones included in this class. Rhodopsin mutations are associated with human retinal degeneration diseases (Bunge *et al.*, 1993), and there is evidence in *Drosophila melanogaster* that the inability to properly localize rhodopsin is responsible for photoreceptor cell death (Davidson and Steller, 1998). S-antigen is the rat arrestin, the protein which causes the dissociation of retinal from activated rhodopsin to end the visual signal (Section **1-A2**, **Figure 1-4.**). Mutant arrestin has been shown to form stable complexes with rhodopsin in *D. melanogaster* which result in photoreceptor cell death (Alloway *et al.*, 2000). This arrestin-rhodopsin complex-induced cell death could be prevented by depleting either protein in the cell. Peripherin 2 has been identified as the cause of the retinal degeneration slow (rds) phenotype in mice (Petersen-Jones, 1998). Like S-antigen, peripherin 2 also has a connection to compromised protein trafficking in the photoreceptor cell since it is

normally found as a glycoprotein on the membranes of OS lamellae of the photoreceptor cell where it is suspected it acts to control the structure of the lamella (Arikawa, 1992).

4-J Cytoskeleton Sequences (6, 5%)

Changes in the cytoskeleton could be indicative of gross morphological changes in the cell, but a more subtle function of the cytoskeleton is to act in signal transduction processes. The signals transduced by the cytoskeleton must derive from some component connected to the cytoskeleton (Table 4-10.). Tubulin (Tubg), and tau (Mapt) are involved in microtubule assembly, and tau is implicated in the neurodegenerative disorder, Alzheimer's Disease (Alonso *et al.*, 1996). The sequence of one clone has identity to that of the expressed sequence of the mouse gene talin (Tln). Talin has been implicated in organizing the interactions of vinculin and the integrins (Critchley *et al.*, 1999), and therefore provides a direct connection between the cytoskeleton and the extracellular matrix (ECM). The presence of Sharpin is the strongest suggestion that ECM-cytoskeleton-signalling cascades are an exceptionally important element of LIRD. Sharpin controls the interaction of Shank proteins which are a class of proteins that are hypothesized to be scaffold proteins that connect the cytoskeleton with membrane-bound receptors at synapses (Lim *et al.*, 2001).

Table 4-10. Sequence Identities of Cytoskeleton Clones (*Mm* - *Mus musculus*)

Clone	Sequence Length	Gene Symbol	Accession	Accession Match	E-value
353.03	267	Hnrpu	D14048	137-254/2467-2591(88%)	3.00E-16
63-2	702	Mapt	NM_017212	34-696/3885-4539(96%)	0.00E+00
200-5	180	Mapt	D30628	1-130/978-1107(98%)	1.00E-61
35G45.07	486	Sharpin	AF203906	1-356/586-941 (98%)	0.00E+00
33G43.07	580	Tln (*Mm*)	NM_011602	4-574/4835-5414(90%)	1.00E-174
170-4	595	Tubg	AB015946	31-595/533-1099(97%)	0.00E+00

4-K Apoptosis-related Sequences (4, 3%)

Two of the three mRNAs that these four clones represent, Pea15 and Rtn3 (Table 4-11.), are of interest because of their connection with the process of apoptosis. Neither has been identified as an important player in apoptosis, but both have been identified as peripherally involved. Their identification in this screen suggests that they may be more important than previously considered. (The identification of the mRNA for

Bcl-2 Antagonist of Cell Death needs to be taken very lightly since the alignment of the sequences is very poor, with an E-value of only 10^{-6}.)

The mRNA for the protein reticulon 3 (Rtn3) occurs only once in this class, and its identification attracts attention because the reticulon genes are widely expressed in the neuroendocrine system, and reticulon 3 has been localized to the endoplasmic reticulum (ER). The latter fact is interesting because a related human protein, reticulon XS has been identified as being able to interact with and localize Bcl-2 and Bcl-XL to the ER, acting as an apoptosis inhibitor (Moreira *et al.*, 1999).

Two clones identified in this screen represent the mRNA for astrocytic phosphoprotein, or phosphoprotein enriched in astrocytes (PEA15, Pea15). This small (15 kDa) protein has been noted as a substrate of protein kinase C, which provides a connection to at least one signalling cascade. PEA15 has also been localized to all brain cells, the eye, and astrocytes. In cells it is associated with microtubules, which provides a connection to the cytoskeleton, and it has been implicated in the transport of glucose across the cell membrane, connecting it to cell metabolism. Most importantly, this protein has been implicated as an astrocyte survival factor in mice exposed to tumour necrosis factor, and it has been suggested that the mechanism of protection is the binding of FADD[38] and caspase 8 (Danziger *et al.*, 1995; Estelles *et al.*, 1996; Kitsberg *et al.*, 1999). If some or all of these impressive hints as to the function of PEA15 can be confirmed, then PEA15 could turn out to be a major protective protein of astrocytes.

Table 4-11. Sequence Identities of Apoptosis-related Clones

Clone	Sequence Length	Gene	Accession	Accession Match	E-value
162-2	108	Bad	NM_022698	81-108/973-1000(100%)	7.00E-06
38-3	688	Pea15	AJ243949	10-663/1684-2341(96%)	0.00E+00
70G80.05	525	Pea15	AJ243949	241-525/1639-1937(90%)	8.00E-62
6.05	238	Rtn3	NM_080909	1-180/441-621(98%)	3.00E-90

4-L Protein Degradation Sequences (4, 3%)

The key component of proteasome-mediated protein degradation is the small protein ubiquitin, which is conjugated to proteins that are destined for degradation by the proteasome (Glickman and Ciechanover, 2002). The best sequence identity in this class

[38] Fas-associated via death domain.

(Table 4-12.) is that for the mRNA of the rat polyubiquitin gene (Ubb). The next best sequence identity is for a subunit of the proteasome (Psmb1) itself.

The sequence of clone 19-3 has strong identity to the sequence of another gene that is part of protein degradation, the gene for the small subunit of a rat calpain protein (Capns1). The calpains are calcium-dependent cysteine proteases, and although the exact nature of the calpains is not clear, they have been shown to be active proteases in response to changes in calcium levels (Arthur *et al.*, 2000).

Another sequence identity is for the human gene for the cullin 4B protein (Cul4b). In humans, the function of this protein is not clear, but it is part of a gene family that has been connected to proteasome degradation by virtue of its association with the family member, cullin 1. Cullin 1 acts with an E3 ubiquitin ligase complex, the complex that is involved in the final transfer of ubiquitin to the target protein (Kipreos *et al.*, 1996).

Table 4-12. Sequence Identities of Protein Degradation Clones (*Hs - Homo sapiens*)

Clone	Sequence Length	Gene Symbol	Accession	Accession Match	E-value
19-3	248	Capns1	U53859	2-81/952-1031(97%)	9.00E-32
74G84-4	436	Cul4b (*Hs*)	NM_014700	9-89/3944-4023(93%)	4.00E-23
628-1	227	Psmb1	NM_053590	4-141/659-796(98%)	2.00E-66
42-4	416	Ubb	D16554	1-416/54-469(97%)	0.00E+00

4-M Cell Interaction Sequences (3, 2%)

Table 4-13. Sequence Identities of Cell Interaction Clones (*Mm - Mus musculus*)

Clone	Sequence Length	Gene Symbol	Accession	Accession Match	E-value
27-5(T)	592	AF272892	NM_133324	1-592/99-684(98%)	0.00E+00
220-5	187	Col4a1 (*Mm*)	X92439	1-181/1200-1371(87%)	2.00E-38
221-5	109	Lgals1	NM_019904	2-109/1-105(97%)	3.00E-42

This class of genes (Table 4-13.) includes a recently identified protein, corneal wound healing related protein (AF272892), involved in wound healing and the formation of the epithelium (Yi *et al.*, 2000). As well, the sequence of another clone is highly similar to the expressed sequence of the mouse collagen α1(IV) gene (Col4a1), which is the collagen involved in the formation of basement membrane attachments in the mouse (Wood *et al.*,1988). In connection with the potential importance of ECM-cytoskeleton-signal transduction suggested by the class of Cytoskeleton mRNAs, this provides more

support to the idea that the extracellular environment of the retina is a very important element in LIRD.

4-N Other Sequences (3, 2%)

This class of clones (Table 4-14.) does not lend itself to speculation about the importance of the mRNAs that they represent. Two of the mRNAs are short sequences that have been identified as either brain- or testis-enriched sequences of unknown function. One current hypothesis is that the Bc1 transcripts are structural elements of ribonucleoprotein particles involved in control of translation (Lin *et al.*, 2001; Muslimov *et al.*, 2002). An earlier hypothesis is that the Bc1 elements, often found in introns, control brain-specific gene expression by being trancribed by RNA polymerase III, which promotes the accessibility of RNA polymerase II control regions (Sutcliffe *et al.*, 1984).

No function has been assigned to the germ cell-specific gene 1 (Gsg1) mRNA. The only hint as to its function is its identification in testicular germ cells and the authors' claim that it is a germ cell-specific gene (Tanaka *et al.*, 1994).

Table 4-14. Sequence Identities of Other Clones

Clone	Sequence Length	Gene	Accession	Accession Match	E-value
247-3	92	Bc1	M16113	22-92/10-80(100%)	1.00E-31
50	545	Gsg1	XM_132926	{7-417/89-499(95%)} {426-541/631-746(93%)}	0.00E+00
92	97	Bc1	U25187	17-83/9-75(95%)	1.00E-22

4-O Gene Expression in Light-induced Retinal Degeneration

The sequences of 87 of the clones identified in this study had identity to 65 different rat genes that are putatively differentially expressed during LIRD in rats. In many cases the role of the particular rat genes identified can potentially be explained within the context of rat LIRD. As well, the sequence of 34 of the rat cDNA clones is similar to 30 different genes found in either mice or humans. Some of the human and mouse genes indicated by sequence similarity to the clone inserts also have functions that are explainable within the context of retinal degeneration, and this suggests that the clone sequence represents mRNAs from rat genes orthologous to the identified mouse and human genes, but which are currently uncharacterized in rats. These putative rat orthologues could be expected to have roles in rat LIRD. The functional classes that the

sequenced clones were placed in are arbitrary, but each class reflects a process that could reasonably be expected to occur in a retina treated with intense green light.

The highest number of sequenced clones (22, 18%) was classed as stress-related (Section **4-C**; Table 4-1.). LIRD has a high oxidative stress component, meaning that the stress that the photoreceptor cells are responding to is due to the increase in the concentration of reactive oxygen species (ROS). For a photoreceptor cell to survive, it must immediately act to minimize the oxidative damage to proteins, lipids, and DNA that the increased ROS concentration could cause. It is very exciting then to find that all but one of the mRNAs for stress-related proteins identified in this study belong to the crystallin family of genes, since in the lens the crystallin proteins act to prevent damage to proteins to maintain lens clarity (Bloemendal and de Jong, 1991; Harding, 1997; Hejtmancik, 1998; Oyster, 1999). The large number of identified crystallin clones has meant that the crystallin stress response has been a particular focus of this study through Northern and Western analysis (**Chapter 7**).

Underlying all the cellular processes in the retina is the generation of energy, and the energy requirements of the 4 hour light-treated rat retina will be extremely high. This is true whether the retina is attempting to maintain normal function and regenerate its most important component, lamella membrane-bound rhodopsin, or is attempting to repair general oxidative damage to the retina. This is reflected in this study which identified a large number of mRNAs for proteins involved in the generation of cellular ATP (Section **4-D**; Table 4-2.).

Two classes of mRNAs are of exceptional importance in this study because the proteins they encode are the nuts and bolts that execute a retinal response to light-treatment. The hypothesis of this study is that there is a particular set of genes that change expression as a result of treating dark-reared rats with intense green lights for 4 hours. This hypothesis then depends on a change in RNA and protein synthesis within the retina, and a change in RNA and protein synthesis necessitates a change in the transcriptional and translational proteins. This important corollary of the study's hypothesis has been borne out with the identification of multiple mRNAs for proteins involved in both processes, and in post-transcriptional and post-translational activities. The mRNA synthesis sequences attract attention because many of the identities in this

class are very close to mouse or human genes, and it is evident that they have not been previously identified in the rat.

The retina is made up largely of photoreceptor cells, but other cell types also exist in the retina, *e.g.* neurons: horizontal, bipolar, and ganglion cells, and glial cells: Müller cells and astrocytes (Oyster, 1999), and it is likely that these other cell types will also be poised between survival and apoptosis, as they will be severely affected by the tissue environment of a degenerating retina. If cells are responding to the total cellular environment it means that a significant proportion of genes identified in a screen of a rat LIRD library should be those involved in cell interactions, and by extension, intracellular signalling. While the largest single class of sequences identified in this study is Stress-related (22 clones), the four related classes: Signalling (13 clones), Membrane (10 clones), Cytoskeleton (6 clones), and Cell Interaction (3 clones) together total 32 of the 121 identified clones. The size of this combined group of clones argues that the retina as a whole may be influencing what the end result of the light exposure will be, *i.e.* apoptosis or protection.

It is likely that components of basic metabolic pathways will be required in the process of LIRD, and a very interesting rat mRNA for farnesyl pyrophosphate synthetase was identified. Farnesyl pyrophosphate synthetase seems important in the synthesis of cofactors for numerous essential enzymes. Deficiencies in this protein's activity could have profound effects on retinal biology, and mutations in this gene could be studied as a potential contributing factor to hereditary human retinal degeneration. The possibility that farnesyl pyrophosphate synthetase is a human disease gene is strengthened somewhat by this screen's identification of three other genes that have known mutations that cause retinal degeneration in mice and humans, *i.e.* S-antigen, peripherin and rhodopsin. Like farnesyl pyroposphate synthetase these genes are ubiquitously expressed in the retina as basic components of photoreceptor cell metabolism. Section **5-D2** explores the possible connection of farnesyl pyroposphate synthetase, among others, to human retinal disease.

The loss of photoreceptors is apoptotic (Milam and Li, 1995; Abler *et al.*, 1996), so it would be reasonable to expect well-known apoptotic proteins to be identified in a screen of a LIRD library. This study did not identify mRNAs for proteins that are well-known in the process of apoptosis. At first this may seem puzzling, but it is important to

keep in mind that the library screened for this study was a 4 Hour Library made from cDNA representative of the mRNA present in rat retinae after 4 hours of light treatment. After 4 hours of light treatment not many cells have died, and the large increase in mRNAs for the protective crystallins suggests that the primary retinal response to 4 hours of light treatment is protective, not apoptotic. Some sequence identities in this study do hint that the apoptotic program is waiting in the wings. Of the good sequence correspondences in this class, one is for reticulon 3 (Rtn3) and two are for PEA15. These two proteins have been implicated in the inhibition of apoptosis, and their identification supports the contention that the primary retinal response is one geared towards protection of the retina. At the same time, both proteins are suggested to act at the point when cells are poised to enter the apoptotic pathway; both proteins remove very early components of the apoptotic pathway, like Bcl-2 (Rtn3; Moreira *et al.*, 1999) and caspase 8 (PEA15; Kitsberg *et al.*, 1999). An important point to note is that PEA15 is noted for being expressed primarily in astrocytes, and any anti-apoptotic effect that it may have could be geared towards protecting the retinal astrocytes (Danziger *et al.*, 1995; Estelles *et al.*, 1996).

Related to the protein-protective response of the crystallins is the necessity for the photoreceptor cell to be able to remove unrecoverable proteins. One pathway to be rid of damaged proteins is the ubiquitin-mediated proteasomal degradation pathway (Glickman and Ciechanover, 2002). That this study identifies mRNAs for components of this pathway is important because the end result of increased light exposure is the loss of photoreceptor cells through apoptosis, and this involves protein degradation. The oxidative environment of the light treated retinae is certain to damage some proteins, despite the protective crystallins, and the damaged proteins will have to be removed.

The sequence information has also identified a number of genes that have not been identified in the rat before, including novel genes or the newly discovered putative rat orthologues of known mouse and human genes. In total, 82 of the 167 clones identified and characterized in this study represent new rat sequences. This information immediately offers the possibility that previously unknown genes contribute to the LIRD phenotype.

The sequence data and gene identifications can be used for bioinformatic analysis, which makes use of the data collected by the NIH NCBI and allows the researcher to glean useful information from the data that researchers submit to the NCBI. Examples of the information that can be obtained from bioinformatic analysis are found in **Chapters 5** and **6**.

The sequence of the clones generated in this study immediately suggested one area of investigation, the stress-related crystallins (**Chapter 7**). The high prevalence of the mRNAs for these proteins, which are known mainly for their expression in the lens, suggests that they have some previously unknown role in LIRD. Characterization of the change in crystallin gene expression in LIRD could indicate what the crystallin proteins are doing in the rat retina.

Chapter 5 Bioinformatics: Chromosomal Localization

Chapter 5 Bioinformatics: Chromosomal Localization

The differential cross screen on which this work is based has identified ninety-three[39] different rat genes whose expression changes during light-induced retinal degeneration (LIRD). The hypothesis of the author is that these are genes whose change in expression results in the net effect of retinal degeneration. The products of some genes will not be required in a cell that is either committed to apoptosis (Milam and Li, 1995; Abler *et al.*, 1996) because of irrevocable damage caused by the light insult, or a cell that is attempting to survive the light insult. This could be because the gene products interfere with the execution of the apoptotic cascade or because the presence of the gene product interferes with the ability of the cell to repair the damage done to the cell. Conversely, some gene products will be required to commit an irrevocably damaged cell to apoptosis, or will be needed to ensure that a cell survives. When the sum metabolic effect of the expression of all these genes is considered, it would be correct to say that any gene whose expression changes during the course of LIRD is part of the process of LIRD. At the same time, the number and variety of the genes identified in this study suggests that it would be very difficult to identify the single gene product whose change in expression touches off the process.

5-A LIRD as a Model for Human Disease

Rat LIRD has several features in common with human retinitis pigmentosa (RP) and macular degeneration (MD). Retinal metabolism in both species is essentially identical, *i.e.* both species have similar retinal physiology, and use the same components of visual transduction. LIRD, RP, and MD all result in the death of photoreceptor cells within the retina. In all three cases, the photoreceptor cell death occurs by the process of apoptosis (Milam and Li, 1995; Abler *et al.*, 1996); in the case of RP, a common feature with LIRD is that both can involve rhodopsin dysfunction. An important distinction between LIRD and the human diseases is that LIRD is an injury response occurring in rats while the human diseases are the result of mutation in, most likely, a single gene. Since the common features of the three conditions are fundamental physiological and

[39] Ninety-five different mRNAs were identified, but two of them, the brain and testis ID transcripts, are not considered here since they could be derived from any number of genes, and their function is not clear (Sutcliffe *et al.*, 1984; Lin *et al.*, 2001; Muslimov *et al.*, 2002).

metabolic features, it is reasonable to hypothesize that at least some of the genes and gene products that effect the apoptotic process in rat LIRD will be orthologous to those that, when mutated, are known to result in human diseases like RP and MD. A corollary to this hypothesis is that some of the genes identified in rat LIRD may have human orthologues that would result in a human retinopathy if mutated.

5-B Determining Gene Location

The rat genome has not yet been as extensively sequenced and mapped as the mouse or human genomes[40]. Nonetheless, significant bioinformatic resources exist for determining the location of known genes within the rat genome.

The first of these is the LocusLink (www.ncbi.nlm.nih.gov/LocusLink) query found on the National Institutes of Health's (NIH) National Centre for Biotechnology Information (NCBI). LocusLink allows a user to submit a gene name and retrieve annotated data about genetic loci associated with the gene from a database maintained and updated by the NIH NCBI. The database currently contains information about genetic loci in humans, rats, mice, and a few other species. This resource can be used to identify the location of known genes within rats, mice and humans if the location has been determined.

LocusLink is a good beginning when attempting to determine gene locations, but one drawback is that the nature of the localization, *e.g.* physical, genetic or cytogenetic mapping, is not immediately obvious. In order to know what methods have been used to determine a gene's location it is necessary to utilize other resources. For rats, the RatMap (ratmap.gen.gu.se/) and Gene and Position Predictor (gapp.gen.gu.se/) queries, maintained by the Swedish Research Council and others at Göteborg University are excellent tools that allow a user to submit the gene name and retrieve information regarding its localization in both rats and mice. For the mouse, a comprehensive database of gene localization, Mouse Genome Informatics (www.informatics.jax.org), provides details about the mouse gene locations. Extensive data on human gene locations can be found with the NIH NCBI Online Mendelian Inheritance in Man query site.

---

[40] As of February 8th, 2003, the rat genome is 0.5% complete, the mouse genome is 26.8% complete, and the human genome is 98.8% complete.

These bioinformatic tools can be used to identify the location of known rat genes and their orthologues in mice and humans. Of the ninety-three rat genes identified in the differential cross screen and considered here, forty-nine (53%) of the rat genes have gene location data available, while gene location is known for ninety (97%) of the orthologous human genes and eighty-four (90%) of the orthologous mouse genes (Table 5-1. Descriptive gene names are found in **Appendix 2.**).

5-C Human Retinopathy Genes

The differential cross screen has identified several (5) rat genes orthologous to those that result in retinal disorders when mutated in humans (Table 5-2.). Mutation in transducin (Gnat1) results in the Nougaret form of congenital stationary night blindness (CSNB), in which affected individuals are unable to see in dim light, but have normal vision in normal light (Dryja *et al.*, 1996). The autosomal recessive Oguchi disease is a form of CSNB caused by mutations in the S-antigen gene (Sag: Fuchs *et al.*, 1995). A dominant cone-rod dystrophy that results in the atrophy of the macula has been identified as a mutation in the human Unc119 homologue, and is suspected to be effected by disruption of neurotransmitter release at the synaptic ribbon (Kobayashi *et al.*, 2000). Mutations in peripherin-rds (Rds) result in various phenotypes, including RP and MD, depending on the mutation (Brecher and Bird, 1990; Farrar *et al.*, 1991; Jordan *et al.*, 1992; Kajiwara *et al.*, 1993; Kikawa *et al.*, 1994; Kim *et al.*, 1995b; Felbor *et al.*, 1997). The implication of the Prph2 gene in numerous retinal dystrophies is likely due to its suspected role as an adhesion molecule in the rod outer segment where it maintains the structure of the lamellae (Travis *et al.*, 1991; Ali *et al.*, 2000). The gene whose expression is centrally important to rod photoreceptor cells, rhodopsin (Rho), is another gene with many known mutations that result in RP (Dryja *et al.*, 1990; Farrar *et al.*, 1990a,b, 2002; Humphries *et al.*, 1990, 1992; Sung *et al.*, 1991). The identification of all five orthologous rat genes in the rat LIRD library is important because it suggests that the rat orthologues of these human disease genes have some role in LIRD. The hypothesis that orthologues of human disease genes would be identified in a LIRD library has been shown to be correct by the identification of these five genes. This lends support to the corollary to this hypothesis, that rat genes identified in the differential cross screen

Table 5-1. Gene Localizations in Rat, Mouse, and Human

Arranged numerically by human chromosome.

Gene	Rat	Mouse	Human
Stmn1	5	4 (65.7 cM)	1p36.1-p35
Eno1	5q36	4 (79.00 cM)	1p36.3-p36.2
Pea15	13q24-q26	1 (93.8 cM)	1q21.1
Fdps	2	3 (42.6 cM)	1q21.2
Atp1a2	13q24-q26	1 (94.20cM)	1q21-q23
Hnrpu	14	1	1q43
Crygb	9q31-q34	1 (32 cM)	2q33-q35
Cryba2	9q31-q34	1 (40.80 cM)	2q34-q36
Sag	9q35-q36	1 (53.6 cM)	2q37.1
Caps		14	3p14.3
Gnai2	8q31-q32	9 (59.00 cM)	3p21
Gnat1	8q31-q32	9 (59.00 cM)	3p21
Glb1	8q31-q32	9 (66.0 cM)	3p21.33
Rho	4q41-q42	6 (51.50 cM)	3q21-q24
Schip1		3	3q25.32
Crygs	11q23	16 (16.10 cM)	3q25-qter
Tloc1		3	3q26.2-q27
Polr2h			3q28
Ctbp1		5	4p16
Sec3		5	4q11
Rpl34			4q24
Rtn3			4q31.21
Il6st	2q14-q16	13	5q11
Cplx2		13	5q35.3
Rds	20p12	17 (18.84 cM)	6p21.2-p12.3
Abcf1		17 (20.50 cM)	6p21.33
Rpl10a		17	6p21.3-p21.2
Psmb1		17 (8.25 cM)	6q27
Rala		13 (10.00 cM)	7p22-p15
Ywhag	12q12-q16	5 (75.00 cM)	7q11.23
Ndufa5			7q32
Aldr1	4q21-q22	6 (13.00 cM)	7q35
Tln		4	9p13
AF272892		13	9q21.33
Rpl7a	3q11-3q12	2 (18.0 cM)	9q34
Pp	20p11-q11	10 (36.00 cM)	10q11.1-q24
Sip30			10q21-q22
Cry2		2	11p11.1
Chst1		2	11p11.2-p11.1
Cntf	1q43-q53	19 (7.0 cM)	11q12.2
Bad		19	11q13.1
Fkbp2		19	11q13.1-q13.3
Rps3		7	11q13.3-q13.5
Pak1	1q22	7 (46.50 cM)	11q13-q14
Ddx6	8	9 (26.0 cM)	11q23.3

Table 5-1. (continued)

Gene	Rat	Mouse	Human
Itpr2		6 (73.00 cM)	12p11
Gpr19		6	12p12.3
Eno2	4q42	6 (60.21 cM)	12p13
Gsg1	4q34-q42	6 (66.30 cM)	12p13.31
Gapd	4q42	6 (56.0 cM)	12p13.31-p13.1
Atp5g2		15	12q12
Prph	7q34	15 (55.5 cM)	12q12-q13
Rpl41			12q13
Col4a1	16q12.2-q12.5	8 (5.00 cM)	13q34
Hnrpc	5q13-5q24	4 (21.50 cM)	14q11.1
Nfkbia		12	14q13
Sfrs5		12	14q24
Hsp86-1	6q24-q32	12 (48.0 cM)	14q32.33
Pkm2	8q31	9 (52.00 cM)	15q22
Rplp1		9	15q22
Hspc121		9	15q22.2
Tceb2		17	16p12.3
Cdh1	19p11-19q12	8 (53.3 cM)	16q22.1
Aldoc	10q23-q32.1	11 (44.98 cM)	17cen-q12
Ubb		11 (35.0 cM)	17p12-p11.1
Unc119		11	17q11.2
Cryba1	10q23-q32.1	11 (44.71 cM)	17q11.2-q12
Rpl19		11	17q11.2-q12
Atp6n1a	10q23-q32.1	11(55.8 cM)	17q21
Tcfl4		11	17q21
Tubg1	10q31.2	11 (60.0 cM)	17q21
Mapt	10	11 (64.0 cM)	17q21.1
Mel	16p14-q11	8 (33 cM)	19p13.1
Capns1		7 (9.5 cM)	19q13.13
Pld3		7	19q13.2
Vapb		2	20q13
Ywhab		2	20q13.1
Cryaa	20p12	17 (17.4 cM)	21q22.3
Lztr1		16	22q11.21
Crybb3	12q16	5 (60.00 cM)	22q11.23
Cryba4	12q16	5 (59.00 cM)	22q12.1
Crybb1	12q16	5 (59.00 cM)	22q12.1
Crybb2	12q16	5 (59.00 cM)	22q12.1
Lgals1	7q33-q34	15 (44.9 cM)	22q13.1
Cul4b		X	Xq23
Upf3b		X	Xq25-q26
Aldh2	Mitoch.	Mitoch.	Mitoch.
Mtco2	Mitoch.	Mitoch.	Mitoch.
Mtcyb	Mitoch.	Mitoch.	Mitoch.
Rnr(#)	3,11,12		(13,14,15,21,22)p12
Sharpin	7		
Mipp65			
Rrp41		15	

could have human orthologues that result in retinal disease. The sections that follow will explore this possibility using a positional candidate approach.

Table 5-2. Known Human Retinal Disease Genes Identified in Rat LIRD Differential Cross Screen

Gene Name	Gene	Rat	Human
Guanine nucleotide binding protein, alpha transducing 1	Gnat1	8q31-q32	3p21
S-antigen	Sag	9q35-q36	2q37.1
Peripherin (retinal degeneration slow)	Rds	20p12	6p21.2-p12.3
Rhodopsin	Rho	4q41-q42	3q21-q24
UNC-119 homologue	Unc119		17q11.2

5-D Potential Human Retinopathy Genes

That human orthologues of rat genes identified in a LIRD library could be retinal disease genes is another hypothesis of this study. In order to determine whether this hypothesis is correct, it was necessary to identify as many known human retinal disease loci as possible, for which the disease gene has not been positively identified. Then the locations of the retinal disease loci could be compared to the locations of the human orthologues of the identified rat genes. All genes that are found in retinal disease loci are potential candidates for causing that retinal disease, but the identification of rat genes in a LIRD differential cross screen which have human orthologues in retinal disease loci suggests that those human orthologues be considered first.

This process is known as the positional candidate approach to identification of disease genes. An unknown disease gene is localized to a particular chromosomal region, genes that lie within that region are identified, and the gene sequences are analyzed for mutations that could result in the disease phenotype. This method has been made very powerful by the large amount of data collected by the NIH NCBI and others and published on the World-wide Web.

Human retinal disease regions can be identified using the NIH NCBI's Online Mendelian Inheritance in Man (OMIM) database query (www.ncbi.nlm.nih.gov:80/entrez/query.fcgi?db=OMIM). OMIM is a database maintained jointly by Johns Hopkins University and the NIH NCBI. It is an annotated catalogue of human genetic disorders with references and information pertaining to each genetic disorder, including mapping

information of the genetic location of the disease. From this database information can be gleaned on retinal diseases that are currently under investigation (Table 5-3.).

Table 5-3. Retinal Disease Regions and Disease Genes

Bold entries indicate *loci* in which a human orthologue of a rat gene identified in the LIRD differential cross screen occurs.

Disease		Location	Disease Gene
Age-related macular degeneration, 1	ARMD1	1q25-q31	
Age-related macular degeneration, 2	ARMD2	1p21-p13	
Cone dystrophy 1	COD1	Xp21.1	Rpgr
Cone dystrophy 3	COD3	6p21.2	Guca1a
X-linked cone dystrophy with tapetal-like sheen	COD-X	X	
Cone-rod dystrophy 2	CORD2	19q13.3	Crx
Cone-rod dystrophy 5	CORD5	17p13-p12	
Cone-rod dystrophy 6	CORD6	17p13.1	Gucy2d
Cone-rod dystrophy 7	CORD7	6cen-q14	
Cone-rod dystrophy 8	**CORD8**	**1q12-q24**	
Congenital stationary night blindness type 1	CSNB1	Xp11.4	Nyx
Congenital stationary night blindness, type 2	CSNB2	Xp11.23	Cacna1f
Cystoid macular edema	**CME**	**7p21-p15**	
Doyne honeycomb retinal dystrophy	DHRD	2p16	Efemp1
Congenital hypotrichosis with juvenile MD	HJMD	16q22.1	Cdh3
Joubert syndrome 1	**JBTS1**	**9q34.3**	
Leber congenital amaurosis, Crb1-related	LCA(Crb1)	1q31-q32.1	Crb1
Leber congenital amaurosis Crx-related	LCA(Crx)	19q13.3	Crx
Leber congenital amaurosis, type I	LCA1	17p13.1	Gucy2d
Leber congenital amaurosis, type II	LCA2	1p31	Rpe65
Leber congenital amaurosis, type III	**LCA3**	**14q24**	
Leber congenital amaurosis, type IV	LCA4	17p13.1	Aipl1
Leber congenital amaurosis, type V	LCA5	6q11-q16	
Leber congenital amaurosis, type VI	LCA6	14q11	Rpgrip1
Retinal degeneration, slow	RDS	6p21.1-cen	Rds
Retinitis pigmentosa, Mertk-related	RP(Mertk)	2q14.1	Mertk
Retinitis pigmentosa 2	RP2	Xp11.3	Rp2
Retinitis pigmentosa 3	RP3	Xp21.1	Rpgr
Retinitis pigmentosa, Rhodopsin-related	RP4	3q21-q24	Rho
Retinitis pigmentosa 9	RP9	7p15.1-p13	
Retinitis pigmentosa 11	RP11	19q13.4	Prpf31
Retinitis pigmentosa 13	RP13	17p13.3	
Retinitis pigmentosa 15	RP15	Xp21.1	Rpgr
Retinitis pigmentosa 19	RP19	1p21-p13	Abca4
Retinoschisis 1, X-linked, juvenile	RS1	Xp22.2-p22.1	Rs1
Sorsby fundus dystrophy	SFD	22q12.1-q13.2	Timp3
Senior-Løken syndrome 1	SLSN1	2q13	
Senior-Løken syndrome 3	**SLSN3**	**3q21-q22**	
Senior-Løken syndrome 4	**SLSN4**	**1p36.31**	
Stargardt disease 1	STGD1	1p21-p13	Abca4
Stargardt disease 3	STGD3	6q14	Elovl4
Stargardt disease 4	STGD4	**4p**	
Vitelliform macular dystrophy	VMD2	11q13	Vmd2
Neovascular inflammatory vitreoretinopathy	**VRNI**	**11q13**	

When the retinal disease regions are examined relative to the location of the human orthologues of the LIRD-identified genes it becomes apparent that fourteen of the orthologous genes are found in eight disease regions where the disease gene is unknown (Table 5-4.). This does not mean that the orthologous gene is the disease gene, but does mark it for further investigation.

Table 5-4. Retinal Disease Regions and LIRD-identified Orthologues in the Same Region

Arranged by chromosome.

Disease	Disease Location	Orthologue Location	LIRD-identified Orthologue	
SLSN4	1p36.31	1p36.1-p35	Stathmin 1	Stmn1
		1p36.3-p36.2	Enolase 1, alpha	Eno1
CORD8	1q12-q24	1q21.1	Phosphoprotein enriched in astrocytes 15	Pea15
		1q21.2	Farnesyl diphosphate synthetase	Fdps
		1q21-q23	ATPase, Na+K+ transporting, alpha 2	Atp1a2
SLSN3	3q21-q22	3q21-q24	Rhodopsin	Rho
STGD4	4p	4p16	C-terminal binding protein 1	Ctbp1
CME	7p21-p15	7p22-p15	v-ral simian leukemia viral oncogene homolog A (ras related)	Rala
JBTS1	9q34.3	9q34	Ribosomal protein L7a	Rpl7a
VRNI	11q13	11q13.1	Bcl-2 associated death agonist	Bad
		11q13.1-q13.3	FK506 binding protein 2	Fkbp2
		11q13.3-q13.5	Ribosomal protein S3	Rps3
		11q13-q14	p21 (CDKN1A)-activated kinase 1	Pak1
LCA3	14q24	14q24	Splicing factor, arginine/serine-rich 5	Sfrs5

The NIH NCBI MapViewer (www.ncbi.nlm.nih.gov/cgi-bin/Entrez/maps.cgi), which is a graphical database that maps human genes and markers on the chromosomes, and the NIH NCBI UniSTS database (www.ncbi.nlm.nih.gov/entrez/), which is a database of chromosomal markers, can be used to determine the relative location of diseases, their markers and genes of interest.

5-D1 Senior-Løken Syndrome Type 4: Using these tools with regard to the SLSN4 region, it becomes evident that Eno1 (Chr1: 8541356- 8559641; D'Ancona *et al.*, 1977) and Stmn1 (Chromosome 1 bases: 25706771- 25713644; Ferrari *et al.*, 1990) are not likely to be the disease genes because they are 2 x 10^6 base pairs (Mbp) and 19 Mbp, respectively, from the marker used to localize the disease, D1S214 (Chr1: 6538644-6538839; Schuermann *et al.*, 2002). Eno1 could still be the cause of SLSN4, but the 2 Mbp distance is discouraging since there are likely to be a number of genes between the telomere and the marker (≅7 Mbp), and the marker and Eno1.

5-D2 Cone-rod dystrophy 8: The cone-rod dystrophies are genetic diseases in which the cone photoreceptor cells degenerate, resulting in an inability to distinguish colour and loss of central vision, followed by a degeneration of the rod photoreceptor cells, loss of peripheral vision, and night-blindness. CORD8 was localized to 1q12-q24 (**Figure 5-1a.**) between the markers D1S442 and D1S2681 (Chr1: 144150962-163688435; Khaliq *et al.*, 2000). The maximum logarithm of odd (LOD) scores were found with two markers within this region, D1S2635 (Chr1: 156962448-156962604) and D1S484 (Chr1: 158559640-158559772). Three of the LIRD-identified orthologous genes fall within this 20 Mbp region: Fdps (Chr1: 153136211-153147962; Wilkin *et al.*, 1990), Atp1a2 (Chr1: 157877856-157905525; Oakey *et al.*, 1992), and Pea15 (Chr1: 157967199-157977232; Hwang *et al.*, 1997).

The product of Fdps is farnesyl diphosphate synthetase which is one of the enzymes of isoprene metabolism which produces cholesterol, ubiquinone and other metabolites, the most important for the functioning of the retina being all-*trans* retinal, rhodopsin's cofactor (Kellogg and Poulter, 1997; Nicholson, 2001). Finding that the gene for an enzyme essential to the functioning of the retina is within a retinal disease region is very interesting. While Fdps can be considered as a candidate gene for CORD8, two notes of caution must be made. First, Fdps is not only essential to the retina, but to the entire organism because it plays a role in the synthesis of cholesterol and one would expect other complications beside retinal degeneration. Second, while Fdps is within 4 Mbp centromeric to the marker with the greatest LOD score (D1S2635), it is the furthest of the three LIRD-identified orthologues from this marker (Khaliq *et al.*, 2000). Fdps is a possible candidate for the gene causing CORD8, but Atp1a2 and Pea15 seem more likely candidates.

The two maximum LOD scores obtained (Khaliq *et al.*, 2000) are for markers that bracket Atp1a2 (D1S2635 and D1S484). Atp1a2 is 0.9 Mbp telomeric from D1S2635, and 0.7 Mbp centromeric from D1S484. Atp1a2 is significantly linked to respiration in humans, and appears to be a strong contributor to respiration in younger individuals (Katzmarzyk *et al.*, 1999). One of the hallmarks associated with CORD8 is loss of both rod and cone cells (Khaliq *et al.*, 2000) which could both be explained by a defect in

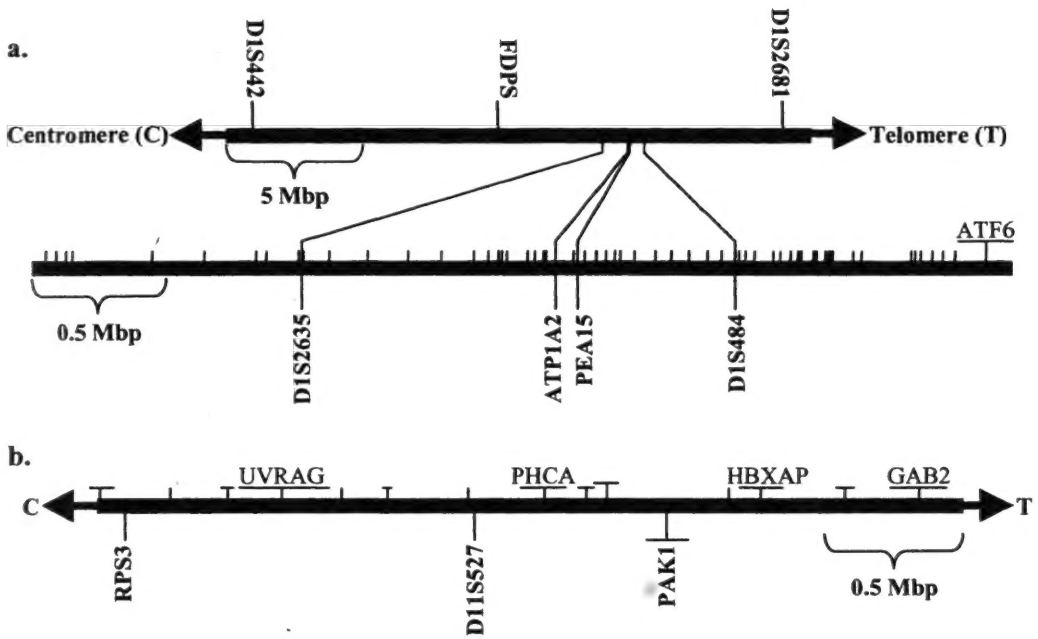

Figure 5-1. Human Retinal Dystrophy Regions.

Each unlabelled vertical bar indicates a sequence-confirmed gene in the region. Each labelled horizontal bar indicates the size of a sequence-confirmed gene big enough to show up at the scale used. The direction to the centromere and telomere are indicated.

a. CORD8 region on chromosome 1 (1q12-q24). The top ideogram represents the 20 Mbp region first identified (Scale: 2.5 Mbp/cm), and the connected ideogram represents the region surrounding the two markers with the highest LOD scores.
(Scale: 0.25 Mbp/cm)

b. VRNI region on chromosome 11 (11q13). (Scale: 0.25 Mbp/cm)

respiration leading to inefficient or ineffective use of oxygen in the retina. CORD8 patients have poor central vision, colour blindness, and night blindness. Katzmarzyk *et al.* (1999) point out that Atp1a2 is only part of the respiratory machinery which also includes Atp1a1 and Atp1a3, which might explain why any putative mutation in Atp1a2 is recessive, and could explain why minor mutations are not homozygous lethal.

Pea15 is also bracketed by D1S2635 and D1S484, being 1.0 Mbp telomeric from D1S2635 and 0.5 Mbp centromeric from D1S484. Pea15's product, phosphoprotein enriched in astrocytes 15, has been shown to function in glucose transport (Condorelli *et al.*, 1998) and to be an anti-apoptotic protein (Condorelli *et al.*, 1999; Kitsberg *et al.*, 1999). Astrocytes can be considered caretaker cells which provide nutrients to neurons and maintain a healthy cellular environment within the tissue (Araujo *et al.*, 1993; Kirchoff *et al.*, 2001). The retina is a highly ordered structure composed of neurons and photoreceptor cells, and delivering nutrients to these highly active cells is made difficult by the necessity for small blood vessels that will not interfere with the reception of light by the photoreceptor cells (Otani *et al.*, 2002). Astrocytes could be mediators of nutrient transport that are resistant to cell death in order to be able to provide nutrients to the retina even in times of stress. Impairing the activity of a central protein of the astrocyte might allow daily stresses to do damage to the retina, and result in the loss of photoreceptor cells. A drawback to this line of thought is that the brain also contains astrocytes (Kirchoff *et al.*, 2001), and CORD8 is not noted to be accompanied by neurological problems (Khaliq *et al.*, 2000). Pea15 is correctly localized to be a candidate gene for CORD8, and its diverse activity in astrocytes suggests that it could be a disease gene.

5-D3 Senior-Løken Syndrome Type 3: The SLSN3 locus, 3q21-q22, could potentially include some parts of Rho (3q21-q24) according to the initial analysis, but this is not the case. Two markers used to localize the SLSN3 locus, D3S1587 and D3S621, flank the SLSN3 locus (Chr3: 127710504-141847705; Omran *et al.*, 2002), and Rho (Chr3: 126073168- 126079873; Nathans *et al.*, 1986) starts almost 2 Mbp centromeric from D3S1587. Rho cannot be the gene which causes SLSN3.

5-D4 Stargardt disease 4: When considering the STGD4 locus, it was unlikely that the single LIRD-identified orthologue found on the short arm of chromosome 4

would be the disease gene because, according to the NIH NCBI OMIM database, the putative locus of STGD4 is the entire short arm. One of the papers cited in the OMIM entry reveals that STGD4 is expected to lie between the markers D4S1582 and D4S2397 (Chr4: 10375864-27407758; Kniazeva *et al.*, 1999), although this information is not reflected in the localization provided by the OMIM entry. The putative STGD4 locus is then 9 Mbp from the telomeric Ctbp1 gene (Chr4: 1211259- 1248796; Katsanis *et al.*, 1998). Ctbp1 is not likely to be the gene that causes STGD4.

5-D5 Cystoid macular edema: The CME locus (7p21-p15) is bounded by two markers, D7S493 and D7S526 (Chr7: 21449638-30591340; Kremer *et al.*, 1994). Rala (7p22-p15; Chr7: 39309537- 39394118; Rousseau-Merck *et al.*, 1988) lies 9 Mbp centromeric to D7S526, which means that Rala cannot be the CME disease gene.

5-D6 Joubert Syndrome Type 1: The JBTS1 locus at 9q34.3 is linked to marker D9S158 (Chr9: 130248894-130249116; Saar *et al.*, 1999). Rpl17a (Chr9: 127304808-127308019) is in a cluster of other ribosomal protein genes at 9q33-q34 (Yon *et al.*, 1989). It is only 3 Mbp centromeric to D9S158, so it cannot be excluded as being the disease gene for JBTS1, and could be considered a candidate in the absence of any other information.

5-D7 Vitreoretinopathy neovascular inflammatory disease: VRNI is characterized by ocular inflammation, obstructive growth of blood vessels, and retinal detachment that combine to result in blindness (Stone *et al.*, 1992). There are four LIRD-identified human orthologues in the VRNI region: Bad (Chr11: 66553032- 66567894; Ottilie *et al.*, 1997), Fkbp2 (Chr11: 66524143-66527416; DiLella *et al.*, 1992), Rps3 (Chr11: 77437507- 77443786; Polakiewicz *et al.*, 1995), and Pak1 (Chr11: 79360030- 79511729; Bekri *et al.*, 1997). VRNI (11q13; **Figure 5-1b.**) has been linked to the marker D11S527 (Chr11: 78725451-78725608; Stone *et al.*, 1992), which means that while Bad and Fkbp2 are 12 Mbp centromeric from the marker, Rps3 is 1.3 Mbp centromeric from D11S527 and Pak1 is 0.6 Mbp telomeric from D11S527. The large distance from the marker means that Bad and Fkbp2 are unlikely to be the VRNI disease gene. In contrast, Rps3 and Pak1 are as good candidates due to their map location relative to the marker.

There is nothing obvious about the protein function of Rps3 or Pak1 that would suggest that these genes are not good candidates. Ribosomal protein S3 has two roles,

acting as both a structural protein of the ribosome, but also having *in vivo* apurinic (AP) endonuclease activity (Kim *et al.*, 1995a; Wimberley *et al.*, 2000; Jung *et al.*, 2001). While the structural function in ribosomes implies that Rps3 is an essential gene (Fingen-Eigen *et al.*, 1996), it does not preclude mutations occurring that affect the AP endonuclease activity (Kim *et al.*, 1995a). Why this would result in the phenotype seen in VRNI is not clear, but not necessarily impossible.

Pak1 is a promising candidate disease gene for VRNI because its product, p21-activated kinase 1 (PAK1), has been implicated in the control of cytoskeleton rearrangements (Zhang *et al.*, 1995; Frost *et al.*, 1998; Sanders *et al.*, 1999; Parrini *et al.*, 2002). In part, this means that PAK1 activity impacts the formation and dissolution of focal adhesions, and cell motility (Frost *et al.*, 1998; Sells *et al.*, 1999). The retina is a highly organized, layered tissue, and some of this organization and layering is due to focal adhesions (Oyster, 1999). It is not difficult to reconcile VRNI retinal detachment and neovascularization with a defect in cytoskeletal control, but it is harder to reconcile why the defect would be manifested in the eye and not in other highly ordered tissues. Nonetheless, Pak1 is a good candidate for being the disease gene for VRNI.

5-D8 Leber congenital amaurosis type III: LCA3 has been linked to 14q24 by the marker D14S74 (Chr14: 76164129-76164432; Stockton *et al.*, 1998). This means that the LIRD-identified orthologue in this region, Sfrs5 (Chr14: 67739049-67743909; Bermingham Jr. *et al.*, 1995) is not a good candidate for LCA3 because it is 8 Mbp from the marker.

5-E Conserved Synteny

The identification of LIRD rat genes with human orthologues in human retinal disease regions provides some support for the contention that these genes are potential candidate genes for retinal diseases. If the rat and human genes are found in regions of conserved synteny, it is likely that they are orthologous genes with similar functions. This contention is more difficult to support in species that are widely separated by evolutionary time, but easier in species like rats and humans that are closely related. It has been estimated by comparison of 104 orthologous protein amino acid sequences from five species that mice and rats (Order: Rodentia) and humans (Order: Primates) have

been separated for 96 MY (**Figure 5-2.**; Nei *et al.*, 2000). The same analysis estimates the divergence of mice (*Mus* spp.) and rats (*Rattus* spp.) as being 33 MY.

It is well known that humans and mice show significant conservation of synteny, and the NIH NCBI Human-Mouse Homology Map (http://www.ncbi.nlm.nih.gov/Homology) uses several sequence- and locus-based techniques to identify regions of conserved synteny in human and mouse chromosomes. The identification of human and mouse synteny is useful in terms of this study because it is reasonable to hypothesize that if human and mouse show significant conserved synteny, mouse and rat will show at least as much conserved synteny (Gómez-Fabre *et al.*, 2002), and so human and rat will show conserved synteny (**Figure 5-3.**). The identification of conserved synteny between rat and humans can be used to reinforce the likelihood that rat genes identified in a LIRD library may have human orthologues that result in retinal dystrophies when mutated.

5-F Bioinformatic Analysis and the Laboratory

The use of readily available bioinformatic tools to identify gene loci and disease regions is a powerful approach to identify genes that could possibly cause genetic diseases. All that is required is a rational reason for examining a particular gene in connection to a particular disease. Even if the model system used is not human, it is still possible to identify orthologous genes in the human and use their locations in order to add depth to possible family studies of diseases in that region.

The bioinformatic approach to identifying candidate genes is powerful, but does not mean that laboratory work is superfluous. There still must be a rational reason to consider a particular gene as a candidate for causing disease. There must be a connection made between the biology of the system that is being investigated and the bioinformatic research. It is also necessary to recognize that candidate genes for genetic diseases must still be confirmed by genetic and molecular biology analysis. Further, if the candidate is shown to be the disease gene, the gene product needs to be biochemically characterized.

In this study, the differential cross screen of a rat LIRD library is the connection between the biology of retinal degeneration and the bioinformatic examination of the genes identified in the screen. LIRD in rats is a well-characterized system, which models

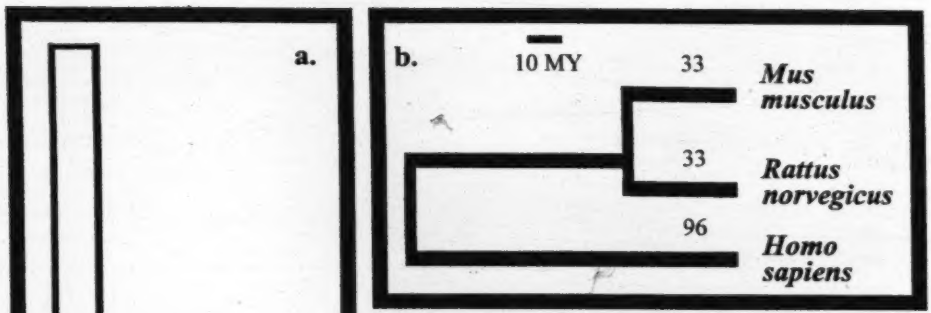

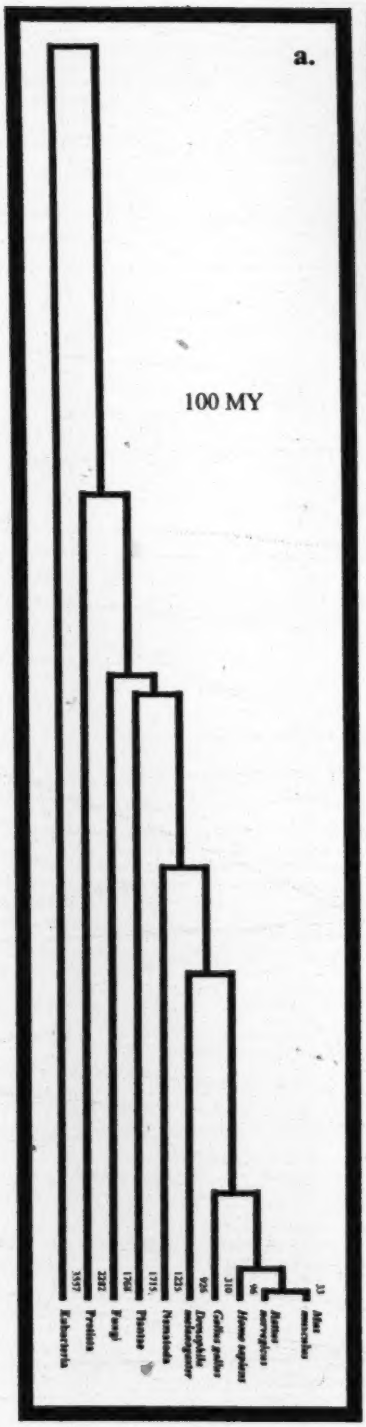

Figure 5-2. Evolutionary Divergence. (After Nei *et al.*, 2000)

Estimated divergence from comparison of 104 protein sequences.

Units: million years (MY).

a. Divergence of several different clades.

b. Divergence of humans from rats, and rats from mice.

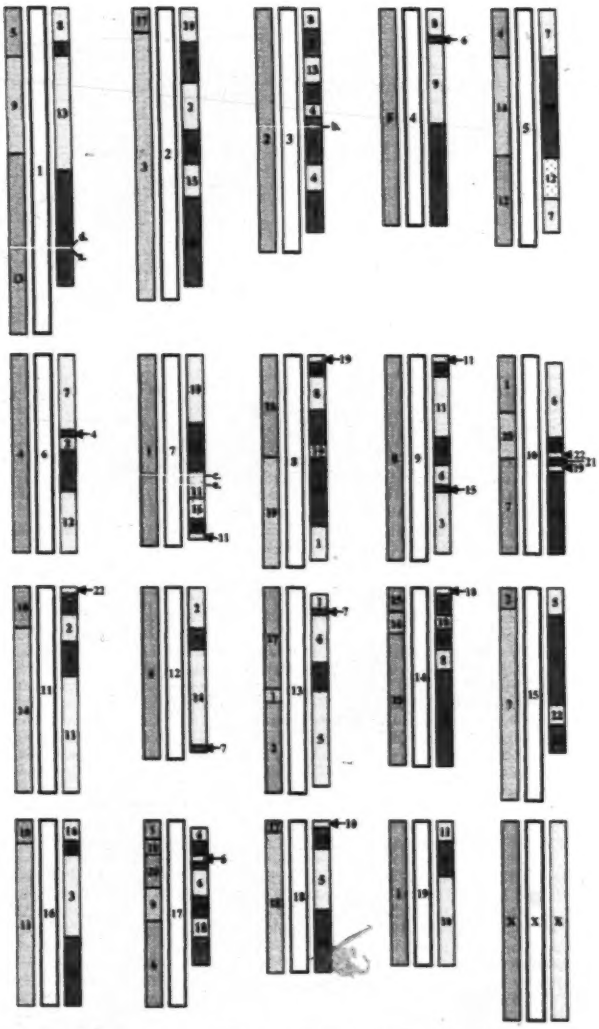

Figure 5-3. Ideogram of Gross Rat, Mouse and Human Conserved Synteny.

Illustration of regions of conserved synteny that occur between rat, mouse, and human chromosomes with the mouse chromosomes as the unifying link. Arranged numerically, left to right, by mouse chromosome. The mouse chromosome is contiguous and appears in white. Rat chromosomal regions are in blue. Human chromosomal regions are in grey. Regions of conserved synteny and chromosome sizes are proportional to the mouse chromosome. White lines indicate the known location of orthologous genes: **a.** Atp1a2 [*Rn* 13q24-q26; *Mm* 1 (94.2 cM); *Hs* 1q21-q23], **b.** Fdps [*Rn* 2; *Mm* 3 (42.6 cM); *Hs* 1q21.2], **c.** Pak1 [*Rn* 1q22; *Mm* 7 (46.50 cM); *Hs* 11q13-q14], **d.** Pea15 [*Rn* 13q24-q26; *Mm* 1 (93.8 cM); *Hs* 1q21.1], **e.** [*Mm* 7; *Hs* 11q13.3-q13.5]. Information obtained from RatMap (gapp.gen.gu.se) and Mouse Genome Informatics (www.informatics.jax.org).

the process of retinal degeneration seen in human genetic diseases. Since the processes in the rat model and the human diseases are similar, the molecular machinery that effects the degeneration should be similar. Genes that are identified as being differentially expressed in rat LIRD can be expected to play a role in some human genetic diseases. The fact that the differential screen identified five genes which, when mutated, cause retinal degeneration in humans is one indication of the effectiveness of the differential cross screen approach. As well, the screen identified several genes whose orthologues are located near known disease loci and provides a reason to examine some of those genes in relation to the diseases, and ignore others. The combination of laboratory and bioinformatic research is an important approach that increases efficiency by highlighting potential avenues and indicating likely blind alleys. From the initial analysis it is clear that two human retinal dystrophies, CORD8 and VRNI, could be the result of defects in genes orthologous to those identified in this LIRD study. The importance of Atp1a2, Fdps, and Pea15 in the etiology of CORD8, and the importance of Rps3 and Pak1 in the etiology of VRNI could be determined in a future study.

Chapter 6 Bioinformatics: *In silico* Northern Analysis

Chapter 6 Bioinformatics: *In silico* Northern Analysis

6-A Northern Analysis

The standard procedure for the determination of gene expression in various tissues is the transfer of RNA from various tissues from a denaturing gel to a nylon membrane (Thomas, 1980; Sambrook *et al.*, 1989; Ausubel *et al.*, 1994), and subsequent hybridization of a labelled probe to the nylon membrane at appropriate conditions. This process, referred to as Northern analysis, is a powerful technique which can provide a wealth of information about mRNAs that are complementary to the probe used. The technique is sensitive, and can detect as little as 50 pg of RNA (Thomas, 1980), giving a good indication of the presence or absence of the target RNA. Beside the answer to this absolute question, Northern analysis is also capable of providing other useful information. The detection of multiple bands of different sizes when the hybridization conditions are stringent is an indication that the heterogeneous nuclear RNA (hnRNA) could be processed into several forms by differential splicing. The detection of multiple bands of different sizes at lower stringency of hybridization could indicate differential splicing of hnRNA, but could also indicate the presence of mRNAs from a closely related gene or gene family. As well, the detection of mRNAs of different sizes at high stringency of hybridization in different tissues indicates that the gene is likely differentially post-transcriptionally regulated in different tissues.

Other methods of RNA detection and quantitation have been developed such as quantitative reverse transcriptase PCR (Sambrook and Russell, 2001) and the nuclease protection assay (Ausubel *et al.*, 1994). Both methods provide useful ways of examining RNA, but for both assays the RNA used cannot be recovered or reused, and RNA is the limiting reagent in this study. Northern analysis allows detection of, and an accurate quantification of specific transcripts, and moreover, allows the researcher to re-examine Northern blots by stripping the probe from analyzed blots and rehybridizing the blot with a different probe.

6-B UniGene Database

This study has identified ninety-three genes that are expressed in the rat retina during light-induced retinal degeneration (LIRD). Since these genes were identified in a

library prepared from mRNA from a rat retina treated with 4 hours of intense green light, it is clear that their gene products are expressed in the retina after exposure to intense green light, but the role of each of these gene products in the process of LIRD is not clear.

In the present case, Northern analysis of ninety-three different genes was considered impractical due to time constraints and the amount of material necessary for such an analysis. At the same time, any information about the genes identified could be useful in indicating the role of the genes in the retina. The information resources of the National Institutes of Health (NIH) National Centre for Biotechnology Information (NCBI) can provide information about the expression of genes through one of its databases, UniGene (www.ncbi.nlm.nih.gov/entrez/query.fcgi?db=unigene).

The UniGene database is a collection of clone sequences from cDNA libraries, *i.e.* libraries derived from the mRNA present in a particular tissue (Sections **2-G-2-H**). These expressed sequence tags (ESTs) have been clustered according to their identity to known genes. The database indicates the tissue from which the library containing the sequenced clone was derived, an indication of the number of ESTs that are in each cluster, and the total number of clones in the database that are derived from a particular tissue source. This information can be collected for a particular gene, and will provide an indication of what tissues the gene is expressed in. Ideally, the proportional occurrence of the cDNA in the libraries made from those tissues should give a relative idea of gene expression levels within a given tissue. This could be likened to an *in silico* Northern analysis, since it provides similar information to true Northern analysis: the presence or absence of the mRNA in a particular tissue, and the amount of mRNA present in a particular tissue.

One limitation of the UniGene database is that rat ESTs are not well represented in terms of the tissues from which they are derived. There are 335 319 rat sequences in the UniGene database, making it the third most represented organism in the database after human (3 905 320 sequences) and mouse (2 495 184 sequences). Unfortunately, 253 616 (76%) of the rat sequences present in the database do not indicate from which tissue they are derived, and 43250 (13%) are derived from only six different tissue sources: mixed tissue (21857, 34%), dorsal root ganglion (11229, 18%), chondrosarcoma (3476, 6%),

cartilage (3144, 5%), vibrissae (2527, 4%), and prostate (1017, 2%)[41]. This is not a representative sample of the tissue types of the rat, and is not useful for a survey of gene expression in the rat. Mouse tissues are far better represented in the database than rat tissues, and human tissues are even better represented than mouse tissues. One advantage found in the human information is that various eye tissues are well represented, which is not the case for the mouse information—presumably because of the tiny size of the mouse eye relative to the human eye. The rat information was surveyed only for the presence of the gene in the rat tissues represented in the database by any number of entries, not for the proportional representation of the genes by ESTs from particular libraries (**Figure 6-1.**). Since the rat tissues are not well represented and the human tissues are the best represented and include many different eye tissues, a survey of the UniGene data for the human orthologues of the ninety-three identified rat genes was undertaken. The human survey examined both the presence of the mRNA in tissues represented in the database (**Appendix 3.**), and the proportional representation of each mRNA in the database for major organs (**Figure 6-2.**), and for eye tissues (**Figure 6-3.**).

6-C Testing the Predictions of the *In silico* Analysis

The survey of human ESTs allows predictions about the tissue expression of particular genes to be made in humans. The information can also be used to predict the particular gene's expression in the rat since the two species are relatively closely related and in the same class (Mammalia). These predictions can then be tested by performing true Northern analysis. For practical reasons, involving the availability of human tissue for Northern analysis, this study concentrated on the predictive ability of the human UniGene data to correctly predict rat orthologous gene expression. Four genes identified as possible human disease candidates by bioinformatic analysis (**Chapter 5**) were chosen to test the accuracy and validity of the *in silico* Northern analysis described here. These genes are: Atp1a2, Fdps, Pak1, and Pea15, and were chosen because they may be important factors in retinal degeneration (**Chapter 5**) and the information describing them deserves to be extended. The inserts from the clones representing these genes were used as probes of rat multi-tissue Northern blots (MTNs).

[41] As of October 4th, 2002.

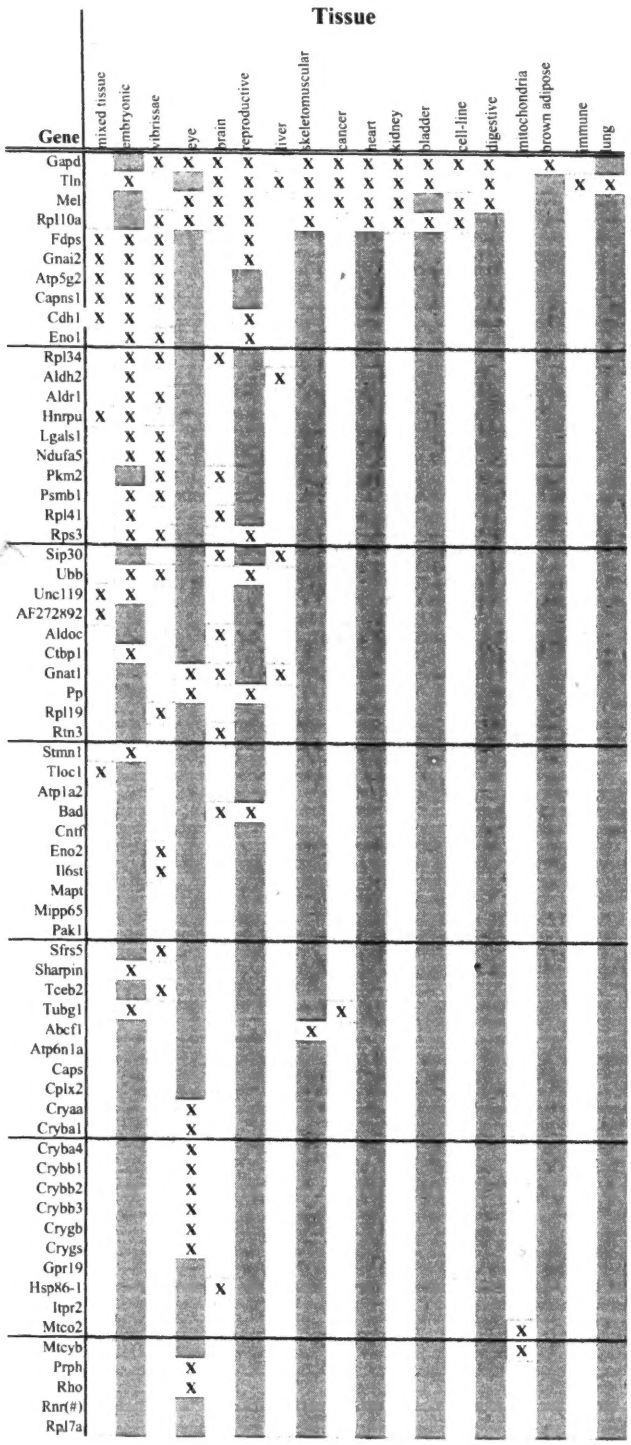

Figure 6-1. Tissue Distribution in the UniGene Database of Rat Sequences.

Presence of rat ESTs corresponding to the identified genes in the UniGene database is indicated with an "X". Only 65 of the 95 identified genes had any ESTs associated with them in the UniGene database.

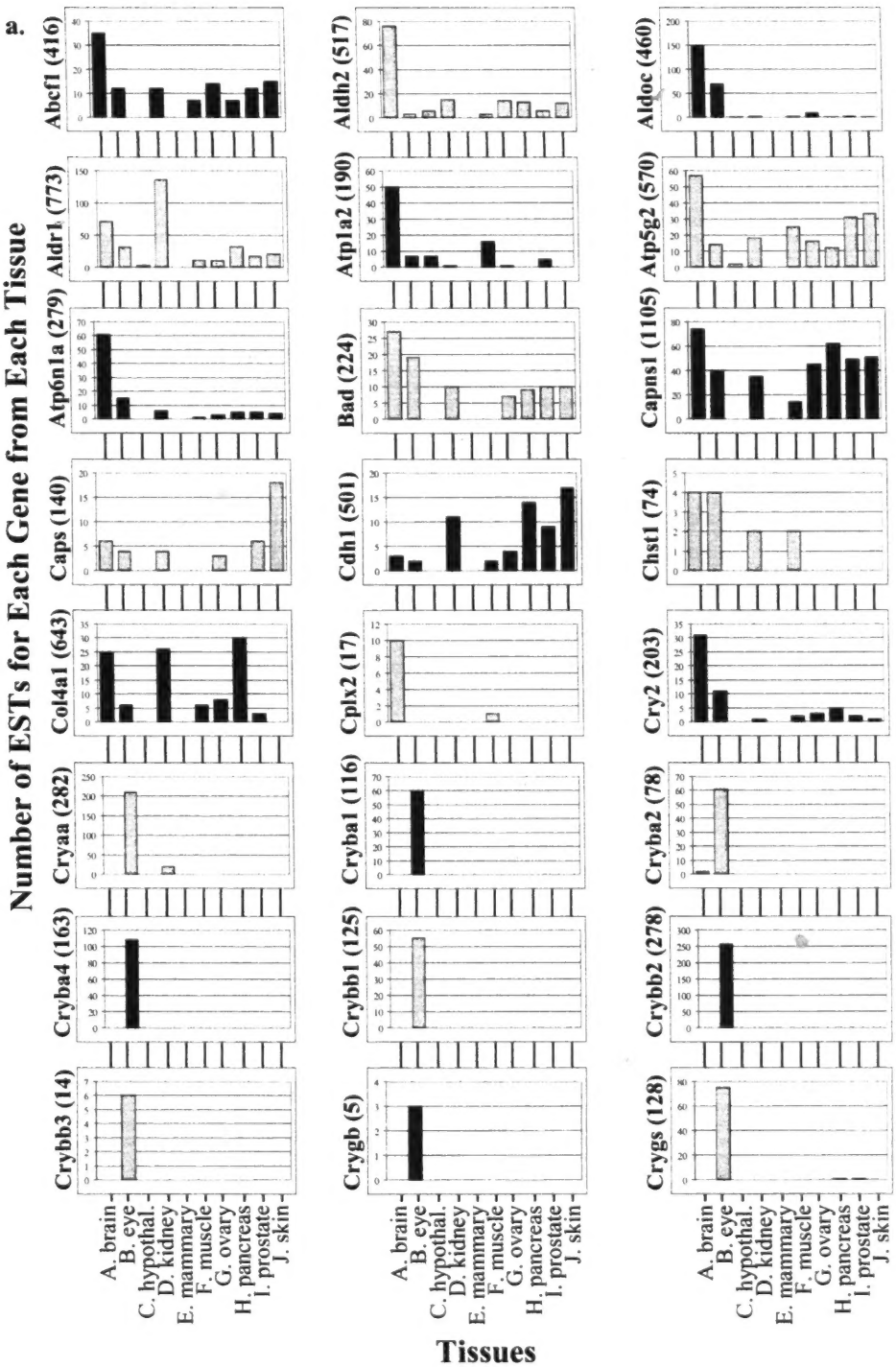

Figure 6-2. Tissue Distribution in the UniGene Database of Human Sequences.
(See page **126** for legend.)

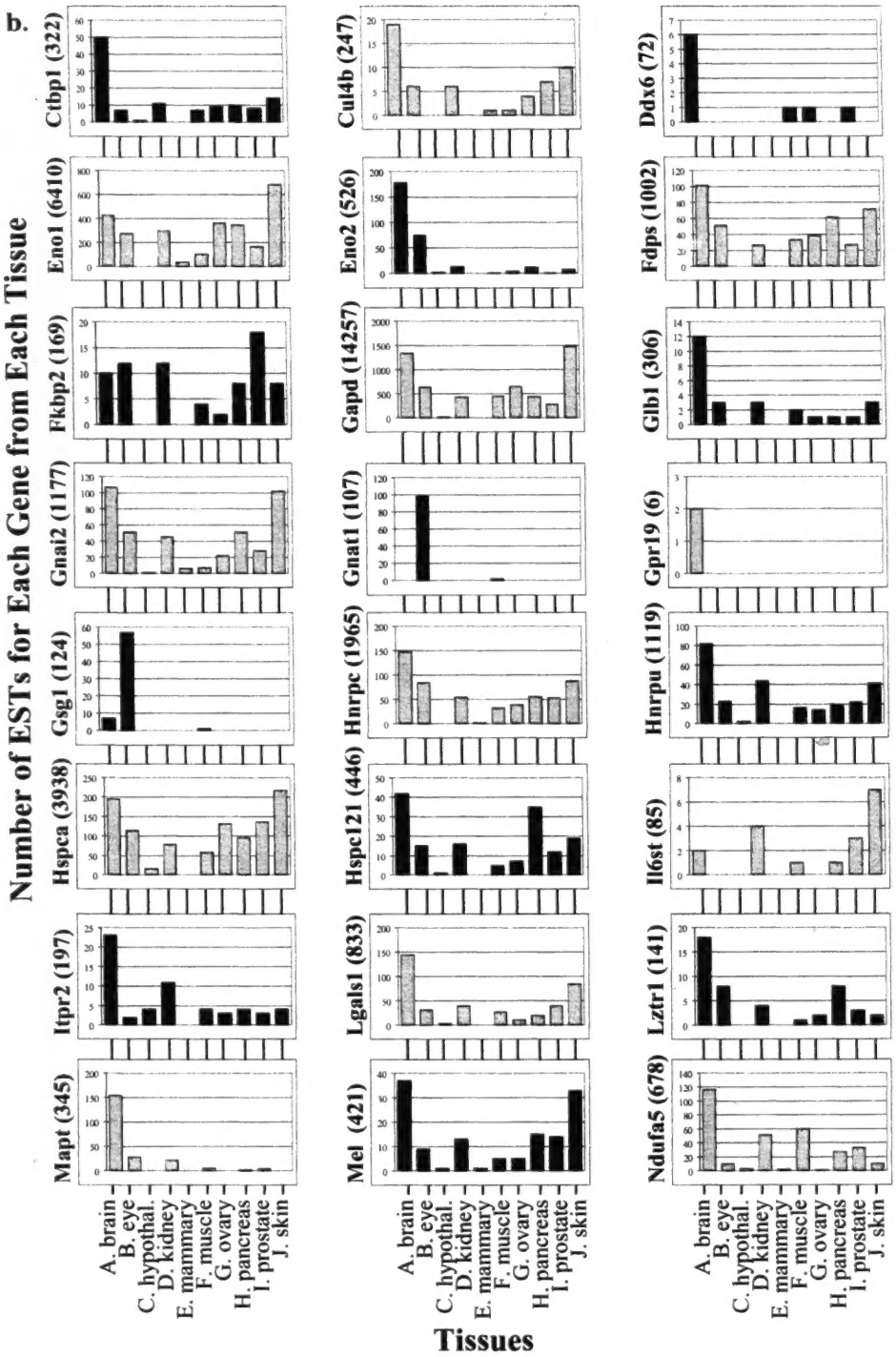

Figure 6-2. Tissue Distribution in the UniGene Database of Human Sequences.
(See page **126** for legend.)

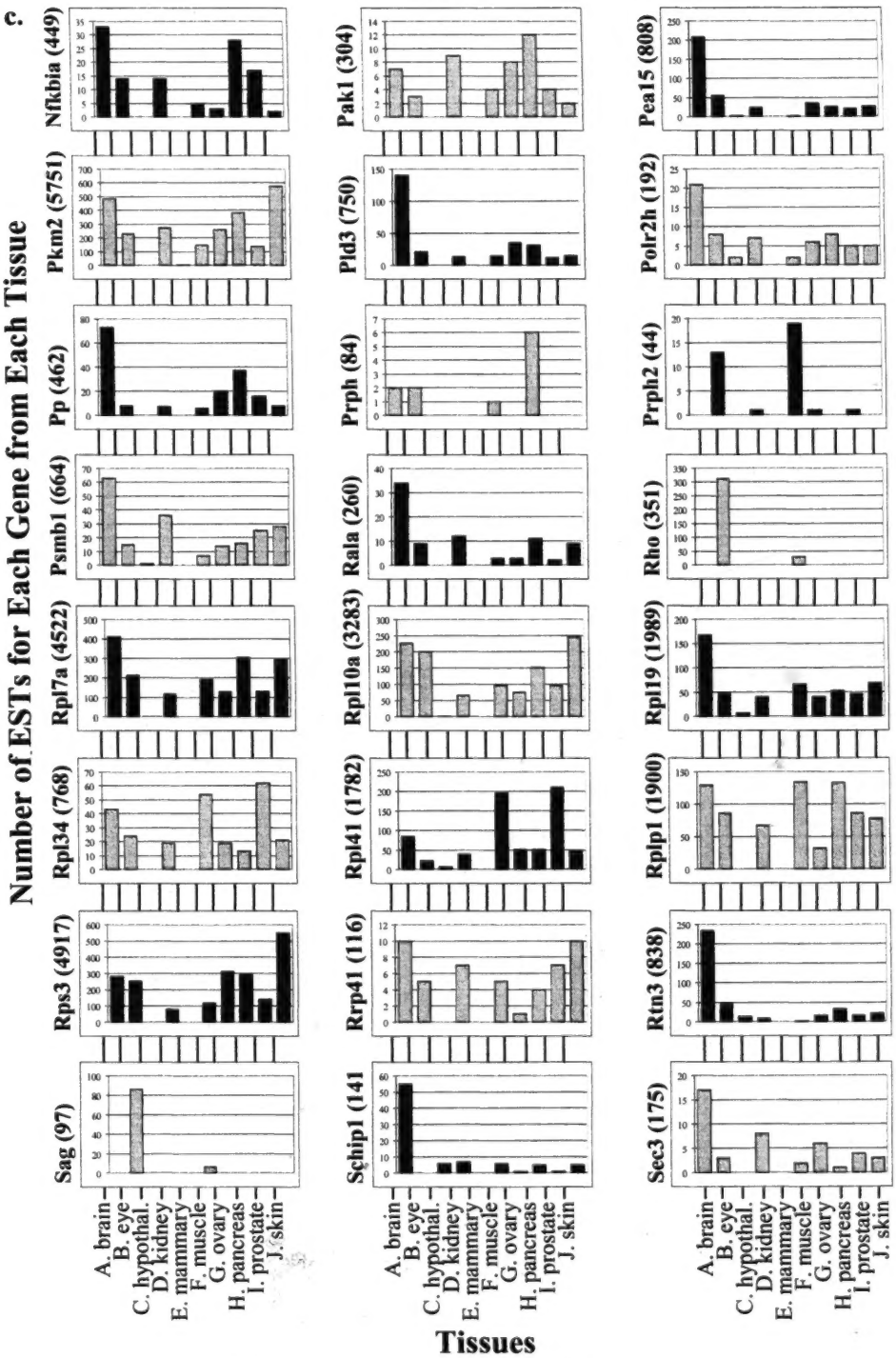

Figure 6-2. Tissue Distribution in the UniGene Database of Human Sequences.
(See page **126** for legend.)

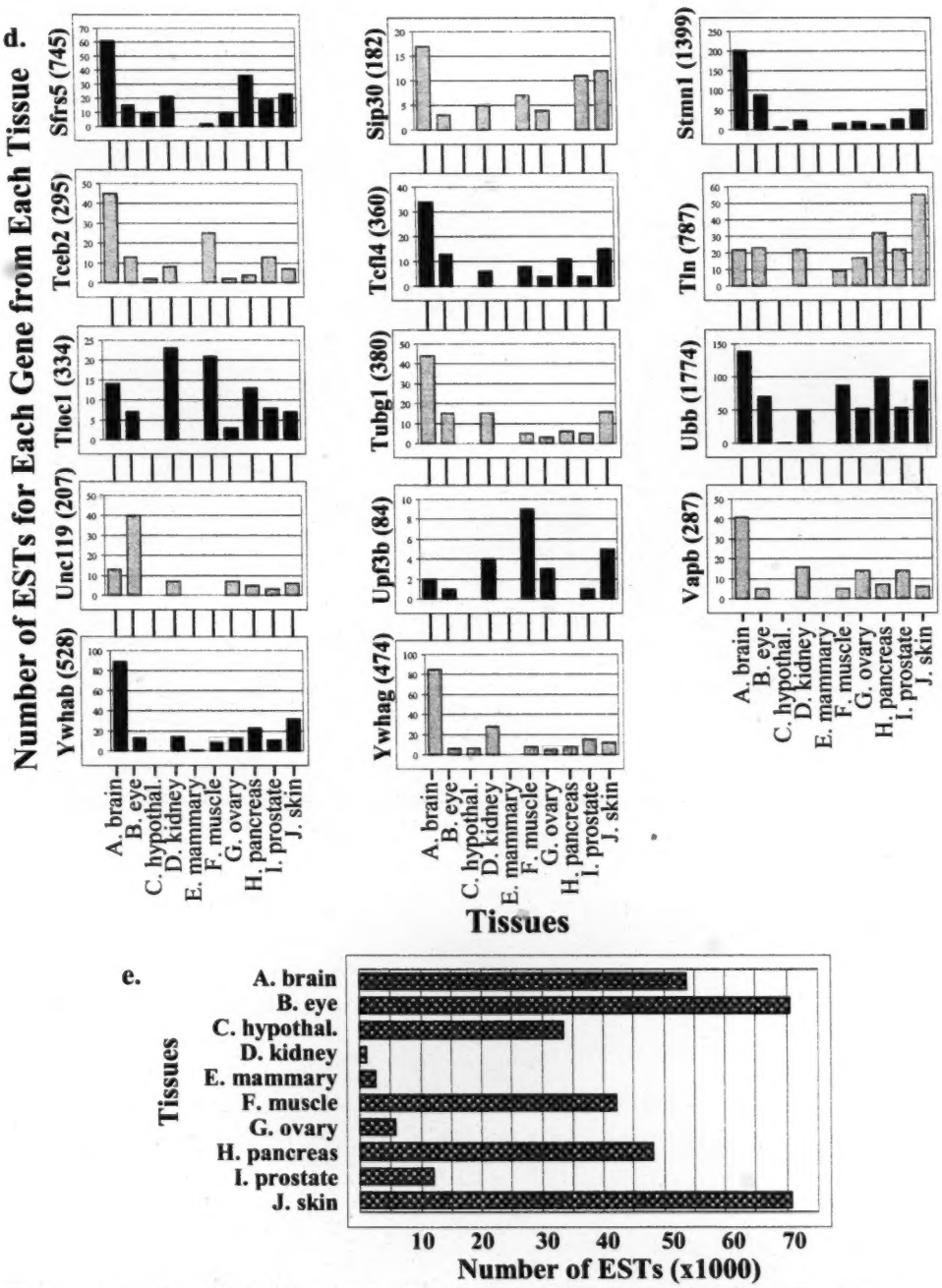

Figure 6-2. Tissue Distribution in the UniGene Database of Human Sequences.
a.-d. Number of expressed sequenced tags (ESTs) in the UniGene database (www.ncbi.nlm.nih.gov/) matching the sequence for the given gene follows the gene name. The distribution of those sequences among ten major organs is indicated in the graph. From left to right the tissues on each graph are: A. brain, B. eye, C. hypothalamus, D. kidney, E. mammary gland, F. skeletal muscle, G. ovary, H. pancreas, I. prostate, J. skin. **e.** The total number of ESTs in the UniGene database that are from each tissue. In the same order as above, except from top to bottom. The scale of the Number of ESTs axis is in thousands.
No human UniGene information was available for AF272892, Cntf, Mipp65 or Sharpin at the time of analysis (October 4th, 2002). Mtco2, Mtcyb, and Rnr(1-5) were considered too ubiquitous to be considered in this analysis.

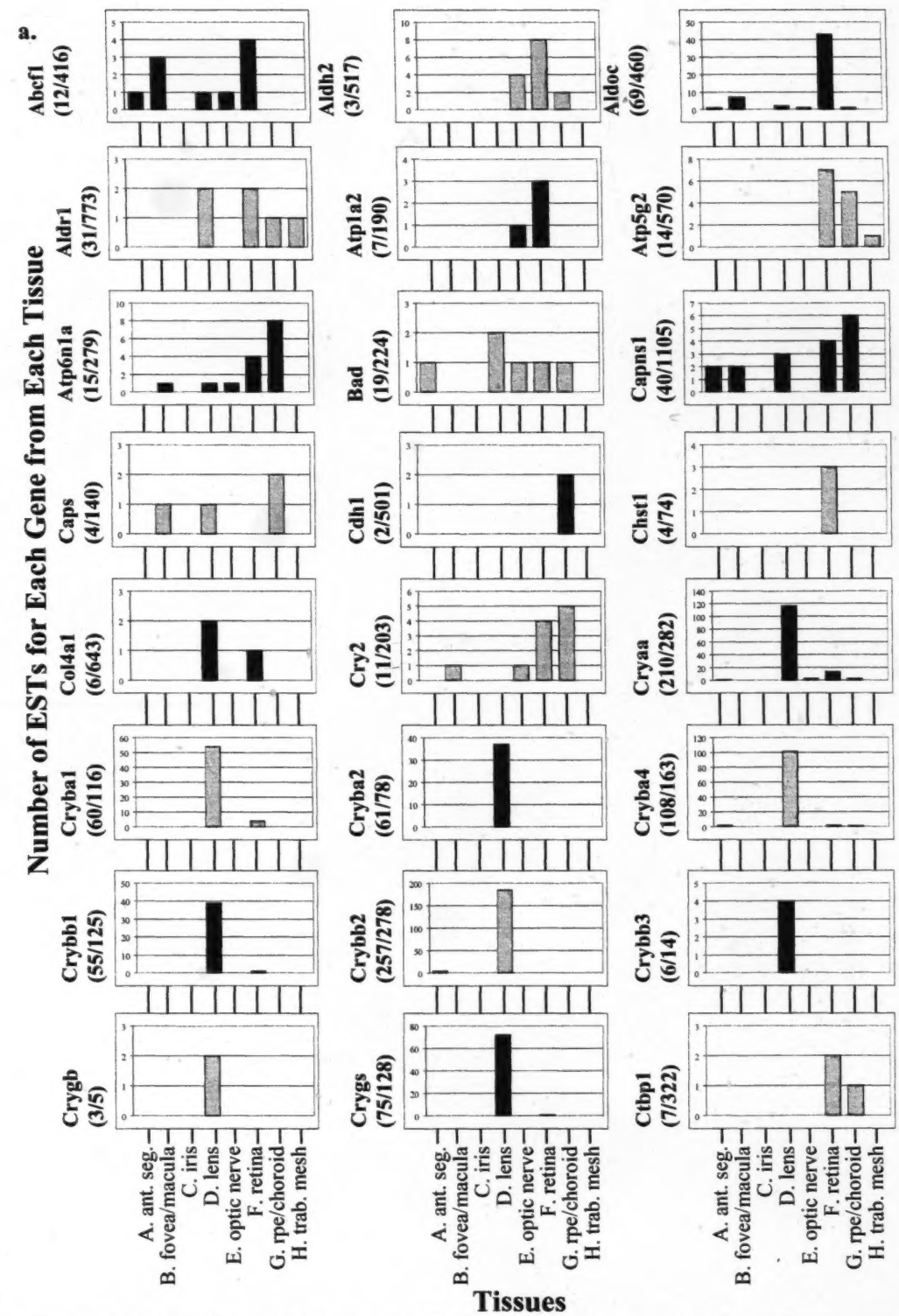

Figure 6-3. Eye Tissue Distribution in the UniGene Database of Human Sequences.
(See page **130** for legend.)

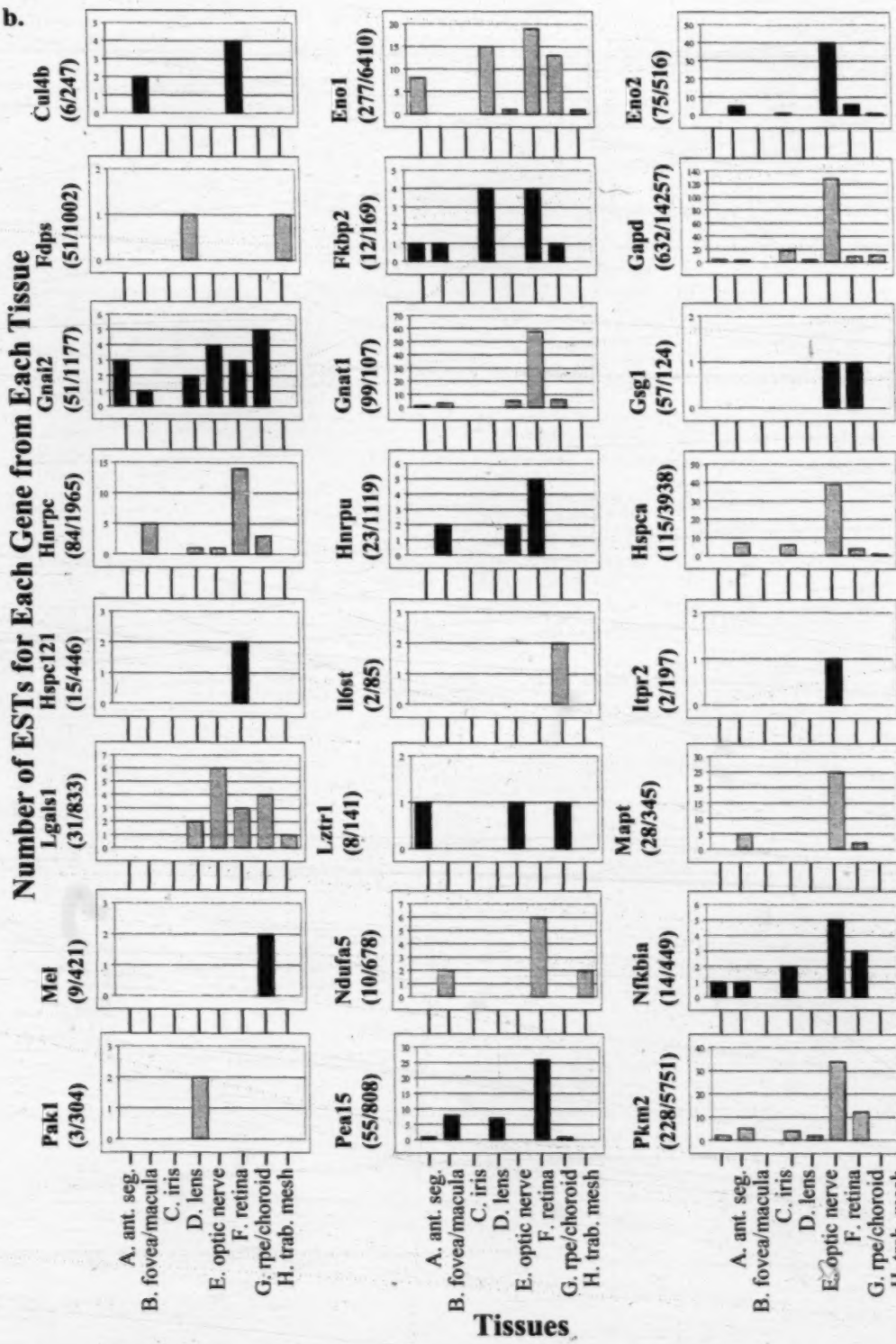

Figure 6-3. Eye Tissue Distribution in the UniGene Database of Human Sequences.
(See page 130 for legend.)

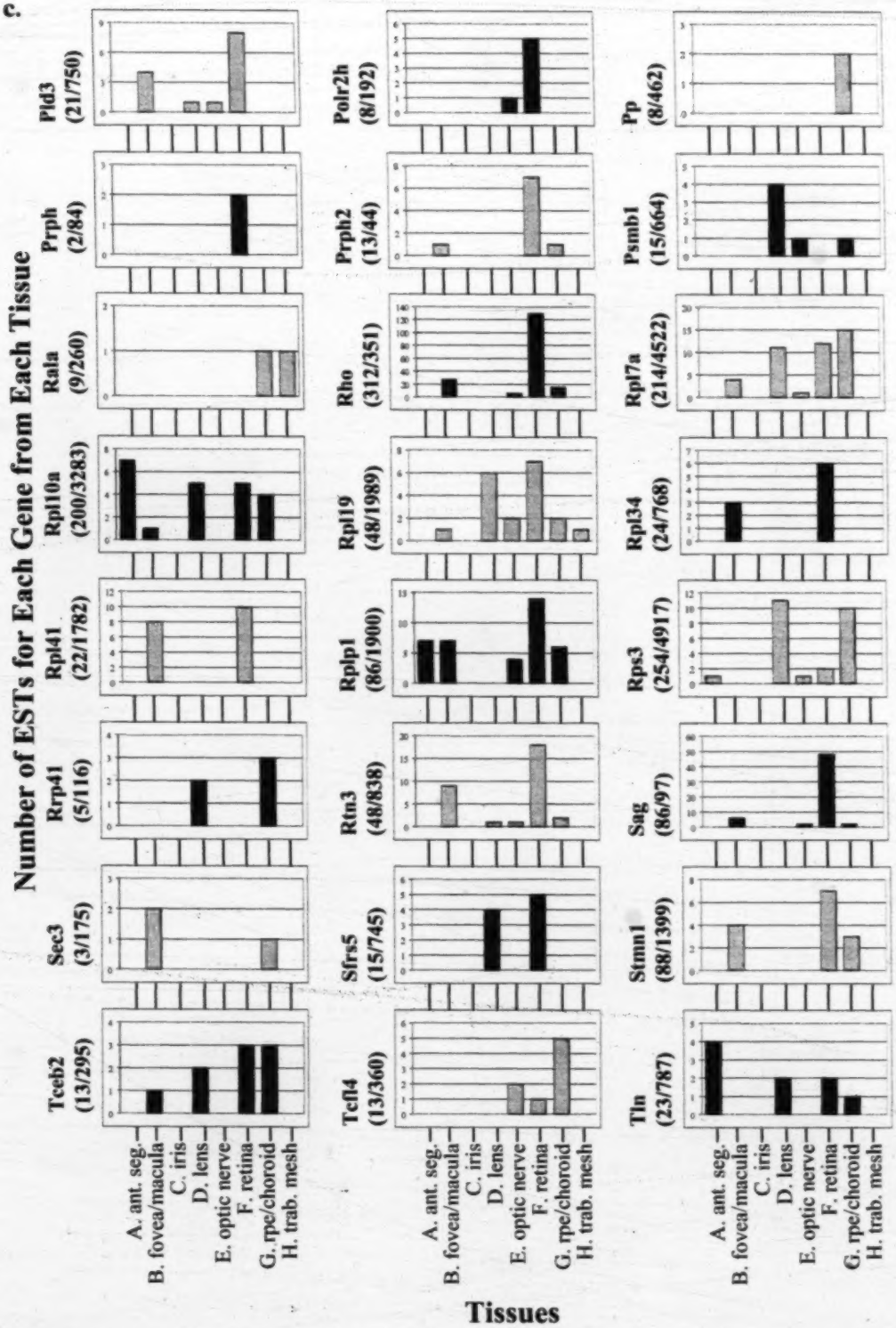

Figure 6-3. Eye Tissue Distribution in the UniGene Database of Human Sequences.
(See page 130 for legend.)

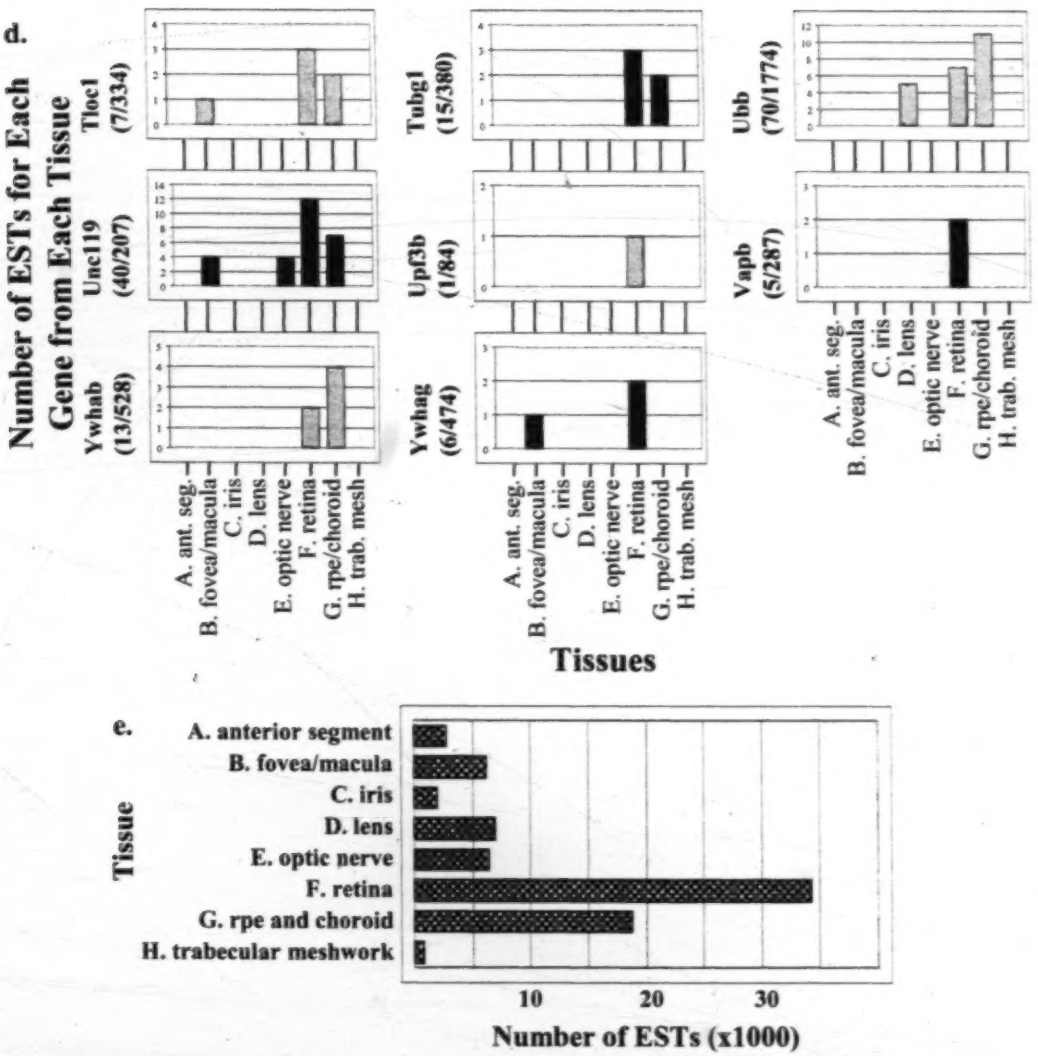

Figure 6-3. Eye Tissue Distribution in the UniGene Database of Human Sequences.
a.-d. Number of expressed sequenced tags (ESTs) in the UniGene database matching the sequence for the given gene follows the gene name, *e.g.* Ywhag (6/474) indicates that there are six eye-derived ESTs in the 474 total ESTs. The distribution of those sequences among ten tissues in the eye is indicated in the graph. From left to right the tissues on each graph are: A. anterior segment, B. fovea and macula, C. iris, D. lens, E. optic nerve, F. retina, G. retinal pigment epithelium and choroid, H. trabecular meshwork. **e.** The total number of ESTs in the UniGene database that are from each tissue. In the same order as above, except from top to bottom. The scale of the Number of ESTs axis is in thousands.
No human UniGene information was available for AF272892, Cntf, Mipp65 or Sharpin at the time of analysis (October 4th, 2002). Mtco2, Mtcyb, and Rnr(1-5) were considered too ubiquitous to be considered in this analysis. Cplx2, Ddx6, Gpr19, and Sip30 are not represented by any human eye-derived sequences in UniGene. Glb1 is represented by 3 (/306) whole eye sequences, and Schip1 is represented by 2 (/141) whole fetal eye sequences. (When the number of eye ESTs and the number of ESTs indicated in the graph are not equal, the ESTs mising from the graph are derived from either whole eye or whole fetal eye.)

6-C1 Atp1a2 Expression: The UniGene survey of Atp1a2 expression predicts that Atp1a2 is most highly expressed in the brain but is also expressed in the eye, the kidney and the ovary (**Figure 6-2a.**). Expression in the eye is predicted to be highest in the retina (**Figure 6-3a.**). Northern analysis confirms that Atp1a2 is expressed in the brain and the retina, but no detectable expression in the kidney or ovary is seen (**Figure 6-4a.**).

6-C2 Fdps Expression: Rat MTN Northern analysis shows that rat Fdps expression is highest in liver and retina, but also occurs in brain, kidney, and ovary (**Figure 6-4b.**). Liver expression was not considered in the *in silico* analysis, but the detection of retina expression was not predicted by the human UniGene data (**Figure 6-3b.**). The rat Fdps expression in brain, kidney and ovary was predicted by the human UniGene data, but large differences in the level of expression in these tissues was not expected (**Figure 6-2b.**), although the data suggested that expression in the brain would be higher than in the kidney or ovary, which is seen on the rat MTN.

6-C3 Pak1 Expression: The *in silico* analysis predicts that rat Pak1 will be expressed at about equal levels in the brain, the kidney, and the ovary (**Figure 6-2c.**). It is also predicted to be expressed in the eye, but not in the retina (**Figure 6-3b.**). True Northern analysis (**Figure 6-4c.**) indicates that Pak1 is expressed in the brain and kidney although brain expression is greater. The rat MTN also indicates that the predicted expression in the rat ovary is not seen, and retinal expression at levels almost as high as the brain's expression levels is seen where it was not predicted.

6-C4 Pea15 Expression: The Northern analysis of Pea15 shows that Pea15 is expressed in the brain, the kidney, and very highly in the retina (**Figure 6-4d.**). This supports the predictions of the UniGene data, but there are discrepancies. According to the UniGene data, expression of Pea15 is expected to be higher in the brain than the retina, and this is clearly not the case. As well, expression in the ovary is expected, but not seen (**Figures 6-2c.** and **6-3b.**).

6-C5 Gene Expression in the Eye: Ninety-three different genes were examined for bioinformatic data. Of these, 4 had no human sequences related to them in the UniGene database, and 3 were ribosomal RNA or mitochondrial genes that were

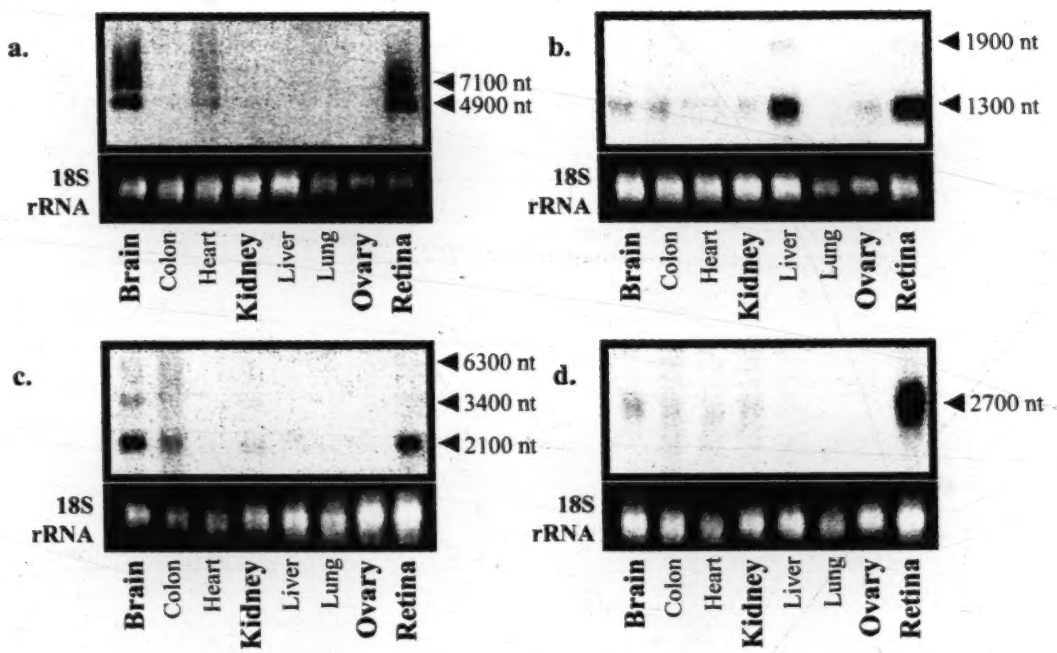

Figure 6-4. Multi-tissue Northern Analysis of Rat Gene Expression .
Levels of gene expression in various indicated rat tissues.
a. Atp1a2 gene expression. Expected size (Accession: NM_012505): 5109 nt. **b.** Fdps gene expression. Expected size (Accession: NM_031840): 1271 nt. **c.** Pak1 gene expression. Expected size (Accession: NM_017198): 2539 nt. **d.** Pea15 gene expression. Expected size (Accession: NM_008556): 1770 nt.
Tissues indicated in bold are tissues common to the UniGene data analysis. The 18S rRNA for each blot is included to indicate that RNA levels are relatively constant.

considered to be too ubiquitously expressed to consider (Mtco2,Mtcyb, and Rnr). The other 86 were all represented in the database by an average of 938 sequences (Range: 5-14257). Not all of these 86 genes were identified in UniGene as being expressed in the eye. Four genes (Cplx2, Ddx6, Gpr19, Sip30) had no eye-related sequences related to them in the database. Glb1 was represented by 3 (/306) whole eye sequences, and Schip1 was represented by 2 (/141) fetal eye sequences.

The human UniGene sequences contain a wide range of sequences from many different eye tissues. This allowed the genes to be analyzed in terms of their expression within the eye. Fifteen of the genes do not have sequences in the database that are derived from human retina (Table 6-1.), despite the fact that the largest class of human eye-related sequences is the retina sequences (34307). The rat orthologues of these 15 genes (/93; 16%) were identified in a screen of a retinal library, and it is interesting to note that this study is the first to associate these genes with expression in the human retina.

Table 6-1. Genes with No UniGene Retina-derived Sequences

Gene	Eye Sequences	Total Sequences	Gene	Eye Sequences	Total Sequences
Caps	4	140	Lztr1	8	141
Cdh1	2	501	Mel	9	421
Cryba2	61	78	Pak1	3	304
Crybb2	257	278	Pp	8	462
Crybb3	6	14	Psmb1	15	664
Crygb	3	5	Rala	9	260
Fdps	51	1002	Rrp41	5	116
Il6st	2	85	Sec3	3	175

6-D Conclusion

The possibility of *in silico* expression analysis is an enticing prospect, but has far to go before it can seriously be considered as an essential tool in research. The predictive value of *in silico* analysis was tested by comparing the human predictions of gene expression in particular tissues with Northern analysis of rat gene expression in rat tissues, and found that the predictions were of limited accuracy. This is not to suggest that the information gained from an exhaustive analysis of the UniGene data is not useful. The data indicates which tissues genes can be expected to be expressed in, based on

previous observations. One drawback for this study is that the sequences available for the rat do not provide enough breadth to the analysis of tissue expression. A second drawback is that the mouse sequences do not contain high levels of retina-derived sequences. These two elements mean that the most useful set of sequences is the human set, which exacerbates the problem of species-specific gene expression beyond even the mouse to rat differences. While some gene expression should be relatively consistent among all three species, some orthologous gene expression in mice and rats should be much more similar than the expression of orthologous genes in rats and humans. The potential differences mean that less confidence can be placed in the predictions made about rat gene expression using data derived from the human sequences in UniGene. It is possible that the predictions that these data make for human gene expression are more accurate than for rat gene expression, but this study cannot address that question.

The problem of lack of depth in the rat and mouse sequences is only one of the problems facing an *in silico* approach to gene expression analysis. It must also be considered that the sequences present in UniGene have many unknowable biases derived from the fact that the sequences are submitted to the NCBI from a host of sources across North America. This means that one cannot be certain: that the tissue the mRNA is isolated from is sufficiently similar to other tissues used for preparation of a different cDNA library, that a particular library is weighted towards either short or long cDNA inserts, that the sequences submitted are a representative portion of the total cDNAs present in the library—*i.e.* whether the libraries are normalized or not (Soares *et al.*, 1994), that duplicate sequences from a particular library are submitted instead of being winnowed out as redundant, *etc.*

In a more positive light, the UniGene sequences do identify tissues in which other researchers have found the genes. Some of the very specific tissues that have been used to make up libraries include relatively small tissues, like human amygdala or pineal gland, even rarer tissues, like human lymphomas, and even odder tissues like rat vibrissae. In many cases, tissues that are commercially available are defined at the level of the organ, *e.g.* heart, brain, eye, pancreas, *etc.* The UniGene database contains many examples of sequences derived from tissues within these organs, like aorta and ventricle, retina and fovea, and even pancreatic islet cells. With this ready-to-hand dissection of the

human organs, and to lesser extent rat and mouse organs, gene expression can be traced to specific areas within the organ, not just the organism.

In silico gene analysis cannot yet, and probably will not ever, replace true Northern analysis—or other methods of RNA analysis. Despite this, UniGene does provide concrete data as to whether or not expression of a particular gene has been identified in a tissue. Using UniGene for analysis of gene expression is probably more useful as background for setting up experiments that test the mechanism of a particular gene's expression. The researcher can determine tissues that are known to express the gene of interest at high levels because of a high representation of the mRNA in a particular library or tissue type found in UniGene. This would remove the necessity of a preliminary broad spectrum of Northern analysis, and conceivably help focus the research project from the start.

Chapter 7 Crystallin Gene Expression

Chapter 7 Crystallin Gene Expression

The differential cross screen of the 4 Hour Library (Sections **2-I**, **2-J**, and **Chapters 3** and **4**) selected 121 clones with known or putative identities, and these 121 clones represent 93 different mRNAs (**Chapters 5** and **6**). These sequences include 21 clones whose inserts match the sequence of crystallin mRNAs. This means that 17% of the identified clones (21/121) represent crystallin genes. The high incidence of crystallin mRNAs suggested that the crystallins be examined with regard to their expression in light-induced retinal degeneration (LIRD) in rats. This examination has identified a change in crystallin gene expression and protein localization, which, taken with the special characteristics of the crystallin proteins, suggest a role for the crystallins in rat retina and the process of LIRD.

7-A Crystallin Superfamily

For many of the crystallin genes studied, this thesis represents the first time that they have been identified in the rat retina. There is increasing evidence that the crystallins are expressed outside the lens, but this has been limited to mouse retinal expression of the genes for the α- and γ-crystallins (Sinha *et al.*, 1998; Jones *et al.*, 1999), and rat expression of the α-crystallins, and Crybb2 (Srinivasan *et al.*, 1992; Dirks *et al.*, 1998; Maeda *et al.*, 1999; Magabo *et al.*, 2000; Machida *et al.*, 2001). This study extends these observations by the identification of nine crystallin mRNAs in the rat retina—including Cryaa, all the β-crystallin genes, Crygb, and Crygs (**Chapter 4**)—out of the fifteen known crystallins (**Figure 7-1.**). An examination of the changes in expression of the crystallin genes during LIRD could help identify what role they play outside the lens.

In mammals, the crystallins are related proteins (**Figure 7-1.**) from three protein families: α-, β-, and γ-crystallins (Wistow and Piatigorsky, 1988). Crystallins are the major protein component of the mammalian lens where they are found in high-molecular weight (HMW) aggregates that act to maintain the transparency of the lens (Bloemendahl and de Jong, 1991; Horwitz *et al.*, 1998, 1999; Hejtmancik, 1998). The role of crystallins in protecting against cataracts is evidenced by several biochemical studies which show

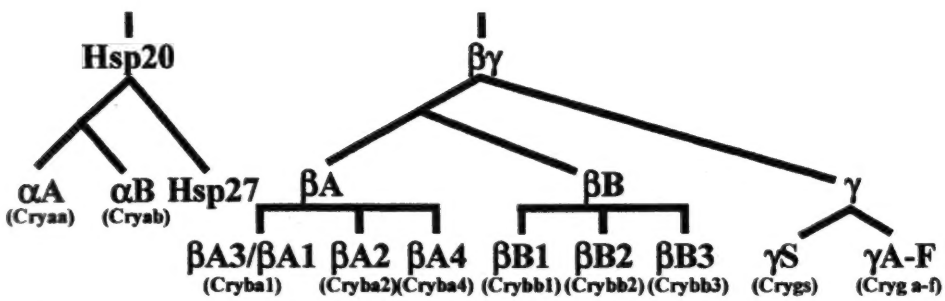

Figure 7-1. The Crystallin Proteins.

Through protein and nucleotide similarity and identity, it is evident that the crystallin proteins make up three families, the α-, β-, and γ-crystallins. The α-crystallins are part of the Hsp20, small heat shock protein, superfamily which share a conserved α-crystallin domain (pfam00011.5, HSP20). The α-crystallins have two family members, αA- and αB-crystallin, which differ by being acidic (A) or basic (B). The βγ-crystallin superfamily are a group of 14 proteins which share a common βγ motif (pfam00030.5, crystall). The superfamily is divided into the β- and γ-crystallins by the prescence of a relatively long N-terminus in the β-crystallins. The β-crystallins are further divided into acidic (A) or basic (B) proteins by the prescence in the basic β-crystallins of a free C-terminus. One of the βA-crystallin genes, βA1 gives rise to two protein products because of an alternate translation start site in the transcript, βA3 is the larger of these two proteins. The γ-crystallins are made up of 7 proteins which are all very similar to one another, although γS-crystallin is a noted outlier of the extremely closely related γA-F-crystallins, the genes for which occur in a single cluster that also includes the gene for βA2-crystallin. γS-Crystallin is considered to be the oldest member of the γS-crystallin family, and is highly conserved in mammals.

that the hydrophilic crystallin aggregates prevent the aggregation of hydrophobic misfolded proteins (Horwitz *et al.*, 1998; Rawat and Rao, 1998; Marini *et al.*, 2000), and by genetic studies which indicate that mutations in crystallin genes are the cause of familial cataractogenesis (Litt *et al.*, 1997, 1998; Kannabiran *et al.*, 1998; Vicart *et al.*, 1998; Der Perng *et al.*, 1999; Graw *et al.*, 1999; Héon *et al.*, 1999). The biology of the lens requires that specialized proteins exist that will prevent the aggregation of misfolded proteins because the central cells of the lens lose their nuclei and are incapable of producing proteins *de novo* to replace or repair misfolded or damaged proteins. Proteins in the central region of the lens are some of the oldest proteins in the mammalian body and must be exceptionally stable so as not to disrupt the clarity of the lens (Bloemendahl and de Jong, 1991; Graw, 1997; Oyster, 1999).

7-A1 α-Crystallins: There are two α-crystallin genes in the rat, mouse and human, these are the genes for αA-crystallin (Cryaa) and αB-crystallin (Cryab). The two protein products are distinguished on the basis of being acidic (A) or basic (B). *In vivo*, the two protein products function as a heterogeneous multimeric α-crystallin protein with an average size of 800 kiloDaltons (kDa), which exists in 3 αA-:1 αB- proportions (Graw, 1997; Derham and Harding, 1999; Horwitz *et al.*, 1999; Slingsby and Clout, 1999). The α-crystallin proteins are related to the small heat shock proteins (sHSPs) which are 20-30 kDa proteins which are upregulated in response to stress. In fact, a common amino acid motif of the sHSPs and the α -crystallins is referred to as the α-crystallin domain (pfam00011.5, HSP20; Wistow and Piatigorsky, 1988; de Jong *et al.*, 1993; Derham and Harding, 1999).

αA-crystallin is a member of the sHSP family that is not known to be induced by stress. Despite this, αA-crystallin has been shown to have a chaperone-like function *in vitro*, where it binds molten globule proteins and prevents their complete denaturation (**Figure 7-2.**; Horwitz *et al.*, 1998; Rawat and Rao, 1998; Marini *et al.*, 2000). Mutations in human Cryaa have been linked to autosomal dominant congenital cataract (Litt *et al.*, 1998), and it has also been shown in mice that preventing Cryaa expression in the lens results in a severe cataractous phenotype (Brady *et al.*, 1997). Since α-crystallin

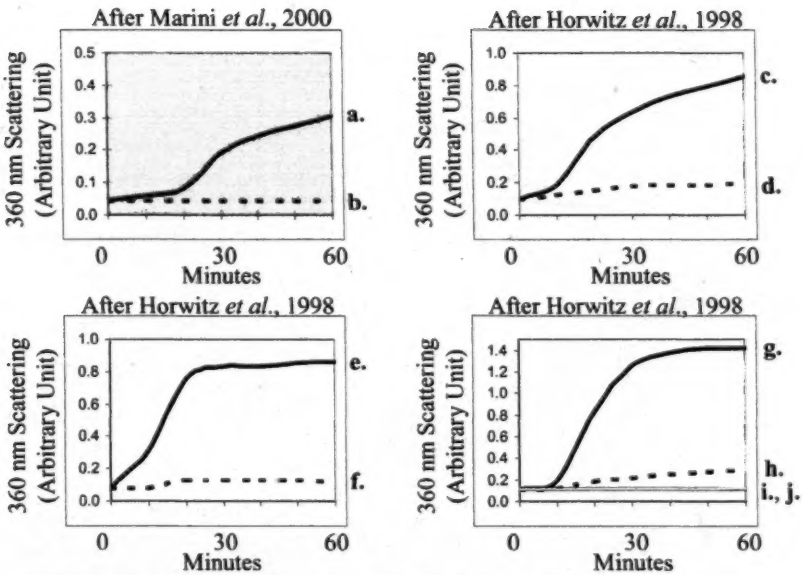

Figure 7-2. α-Crystallin Acts as a Chaperone.

The chaperone properties of α-crystallin were examined (Horwitz *et al.*, 1998; Marini *et al.*, 2000) by determining the amount of light scattering by solutions containing various proteins and α-crystallin. The experiment is based on the fact that non-native proteins in solution aggregate to form large complexes that increase the scattering of light with a wavelength of 360 nm. In all cases, addition of α-crystallin, and particularly αB-crystallin maintained the clarity of the solution and prevented the formation of protein aggregates.

a. *Bos taurus* sorbitol dehydrogenase (0.3 mg/mL) at 55°C. **b.** Cow sorbitol dehydrogenase (0.3 mg/mL) and cow α-crystallin (0.15 mg/mL) at 55°C. **c.** *Saccharomyces* sp. alcohol dehydrogenase (0.5 mg/mL) at 37°C. **d.** Yeast alcohol dehydrogenase (0.5 mg/mL) and *Homo sapiens* αB-crystallin (0.1 mg/mL) at 37°C. **e.** Human insulin (0.25 mg/mL) at 37°C. **f.** Human insulin (0.25 mg/mL) and human αB-crystallin (0.13 mg/mL)at 37°C. **g.** Cow α-lactalbumin (III) (1.25 mg/mL) at 37°C. **h.** Cow α-lactalbumin (III) (1.25 mg/mL) and human αA-crystallin (2.5 mg/mL) at 37°C. **i.** Cow α-lactalbumin (III) (1.25 mg/mL) and human α-crystallin (1.25 mg/mL) at 37°C. **j.** Cow α-lactalbumin (III) (1.25 mg/mL) and human αB-crystallin (1.25 mg/mL) at 37°C.

normally consists of both A and B subunits, it has been suggested that αA-crystallin is necessary for the proper function of αB-crystallin by maintaining αB-crystallin's solubility, and this is supported by the finding that αA-crystallin protein is less efficient as a chaperone than αB-crystallin (Datta and Rao, 1999; Andley *et al.*, 2000; Reddy *et al.*, 2000; Liao *et al.*, 2002). αA-crystallin was originally considered to be a lens-specific protein, but it has been identified in non-lens tissues, notably brain and spleen (Kato *et al.*, 1991a; Srinivasan *et al.*, 1992).

αB-crystallin has been identified as a sHSP that responds to various stresses (Klemenz *et al.*, 1991; Ray *et al.*, 2001), and biochemical studies of αB-crystallin *in vitro* indicate that it acts to prevent the unfolding of denaturing, molten globule proteins (Das *et al.*, 1996, 1999; Horwitz *et al.*, 1998; Rawat and Rao, 1998; Marini *et al.*, 2000; Rajaraman *et al.*, 2001; Carver *et al.*, 2002; Tanksale *et al.*, 2002). This activity is not a repair function, but rather a sequestering of misfolded or damaged proteins by α-crystallin. This presumably allows repair or degradation proteins to be recruited to the αB-crystallin-damaged protein complex before the damaged protein causes an irreversible aggregation of other misfolded proteins that could lead to dense light-scattering bodies in the lens (Wagner and Margolis, 1995; Brady *et al.*, 1997; Mathew and Morimoto, 1998; Wickner *et al.*, 1999; Connell *et al.*, 2001; Wang and Spector, 2000; Boscia *et al.*, 2000; Abgar *et al.*, 2001; Höhfeld *et al.*, 2001). While at first all the crystallins were considered to be lens-specific proteins, it was found that αB-crystallin is expressed in many tissues (Bhat and Nagineni, 1989; Kato *et al.*, 1991b, 2002; Vicart *et al.*, 1998), and has been implicated in many neurodegenerative diseases, including Alzheimer Disease where it is found as a component of neurofibrillary tangles (Gai *et al.*, 1999; Stege *et al.*, 1999; Yoo *et al.*, 2001).

7-A2 βγ-Crystallin Superfamily: The members of the βγ-crystallin superfamily all share an extremely stable characteristic secondary structure (pfam00030.5, crystall; Slingsby *et al.*, 1988; Wistow and Piatigorsky, 1988). This γ motif consists of four β strands which form a β-pleated sheet with portions of one strand exposed to the cytoplasm. The presence of four γ motifs in all the βγ-crystallins allowed the βγ-crystallin genes to be identified as a gene family which likely arose due to gene

duplication and fusion events (Slingsby *et al.*, 1988; Wistow and Piatigorsky, 1988; Clout *et al.*, 2000). The βγ-crystallin's role in the lens, alongside α-crystallin, seems to be to maintain lens clarity. They are considered to act as a hydrophilic, malleable, intracellular crystal that allows fine homeostatic control of the refractive index of the lens in response to systemic or ocular physiological changes (Graw, 1997; Oyster, 1999). In this view, α-crystallin also provides this fine control because of its structure, but has another role as a chaperone, preventing nascent hydrophobic regions of damaged or misfolded proteins from precipitating other hydrophobic proteins to form a light-scattering inclusion body within the lens (Bloemendahl and de Jong, 1991; Wang and Spector, 1995; Graw, 1997; Oyster, 1999).

The β-crystallin proteins are divided into two classes: acidic (A) or basic (B), which classification is dependent on the presence (basic) or absence (acidic) of C-terminal peptides extending from the common βγ-crystallin structure. The β-crystallins are distinguished from the γ-crystallins by the presence of a 10-58 amino acid (aa) N-terminal peptide extending from the common βγ-crystallin structure where the γ-crystallins have a 2-4 aa N-terminal extension (Slingsby *et al.*, 1988; Wistow and Piatigorsky, 1988; Graw, 1997).

Seven β-crystallins, the products of six genes, have been identified in mammals to date. The proteins are found in 50-200 kDa dimeric or heteromeric aggregates of β-crystallins within the lens (Wistow and Piatigorsky, 1988; Slingsby and Clout, 1999). Mutations in the genes for two of the β-crystallins, Cryba1 (βA3/A1) and Crybb2 (βB2), have been associated with diseases that result in congenital cataractogenesis (Litt *et al.*, 1997; Graw *et al.*, 1999; Kannabiran, 1998), but the other β-crystallin genes: Cryba2,Cryba4, Crybb1, and Crybb3 have not yet been associated with any genetic disease. Crybb2 is distinct from the other β-crystallins in that its expression has been identified in non-lens mammalian tissue, including the retina (Dirks *et al.*, 1998; Magabo *et al.*, 2000). No other β-crystallin gene has been identified as being expressed outside the mammalian lens, although Cryba1 expression was identified in *Gallus gallus* (chicken) retina (Ishibashi *et al.*, 2000).

Table 7-1. Crystallin Gene Locations in Rat, Mouse and Human

Arranged numerically by human chromosome.

Gene	*Rattus norvegicus*	*Mus musculus*	*Homo sapiens*
Cryga-Crygf	9q31-q34	1 (32 cM)	2q33-q35
Cryba2	9q31-q34	1 (40.80 cM)	2q34-q36
Crygs	11q23	16 (16.10 cM)	3q25-qter
Cryab	8q24	9 (29.00 cM)	11q22.3-q23.1
Cryba1	10q23-q32.1	11 (44.71 cM)	17q11.2-q12
Cryaa	20p12	17 (17.4 cM)	21q22.3
Crybb3	12q16	5 (60.00 cM)	22q11.23
Cryba4	12q16	5 (59.00 cM)	22q12.1
Crybb1	12q16	5 (59.00 cM)	22q12.1
Crybb2	12q16	5 (59.00 cM)	22q12.1

There are also seven members of the γ-crystallin family, and they are very closely related. Six of the genes: Cryga, Crygb, Crygc, Crygd, Cryge, and Crygf, are found clustered on the same chromosome near Cryba2 in humans, rats, and mice. This clustering is also seen with the Crybb1-3 and Cryba4 genes (Table 7-1), which is consistent with the hypothesis that the βγ-crystallins arose from gene duplication events (Slingsby *et al.*, 1988; Wistow and Piatigorsky, 1988; Clout *et al.*, 2000). The clustering also serves to underscore the uniqueness of the occurrence of four genes on different, separate chromosomes: Cryaa, Cryab, Cryba1, and Crygs.

Crygd has been associated with a form of juvenile cataractogenesis (Stephan *et al.*, 1999), but there is little else of significance to distinguish the products of Cryga-Crygf from each other, *e.g.* the coding regions of the mouse genes are 79-97% identical to each other, the mouse proteins are 72-90% identical and, when conservative amino acid substitutions are considered, the proteins are 87-94% similar. In contrast to the α- and β-crystallins, the γ-crystallins are known to be monomeric proteins with a high thiol content. The cysteine and methionine contents of the mouse γ-crystallin proteins are both on average 4% of the total amino acids, while the average cysteine and methionine content of all the crystallins is 2 and 3% respectively (**Figure 7-8.**). The prevalence of thiol groups in the γ-crystallins is thought to maintain the structure of the γ-crystallins in the face of oxidative stress, since the thiol groups can be reduced by glutathione, which is present in high concentrations in the lens (Giblin, 2000). The γ-crystallin-glutathione reaction is considered important because it would maintain the γ-crystallins in a near

native state that cannot form protein-protein disulfide bonds, which would serve as the nucleus for protein aggregation, and the reaction also scavenges electrons which results in a reduction of free radicals and peroxides so that they cannot damage cellular components (Puertas *et al.*, 1993; Wang *et al.*, 1997; Tanito *et al.*, 2002b). The γA-F-crystallins were considered lens-specific until they were identified in the mouse retina (Jones *et al.*, 1999).

An outlier of the γ-crystallin family is γS-crystallin. Of all the γ-crystallins, this protein has the most similarity to the β-crystallins, and is the most different of the γ-crystallins, at both the protein and mRNA level. While it is the most different of the γ-crystallins, it is still more similar to the γ-crystallins than to the β-crystallins, and shares the γ-crystallin features of being a monomeric protein with a high thiol content. These considerations suggest that γS-crystallin is the earliest member of the γ-crystallin family (Wistow and Piatigorsky, 1988). γS-crystallin was also considered to be lens-specific until it was identified in the mouse retina (Sinha *et al.*, 1998).

7-B Stress Proteins

LIRD treatment results in oxidative stress to the rat retina (Organisciak *et al.*, 1991, 1992a,b, 1999b), and the increased expression of known stress response genes like Hmox1 which produces the antioxidant protein heme-oxygenase-1 (HO-1; Kutty *et al.*, 1995; Organisciak *et al.*, 1995; Wong *et al.*, 2001). Other stress response proteins should also be required by the light-treated rat retina, and systemic stress response proteins are likely to be involved in this protection. For this reason, Hsp70, Hsp90, and copper-zinc superoxide dismutase (SOD1) were also examined in the context of LIRD.

Systemic stress is known to induce expression of Hsp70 and Hsp90 proteins (Fink, 1999; Frydman, 2001), so it is reasonable to think that the regulation of the genes for these proteins, Hspa1a and Hspca[42] respectively, is changed in response to oxidative stress in the rat retina. These proteins are known to function in the ATP-dependent folding of nascent proteins, and the recruitment of proteases for degradation of damaged proteins (Mathew and Morimoto, 1998; Wickner *et al.*, 1999; Connell *et al.*, 2001;

[42] In rats, this gene is not yet identified except by expected synteny (Gómez-Fabre *et al.*, 2001). The mouse gene name is Hsp86-1, and the human gene name is HSPCA. The rat gene name usually matches the orthologous human gene name (www.ncbi.nlm.nih.gov/LocusLink/).

Höhfeld *et al.*, 2001). Since LIRD is known to involve the *de novo* synthesis of both pro- (*e.g.* caspases) and anti- (*e.g.* HO-1) apoptotic proteins and the apoptotic degradation of proteins by the caspases and proteasomes (Chang *et al.*, 1993; Portera-Cailliau *et al.*, 1994; Milam and Li, 1995; Carmody and Cotter, 2000; Höhfeld *et al.*, 2001), Hsp70 and Hsp90 levels should be expected to increase in LIRD.

Since LIRD results in oxidative stress it is reasonable to suppose that antioxidant proteins other than HO-1, such as SOD1 (Mittag *et al.*, 1999; Borg and London, 2002), should be induced in the rat retina. SOD1 reduces the superoxide anion (O_2^-), a reactive oxygen species (ROS), to oxygen (O_2) and hydrogen peroxide (H_2O_2). H_2O_2, another ROS, is in turn oxidized by either a glutathione peroxidase or a catalase, and the products of these reactions are not toxic (Section **1-B3**, **Figure 1-6.**; Fridovitch, 1995).

7-C Experimental Outline

Given the predominance of crystallin genes identified in the differential cross screen (**Chapters 3 and 4**), the crystallins were selected for closer study of their expression patterns in LIRD. Known stress response genes: Hspa1a (Hsp70), Hspca (Hsp90), and Sod1 (SOD1), were also examined to illustrate the effect of light exposure on expression of these stress and antioxidant genes. The known stress-response genes were expected to show increased expression with increasing exposure to intense green light.

Table 7-2. Gene and Protein Expression Analyses Performed

Gene	Northern Analysis	Western Analysis	Immuno-histochemistry
Cryaa	Yes	Yes	
Cryab	Yes	Yes	Yes
Cryba1	Yes	Yes	
Crybb2	Yes		
Crygs	Yes	Yes	Yes
Hspa1a	Yes	Yes	
Hspca	Yes		
Sod1	Yes		

Representative genes of the crystallins and other stress proteins were examined for the level of expression of their transcripts or gene products (Table 7-2.). Cryaa, Cryab, Cryba1, Crybb2, Crygs, Hspa1a, Hspca[42], and Sod1 levels were determined by Northern analysis of the LIRD Profile (Sections **2-B-2-E** and **2-K**, **Figure 7-3.**), using cDNA clones representing the mRNAs. As well, Western analysis of αA-crystallin, αB-

crystallin, the β-crystallins, γS-crystallin, and Hsp70 was performed (Sections **2-L** and **2-M**, **Figure 7-4.**). Finally, immunohistochemistry was performed to determine the localization of αB-crystallin and γS-crystallin in the retina (Section **2-N**, **Figures 7-5.** and **7-6.**).

7-D Northern Analysis

Northern analysis was performed as described in Section **2-K**. The results of densitometric analysis were normalized to the 18S ribosomal RNA band of the gel (Section **2-K5**). Multiple blots were probed with the same probe, and densitometry was determined for each separate blot. The normalized results for each blot were then made relative to the intensity of the band in the untreated dark-reared rat retinae (Dark), and pooled to find the average level of expression in the retinae of dark-reared rats treated with either 4 hours (4 Hour) or 8 hours (8 Hour) of intense green light.

7-D1 Cryaa: The 4 Hour retinal expression of the Cryaa transcript (**Figure 7-3a.**) increases to 121% of Dark levels with a standard deviation (s.d.) of 18% (n=3). This marginal increase is improved on when 8 Hour mRNA levels increase to 172% (s.d. 35%) of Dark levels. The detected transcript is 1275 nucleotides (nt) in length (n=3), which accords well with the 1056 nt size of the mRNA, Accession (Acc.): NM_012534, listed in the National Centre for Biotechnology Information (NCBI) GenBank database (www.ncbi.nlm.nih.gov).

7-D2 Cryab: Retinal expression of the Cryab transcript (**Figure 7-3b.**) increases to 121% (s.d. 7%, n=3) of Dark levels in the 4 Hour sample, and increases to 158% (s.d. 9%, n=3) in the 8 Hour sample. The detected trancript size is 661 nt (n=3), which is very close to the 528 nt mRNA listed in GenBank (Acc.: NM_012935).

7-D3 Cryba1: The transcript of the Cryba1 gene shows the greatest change in expression of the crystallins examined (**Figure 7-3c.**). Levels of this transcript in the 4 Hour sample are 527% (s.d. 118%, n=3) of Dark levels. After the initial increase in Cryba1 mRNA, the levels of this transcript in the 8 Hour sample then decline to 138% (s.d. 18%, n=3) of the Dark levels. The 720 nt band (n=3) identified on the autoradiograph matches the size of the 650 nt Cryba1 mRNA in the NCBI database (Acc.: X15143).

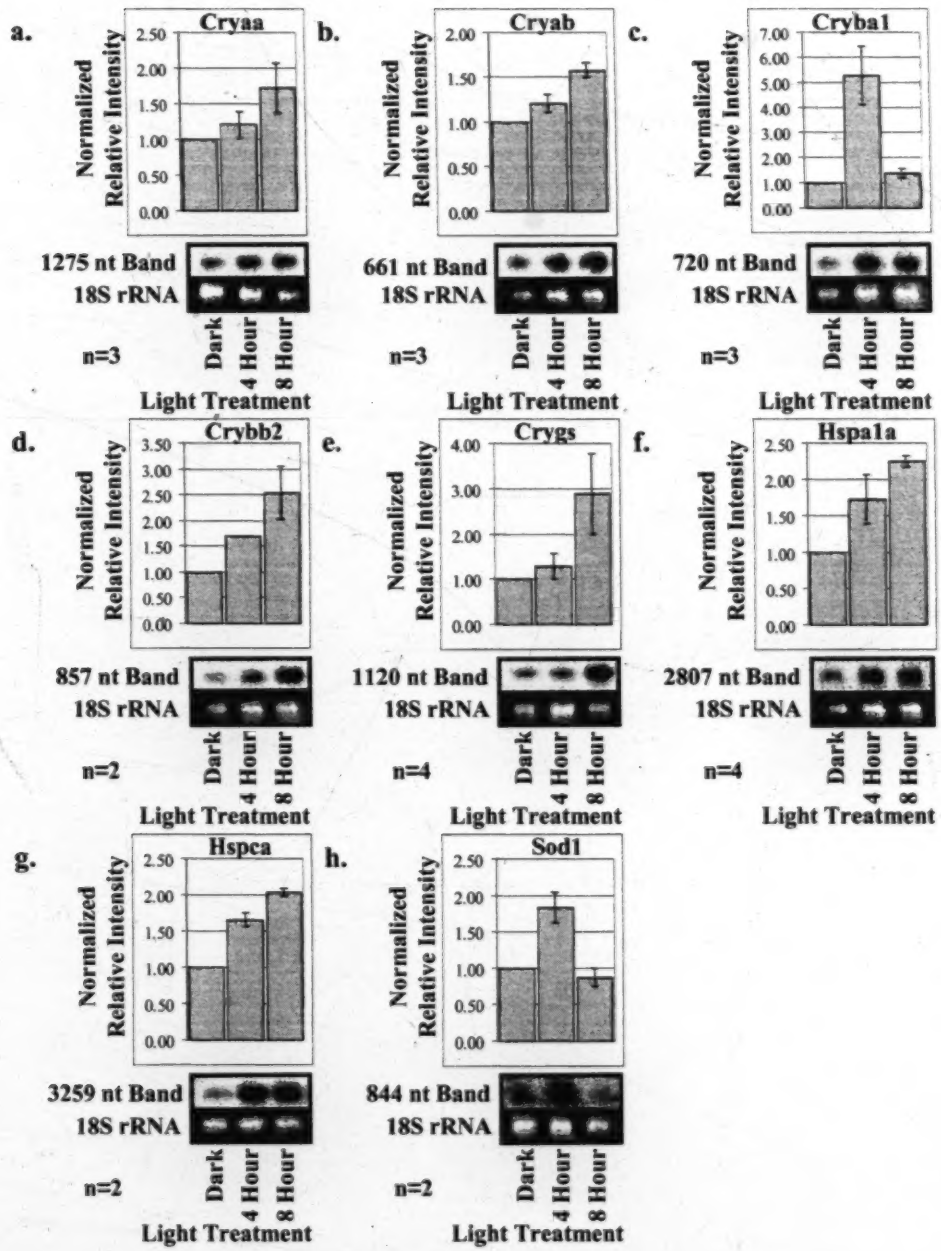

Figure 7-3. Normalized Relative Intensity of Autoradiograph Bands of LIRD Northern Blots.

a. Cryaa, **b.** Cryab, **c.** Cryba1, **d.** Crybb2, **e.** Crygs, **f.** Hspa1a, **g.** Hspca, **h.** Sod1

Error Bars indicate the standard deviation of the sample set where n>2, and the mean difference between blots where n=2. Autoradiograph band intensity determined by densitometry is normalized to the intensity of the ethidium bromide stained 18S rRNA band of the gel from which the Northern blot was made. A representative autoradiograph is shown for each transcript.

7-D4 Crybb2: Crybb2 transcripts increase to 170% (mean difference 1%, n=2) of Dark levels in the 4 Hour sample, and this increase continues to 254% (mean difference 50%, n=2) of Dark levels in the 8 Hour sample (**Figure 7-3d.**). The detected band is 857 nt in length (n=2), which matches the 735 nt length of the Crybb1 mRNA in the database (Acc.: NM_012937).

7-D5 Crygs: The detected Crygs transcript on the LIRD profile is 1120 nt in length (n=4), which is larger than the 703 nt size of the mouse Crygs mRNA in the NCBI database (Acc.: NM_009967). Crygs transcript levels increase to 128% (s.d. 28%, n=4) in the 4 Hour sample as compared to the Dark sample. The transcript levels in the 8 Hour sample are 289% (s.d. 88%, n=4) of the levels in the Dark (**Figure 7-3e.**).

7-D6 Hspa1a: The levels of the transcript for Hsp70-1 increase to 172% (s.d. 33%, n=4) of Dark levels in the 4 Hour sample. This increase is then followed by an increase to 225% (s.d. 7%, n=4) of Dark levels in the 8 Hour sample (**Figure 7-3f.**). The detected transcript size of this mRNA was 2807 nt (n=4) which is close to the 2455 nt size noted in the NCBI database for (Acc.: NM_031971).

7-D7 Hspca[42]: mRNA expression of Hspca is similar to Hspa1a (**Figure 7-3g.**). The 4 Hour sample indicates that Hspca transcript levels rise to 165% (mean difference 10%, n=2) of Dark levels, and at 8 Hour are at 204% (mean difference 5%, n=2). The identified transcript size is 3259 nt (n=2) which is close to the 2975 nt size of the mouse mRNA for Hsp86-1 in Genbank (Acc.: NM_010480).

7-D8 Sod1: Sod1 mRNA levels increase in the 4 Hour samples to 183% (s.d. 20%, n=3) of Dark, but then decrease to 87% (s.d. 12%, n=3) of Dark levels in the 8 Hour samples (**Figure 7-3h.**). The observed transcript size on the autoradiograph is 844 nt (n=3), and the mRNA size in Genbank is 650 nt (Acc.: NM_017050).

7-E Western Analysis

7-E1 αA-Crystallin (Cryaa): The anti-αA-crystallin antibody detects an approximately 32 kDa protein over the course of the Western LIRD Profile (**Figure 7-4a.**). The molecular mass observed on a Western blot derived from an SDS-PAGE gel (Section **2-M**) is higher than that predicted for an αA-crystallin 19.9 kDa monomer, SwissProt Accession (SwissProt; www.ebi.ac.uk/swissprot): P02489, but it is the only

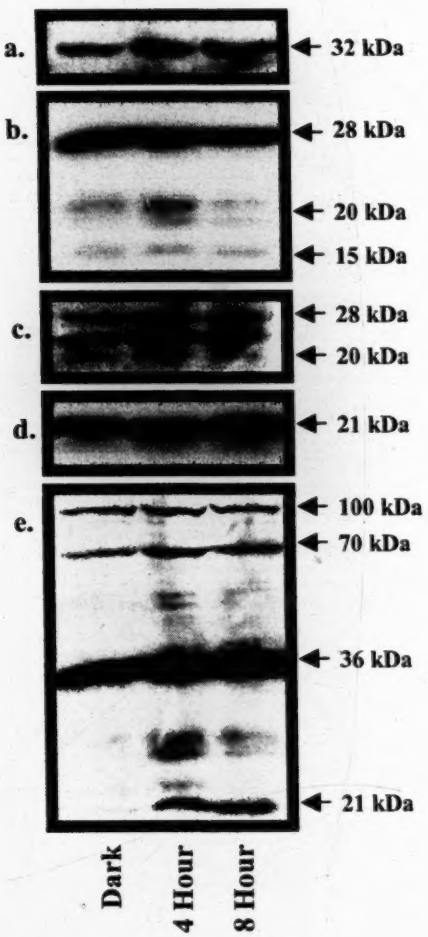

Figure 7-4. Electrochemoluminescence Detection of Peroxidase-conjugated Secondary Antibodies.

Primary antibodies: **a.** Anti-αA-crystallin, **b.** Anti-αB-crystallin, **c.** Anti-β-crystallin, **d.** Anti-γS-crystallin, **e.** Anti-Hsp70. (kDa = kiloDalton)

significant band on the very short (1 s) exposure. The amount of protein detected follows the same general trend of the Cryaa transcript, with an increase (≅120%, n=2) in protein levels from the Dark sample to the 4 Hour sample which is maintained in the 8 Hour sample.

7-E2 αB-Crystallin (Cryab): Western analysis with an anti-αB-crystallin antibody detects four bands ranging in size from approximately 15 kDa to 28 kDa (**Figure 7-4b.**). Two of these bands are a close 20-21 kDa doublet. The observed doublet matches the expected 20.1 kDa size well (SwissProt: P23928), but the most intensely fluorescing band on the 3 s exposure is the 28 kDa band. The doublet and the 15 kDa band show a definite increase in intensity from the Dark sample to the 4 Hour sample, but the intensity of these bands detected in the 8 Hour sample decreases. Of interest with regard to the doublet is that the 20 kDa band is absent in the Dark sample. The 28 kDa band has roughly equal intensity for all three Western LIRD samples.

7-E3 β-Crystallin: The antibody used to detect β-crystallin expression was a monoclonal antibody to a HMW aggregate of β-crystallin from cow lens (Section **2-M**, Table 2-1.). Cow lens β -crystallins are heteromeric aggregates of all the β -crystallin proteins (Wistow and Piatigorsky, 1988; Slingsby and Clout, 1999), so the antibody used is not specific for any particular β-crystallin, and in fact could have as an epitope some common structure in the aggregate. Western blot detection of a triplet of bands indicates that the antibody recognizes three proteins that range between 20 kDa and 28 kDa, which brackets the average size (24.1 kDa) of the β-crystallins (**Figure 7-4c.**). All of the detected proteins appear to be present at equal levels in all of the samples (Dark, 4 Hour, 8 Hour). Predicted protein sizes for all the β-crystallins are not available for the rat, but in human, βA3-cystallin is predicted to be 25.2 kDa (SwissProt: P05813). In rat, βA1-crystallin is predicted to be 23.4 kDa (SwissProt: P02525), and in mouse, βB2-crystallin is predicted to be 23.3 kDa (SwissProt: P26775).

7-E4 γS-Crystallin (Crygs): The rat γS-crystallin is expected to be 21 kDa in size (Wistow, personal communication), and the Western analysis identifies a band that is approximately 21 kDa in size. There seems to be no change in band intensity in the

4 Hour sample, and a marginal (<10%) increase in the 8 Hour sample, compared to the Dark sample (**Figure 7-4d.**).

7-E5 Hsp70 (Hspa1a): The Western analysis of Hsp70 identified an approximately 70 kDa band which is about 20% more highly expressed in the 4 and 8 Hour samples (**Figure 7-4e.**). The antibody (Section **2-M**, Table 2-1.) also identified three other distinct bands: one at 21 kDa, one at 36 kDa, and one at 100 kDa. The epitope used to generate the polyclonal antibody was a peptide that matches residues 446-641 of rat Hsp70, so it is likely that the 70 kDa band detected is Hsp70. The Conserved Domain Database of the NCBI Structure Group shows that the Hsp70 domain (pfam00012.5, HSP70; PSSM ID: 4036; www.pfam.wustl.edu/) occurs in 69 other Rodentia proteins of various sizes in Genbank. The peptide used to generate the antibody includes the C-terminal, substrate binding portion of the Hsp70 domain.

7-F Immunohistochemistry

7-F1 αB-Crystallin (Cryab): Immunohistochemistry using anti-αB-crystallin antibody, detected by a Cy3-conjugated secondary antibody, to detect αB-crystallin proteins in rat retina cross-sections shows that αB-crystallin is expressed in the retina at all time points of the LIRD Profile (**Figure 7-5.**).

Dark rat retina cross-sections indicate that αB-crystallin is located at the tips of the outer segments (OS), at the inner segments (IS), and in all other regions of the retina except the outer and inner nuclear layers (ONL and INL) and the portion of the OS closest to the IS (**Figure 7-5a.**; Retinal morphology: Section **1-A1 Figure 1-2.**). αB-Crystallin is not detected in the retinal pigment epithelium (RPE). The strongest fluorescent signal intensity in Dark retina cross-sections is at the outer plexiform (OPL) and ganglion cell layers (GCL), but this maximum signal occurs at discrete points with small areas within these layers. Most of the signal intensity in the retinal layers is relatively uniform, ranging from 35-75% of the maximum signal, with an approximate average signal intensity of 60% of maximum.

4 Hour rat retina cross-sections localize αB-crystallin to all the layers noted in the Dark cross-section: OS, IS, OPL, inner plexiform layer (IPL), and GCL. In addition,

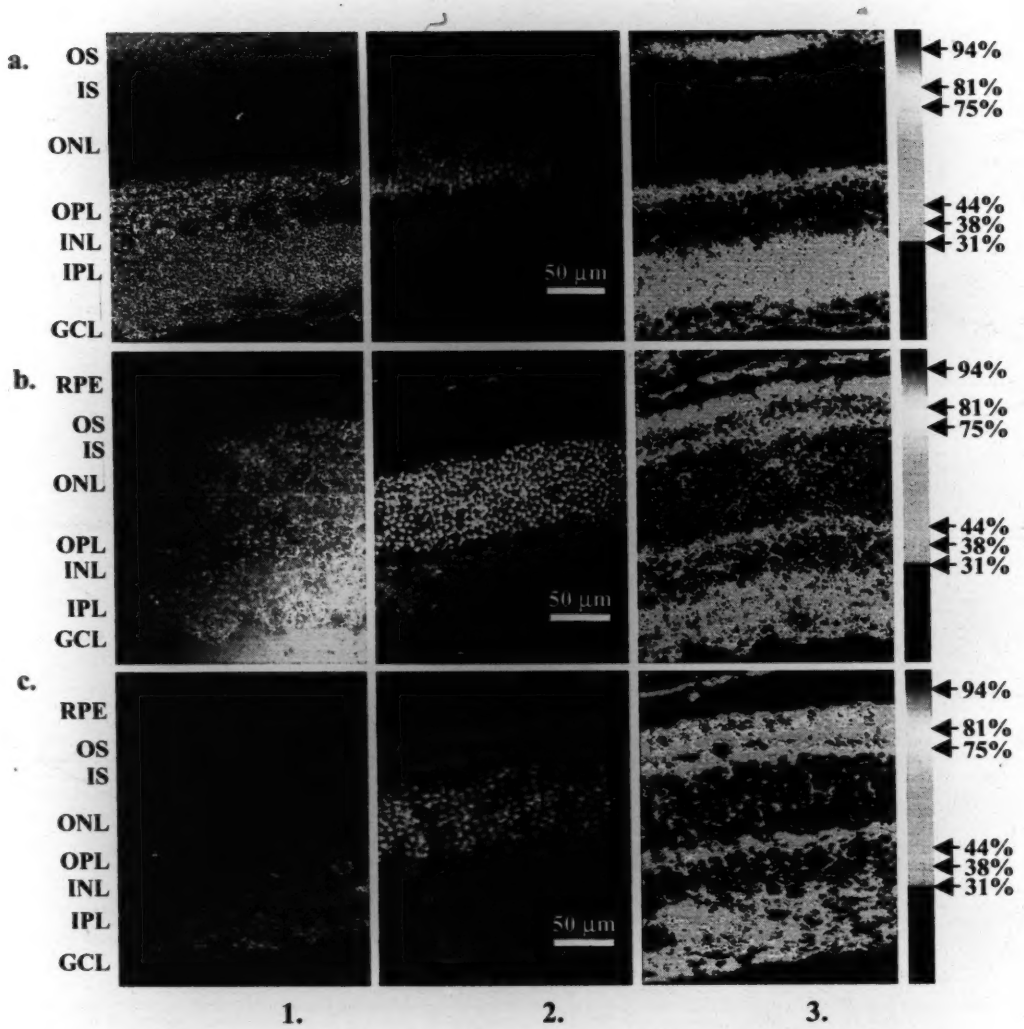

Figure 7-5. Fluorescent Microscopy of αB-Crystallin Immunohistochemistry.

Representative retinal sections from untreated (Dark; **a.**), 4 Hour light-treated (4 Hour; **b.**), and 8 Hour light-treated (8 Hour; **c.**) rats were treated with anti-αB-crystallin antibody, and this antibody was detected by a Cy3-conjugated secondary antibody (Excitation: 550 nm, Emission: 615 nm). Sections were also stained with 4'-6- diamidine-2- phenylindole (DAPI; Excitation: 350 nm, Emission: 470 nm).

From left to right in each row: **1.** reflective image of tissue section, **2.** DAPI/Cy3 signal merged image of same section, and **3.** pseudo-coloured Cy3 signal intensity image of same section. Retinal layers are indicated on the left: RPE = retinal pigment epithelium, OS = outer segments, IS = inner segments, ONL = outer nuclear layer, OPL = outer plexiform layer, INL = inner nuclear layer, IPL = inner plexiform layer, GCL = ganglion cell layer. Cy3 signal is red, while DAPI signal is cyan (**2.**). Cy3 signal intensity was translated into a red (100% of maximum) to blue (31% of maximum) spectrum (**3.**). Signal intensity below 31% of maximum was coloured black for clarity.

significant levels of signal are detected in the ONL and INL in small, discrete areas (**Figure 7-5b.**). αB-Crystallin is detected in the RPE, and the signal intensity in the RPE is at, or approaches, maximum levels. The amount of maximum signal intensity in the OPL and GCL also increases, and maximum signal intensity is also seen in the IPL. In the OS and IS, the signal intensity remains at about 60% of the maximum, and the same pattern of localization to the tips of the OS rather than the region of the OS closest to the IS is seen.

The localization of αB-crystallin in 8 Hour retina cross sections is different from the localization in 4 Hour retina cross-sections mainly in that higher amounts of maximum signal intensity are seen in the tips of the OS and in the IS (**Figure 7-5c.**). The gap of low signal intensity between the OS tips and the IS is still maintained, although signal intensity from this region is higher than in 4 Hour cross-sections.

7-F2 γS-Crystallin (Crygs): Immunohistochemistry using the anti-γS-crystallin antibody indicates that γS-crystallin is primarily located in the RPE and the tips of the OS in Dark retina cross-sections (**Figure 7-6a.**). In these areas, maximum signal intensity is seen, while in other areas, *e.g.* the IS, the OPL and the IPL, the signal intensity ranges from 30-50% of maximum with approximately 40% of maximum being the average signal intensity. No signal is present in the ONL and INL in the Dark cross-section.

In 4 Hour retina cross-sections maximum signal intensity is again seen in the RPE (**Figure 7-6b.**). The OS signal intensity changes from maximal in the Dark cross-sections to approximately 40% of maximum, especially at the tips of the OS. The IS signal intensity increases from an approximate average of 40% of maximum in Dark cross-sections to an approximate average of 60% of maximum with scattered points of maximum signal intensity. The most marked change comes in the OPL and IPL where signal intensity increases from 30% of maximum in Dark cross-sections to maximum signal intensity in 4 Hour cross-sections. As well, in the ONL and INL of the 4 Hour cross-section scattered areas of 30% maximum signal intensity occur.

The 8 Hour cross-section maintains maximum signal in the RPE, and the diffuse 30% maximum signal intensity seen in the ONL and INL (**Figure 7-6c.**). In the other cell layers, the change from signal intensity in the Dark and 4 Hour sections is marked.

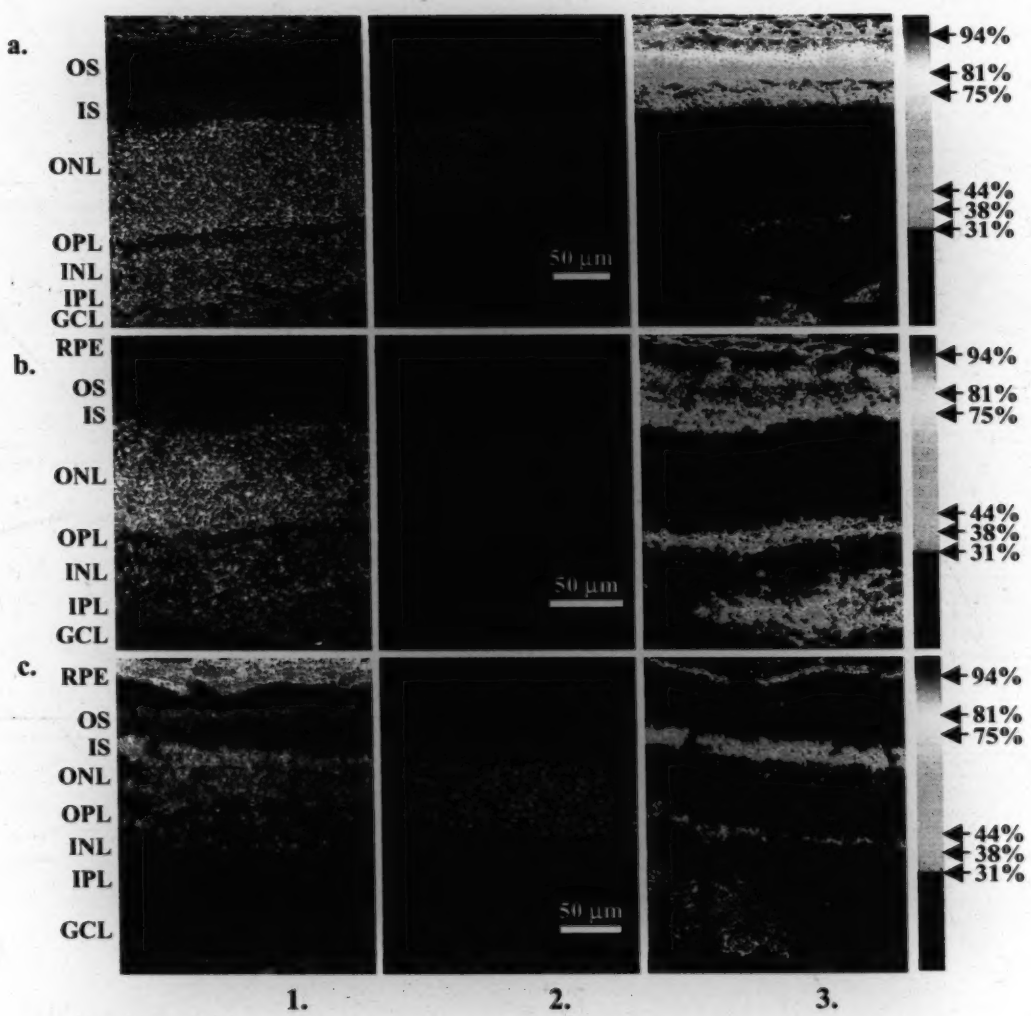

Figure 7-6. Fluorescent Microscopy of γS-Crystallin Immunohistochemistry.

Representative retinal sections from untreated (Dark; **a.**), 4 Hour light-treated (4 Hour; **b.**), and 8 Hour light-treated (8 Hour; **c.**) rats were treated with anti-γS-crystallin antibody, and this antibody was detected by a Cy3-conjugated secondary antibody (Excitation: 550 nm, Emission: 615 nm). Sections were also stained with 4'-6- diamidine-2- phenylindole (DAPI; Excitation: 350 nm, Emission: 470 nm).

From left to right in each row: **1.** reflective image of tissue section, **2.** DAPI/Cy3 signal merged image of same section, and **3.** pseudo-coloured Cy3 signal intensity image of same section. Retinal layers are indicated on the left: RPE = retinal pigment epithelium, OS = outer segments, IS = inner segments, ONL = outer nuclear layer, OPL = outer plexiform layer, INL = inner nuclear layer, IPL = inner plexiform layer, GCL = ganglion cell layer. Cy3 signal is red, while DAPI signal is cyan (**2.**). Cy3 signal intensity was translated into a red (100% of maximum) to blue (31% of maximum) spectrum (**3.**). Signal intensity below 31% of maximum was coloured black for clarity.

Maximum signal intensity is seen at the IS, while in all other areas signal intensity ranges from 30-60% of maximum. The signal intensity from the OS, where it occurs as scattered points of about 30% maximum, is much lower than the other two cross-sections. Signal intensity in the OPL decreases to an approximate average of 50% of maximum, while signal intensity in the IPL decreases to an approximate 40% of maximum.

7-G Discussion

The data presented here indicate that the crystallins are a component of both the normal retina and LIRD. The changes in crystallin transcription and translation mirror or exceed the changes in known stress response genes (**Figure 7-7.**). Expression of the crystallin genes in the face of the oxidative stress conditions created by light exposure indicates that the crystallins have a LIRD-related function. This conclusion is supported by the change in αB- and γS-crystallin protein localization observed in light-exposed (4 Hour, 8 Hour) retina as compared to unexposed (Dark) retina. This suggests that some aspect of the function of these two proteins is required as part of the LIRD tissue environment.

The known stress-response crystallin, α-crystallin, is composed of two proteins αA- and αB-crystallin. The levels of mRNA for both of these crystallins increase with increasing light exposure in dark-reared rats (**Figure 7-3a.,b.**). The proteins are both present in the rat retina (**Figure 7-4a.,b.**), and αB-crystallin localization changes with increasing light exposure (**Figure 7-5.**). This indicates that α-crystallin is present in the retina, and responds to increasing light exposure and the increased oxidative stress caused by the light exposure. The most likely activity of α-crystallin in the retina is its well-documented role as a chaperone that binds molten globule proteins to prevent protein aggregation (Horwitz *et al.*, 1998; Rawat and Rao, 1998; Marini *et al.*, 2000).

Confidence in this prediction is promoted by the fact that an oxidative environment is known to result in the oxidation of proteins which results in the formation of protein aggregates because the oxidized proteins are unable to maintain their correct conformation and unfold (Liang and Pelletier, 1987, 1988; Kono *et al.*, 1990; Hanson *et al.*, 1999). Cryaa and Cryab mRNA levels increase at a very similar rate to the increases seen in the mRNA levels of Hspa1a and Hspca (**Figure 7-3f.,g.** and **Figure 7-7.**). All

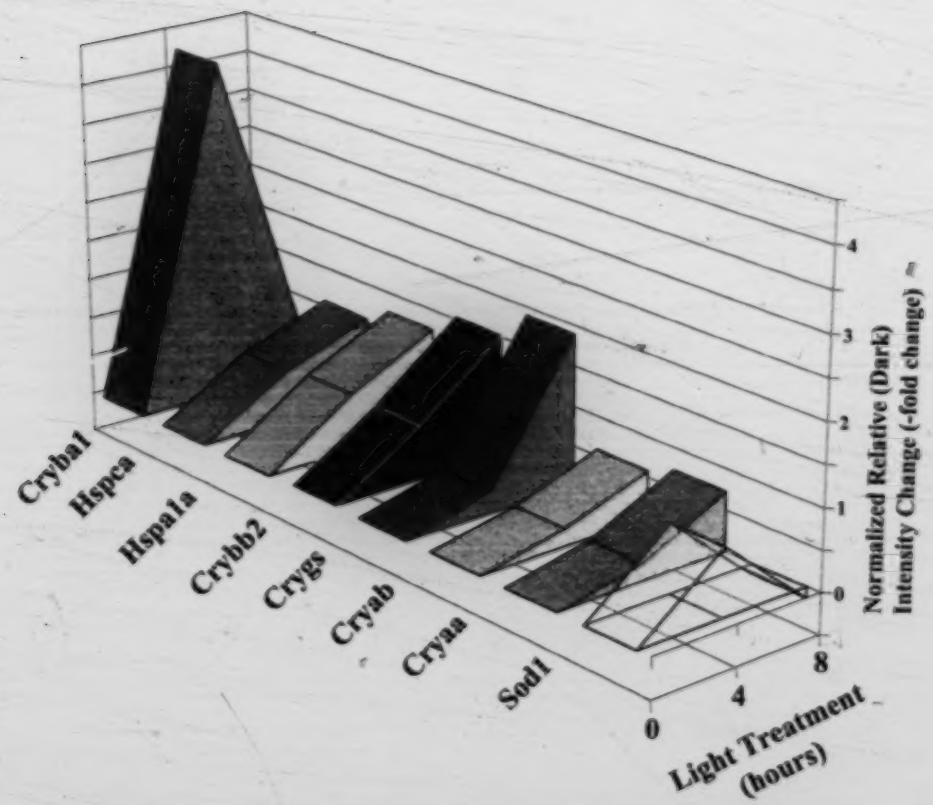

Figure 7-7. Change in mRNA Levels of Crystallins and Stress Proteins During Light-induced Retinal Degeneration.

The change in normalized relative intensity of autoradiograph band intensity corresponding to mRNA transcripts of Sod1, Cryaa, Cryab, Crygs, Crybb2, Hspa1a, Hspca, and Cryba1.

four transcript levels increase after 4 hours of light treatment, and this increase continues after 8 hours of light exposure. The increase of the Cryaa and Cryab transcripts is less than that of the Hspa1a and Hspca transcripts, but the trend is the same. This similarity in rate of change of mRNA levels suggests that Cryaa, Cryab, Hspa1a, and Hspca gene expression changes in response to similar stimuli.

A possible explanation for the slower rate of increased transcription of Cryaa and Cryab could be that α-crystallin in the retina is ubiquitous, as seen by the strong signal of αA- and αB-crystallin in the Dark protein sample (**Figure 7-4a.,b.**). Expression of α-crystallin in untreated tissue suggests that α-crystallin is part of the first line of response against cytotoxic oxidative damage to proteins. α-Crystallin in this view would sequester misfolded proteins and hold them until sufficient levels of Hsp70 and Hsp90 accumulated, and, in fact, Hsp70 levels do increase in 4 and 8 Hour samples (70 kDa Band, **Figure 7-4e.**). Hsp70 and Hsp90 are involved in folding nascent or misfolded proteins and in marking irreparable proteins for degradation, neither of which activities are properties of α-crystallin (Horwitz *et al.*, 1998; Mathew and Morimoto, 1998; Rawat and Rao, 1998; Wickner *et al.*, 1999; Connell *et al.*, 2000; Wang and Spector, 2000; Abgar *et al.*, 2001; Höhfeld *et al.*, 2001). Cryaa and Cryab transcription would not be immediately required, because the α-crystallin levels would at first be sufficient to deal with damaged proteins. Only when the level of damaged protein to free α-crystallin levels are too high would it be necessary to generate more α-crystallin. At the same time, the presence of α-crystallin-oxidized protein complexes could be part of the stress signal that induces transcription of Hspa1a and Hspca by reducing the levels of uncomplexed α-crystallin, which would be indicative of higher levels of protein denaturation.

The change in localization of αB-crystallin to the rat OS and IS after 4 and 8 hours of light treatment (**Figure 7-5.**) suggests that the source of oxidative damage to proteins in the retina is in the OS and IS. Oxidative damage occurs through reaction with ROS or radicals generated by ROS. ROS and radicals are very reactive, and could not be expected to travel far from their source (Halliwell, 1991; Winkler *et al.*, 1999). There are three reasonable sources of ROS and radicals in the retina (**Figures 1-2., 1-7.**): the mitochondria of the IS, the high concentration of retinal in the OS, and the high

concentration of docosahexaenoic acid (DHA) in the OS (Section **1-B3**). The mitochondria of photoreceptor cells are clustered at the base of the outer segments in the endoplasmic reticulum and mitochondria-rich region that makes up the IS. Retinal and DHA are integral components of the lamellae of the OS, retinal because it is rhodopsin's co-factor (Oyster, 1999), and DHA because it is a major component of the folded lipid bilayer that is the lamella (Organisciak *et al.*, 1996, 1998; Rodriguez de Turco *et al.*, 1997). All three are reasonable candidates as a source of radicals and they occur in the same regions that show the greatest increase in localization of αB-crystallin.

The possible generation of radicals from DHA could explain why the transcript levels of Sod1 increase and then decrease (**Figure 7-3h.**). SOD1 is a cytoplasmic antioxidant enzyme that generates H_2O_2 from O_2^- and water (Section **1-B3** and **Figure 1-7c.**; Fridovitch, 1995; Mittag *et al.*, 1991). In an unstressed retina, this reaction is not deleterious because other enzymes oxidize H_2O_2 to generate relatively innocuous compounds, *e.g.* glutathione peroxidase, thioredoxin peroxidase, and catalase. In a retina which is subjected to a long, continuous light stress, the generation of H_2O_2 by SOD1 might outpace the ability of the other enzyme systems to oxidize H_2O_2. Increasing H_2O_2 concentrations can result in the generation of the most reactive ROS, the hydroxyl radical, when H_2O_2 oxidizes iron (**Figure 1-7d.**; Halliwell, 1991; Winkler *et al.*, 1999). Since SOD1 activity is potentially protective and antioxidant, an increase in Sod1 transcript levels for the enzyme might be an early response of the retina. Later, if the concentration of ROS increases, removing a possible generator of ROS, SOD1, would allow the other antioxidant enzyme systems time to reduce the ROS levels and would explain why Sod1 transcript levels decrease.

The possible link between protein oxidation, the α-crystallin-Hsp70-Hsp90 stress response, and SOD1 activity, lies in βγ-crystallin expression in the retina. Protein oxidation has a major target in the amino acid cysteine (Cys), which is an important target for oxidation because one of its roles in protein formation is oxidation of two Cys to provide an intra- or inter-molecular covalent bond that, respectively, maintains secondary and tertiary structure of the protein, or links protein subunits to form functional enzymes (Voet and Voet, 1995). One of the noted characteristics of the γ-crystallins is their high Cys content (Graw, 1997; Hanson *et al.*, 1999; Skouri-Panet *et al.*, 2001). An

analysis of the primary structure of all the mouse crystallins confirms this observation (**Figure 7-8.**). The γ-crystallins, and the βA1-, βA2-, and βA3-crystallins, all have Cys contents (%) that are at least twice the average Cys content of sixty-seven other mouse proteins (1.54%). The proteins from which the average Cys and methionine[43] were derived were chosen by two criteria: identification of their orthologous gene in a rat LIRD cross screen (**Chapter 4**), and the availability of complete protein sequence (www.ncbi.nlm.nih.gov:80/). Mouse proteins were used because more protein sequence is available for mouse, rat and mouse are closely evolutionarily related (Section **5-E**), and the close sequence alignment of the known rat and mouse crystallin proteins (96% identity, n=7; **Appendix 5.**).

The high Cys content of the γ-crystallins suggests that these proteins should be excellent targets for oxidation of the thiol group in Cys residues which are accessible. The molecule that is normally used for oxidation of thiols (R–SH) in the cell is the tripeptide glutathione, which also contains a Cys thiol (Giblin, 2000). Glutathione (GSH)-mediated oxidation of Cys in the γ-crystallins is well-established in cow lens systems. Cow γB-crystallin, orthologous to mouse γB-crystallin, has been noted to have two of its seven Cys oxidized by GSH *in vitro* (Slingsby and Miller, 1985; Hanson *et al.*, 1999; Skouri-Panet *et al.*, 2001).

The other role of the γ-crystallins is as a structural protein of the lens where they appear as monomers (Wistow and Piatigorsky, 1988; Graw, 1997). There is a paradox between the function and structure of the γ-crystallins if their only role is as monomeric structural proteins. The high number of Cys residues, at least some of which are accessible for oxidation, means that γ-crystallins could oxidize each other and form covalent bonds, and this covalently bound dimer could serve as the nucleus for further γ-crystallin oxidation and, potentially, protein aggregation. In the lens, this protein aggregation could result in light-scattering bodies, which is at odds with the physiological role of the lens (Brady *et al.*, 1997; Boscia *et al.*, 2000). Although the incidence of oxidized crystallins in the lens increases with age, it is abnormal for sufficient crystallin aggregation to occur to occlude the passage of light through the lens (Oyster, 1999;

[43] The other sulfur-containing amino acid methionine can also be oxidized, but less readily than Cys.

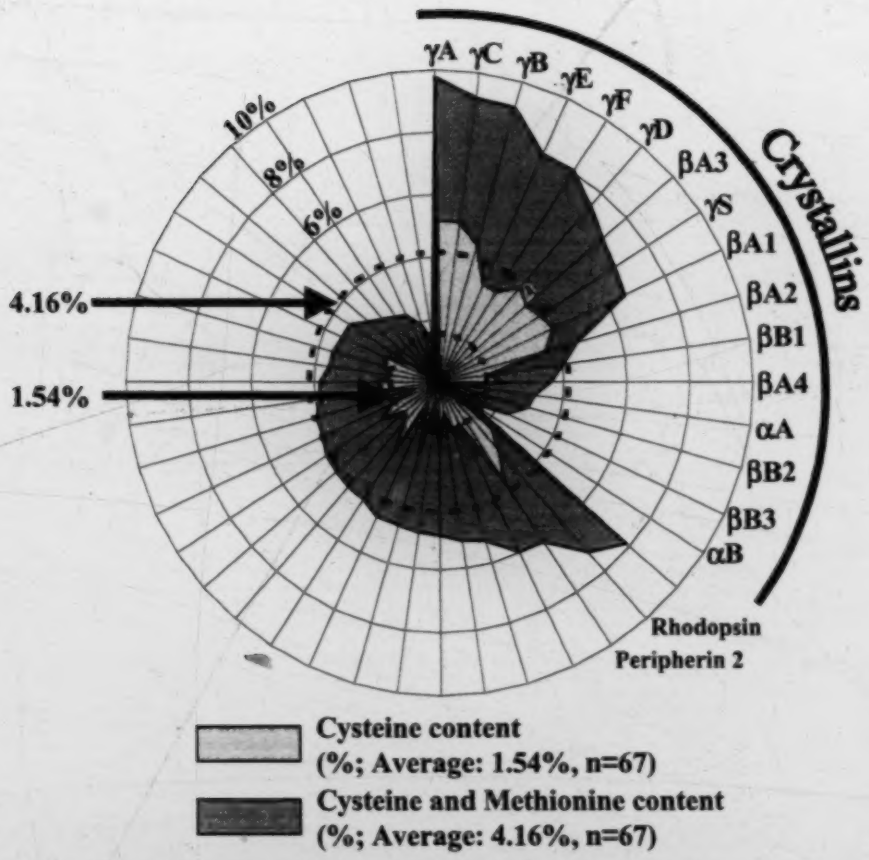

Figure 7-8. Sulfur Containing Amino Acids in the Crystallins.

Cysteine (Cys) and methionine (Met) can be oxidized by oxidizing agents to give substituted amino acids that can change the conformation of the protein, and can potentially create proteins linked by disulfide bonds. The Cys thiol (R–S–H) group is easier to oxidize than the Met sulfide (R–S–CH_3) and Cys is the usual residue oxidized to form disulfide bonds.

The data in this figure represent the Cys and Met content (%) of the sixteen *Mus musculus* crystallins (under the arc), and a representative sample (28) of sixty-seven other mouse proteins. The proteins from which the average Cys and Met content were derived were chosen by two criteria: identification of their orthologous gene in a *Rattus norvegicus* light-induced retinal degeneration cross-screen (Section **SA**), and the availability of complete protein sequence (www.ncbi.nlm.nih.gov:80/). Note the high sulfur content of rhodopsin (2nd of 67, 8th of 83) and peripherin 2 (6th of 67, 15th of 83), and the extremely low sulfur content of αB-crystallin (2 Met/175, 83rd of 83).

The interior dashed circle represents the average cysteine content of the non-crystallins, while the outer dashed circle represents the average Cys and Met content of the non-crystallins. The crystallins that do not have at least twice the average cysteine content (6/16) are: the α-crystallins (2/16), βA4-crystallin, and the βB-crystallins (3/16).

Boscia *et al.*, 2000). In healthy lenses, the crystallins retain their proper structure to maintain lens transparency. In order to resolve this apparent paradox, it is considered that the γ-crystallins remain monomeric because their accessible Cys residues are oxidized by GSH when oxidizing conditions in the lens occur to form a mixed disulfide of the γ-crystallin and GSH (PSSG; Slingsby and Miller, 1985, Liang and Pelletier, 1987, 1988; Lou and Dickerson Jr., 1992).

The implications of γ-crystallin function and structure for the retina are important. γS-Crystallin is definitely expressed at both the mRNA and protein level in the rat retina (**Figures 7-3e., 7-4d.**, and **7-6.**), and γB-crystallin was also identified in a rat LIRD differential cross screen (Section **4-B**). Immunohistochemistry suggests that there is a significant amount of γS-crystallin in untreated rat retinae, primarily in the OS (**Figure 7-5a.**). γS-Crystallin is likely not unique among the γ-crystallins for its expression in the retina because γA-F-crystallins have been identified in the mouse retina, where they are also detected in the OS (Jones *et al.*, 1999). Even if γS-crystallin were unique among the γ-crystallins in being expressed in the retina, its function, suggested by the γ-crystallin role in the lens, would still be valid. That is, γ-crystallins in the lens are structural proteins that maintain the shape and structure of the lens, and they are oxidized by GSH to maintain them in the correct conformation, and their function in the retina is likely to be exactly what it is in the lens.

The structural role of the γ-crystallins can be reconciled with expression in the retina OS because the OS is a tissue layer that must be kept in a very particular conformation just as the lens must be (**Figure 1-2.**). The OS of each photoreceptor cell must remain attached to the main body of the cell so that its store of metabolites and proteins is continually replenished. The necessity for replenishment is due to the phagocytosis of the tips of the OS by the RPE as the lamellae of the OS move towards the RPE. This phagocytosis creates a means of replacing the oldest, and presumably most damaged, lamellae of the cell without the continual increase in size of the OS. Replacement of potentially damaged lamellae is necessary to maintain the retina's ability to detect light (Young, 1971, 1972, 1978; Oyster, 1999). The OS is also constrained along its axis by its neighbour's OS which have the same terminal constraints. This

means that the OS must be long and rod-like with well defined termini. Internally, the OS must also be specifically arranged. The lamellae of the OS are flattened spheres formed from a lipid bilayer. Rhodopsin and other proteins are embedded in this membrane, and there are cytoplasmic spaces between the external faces of the lamellae (Hart, 1992; Oyster, 1999; Kolb *et al.*, 2002). The inter-lamella space suggests that some agent maintains the lamellae as discrete units and prevents the likely membrane fusion that would occur if the lamellae were to contact each other. γ-Crystallins maintain lens structure, along with the α- and β-crystallins, and it is a reasonable hypothesis to suggest that they could have a similar function in the OS given the physiological constraints of a photoreceptor OS. Localization of γS-crystallin to the OS in untreated rats provides support for this hypothesis (**Figure 7-6a.**).

A potential structural role of the γ-crystallins in the retina does not address the role of γ-crystallins in the oxidative environment created by light exposure. Two systems for reducing ROS exist in cells, the thioredoxin peroxidase (TrxP) and the glutathione peroxidase (Gpx) systems. Enzymes with Gpx activity reduce H_2O_2 by oxidizing the Cys of two GSH to form a glutathione disulfide (GSSG; **Figure 7-9.**). This reaction removes the H_2O_2 created by SOD1, and so depletes a potential source of more reactive ROS, *i.e.* the hydroxyl radical (Ziegler, 1985; Halliwell, 1991). In the retina, convincing evidence exists that Gpx activity is absent from the OS (Organisciak *et al.*, 1998). It is important to note that the assay for Gpx activity involves measuring the oxidation of reduced nicotinamide adenine dinucleotide phosphate (NADPH) to $NADP^+$ in the reduction of GSSG to GSH by enzymes with glutathione reductase (Glr) activity, which are present in excess in the assay (Flohé and Günzler, 1984). TrxP activity has a similar reaction course, oxidizing the thioredoxin protein (Trx) to reduce H_2O_2 (Powis and Montfort, 2001). The oxidized form of Trx can be reduced by an enzyme with thioredoxin reductase (TrxR) activity, at the cost of oxidation of NADPH (Powis and Montfort, 2001). TrxR oxidation of NADPH is important to note because Gpx activity in OS was measured indirectly by determining the amount of oxidation of NADPH by excess Glr, so TrxP and TrxR activity is also measured indirectly (**Figure 7-9.**), and no activity was observed (Organisciak *et al.*, 1998).

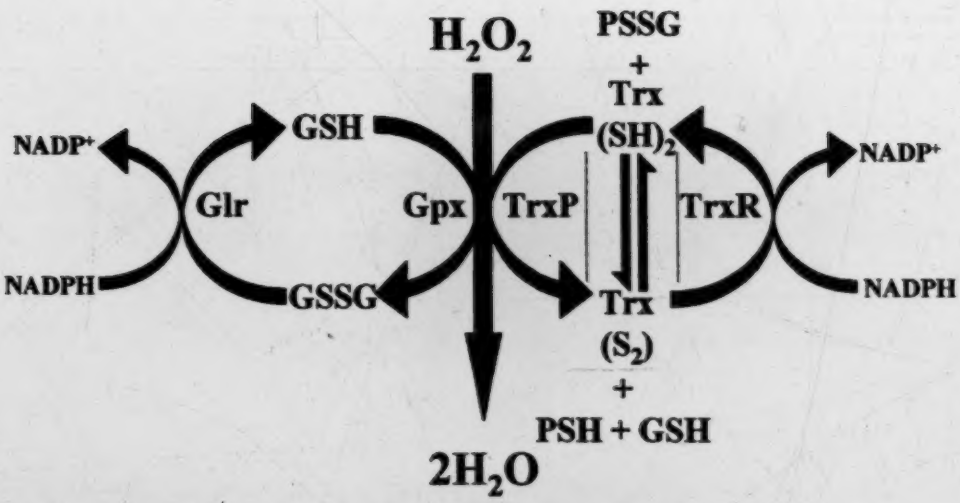

Figure 7-9. Glutathione and Thioredoxin Peroxidase Reactions.
A representation of two antioxidant metabolic activities of the mammalian cell.
GSH: glutathione, **GSSG**: GSH disulfide, **PSH**: protein thiol, **PSSG**: mixed protein-GSH disulfide, **Glr**: GSH reductase activity, **Gpx**: GSH peroxidase activity, **Trx $(SH)_2$**: reduced thioredoxin, **Trx (S_2)**: oxidized Trx, **TrxR**: Trx reductase activity, **TrxP**: Trx peroxidase activity, **NADP+**: oxidized nicotinamide adenine dinucleotide phosphate, **NADPH**: reduced NADP+

It is known that Trx promotes the oxidation of proteins and GSH to produce a mixed protein-GSH disulfide (PSSG) without requiring cofactors, and there is also evidence that PSSG can be reduced by Trx to protein and GSH (Engström *et al.*, 1974; Holmgren, 1985; Wetlaufer, 1984; Powis and Montfort, 2001; Casagrande *et al.*, 2002). This non-peroxidase activity of thioredoxin does not occur in the Gpx system, and would allow Trx to regenerate reducing potential from a wider range of sources. Where the Gpx system is limited to find reducing potential in the GSH and NADPH pools, Trx may be able to draw from the pool of readily oxidized proteins in a process which would be undetectable by the Gpx activity assay (**Figure 7-9.**). Trx has been shown to be expressed in both rat and mouse retina (Yamamoto *et al.*, 1997; Tanito *et al.*, 2002a,b), and, more specifically, to be present in the OS of light-exposed mice (Tanito *et al.*, 2002a,b)

γ-Crystallins in the lens can be oxidized to mixed disulfides (PSSG), and this aspect of γ-crystallin biochemistry is more important in the context of oxidative stress in the retina. γS-crystallin has a high Cys content and can be readily oxidized by oxidized Trx to form a PSSG, which reduces Trx. Reduced Trx is capable of being oxidized by TrxP to reduce H_2O_2 without generating $NADP^+$. In this scheme, H_2O_2 would be reduced, Trx would be kept in a reduced form for as long as there is easily oxidized GSH and crystallin available, and TrxP activity could not be detected by assaying for $NADP^+$ (Flohé and Günzler, 1984; Organisciak *et al.*, 1998). Expression of γS-crystallin (**Figure 7-6a.**), and possibly the other γ-crystallins (Jones *et al.*, 1999), in the OS and IS could provide a peroxide 'sink' for the OS and IS at a location that is close to the likely origin of ROS within the retina. This sink would serve two purposes: its primary purpose of providing reducing potential for TrxP activity to reduce H_2O_2, and a secondary purpose of maintaining the easily oxidized structural crystallins in an oxidized form that does not allow the formation of inter-protein bonds.

This hypothesis of the γ-crystallins being a retinal sink for oxidative reactions could explain the decreased localization of γS-crystallin in the OS of light-treated rat retinae (**Figure 7-6b.,c.**). Perhaps oxidized γS-crystallin is targeted for degradation by chaperones, other than α-crystallin, and this would explain the lack of an increase in band intensity seen by Western analysis (**Figure 7-4d.**); as fast as the protein is formed it is

being oxidized to PSSG, and then degraded. Perhaps αB-crystallin is localized to the OS to prevent γS-crystallin-nucleated aggregates from forming, and the anti-γS-crystallin antibody has a reduced affinity for the α/γS-crystallin complex, or the antibody has reduced affinity for the conformational changes of the oxidized γS-crystallin.

Another possibility that does not preclude the other possibilities is that the normal level of γS-crystallin in the rat retina provides a buffer of time for a stress response to be enacted, such as the increased expression of α-crystallin, Hsp70, Hsp90, and SOD1, and perhaps this stress response includes increased expression of the other βγ-crystallins, especially the other γ-crystallins, and the βA1-A3 crystallins. These crystallins, with their high Cys content, could bolster the reducing potential of the retina and, as structural proteins, make up for any degradation of γS-crystallin. After 8 hours of light treatment the mRNA levels of Crygs are higher than levels for the known stress-response genes (**Figure 7-7.**), so replenishment of the γS-crystallin pool could occur. The largest change in transcript levels (527% of Dark) seen in this study was for Cryba1, which encodes both βA3- and βA1-crystallin, although levels of Cryba1 drop after 8 hours of light treatment to levels comparable to Cryaa and Cryab transcripts. The mRNA level for the basic crystallin that was examined, βB2-crystallin (Crybb2), also increases sharply after 4 hours of light treatment and continues to increase to levels greater than the mRNA for the known stress-response proteins. The Crybb2 transcript levels suggest that a high Cys content in the gene product is not the only factor that results in the expression of the βγ-crystallins in the retina.

This study has clearly established that at least a representative number of the crystallins are expressed within the rat retina, including those that have long been considered lens-specific. As well, this expression changes with increasing light exposure and an increasingly oxidative environment. A functional role for αB- and γS-crystallin in rat LIRD is also strongly predicted due to the change in localization of the protein as determined by immunohistochemistry (**Figure 7-10.**). Primary sequence analysis of the crystallin proteins identified a significant departure from the average in terms of Cys and methionine content, and established the fact that even simple bioinformatic analysis can result in intriguing hypotheses.

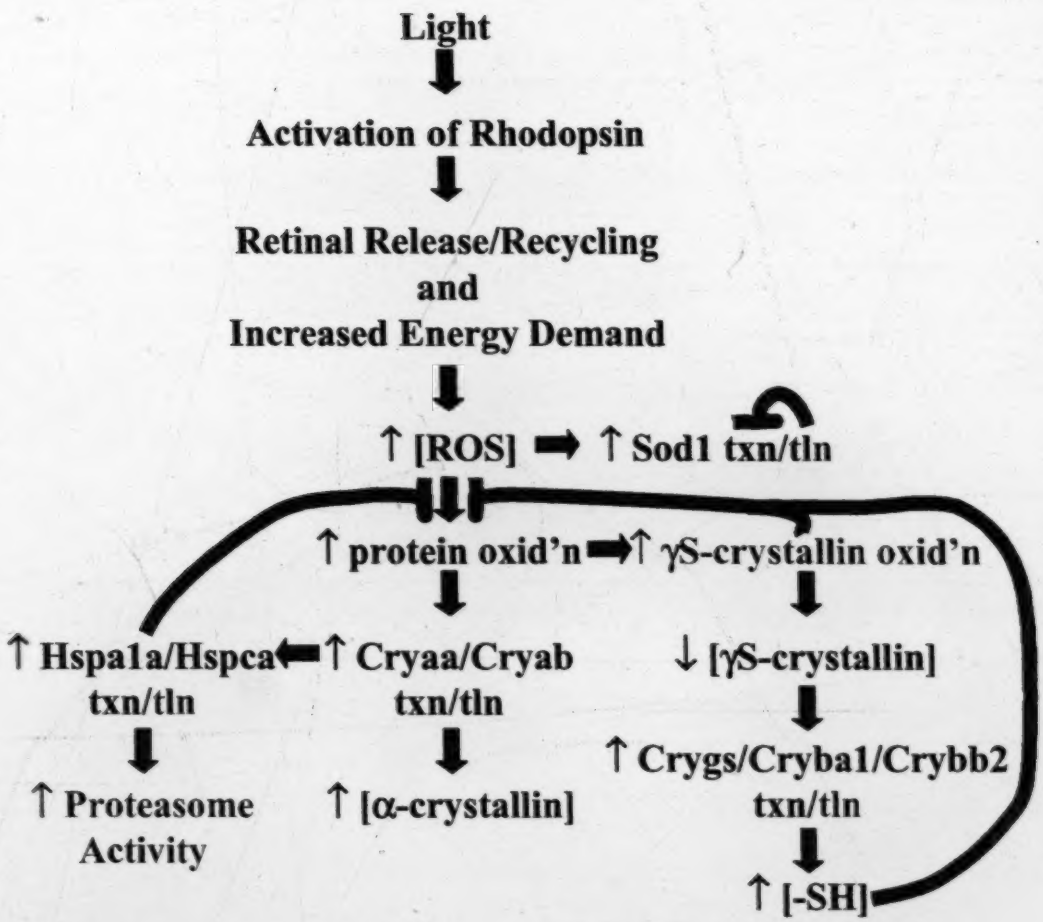

Figure 7-10. Proposed Role of the Crystallins in the Response of Rat Retinae to Light Exposure.

Light exposure causes increased activation of rhodopsin, and so increased release of retinal, and a greater energy requirement. This would result in an increase in ROS, and therefore protein oxidation. Protein oxidation would lead to α-crystallin (Cryaa and Cryab), Hsp70 (Hspa1a), and Hsp90 (Hspca) interactions with the oxidized proteins, which could result in increased protein degradation, or repair of damaged proteins. Among the proteins oxidized would be the βγ-crystallins, which might result in increased expression of the βγ-crystallins. The high cysteine content of the βγ-crystallins could have the effect of increasing the reducing potential of the photoreceptor cell, and decreasing the effect of ROS on other cellular proteins. Superoxide dismutase (Sod1) expression might initially increase in response to increased ROS, but since it also generates ROS, high levels of SOD1 could inhibit further transcription of Sod1. Elements of this response for which evidence exists are indicated in black. Elements in grey require further research. (txn = transcription, tln = translation, oxid'n = oxidation, -SH = cysteine thiol.)

One strong hypothesis with regards to these results has been suggested, that the crystallins are structural proteins of the retina which have the capacity to generate a reducing environment by the action of thioredoxin peroxidase and thioredoxin in oxidizing the Cys residues of the crystallins, which also means that covalent inter-linkage of the crystallins cannot occur. This hypothesis needs to be tested to see if the predicted GSH-modified crystallins can be detected in a rat retina treated with light. As well, a definitive determination of the oxidoreductases, if any, that could perform as predicted by the hypothesis needs to be done. If these turn out to be thioredoxin peroxidase and thioredoxin, then the expression, localization, and activity of these enzymes should be examined in rat retina to refine this hypothesis. The groundwork laid by this study suggests several biochemical and genetic studies that could be pursued, ranging from fluorescent microscopy, to retina proteome analysis, to transgenic manipulation of model organisms.

Chapter 8 Conclusion

Chapter 8 Conclusion

This study is based on the hypothesis that exposure of rats to intense green light will generate a characteristic molecular phenotype in the retina as a result of an increase in oxidative stress (Section **1-C.**). One aspect of this molecular phenotype is the change in transcription of genes whose products have some effect on the final result of the light exposure, light-induced retinal degeneration (LIRD). This study has identified ninety-five different genes whose transcript levels change after 4 hours of light exposure. These genes were identified by sequencing 121 clones selected in a differential cross screen of a retinal cDNA library that compared the level of expression of mRNA transcripts in retinae of dark-reared rats that were not treated with light (Dark) with the level of expression of mRNA transcripts in retinae of dark-reared rats exposed to 4 hours of intense green light (4 Hour; **Chapters 2-4**).

The sequence data and subsequent gene identification obtained in this study is a starting point for designing experiments aimed at examining the role of specific genes in the context of LIRD and so perhaps in the context of human retinal degeneration. Useful information can be obtained by bioinformatic analysis, using readily available research tools from the National Institutes of Health (NIH) National Centre for Biotechnology Information (NCBI; www.ncbi.nlm.nih.gov). This study used these resources to identify sequences derived from 121 differentially expressed clones as known rat genes (86/121), or as potential rat genes orthologous to known human or mouse genes (35/121).

Northern analysis of nine of the one hundred and twenty-one clones, representing nine different genes (9/95, 9%), confirmed that eight of the nine clones (89%) represented mRNAs that were differentially expressed between the two conditions (**Chapters 3 and 4**). Given that 89% of the clones tested by Northern analysis did show a differential pattern of expression, it is likely that at least 89% of the mRNAs represented by all the isolated clones are differentially expressed between Dark and 4 Hour rat retinae.

Many of the products of the identified genes have known functions that suggest a tissue environment where there is a marked change in the rate of basic metabolism (Table 4-2.), photoreceptor metabolism (Table 4-9.), the rate of both transcription and translation (Tables 4-3.-4-6.), a change in the nature of intercellular and intracellular

communication (Tables 4-7., 4-8., 4-10., and 4-13.), and the control of apoptosis (Tables 4-11.). A change in cellular metabolism, cell signalling, and apoptosis control is a reasonable expectation given that the light exposure (4 Hour) induces a drastic change in retina tissue environment in the dark-reared animals, a state of oxidative stress. These basic processes should show a change as the cells of the retina respond to the light stimulus and increasingly oxidative environment of the retina (Organisciak *et al.*, 1992a, 1992b, 1995, 1999a; Kutty *et al.*, 1995; Specht *et al.*, 1999). Many of the genes in these classes (Tables 4-2.-4-11. and 4-13.) could be examined to provide additional details about other important elements of retinal function.

The bioinformatic resources of the NCBI were used to identify the chromosomal locations of the identified genes in the human, mouse, and rat genomes, and to examine whether any of the human orthologues of the identified rat genes occurred in human chromosomal regions that coincided with known minimum critical regions associated with genetic retinal dystrophies for which the mutation is not known. This analysis identified four of the identified rat genes as having human orthologues that occur in minimum critical regions linked to two retinal dystrophies. Atp1a2 and Pea15 are good candidates for cone-rod dystrophy 8 (CORD8) because mapping of the two loci in humans places them within the minimum critical region of CORD8 on chromosome 1 (Oakey *et al.*, 1992; Hwang *et al.*, 1997; Khaliq *et al.*, 2000; Section **5-D2**). In addition, the known biological functions of Atp1a2 and Pea15 suggest that they could play an important functional role in the context of retinal biology (Condorelli *et al.*, 1998, 1999; Katzmarzyk *et al.*, 1999; Kitsberg *et al.*, 1999). Similarly, Rps3 and Pak1 (Bekri *et al.*, 1991; Kim *et al.*, 1995a; Knauss *et al.*, 1995; Polakiewicz *et al.*, 1995; Frost *et al.*, 1998; Sanders *et al.*, 1999; Wimberley *et al.*, 2000; Jung *et al.*, 2001; Parrini *et al.*, 2002) are good candidates for vitreoretinopathy neovascular inflammatory disease (VRNI) which has been localized to chromosome 11 (Stone *et al.*, 1992; Section **5-D7**). These four human genes are good candidates by position and function for CORD8 or VRNI, but this does not mean that any one of them is the gene responsible for either of these diseases. On the other hand, their identification as candidates could help focus attempts to identify the genes causing the diseases. The identification of the rat orthologues of these genes in a LIRD screen indicates that at least in the rat these genes are expressed in retinae that

model a human retinal disease, retinitis pigmentosa. This could mean that these genes are important elements of general retinal function, and that mutations in these human genes result in retinal diseases.

Bioinformatic analysis using the NCBI resources was also used to identify rat tissues (**Figure 6-1.**) and human tissues (**Appendix 4.**) in which expressed sequence tags (ESTs) showing high sequence similarities to identified genes have been found. It became clear from the initial examination of the rat EST databases that it was not very extensive. Examination of the mouse and human EST databases revealed a much greater depth of entries than the rat database, but that eye tissue ESTs were better represented in the human database than in the mouse database. For this reason the human database was used for a quantitative analysis of several tissues for the number of ESTs matching human genes orthologous to rat genes identified in the differential cross screen. The occurrence of matching ESTs in major human organ systems are represented in **Figure 6-2.**, and the occurrence of matching ESTs in tissues of the human eye are represented in **Figure 6-3.** Theoretically, this type of analysis might allow prediction of gene expression in tissues by *in silico* Northern analysis. The data generated from the human database were used to predict the expression of the rat genes: Atp1a2, Fdps, Pak1, and Pea15 in rat tissues. These predictions were tested by a multi-tissue Northern analysis of the genes' expression profile. The results of this test suggest that, at least for cross-species predictions, the data available in the NCBI databases are not sufficient to accurately predict tissue gene expression profiles.

There is one very intriguing class of genes identified in the differential cross screen, the crystallins (Table 4-1.). Of the 121 sequenced clones, 21 of them (17%, n=121) represented 9 different (9%, n=95) crystallin transcripts. Clearly the differential cross screen identified a class of genes that is of signal importance in a light-exposed rat retina. The high representation of the crystallin gene family among the sequenced clones, and the fact that these clones represented closely related genes from a single gene family (Slingsby *et al.*, 1988; Wistow and Piatigorsky, 1988) was an immediately intriguing observation. On top of this observation was the realization that the 9 different genes identified in this screen represented 60% of the known mammalian crystallin genes (15). Further, the Cryga-Crygf genes are a cluster of very closely related genes (Section **7-A2,**

Table 7-1.), and the presence of a clone representing Crygb hints that these other 5 transcripts might also be present in the 4 Hour cDNA library, and thus in a 4 hour light-treated rat retina. The high prevalence of the transcripts of individual crystallin genes, especially Cryaa (9 clones; 7%, n=121), strongly suggests that the crystallins are an integral component of LIRD.

To further add to the interest in the crystallins, it was noted that the crystallins, with the exception of the α-crystallins (Cryaa and Cryab; Bhat and Nagineni, 1989; Kato *et al.*, 1991a, 1991b, 2002; Srinivasan *et al.*, 1992; Vicart *et al.*, 1998), are largely considered lens-specific proteins, and only recently have some of them: Crybb2 (βB2), CrygA-F (γA-F), and Crygs (γS), been recognized as genes that are expressed in the mammalian retina (Dirks *et al.*, 1998; Sinha *et al.*, 1998; Jones *et al.*, 1999; Magabo *et al.*, 2000). Of particular interest, Crygs has yet to be fully characterized in rats, and has not been identified previously as being expressed in rat retina. This study is also the first determination that Cryba1-4, Crybb1, Crybb3, and Crygb are expressed in the rat retina. It is also the first implication of Cryba1-4, Crybb1-3, Crygb, and Crygs in retinal degeneration of any sort.

The identification of this large class of clones prompted an examination of the expression patterns of several of the crystallin genes. Northern analysis of Cryaa, Cryab, Cryba1, Crybb2, and Crygs revealed that all five genes are expressed in dark-reared rat retinae (**Figure 7-3.**). Expression levels of all transcripts except that for Cryba1 continually increased with increasing light exposure (4 and 8 hours). The Cryba1 transcript differed from the others in that it showed the greatest observed increase in expression of all the crystallin transcripts after 4 hours of light exposure, but these levels then dropped after 8 hours of light exposure. Western analysis of αA-, αB-, β-, and γS-crystallin indicated that αA-, αB-, and γS-crystallin are present in untreated retinae, but that their levels remain relatively constant with increasing light exposure. β-Crystallin levels also remain relatively constant, but no determination could be made regarding which β-crystallins were present, only that they were present in all three treatments. Immunohistochemistry showed that αB- and γS-crystallin showed a change in localization with increasing light exposure, indicating that some aspect of these proteins' function in the retina changes with light exposure.

A stress-response function for αA- and αB-crystallin has already been well-established (Klemenz *et al.*, 1991; Das *et al.*, 1996, 1999; Horwitz *et al.*, 1998; Rawat and Rao, 1998; Marini *et al.*, 2001; Ray *et al.*, 2001), so it is not surprising to find that the oxidative stress of LIRD is marked by a change in expression of the genes for these proteins, or that αB-crystallin localization in the retina changes. As yet, a definitive role for the other crystallins has not been firmly established in the stress-response. Some studies that examine the role of the crystallins in the lens seem to be examining the hypothesis that the βγ-crystallins are an important part of the reduction-oxidation (redox) balance of the lens (Slingsby and Miller, 1985; Liang and Pelletier, 1987, 1988; Lou and Dickerson Jr., 1992). This study provides a different perspective for βγ-crystallin function. The βγ-crystallins have a primarily structural role in the lens, while in the retina, a structural function for the βγ-crystallins has not been established at all. While the retina is a highly organized tissue, its structure is radically different from lens structure, and suggests that the βγ-crystallin's structural function is of less significance in the retina. This means that the expression of γS-crystallin seen in the retina is more likely related to the other suspected role of the βγ-crystallins, redox balance. The realization of this prompted the formulation of the hypothesis that, in the retina, the βγ-crystallins, with their high cysteine content, provide a readily available pool of reducing potential for a tissue that possesses a very high oxidizing potential (Section **1-B3**; **Figures 1-6.**, and **7-10.**). Oxidative stress is an established characteristic of LIRD (Organisciak *et al.*, 1992a, 1992b, 1995, 1999a; Kutty *et al.*, 1995; Specht *et al.*, 1999), and the retina must be able to respond to this imbalance. The mRNA for antioxidant proteins like heme-oxygenase-1 (Hmox1; Kutty *et al.*, 1995) and copper/zinc superoxide dismutase (Sod1; **Figure 7-3h.**) has been shown to increase after light treatment. Perhaps the βγ-crystallins are part of the suite of antioxidant proteins, as passive donors of reducing potential.

The identification and characterization of crystallin expression in the LIRD retina provides support for the hypothesis that LIRD retinae will have a characteristic molecular phenotype. Light exposure (4 and 8 hours) results in increased mRNA levels of the crystallins, and a change in localization of at least two crystallins in the retina. So, one aspect of the molecular phenotype of LIRD is an increase in crystallin gene expression,

and a change in protein localization. Defining this one element of the LIRD phenotype is important, because it is the first time that crystallin gene expression has been implicated in any form of retinal degeneration. As well, in looking for an explanation for an increase in crystallin gene expression in LIRD, a strong hypothesis for βγ-crystallin function has been generated. The results and hypotheses generated by this study suggest a new avenue of research, an examination of redox balance when proteins are considered part of the cellular reducing potential. More specifically, this thesis suggests that an examination of the effect that increased crystallin expression has on redox balance in photoreceptor cells of the retina will increase our understanding of retinal degeneration.

References

Abgar, S., J. Vanhoudt, T. Aerts, and J. Clauwaert. 2001. Study of the Chaperoning Mechanism of Bovine Lens α-Crystallin, a Member of the α-Small Heat Shock Superfamily. *Biophysical Journal* **80**(4): 1986-1995.

Abler, A., C. Chang, J. Ful, M. Tso, T. Lam. 1996. Photic Injury Triggers Apoptosis of Photoreceptor Cells. *Research Communications In Molecular Pathology and Pharmacology* **92**(2): 177-189.

Akao, Y., and Y. Matsuda. 1996. Identification and Chromosome Mapping of the Mouse Homologue of The Human Gene (DDX6) that Encodes a Putative RNA Helicase of the DEAD Box Protein Family. *Cytogenetics and Cell Genetics* **75**(1): 38-44.

Ali, R., G. Sarra, C. Stephens, M. Alwis, J. Bainbridge, P. Munro, S. Fauser, M. Reichel, C. Kinnon, D. Hunt, S. Bhattacharya, and A. Thrasher. 2000. Restoration of Photoreceptor Ultrastructure and Function in Retinal Degeneration Slow Mice by Gene Therapy. *Nature Genetics* **25**(3): 306-310.

Alloway, P., L. Howard, and P. Dolph. 2000. The Formation of Stable Rhodopsin-Arrestin Complexes Induces Apoptosis and Photoreceptor Cell Degeneration. *Neuron* **28**(1): 129-138.

Alonso, A., I. Grundke-Iqbal, and K. Iqbal. 1996. Alzheimer's Disease Hyperphosphorylated Tau Sequesters Normal Tau into Tangles of Filaments and Disassembles Microtubules. *Nature Medicine* **2**(7): 783-787.

Altschul, S., W. Gish, W. Miller, E. Myers, and D. Lipman. 1990. Basic Local Alignment Search Tool. *Journal of Molecular Biology* **215**(3): 403-410.

Altschul, S., T. Madden, A. Schäffer, J. Zhang, Z. Zhang, W. Miller, and D. Lipman. 1997. Gapped BLAST and PSI-BLAST: A New Generation of Protein Database Search Programs. *Nucleic Acids Research* **25**(17): 3389-3402.

Andley, U., Z. Song, E. Wawrousek, T. Fleming, and S. Bassnet. 2000. Differential Protective Activity of αA- and αB-Crystallin in Lens Epithelial Cells. *The Journal of Biological Chemistry* **275**(47): 36823-36831.

Ann, K., J. Kowalchyk, K. Loyet, and T. Martin. 1997. Novel Ca^{2+}-Binding Protein (CAPS) Related to UNC-31 Required for Ca^{2+}-Activated Exocytosis. *Journal of Biological Chemistry* **272**(32): 19637-640.

Araujo, H., N. Danziger, J. Cordier, J. Glowinski, and H. Chneiweiss. 1993. Characterization of PEA-15, a Major Substrate for Protein Kinase C in Astrocytes. *Journal of Biological Chemistry* **268**(8): 5911-5920.

Arikawa, K., L. Molday, R. Molday, and D. Williams. 1992. Localization of Peripherin/Rds in the Disk Membranes of Cone and Rod Photoreceptors: Relationship to Disk Membrane Morphogenesis and Retinal Degeneration. *Journal of Cell Biology* **116**(3): 659-667.

Arthur, J., J. Elce, C. Hegadorn, K. Williams, and P. Greer. 2000. Disruption of the Murine Calpain Small Subunit Gene, Capn4: Calpain is Essential for Embryonic Development but not for Cell Growth and Division. *Molecular and Cellular Biology* **20**(12): 4474-4481.

Ausubel, F., R. Brent, R. Kingston, D. Moore, J. Sediman, J. Smith, and K. Struhl. 1994. *Current Protocols in Molecular Biology*. John Wiley & Sons, Inc. Etobicoke, Ontario.

Bekri, S.; J.Adelaide, S. Merscher; J. Grosgeorge, F. Caroli-Bosc, D. Perucca-Lostanlen, P. Kelley, M.-J. Pebusque, C. Theillet, D. Birnbaum, P. Gaudray. 1997. Detailed Map of a Region Commonly Amplified at 11q13-Q14 in Human Breast Carcinoma. *Cytogenetics and Cell Genetics* **79**(1-2): 125-131.

Bermingham, Jr., J., K. Arden, A. Naumova, C. Sapienza, C. Viars, X. Fu, J. Khotz J, J. Manley, and M. Rosenfeld. 1995. Chromosomal Localization of Mouse and Human Genes Encoding the Splicing Factors ASF/SF2 (SFRS1) and SC-35 (SFRS2). *Genomics*. **29**(1): 70-79.

Bhat, S., and C. Nagineni. 1989. αB Subunit of Lens-specific α-Crystallin is Present in Other Ocular and Non-ocular Tissues. *Biochemical and Biophysical Research Communication* **158**(1): 319-325.

Bloemendal, H., and W. de Jong. 1991. Lens Proteins and Their Genes. *Progress in Nucleic Acids Research and Molecular Biology* **41**: 259-281.

Borg, J., and J. London. 2002. Copper/Zinc Superoxide Dismutase Overexpression Promotes Survival of Cortical Neurons Exposed to Neurotoxins *In Vitro*. *Journal of Neuroscience Research* **70**(2): 180-189.

Boscia, F., I. Grattagliano, G. Vendemiale, T. Micelli-Ferrari, and E. Altomare. 2000. Protein Oxidation and Lens Opacity in Humans. *Investigative Ophthalmology and Visual Science* **41**(9): 2461-2465.

Boulton, M., M. Rózanowska, and B. Rózanowski. 2001. Retinal Photodamage. *Journal of Photochemistry and Photobiology* **64**(2-3): 144-161.

Brady, J., D. Garland, Y. Douglas-Tabor, W. Robison Jr., A. Groome, and E. Wawrousek. 1997. Targetted Disruption of the Mouse αA-Crystallin Gene Induces Cataract and Cytoplasmic Inclusion Bodies Containing the Small Heat Shock Protein αB-Crystallin. *Proceedings of the National Academy of Sciences, USA* **94**(3): 884-889.

Brecher, R., and A. Bird. 1990. Adult Vitelliform Macular Dystrophy. *Eye* **4**(1): 210-215.

Britten, R., and E. Davidson. 1985. Hybridisation Strategy in *Nucleic Acid Hybridisation: A Practical Approach*. IRL Press Limited. Washington, D.C. pp. 3-15.

Brunori, M., and G. Rotilio. 1984. Biochemistry of Oxygen Radical Species. *Methods in Enzymology* **105**: 22-35.

Brymora, A., V. Valova, M. Larsen, B. Roufogalis, and P. Robinson. 2001. The Brain Exocyst Complex Interacts with RalA in a GTP-Dependent Manner: Identification of a Novel Mammalian Sec3 Gene and a Second Sec15 Gene. *Journal of Biological Chemistry* **276**(32): 29792-29797.

Bunge, S., H. Wedemann, D. David, D. Terwilliger, L. van den Born, C. Aulehla-Scholz, C. Samanns, M. Horn, J. Ott, E. Schwinger, A. Schinzel, M. Denton, and A. Gal. 1993. Molecular Analysis and Genetic Mapping of the Rhodopsin Gene in Families with Autosomal Dominant Retinitis Pigmentosa. *Genomics* **17**(1): 230-233.

Carmody, R., and T. Cotter. 2000. Oxidative Stress Induces Caspase-independent Retinal Apoptosis *In Vitro*. *Cell Death and Differentiation* **7**(3): 282-291.

Carver, J., R. Lindner, C. Lyon, D. Canet, H. Hernandez, C. Dobson, and C. Redfield. 2002. The Interaction of the Molecular Chaperone α-Crystallin with Unfolding α-Lactalbumin: A Structural and Kinetic Spectroscopic Study. *Journal of Molecular Biology* **318**(3): 815-827.

Casagrande, S., V. Bonetto, M. Fratelli, E. Gianazza, I. Eberini, T. Massignan, M. Salmona, G. Chang, A. Holmgren, and P. Ghezzi. 2002. Glutathionylation of Human Thioredoxin: A Possible Crosstalk Between the Glutathione and Thioredoxin Systems. *Proceedings of the National Academy of Sciences, USA*, **99**(15): 9745-9749.

Chambers, M., D. Organisciak, R. Darrow, K. Woltjen, A. Aggarwal, J. Stepczynski, and P. Wong. 1998. Defining the Degeneration Phenotype of Light-induced, Oxidative Stress-Mediated, Retinal Damage in Rats. *Investigative Ophthalmology and Visual Science*, **39**(4): S128.

Chang, G.-Q., Y. Hao, and F. Wong. 1993. Apoptosis: Final Common Pathway of Photoreceptor Death in rd, rds, and Rhodopsin Mutant Mice. *Neuron* **11**(4): 595-605.

Clout, N., A. Basak, K. Wieligmann, O. Bateman, R. Jaenicke, and C. Slingsby. 2000. The N-terminal Domain of βB2-Crystallin Resembles the Putative Ancestral Homodimer. *Journal of Molecular Biology* **304**(3): 253-257.

Colley, N., J. Cassill, E. Baker, and C. Zuker. 1995. Defective Intracellular Transport is the Molecular Basis of Rhodopsin-dependent Dominant Retinal Degeneration. *Proceedings of the National Academy of Sciences, USA*, **92**(7): 3070-3074.

Condorelli, G., G. Vigliotta, C. Iavarone, M. Caruso, C. Tocchetti, F. Andreozzi, A. Cafieri, M. Tecce, P. Formisano, L. Beguinot, and F. Beguinot. 1998. PED/PEA-15 Gene Controls Glucose Transport and is Over-expressed in Type 2 Diabetes Mellitus. *EMBO Journal* **17**(14): 3858-3866.

Condorelli, G., G. Vigliotta, A. Cafieri, A. Trencia, P. Andalo, F. Oriente, C. Miele, M. Caruso, P. Formisano, and F. Beguinot. 1999. PED/PEA-15: An Anti-apoptotic Molecule that Regulates FAS/TNFR1-induced Apoptosis. *Oncogene* **18**(31): 4409-4415.

Connell, P., C. Ballinger, J. Jiang, Y. Wu, L. Thompson, J. Höhfeld, and C. Patterson. 2001. The Co-chaperone CHIP Regulates Protein Triage Decisions Mediated by Heat-shock Proteins. Nature Cell Biology **3**(1): 93-96.

Correa-Rotter, R, Mariash, C, Rosenberg, M. 1992. Loading and Transfer Control for Northern Hybridization. *Biotechniques* **12**(2): 154-8.

Courilleau, D., E. Chastre, M. Sabbah, G. Redeuilh, A. Atfi, and J. Mester. 2000. B-ind1, a Novel Mediator of Rac1 Signaling Cloned from Sodium Butyrate-Treated Fibroblasts. *Journal of Biological Chemistry* **275**(23): 17344-17348.

Critchley, D., M. Holt, S. Barry, H. Priddle, L. Hemmings, and J. Norman. 1999. Integrin-mediated Cell Adhesion: The Cytoskeletal Connection. *Biochemical Society* **65**: 79-99.

D'Ancona, G., C. Chern, P. Benn, and C. Croce. 1977. Assignment of the Human Gene for Enolase 1 to Region pter in Equilibrium p36 of Chromosome 1. *Cytogenetics and Cell Genetics* **18**(6): 327-332.

Daiger, S. 2002. Retnet. What's New in Genes Causing Retinal Diseases. www.sph.uth.tmc.edu/Retnet/. Last updated October 15th, 2002. Visited December 13th, 2002.

Daimon, M., S. Susa, K. Suzuki, T. Kato, K. Yamatani, and H. Sasaki. 1997. Identification of a Human cDNA Homologue to the Drosophila Translocation Protein 1 (Dtrp1). *Biochemical and Biophysical Research Communications* **320**(1); 100-104

Danziger, N., M. Yokoyama, T. Jay, J. Cordier, J. Glowinski, and H. Chneiweiss. 1995. Cellular Expression, Developmental Regulation, and Phylogenic Conservation of PEA-15, the Astrocytic Major Phosphoprotein and Protein Kinase C Substrate. *Journal of Neurochemistry* **64**(3): 1016-1025.

Das, K., J. Petrash, and W. Surewicz. 1996. Conformational Properties of Substrate Proteins Bound to a Molecular Chaperone α-Crystallin. *The Journal of Biological Chemistry* **271**(18): 10449-10452.

Das, K., L. Choo-Smith, J. Petrash, and W. Surewicz. 1999. Insight into the Secondary Structure of Non-native Proteins Bound to a Molecular Chaperone α-Crystallin. *The Journal of Biological Chemistry* **274**(47): 33209-33212.

Datta, S., C. Rao. 1999. Differential Temperature-dependent Chaperone-like Activity of αA- and αB-Crystallin Homoaggregates. *The Journal of Biological Chemistry* **274**(49): 34773-34778.

Davidson, F. and H. Steller. 1998. Blocking Apoptosis Prevents Blindness in *Drosophila* Retinal Degeneration Mutants. *Nature*, **391**(6667): 587-591.

de Jong, W., J. Leunissen, and C. Voorter. 1993. Evolution of the α-Crystallin/Small Heat-shock Protein Family. *Molecular Biology and Evolution* **10**(1): 103-126.

Derham, B., and J. Harding. 1999. α-Crystallin as a Molecular Chaperone. *Progress in Retinal and Eye Research* **18**(4): 463-509.

Der Perng, M., P. Muchowski, P. van den IJssel, G. Wu, A. Hutcheson, J. Clark, and R. Quinlan. 1999. The Cardiomyopathy and Lens Cataract Mutation in αB-Crystallin Alters Its Protein Structure, Chaperone Activity, and Interaction with Intermediate Filaments *In Vitro*. *The Journal of Biological Chemistry* **274**(47): 33235-33243.

DiLella, A., A. Hawkins, R. Craig, S. Schreiber, and C. Griffin. 1992. Chromosomal Band Assignments of the Genes Encoding Human FKBP12 and FKBP13. *Biochemical Biophysical Research Communications* **189**(2): 819-823.

Dirks, R., S. van Genesen, J. Krûse, L. Jorissen, and N. Lubsen. 1998. Letter to the Editors: Extralenticular Expression of the Rodent βB2-Crystallin Gene. *Experimental Eye Research* **66**(2): 267-269.

Dryja, T.; T. McGee, E. Reichel, L. Hahn, G. Cowley, D. Yandell, M. Sandberg, and E. Berson. 1990 A Point Mutation of the Rhodopsin Gene in One Form of Retinitis Pigmentosa. *Nature* **343**(6256): 364-366.

Dryja, T., L. Hahn, T. Reboul, and B. Arnaud. 1996. Missense Mutation in the Gene Encoding the Alpha Subunit of Rod Transducin in the Nougaret Form of Congenital Stationary Night Blindness. *Nature Genetics* **13**(3): 358-360.

Esterbauer, H., and K. Cheeseman. 1990. Determination of Aldehydic Lipid Peroxidation Products: Malonaldehyde and 4-Hydroxynonenal. *Methods in Enzymology* **186**: 407-421.

Engström, N.-E., A. Holmgren, A. Larsson, and S. Söderhall. 1974. Isolation and Characterization of Calf Liver Thioredoxin. *The Journal of Biological Chemistry* **249**(1): 205-210.

Estelles, A., M. Yokoyama, F. Nothias, J. Vincent, J. Glowinski, P. Vernier, and H. Chneiweiss. 1996. The Major Astrocytic Phosphoprotein PEA-15 is Encoded by Two mRNAs Conserved on Their Full Length in Mouse and Human. *Journal of Biological Chemistry* **271**(25): 14800-14806.

Farrar, G., P. Kenna, R. Redmond, P. McWilliam, D. Bradley, M. Humphries, E. Sharp, C. Inglehearn, R. Bashir, M. Jay, A. Watty, M. Ludwig, A. Schinzel, C. Samanns, A. Gal, S. Bhattacharya, S.; and P. Humphries. 1990a. Autosomal Dominant Retinitis Pigmentosa: Absence of the Rhodopsin Proline-to-histidine Substitution (codon 23) in Pedigrees from Europe. *American Journal of Human Genetics* **47**(6): 941-945.

Farrar, G., P. McWilliam, D. Bradley, P. Kenna, M. Lawler, E. Sharp, M. Humphries, H. Eiberg, P. Conneally, J. Trofatter, and P. Humphries. 1990b. Autosomal Dominant Retinitis Pigmentosa: Linkage to Rhodopsin and Evidence for Genetic Heterogeneity. *Genomics* **8**(1): 35-40.

Farrar, G., P. Kenna, S. Jordan, R. Kumar-Singh, M. Humphries, E. Sharp, D. Sheils, and P. Humphries. 1991. A Three Base-pair Deletion in the Peripherin-RDS Gene in One Form of Retinitis Pigmentosa. *Nature* **354**(6353): 478-480.

Farrar, G., P. Kenna, and P. Humphries. 2002. On the Genetics of Retinitis Pigmentosa and on Mutation-independent Approaches to Therapeutic Intervention. *EMBO Journal* **21**(5): 857-864.

Fassler, J., C. Nadell, N. Richardson, J. McEntyre, G. Schuler, S. McGinnis, S. Pongor, and D. Landsman. BLAST Information Guide. www.ncbi.nlm.nih.gov/Education/BLASTinfo/. Last updated June 7th, 2000. Visited December 16th, 2002.

Felbor, U., H. Schilling, and B. Weber. 1997. Adult Vitelliform Macular Dystrophy is Frequently Associated with Mutations in the Peripherin/RDS gene. *Human Mutation* **10**(4): 301-309.

Ferrari, A., H. Seuanez, S. Hanash, and G. Atweh. 1990. A Gene that Encodes for a Leukemia-associated Phosphoprotein (p18) Maps to Chromosome Bands 1p35-36.1. *Genes Chromosomes Cancer* **2**(2): 125-129.

Fink, A. 1999. Chaperone-mediated Protein Folding. *Physiological Reviews* **79**(2): 425-449.

Fingen-Eigen, M., H. Domdey, and K. Kohrer. 1996. The Ribosomal Protein Gene RPS3 is an Essential Single Copy Gene of the Yeast *Saccharomyces cerevisiae*. *Biochemical and Biophysical Research Communications* **223**(2): 397-403.

Flohé , L., and W. Günzler. Assays of Glutathione Peroxidase. *Methods in Enzymology* **105**: 114-121.

Fridovitch, I. 1995 Superoxide Radical and Superoxide Dismutases. *Annual Review of Biochemistry* **64**: 97-112.

Frost, J., A. Khokhlatchev, S. Stippec, M. White, and M. Cobb. 1998. Differential Effects of PAK1-Activating Mutations Reveal Activity-dependent and -Independent Effects on Cytoskeletal Regulation. *Journal of Biological Chemistry* **273**(43): 28191-28198.

Frydman, J. 2001. Folding of Newly Translated Proteins *In Vivo*: The Role of Molecular Chaperones. *Annual Review of Biochemistry* **70**: 603-647.

Fuchs, S., M. Nakazawa, M. Maw, M. Tamai, Y. Oguchi, and A. Gal. 1995. A Homozygous 1 Base-pair Deletion in the Arrestin Gene is a Frequent Cause of Oguchi Disease in Japanese. *Nature Genetics* **10**(3): 360-362.

Gai, W., J. Power, P. Blumbergs, J. Culvenor, and P. Jensen. 1999. Alpha-synuclein Immunoisolation of Glial Inclusions from Multiple System Atrophy Brain Tissue Reveals Multiprotein Components. *Journal of Neurochemistry* **73**(5): 2093-2100.

Giblin, F. 2000. Glutathione: A Vital Lens Antioxidant. *Journal of Ocular Pharmacology and Therapeutics* **16**(2): 121-135.

Glickman, M., and A. Ciechanover. 2002. The Ubiquitin-Proteasome Proteolytic Pathway: Destruction for the Sake of Construction. Physiological Reviews **82**(2): 373-428.

Gómez-Fabre, P., K. Helou, and F. Stahl. 2002. Predictions Based on the Rat-mouse Comparative Map Provide Mapping Information on Over 6000 New Rat Genes. *Mammalian Genome* **13**(4): 189-193.

Goutebroze, L., E. Brault, C. Muchardt, J. Camonis, and G. Thomas. 2000. Cloning and Characterization of SCHIP-1, a Novel Protein Interacting Specifically with Spliced Isoforms and Naturally Occurring Mutant NF2 Proteins. *Molecular and Cellular Biology* **20**(5): 1699-1712.

Graw, J. 1997. The Crystallins: Genes, Proteins, and Diseases. *Biological Chemistry* **378**(11): 1331-1348.

Graw, J., M. Jung, J. Loster, N. Klopp, D. Soewarto, C. Fella, H. Fuchs, A. Reis, R. Balling, M. Hrabé de Angelis. 1999. Mutation in the βA3/A1-Crystallin Encoding Gene *Cryba1* Causes a Dominant Cataract in the Mouse. *Genomics* **62**(1): 67-73.

Green, M., and H. Hill. 1984. Chemistry of Dioxygen. *Methods in Enzymology* **105**: 3-22.

Grimm, C., A. Wenzel, F. Hafezi, and C. Remé. 2000. Gene Expression in the Mouse Retina: The Effect of Damaging Light. *Molecular Vision* **6**: 252-260.

Hafezi, F., C. Grimm, B. Simmen, A. Wenzel, and C. Remé. 2000. Molecular Ophthalmology: An Update on Animal Models for Retinal Degenerations and Dystrophies. *British Journal of Ophthalmology* **84**: 922-927.

Halliwell, B. 1991. Reactive Oxygen Species in Living Systems: Source, Biochemistry, and Role in Human Disease. *American Journal of Medicine* **91**(3C):14S-22S.

Ham, Jr., W., H. Muller, and D. Sliney. 1976. Retinal Sensitivity to Damage from Short Wavelength Light. *Nature* **260**(5547): 153-155.

Ham, Jr., W., H. Muller, J. Ruffalo, J. Millen, D. Guerry, and R. Guerry. 1982. Action Spectrum for Retinal Injury from Near Ultraviolet Radiation in the Aphakic Monkey. *American Journal of Ophthalmology* **93**(3): 299-306.

Ham, Jr., W., H. Muller, J. Ruffalo, J. Millen, R. Guerry, and D. Guerry, 3rd. 1984. Basic Mechanisms Underlying the Production of Photochemical Lesions in the Mammalian Retina. *Current Eye Research* **3**(1): 165-174.

Hanson, S. A. Chen, J. Smith, and M. Lou. Thiolation of the γB-Crystallins in Intact Bovine Lens Exposed to Hydrogen Peroxide. *The Journal of Biological Chemistry* **274**(8): 4735-4741.

Hao, W., A. Wenzel, M. Obin, C.-K. Chen, E. Brill, N. Krasnoperova, P. Eversole-Cire, Y. Kleyner, A. Taylor, M. Simon, C. Grimm, C. Remé and J. Lem. 2002, Evidence for Two Apoptotic Pathways in Light-induced Retinal Degeneration. *Nature Genetics* **32**(2): 254-260.

Harding, J., ed. 1997. *Biochemistry of the Eye*. Chapman & Hall Medical. New York, New York.

Hart, Jr., W., ed. 1992. *Adler's Physiology of the Eye, 9th Edition*. Mosby Year Book, Inc. St. Louis, Missouri.

Hejtmancik, J. 1998. The Genetics of Cataract: Our Vision Becomes Clearer. *American Journal of Human Genetics* **62**(3):520-525.

Hemmerich, S., J. Lee, S. Bhakta, A. Bistrup, N. Ruddle, and S. Rosen. 2001. Chromosomal Localization and Genomic Organization for the Galactose/N-acetylgalactosamine/N-acetylglucosamine 6-O-sulfotransferase Gene Family. *Glycobiology* **11**(1): 75-87.

Héon, E., M. Priston, D. Schorderet, G. Billingsley, P. Girard, N. Lubsen, and F. Munier. 1999. The γ-Crystallins and Human Cataracts: A Puzzle Made Clearer. *American Journal of Human Genetics* **65**(5): 1261-1267.

Higashide, T., M. McLaren, and G Inana. 1998. Localization of HRG4, a Photoreceptor Protein Homologous to Unc-119, in Ribbon Synapse. *Investigative Ophthalmology and Visual Science* **39**(5):690-698.

Höhfeld, J., D. Cyr, and C. Patterson. 2001. From the Cradle to the Grave: Molecular Chaperones that May Choose Between Folding and Degradation. *EMBO Reports* **2**(10): 885-890.

Holmgren, A. 1985. Thioredoxin. *Annual Review of Biochemistry* **54**: 237-271.

Horwitz, J. 1993. Proctor Lecture: The Function of α-Crystallin. *Investigative Ophthalmology and Visual Science* **34**(1): 10-22.

Horwitz, J., Q. Huang, L. Ding, and M. Bova. 1998. Lens α-Crystallin: Chaperone-like Properties. *Methods in Enzymology* **290**: 365-383.

Horwitz, J., M. Bova, L. Ding, S. Haley, and P. Stewart. 1999. Lens α-Crystallin: Function and Structure. *Eye* **13**(3b): 403-408.

Humphries, P., G. Farrar, P. Kenna, P. McWilliam. 1990. Retinitis Pigmentosa: Genetic Mapping in X-linked and Autosomal Forms of the Disease. *Clinical Genetics* **38**(1): 1-13.

Humphries, P.; P. Kenna, G. Farrar. 1992. On the Molecular Genetics of Retinitis Pigmentosa. *Science* **256**(5058): 804-808.

Hwang, S., W. Kuo, J. Cochran, R. Guzman, T. Tsukamoto, G. Bandyopadhyay, K. Myambo, and C. Collins. 1997. Assignment of HMAT1, the Human Homolog of the Murine Mammary Transforming Gene (MAT1) Associated with Tumorigenesis, to 1q21.1, a Region Frequently Gained in Human Breast Cancers. *Genomics* **42**(3): 540-542.

Ishibashi, K., S. Fjii, M. Escaño, Y. Sekiya, and M. Yamamoto. 2000. Up-regulation of Crystallin mRNAs in Form-deprived Chick Eyes. *Experimental Eye Research* **70**(2): 153-158.

Jones, Jr., M. 1997. *Organic Chemistry*. W. W. Norton and Company. New York, New York.

Jones, S., C. Jomary, J. Grist, J. Makwana, and M. Neal. 1999. Retinal Expression of γ-Crystallins in the Mouse. *Investigative Ophthalmology and Visual Science* **40**(12): 3017-3020.

Jordan, S., G. Farrar, R. Kumar-Singh, P. Kenna, M. Humphries, V. Allamand, E. Sharp, and P. Humphries. 1992. Autosomal Dominant Retinitis Pigmentosa (adRP; RP6): Cosegregation of RP6 and the Peripherin-RDS Locus in a Late-onset Family of Irish Origin. *American Journal of Human Genetics* **50**(3): 634-639.

Jung, S., J. Lee, and J. Kim. 2001. Yeast Ribosomal Protein S3 has an Endonuclease Activity on AP DNA. *Molecular Cell* **12**(1): 84-90.

Kajiwara, K., M. Sandberg, E. Berson, and T. Dryja. 1993. A Null Mutation in the Human Peripherin/RDS Gene in a Family with Autosomal Dominant Retinitis Punctata Albescens. *Nature Genetics* **3**(3): 208-212.

Kannabiran, C., P. Rogan, L. Olmos, S. Basti, G. Rao, M. Kaiser-Kupfer, and J. Hejtmancik. 1998. Autosomal Dominant Zonular Cataract with Structural Opacities is Associated with a Splice Mutation in the βA3/A1-Crystallin Gene. *Molecular Vision* **4**(21). (www.molvis.org/)

Kapron, J., G. Hilliard, J. Lakins, M. Tenniswood, K. West, S. Carr, and J. Crabb. 1997. Identification and Characterization of Glycosylation Sites in Human Serum Clusterin. *Protein Science* **6**(10): 2120-2133.

Kato, K., H. Shinohara, N. Kurobe, S. Goto, Y. Inaguma, and K. Ohshima. 1991a. Immunoreactive αA-Crystallin in Rat Non-Lenticular Tissues Detected With a Sensitive Immunoassay Method. *Biochimica et Biophysica Acta* **1080**(2): 173-180.

Kato K, Shinohara H, Kurobe N, Inaguma Y, Shimizu K, Ohshima K. 1991b. Tissue Distribution and Developmental Profiles of Immunoreactive αB-Crystallin in the Rat Determined With a Sensitive Immunoassay System. *Biochimica et Biophysica Acta* **1074**(1): 201-208.

Kato, K., H. Ito, K. Kamei, I. Iwamoto, and Y. Inaguma. 2002. Innervation-dependent Phosphorylation and Accumulation of αB-Crystallin and Hsp27 as Insoluble Complexes in Disused Muscle. *FASEB Journal* **16**(11): 1432-1434.

Katsanis, N., and E. Fisher. 1998. A Novel C-Terminal Binding Protein (CTBP2) is Closely Related to CTBP1, an Adenovirus E1A-binding Protein, and Maps to Human Chromosome 21q21.3. *Genomics* **47**(2): 294-299.

Katzmarzyk, P., T. Rankinen, L. Perusse, O. Deriaz, A. Tremblay, I. Borecki, D. Rao, and C. Bouchard. 1999. Linkage and Association of the Sodium Potassium-adenosine triphosphatase Alpha2 and Beta1 Genes with Respiratory Quotient and Resting Metabolic Rate in the Quebec Family Study. *Journal of Clinical Endocrinology and Metabolism* **84**(6): 2093-2097.

Kellogg, B., and C. Poulter. 1997. Chain Elongation in the Isoprenoid Biosynthetic Pathway. *Current Opinion in Chemical Biology* **1**(4): 570-578.

Khaliq, S., A. Hameed, M. Ismail, K. Anwar, B. Leroy, S. Mehdi, A. Payne, and S. Bhattacharya. 2000. Novel Locus for Autosomal Recessive Cone-rod Dystrophy CORD8 Mapping to Chromosome 1q12-q24. *Investigative Ophthalmology and Visual Science* **41**(12): 3709-3712.

Kikawa, E., M. Nakazawa, Y. Chida, T. Shiono, and M. Tamai. 1994. A Novel Mutation (Asn244Lys) in the Peripherin/RDS Gene Causing Autosomal Dominant Retinitis Pigmentosa Associated with Bull's-eye Maculopathy Detected by Non-radioisotopic SSCP. *Genomics* **20**(1): 137-139.

Kim, J., L. Chubatsu, A. Admon, J. Stahl, R. Fellous, and S. Linn. 1995a. Implication of Mammalian Ribosomal Protein S3 in the Processing of DNA Damage. *Journal of Biological Chemistry* **270**(23): 13620-13629.

Kim, R., H. Dollfus, T. Keen, F. Fitzke, G. Arden, S. Bhattacharya, and A. Bird. 1995b. Autosomal Dominant Pattern Dystrophy of the Retina Associated with a 4 base-pair Insertion at Codon 140 in the Peripherin/RDS gene. *Archives of Ophthalmology* **113**(4): 451-455.

Kim, V., N. Kataoka, and G. Dreyfuss. 2001. Role of the Nonsense-Mediated Decay Factor hUpf3 in the Splicing-Dependent Exon-Exon Junction Complex. *Science* **293**(5536): 1832-1836.

Kipreos, E., L. Lander, J. Wing, W. He, and E. Hedgecock. 1996. cul-1 is Required for Cell Cycle Exit in *C. elegans* and Identifies a Novel Gene Family. *Cell* **85**(6): 829-839.

Kirchhoff, F., R. Dringen, and C. Giaume. 2001. Pathways of Neuron-astrocyte Interactions and Their Possible Role in Neuroprotection. *European Archives of Psychiatry and Clinical Neuroscience* **251**(4): 159-169.

Kiss, T. 2002. Small Nucleolar RNAs: An Abundant Group of Noncoding RNAs with Diverse Cellular Functions. *Cell* **109**(2): 145-148.

Kitsberg, D., E. Formstecher, M. Fauquet, M. Kubes, J. Cordier, B. Canton, G. Pan, M. Rolli, J. Glowinski, and H. Chneiweiss. 1999. Knock-out of the Neural Death Effector Domain Protein PEA-15 Demonstrates that its Expression Protects Astrocytes from TNFα-induced Apoptosis. *Journal of Neuroscience* **19**(19): 8244-8251.

Klemenz, R., E. Fröhli E, R. Steiger, R. Schäafer, and A. Aoyama. 1991. αB-Crystallin is a Small Heat Shock Protein. *Proceedings of the National Academy of Sciences, USA*, **88**(9): 3652-3656.

Kniazeva, M., M. Chiang, B. Morgan, A. Anduze, D. Zack, M. Han, and K. Zhang. 1999. A New Locus for Autosomal Dominant Stargardt-like Disease Maps to Chromosome 4. *American Journal of Human Genetics* **64**(5):1394-1399.

Kobayashi, A., T. Higashide, D. Hamasaki, S. Kubota, H. Sakuma, W. An, T. Fujimaki, M. McLaren, R. Weleber, and G. Inana. 2000. HRG4 (UNC119) Mutation Found in Cone-rod Dystrophy Causes Retinal Degeneration in a Transgenic Model. *Investigative Ophthalmology and Visual Science* **41** (11): 3268-3277.

Kolb, H., E. Fernandez, and R. Nelson. 2002. Webvision: The Organization of the Retina and Visual System. www.webvision.med.utah.edu. Last updated: July, 2002. Visited: August 1st, 2002.

Kono, M., A. Sen, B. Chakrabarti. 1990. Thermodynamics of Thermal and Athermal Denaturation of γ-Crystallins: Changes in Conformational Stability Upon Glutathione Reaction. *Biochemistry* **29**(2):464-70

Kremer, H., A. Pinckers, B. van den Helm, A. Deutman, H. Ropers, and E. Mariman. 1994. Localization of the Gene for Dominant Cystoid Macular Dystrophy on Chromosome 7p. *Human Molecular Genetics* **3**(2): 299-302.

Kutty, R., G. Kutty, B. Wiggert, G. Chader, R. Darrow, and D. Organisciak. 1995. Induction of Heme Oxygenase 1 in the Retina by Intense Visible Light: Suppression by the Antioxidant Dimethylthiourea. *Proceedings of the National Academy of Sciences, USA*, **92**(4): 1177-1181.

Lagali, P., I. MacDonald, I. Griesinger, M. Chambers, R. Ayyagari, and P. Wong. 2000. Autosomal Dominant Stargardt-like Macular Dystrophy Segregating in a Large Canadian Family. *Canadian Journal of Ophthalmology* **35**(6): 315-24.

Lam, S., M. Tso, and D. Gurne. 1990. Amelioration of Photic Injury in Albino Rats by Dimethylthiourea. *Archives of Ophthalmology* **108**(12): 1751-1757.

Lee, H., S. Safieddine, R. Petralia, and R. Wenthold. 2002. Identification of a Novel SNAP25 Interacting Protein (SIP30). *Journal of Neurochemistry* **81**(6): 1338-1347.

Lenzi, D., and H. von Gersdorff. 2001. Structure Suggests Function: The Case for Synaptic Ribbons as Exocytotic Nanomachines. *BioEssays* **23**(9): 831-840.

Lerman, S. 1980. Biological and Chemical Effects of Ultraviolet Radiation in *Radiant Energy and the Eye*. Macmillan, Inc. New York, New York. pp. 115-186.

Lewin, B. 1997. *Genes VI*. Oxford University Press. New York, New York.

Li, Z.-Y., M. Tso, H.-M. Wang,, and D. Organisciak. 1985. Amelioration of Photic Injury in Rat Retina by Ascorbic Acid: A Histopathologic Study. *Investigative Ophthalmology and Visual Science* **26**(11): 1589-1598.

Liang, J., and M. Pelletier. 1987. Spectroscopic Studies on the Mixed Disulfide Formation of Lens Crystallin with Glutathione. *Experimental Eye Research* **45**(2): 197-206.

Liang, J., and M. Pelletier. 1988. Destabilization of Lens Protein Conformation by Glutathione Mixed Disulfide. *Experimental Eye Research* **47**(1): 17-25.

Liao, J.-H., J.-S. Lee, and S.H. Chiou. 2002. Distinct Roles of αA- and αB-Crystallins Under Thermal and UV Stress. *Biochemical and Biophysical Research Communication* **295**(4): 854-861.

Lim, S., C. Sala, J. Yoon, S. Park, S. Kuroda, M. Sheng, and E. Kim. 2001. Sharpin, A Novel Postsynaptic Density Protein that Directly Interacts with the Shank Family of Proteins. *Molecular and Cellular Neuroscience* **17**(2): 385-397.

Lin, Y., J. Brosius, and H. Tiedge. 2001. Neuronal BC1 RNA: Co-expression with Growth-associated Protein-43 Messenger RNA. *Neuroscience* **103**(2):465-479.

Litt, M., R. Carrero-Valenzuela, D. LaMorticella, D. Schultz, T. Mitchell, P. Kramer, and I. Maumenee. 1997. Autosomal Dominant Cerulean Cataract is Associated with a Chain Termination Mutation in the Human β-Crystallin Gene CRYBB2. . *Human Molecular Genetics* **6**(5): 665-668.

Litt, M., P. Kramer, D. LaMorticella, W. Murphey, E. Lovrien, and R. Weleber. 1998. Autosomal Dominant Congenital Cataract Associated with a Missense Mutation in the Human α-Crystallin Gene CRYAA. *Human Molecular Genetics* **7**(3): 471-474.

Lolley, R., H. Rong, and C. Craft. 1994. Linkage of Photoreceptor Degeneration by Apoptosis with Inherited Defect in Phototransduction. *Investigative Ophthalmology and Visual Science* **35**(2): 358-362.

Lou, M., and J. Dickerson Jr. 1992. Protein-thiol Mixed Disulfides in Human Lens. *Experimental Eye Research* **55**(6): 889-896.

Machida, S., P. Chaudry, T. Shinohara, D. Singh, V. Reddy, L. Chylack Jr., P. Sieving, and R. Bush. 2001. Lens Epithelium Derived Growth Factor Promotes Photoreceptor Survival in Light-damaged and RCS Rats. *Investigative Ophthalmology and Visual Science* **42**(5): 1087-1095.

Madden, T., R. Tatusov, and J. Zhang. 1996. Applications of Network BLAST Server. *Methods in Enzymology* **266**:131-141.

Maeda, A., H. Ohguro, T. Maeda, T. Nakagawa, and Y. Kuroki. 1999. Low Expression of αA-Crystallins and Rhodopsin Kinase of Photoreceptors in Retinal Dystrophy Rat. *Investigative Ophthalmology and Visual Science* **40**(12): 2788-2794.

Magabo, K., J. Horwitz, J. Piatigorsky, and M. Kantorow. 2000. Expression of βB2-Crystallin mRNA and Protein in Retina, Brain, and Testis. *Investigative Ophthalmology and Visual Science* **41**(10): 3056-3060.

Marini, I., R. Moschini, A. Del Corso, and U. Mura. 2000. Complete Protection by α-Crystallin of Lens Sorbitol Dehydrogenase Undergoing Thermal Stress. *The Journal of Biological Chemistry* **275**(42): 32559-32565.

Mathew, A., and R. Morimoto. 1998. Role of the Heat-shock Response in the Life and Death of Proteins. *Annals New York Academy of Sciences* **851**: 99-111.

Maw, M., B. Kennedy, A. Knight, R. Bridges, K. Roth, E. Mani, J. Mukkadan, D. Nancarrow, J. Crabb, and M. Denton. 1997. Mutation of the Gene Encoding Cellular Retinaldehyde-binding Protein in Autosomal Recessive Retinitis Pigmentosa. *Nature Genetics* **17**(2): 198-200.

M^{c}Mahon, H., M. Missler, C. Li, and T. Sudhof. 1995. Complexins: Cytosolic Proteins that Regulate SNAP Receptor Function. *Cell* **83**(1): 111-119.

Milam, A. and Z. Li. 1995. Retinal Pathology in Retinitis Pigmentosa: Considerations for Therapy in *Degenerative Diseases of the Retina*. Plenum Press. New York, New York. pp. 275-284.

Mittag, T., A. Bayer, and M. LaVail. 1999. Light-induced Retinal Damage in Mice Carrying a Mutated Sod1 Gene. *Experimental Eye Research* **69**(6): 677-83.

Moreira, E., C. Jaworski, and I. Rodriguez. 1999. Cloning of a Novel Member of the Reticulon Gene Family (RTN3): Gene Structure and Chromosomal Localization to 11q13. *Genomics* **58**(1): 73-81.

Morimura, H., F. Saindelle-Ribeaudeau, E. Berson, and T. Dryja. 1999. Mutations in RGR, Encoding a Light-sensitive Opsin Homologue, in Patients with Retinitis Pigmentosa. *Nature Genetics* **23**(4): 393-394.

Moritz, O., B. Tam, L. Hurd, J. Peränen, D. Deretic, and D. Papermaster. 2001. Mutant rab8 Impairs Docking and Fusion of Rhodopsin-bearing Post-Golgi Membranes and Causes Cell Death of Transgenic *Xenopus* Rods. *Molecular Biology of the Cell* **12**(8): 2341-2351.

Muslimov, I., Y. Lin, M. Heller, J. Brosius, Z. Zakeri, and H. Tiedge. 2002. A Small RNA in Testis and Brain: Implications for Male Germ Cell Development. *Journal of Cell Science* **115**(6):1243-1250.

Nathans, J., D. Thomas, and D. Hogness. 1986. Molecular Genetics of Human Color Vision: The Genes Encoding Blue, Green, and Red Pigments. *Science* **232**(4747): 193-202.

Nei, M., P. Xu, and G. Glazko. 2000. Estimation of Divergence Times from Multi-protein Sequences for a Few Mammalian Species and Several Distantly Related Organisms. *Proceedings of the National Academy of Sciences* USA **98**(5): 2497-2502.

Nicholson, D. 2001. Products of Isoprene Metabolism. International Union of Biochemistry & Molecular Biology. www.tcd.ie/Biochemistry/IUBMB-Nicholson/. Last revised October 24th, 2002. Visited: December 16th, 2002.

Nishimura, Y., M. Hayashi, H. Inada H, and T. Tanaka. 1999. Molecular Cloning and Characterization of Mammalian Homologues of Vesicle-Associated Membrane Protein-Associated (VAMP-Associated) Proteins. *Biochemical and Biophysical Research Communications* **254**(1): 21-26.

Noell, W., V. Walker, B. Kang, and S. Berman. 1966. Retinal Damage by Light in Rats. *Investigative Ophthalmology and Visual Science* **5**(5): 450-473.

Noell, W. 1980. Possible Mechanisms of Photoreceptor Damage by Light in Mammalian Eyes. *Vision Research* **20**(12): 1163-1171.

Noell, W., D. Organisciak, H. Ando, M. Braniecki, and C. Durlin. 1987. Ascorbate and Dietary Protective Mechanisms in Retinal Light Damage of Rats: Electrophysiological, Histological, and DNA Measurement in *Degenerative Retinal Disorders: Clinical Laboratory Investigations*. Alan R. Liss, Inc. New York, New York.

Oakey, R., M. Watson, and M. Seldin. 1992. Construction of a Physical Map on Mouse and Human Chromosome 1: Comparison of 13 Mb of Mouse and 11 Mb of Human DNA. *Human Molecular Genetics* **1**(8): 613-620.

Omran, H., G. Sasmaz, K. Haffner, A. Volz, H. Olbrich, R. Melkaoui, E. Otto, T. Wienker, R. Korinthenberg, M. Brandis, C. Antignac, and F. Hildebrandt. 2002. Identification of a Gene Locus for Senior-Loken Syndrome in the Region of the Nephronophthisis Type 3 Gene. *Journal of the American Society of Nephrology* **13**(1): 75-79.

Organisciak, D., H.-M. Wang, and A. Kou. 1984. Ascorbate and Glutathione Levels in the Developing Normal and Dystrophic Rat Retina: Effect of Intense Light Exposure. *Current Eye Research* **3**(1): 257-267.

Organisciak, D., H.-M. Wang, Z.-Y. Li, and M. Tso. 1985. The Protective Effect of Ascorbate in Retinal Light Damage of Rats. *Investigative Ophthalmology and Visual Science* **26**(11): 1580-1588.

Organisciak, D., H.-M. Wang, and W. Noell. 1987. Aspects of the Ascorbate Protective Mechanism in Retinal Light Damage of Rats with Reduced ROS Docosahexaenoic Acid in *Degenerative Retinal Disorders: Clinical Laboratory Investigations*. Alan R. Liss, Inc. New York, New York.

Organisciak, D. Y.-L. Jiang, H.-M. Wang, and I. Bicknell. 1990. The Protective Effect of Ascorbic Acid in Retinal Light Damage of Rats Exposed to Intermittent Light. *Investigative Ophthalmology and Visual Science* **31**(7): 1195-1202.

Organisciak, D., R. Darrow, I. Bicknell, Y.-L. Jiang, M. Pickford, and J. Blanks. 1991. Protection Against Retinal Light Damage by Natural and Synthetic Antioxidants in *Retinal Degenerations*. CRC Press. Boca Raton, Florida. pp. 189-201.

Organisciak, D., I. Bicknell, and M. Darrow. 1992a. The Effects of L- and D-Ascorbic Acid Administration on Retinal Tissue Levels and Light Damage in Rats. *Current Eye Research* **11**(3): 231-241.

Organisciak, D., R. Darrow, Y. Jiang, G. Marak, and J. Blanks. 1992b. Protection by Dimethylthiourea Against Retinal Light Damage in Rats. *Investigative Ophthalmology and Visual Science*, **33**(5): 1599-1609.

Organisciak, D., and B. Winkler. 1994. Retinal Light Damage: Practical and Theoretical Considerations. *Progress in Retinal and Eye Research* **13**(1): 1-29.

Organisciak, D., R. Kutty, M. Leffak, P. Wong, S. Messing, B. Wiggert, R. Darrow, and G. Chader. 1995. Oxidative Damage and Responses in Retinal Nuclei Arising from Intense Light Exposure in *Degenerative Diseases of the Retina*. Plenum Press. New York, New York.

Organisciak, D., R. Darrow, Y.-L. Jiang, and J. Blanks. 1996. Retinal Light Damage in Rats with Altered Levels of Rod Outer Segment Docosahexaenoate. *Investigative Ophthalmology and Visual Science*, **37**(11): 2243-2257.

Organisciak, D., R.M. Darrow, R.A. Darrow, and L. Linninger. 1998. Environmental Light and Age-related Changes in Retinal Proteins in *Photostasis and Related Phenomenon*. Plenum Press. New York, New York. pp. 79-92.

Organisciak, D., M. Li, R. Darrow, and D. Farber. 1999a. Photoreceptor Cell Damage by Light in Young Royal College of Surgeon rats. *Current Eye Research* **19**(2): 188-196.

Organisciak, D., R.A. Darrow, L. Barsalou, R.M. Darrow, and L. Linninger. 1999b. Light-induced Damage in the Retina: Differential Effects of Dimethylthiourea on Photoreceptor Survival, Apoptosis and DNA Fragmentation. *Photochemistry and Photobiology* **70**(2): 261-268.

Organisciak, D., R. Darrow, L. Barsalou, R. Kutty, and B. Wiggert. 2000. Circadian-dependent Retinal Light Damage in Rats. *Investigative Ophthalmology and Visual Science* **41**(12): 3694-3701.

Ossola, J. and M. Tomaro. 1998. Heme Oxygenase Induction by UVA radiation: A Response to Oxidative Stress in Rat Liver. *International Journal of Biochemistry and Cell Biology* **30**(2): 285-292.

Otani, A., K. Kinder, K. Ewalt, F. Otero, P. Schimmel, and M. Friedlander. 2002. Bone Marrow–derived Stem Cells Target Retinal Astrocytes and Can Promote or Inhibit Retinal Angiogenesis. *Nature Medicine* **8**(9): 1004-1010.

Ottilie, S., J. Diaz, W. Horne, J. Chang, Y. Wang, G. Wilson, S. Chang, S. Weeks, L. Fritz, and T. Oltersdorf. 1997. Dimerization Properties of Human BAD. Identification of a BH-3 Domain and Analysis of Its Binding to Mutant BCL-2 and BCL-XL Proteins. *Journal of Biological Chemistry* **272**(49): 30866-30872.

Oyster, C. 1999. *The Human Eye: Structure and Function*. Sinauer Associates, Inc. Sunderland, Massachusetts.

Parrini, M., M. Lei, S. Harrison, and B. Mayer. 2002. Pak1 Kinase Homodimers are Autoinhibited in Trans and Dissociated upon Activation by Cdc42 and Rac1. *Molecular Cell* **9**(1):73-83.

Patterson, C., J. Gao, A. Rooney, and E. Davis. 2002. Genomic Organization of Mouse and Human 65 kDa FK506-Binding Protein Genes and Evolution of the FKBP Multigene Family. *Genomics* **79**(6): 881-889.

Perin, M., V. Fried, D. Stone, X Xie, and T. Sudhof. 1991. Structure of the 116-kDa Polypeptide of the Clathrin-Coated Vesicle/Synaptic Vesicle Proton Pump. *Journal of Biological Chemistry* **266**(6): 3877-3881.

Petersen-Jones, S. 1998. Animal Models of Human Retinal Dystrophies. *Eye* **12**(3b):566-570.

Polakiewicz, R., D. Munroe, S. Sait, K. Tycowski, N. Nowak, T. Shows, D. Housman, and D. Page. 1995. Mapping of Ribosomal Protein S3 and Internally Nested snoRNA U15A Gene to Human Chromosome 11q13.3-q13.5. *Genomics* **25**(2):577-580.

Portera-Cailliau, C., C. Sung, J. Nathans, and R. Adler. 1994. Apoptotic Photoreceptor Cell Death in Mouse Models of Retinitis Pigmentosa. *Proceedings of the National Academy of Sciences, USA*, **91**: 974-978.

Powis, G., and W. Montfort. 2001. Properties and Biological Activities of Thioredoxins. *Annual Review of Pharmacology and Toxicology* **41**: 261-295.

Puertas, F., M. Díaz-Llopis, E. Chipont, J. Romá, Á. Raya, and F. Romero. 1993. Glutathione System of Human Retina: Enzymatic Conjugation of Lipid Peroxidation Products. *Free Radical Biology & Medicine* **14**(5): 549-551.

Rajaraman, K., B. Raman, T. Ramakrishna, and C. Rao. 2001. Interaction of Human Recombinant αA- and αB-Crystallins with Early and Late Unfolding Intermediates of Citrate Synthase on Its Thermal Denaturation. *FEBS Letters* **497**(2-3): 118-123.

Rapp, L., and T. Williams. 1980. The Role of Ocular Pigmentation in Protecting Against Retinal Light Damage. *Vision Research* **20**(12): 1127-1131.

Rattner, A., H. Sun, and J. Nathans. 1999. Molecular Genetics of Human Retinal Disease. *Annual Review of Genetics* **33**: 89-131

Rawat, U. and M. Rao. 1998. Interactions of Chaperone α-Crystallin with the Molten Globule State of Xylose Reductase. *The Journal of Biological Chemistry* **273**(16): 9415-9423.

Ray, P., J. Martin, E. Swanson, H. Otani, W. Dillman, and D. Das. 2001. Transgene Overexpression of αB-Crystallin Confers Simultaneous Protection Against Cardiomyocyte Apoptosis and Necrosis During Myocardial Ischemia and Reperfusion. *FASEB Journal* **15**(2): 393-402.

Reddy, G., K. Dast, J. Petrash, and W. Surewicz. 2000. Temperature-dependent Chaperone Activity and Structural Properties of Human αA- and αB-Crystallins. *The Journal of Biological Chemistry* **275**(7): 4565-4570.

Reim, K., M. Mansour, F. Varoqueaux, H. McMahon, T. Sudhof, N. Brose, and C. Rosenmund. 2001. Complexins Regulate a Late Step in Ca^{2+}-Dependent Neurotransmitter Release. *Cell* **104**(1): 71-81.

Remé, C., M. Weller, P. Szczesny, K. Munz, F. Hafezi, J.-J. Reinboth, and M. Clausen. 1995. Light-induced Apoptosis in the Rat Retina *In Vivo*: Morphological Features, Threshold and Time Course in *Degenerative Diseases of the Retina*. pp. 19-25.

Richard, M., R. Drouin, and A. Beaulieu. 1998. ABC50, a Novel Human ATP-Binding Cassette Protein Found in Tumor Necrosis Factor-Alpha-Stimulated Synoviocytes. *Genomics* **53**(2): 137-145.

Roberts, J. 2001. Ocular Phototoxicity. *Journal of Photochemistry and Photobiology* **64**(2-3): 136-143.

Rodriguez de Turco, E., D. Deretic, N. Bazan, and D. Papermaster. 1997. Post-Golgi Vesicles Cotransport Docosahexaenoyl-phospholipids and Rhodopsin During Frog Photoreceptor Membrane Biogenesis. *Journal of Biological Chemistry* **272**(16): 10491-10497.

Ross, J. 1995. mRNA Stability in Mammalian Cells. *Microbiological Reviews* **59**: 423-450.

Rousseau-Merck, M., A. Bernheim, P. Chardin, R. Miglierina, A. Tavitian, and R. Berger. 1988. The Ras-related Ral Gene Maps to Chromosome 7p15-22. *Human Genetics* **79**(2): 132-136.

Saar, K., L. Al-Gazali, L. Sztriha, F. Rueschendorf, M. Nur-E-Kamal, A. Reis, and R. Bayoumi. 1999. Homozygosity Mapping in Families with Joubert Syndrome Identifies a Locus on Chromosome 9q34.3 and Evidence for Genetic Heterogeneity. *American Journal of Human Genetics* **65**(6): 1666-1671.

Sambrook, J., E. Fritsch, and T. Maniatis. 1989. *Molecular Cloning: A Laboratory Manual, Second Edition*. Cold Spring Harbor Laboratory Press. Plainview, New York.

Sambrook, J., and D. Russell. 2001. *Molecular Cloning: A Laboratory Manual, Third Edition*. Cold Spring Harbor Laboratory Press. Cold Spring Harbor, New York.

Sancar, A. 2000. Cryptochrome: The Second Photoactive Pigment in The Eye and Its Role in Circadian Photoreception. *Annual Review of Biochemistry* **69**:31-67.

Sanders, L., F. Matsumura, G. Bokoch, and P. de Lanerolle. 1999. Inhibition of Myosin Light Chain Kinase by p21-activated Kinase. *Science* **283**(5410):2083-2085.

Schuermann, M., E. Otto, A. Becker, K. Saar, F. Ruschendorf, B. Polak, S. Ala-Mello, J. Hoefele, A. Wiedensohler, M. Haller, H. Omran, P. Nurnberg, and F. Hildebrandt. 2002. Mapping of Gene Loci for Nephronophthisis Type 4 and Senior-Loken Syndrome, to Chromosome 1p36. *American Journal of Human Genetics* **70**(5): 1240-1246.

Sells, M., J. Boyd, and J. Chernoff. 1999. p21-activated Kinase 1 (Pak1) Regulates Cell Motility in Mammalian Fibroblasts. *Journal of Cell Biology* **145**(4):837-849.

Shull, G., J. Greeb, and J. Lingrel. 1986. Molecular Cloning of Three Distinct Forms of the Na+,K+-ATPase Alpha-Subunit From Rat Brain. *Biochemistry* **25**(25): 8125-8132.

Sinha, D., N. Esumi, C. Jaworski, C. Kozak, E. Pierce, and G. Wistow. 1998. Cloning and Mapping the Mouse Crygs Gene and Non-lens Expression of γS-Crystallin. *Molecular Vision* **4**: 8-12.

Skouri-Panet, F., F. Bonneté, K. Prat, O. Bateman, N. Lubsen, and A. Tardieu. 2001. Lens Crystallins and Oxidation: The Special Case of γS. *Biophysical Chemistry* **89**(1): 65-76.

Slingsby, C., H. Driessen, D. Mahadevan, B. Bax, and T. Blundell. 1988. Evolutionary and Functional Relationships Between the Basic and Acidic β-Crystallins. *Experimental Eye Research* **46**(3): 375-403.

Slingsby, C., and N. Clout. 1999. Structure of the Crystallins. *Eye* **13**(3b): 395-402.

Slingsby, C., and L. Miller. 1985. The Reaction of Glutathione with the Eye-lens Protein γ-Crystallin. *Biochemical Journal* **230**(1): 143-150.

Smillie, D., J. Sommerville. 2002. RNA Helicase p54 (DDX6) is a Shuttling Protein Involved in Nuclear Assembly of Stored mRNP Particles. *Journal of Cell Science* **115**(2):395-407.

Soares, M., M. Bonaldo, P. Jelene, L. Su, L. Lawton, and A. Efstratiadis. 1994. Construction and Characterization of a Normalized cDNA Library. *Proceedings of the National Academy of Sciences, USA* **91**(20): 9228-9232.

Specht, S., M. Leffak, R. Darrow, and D. Organisciak. 1999. Damage to Rat Retinal DNA Induced *In Vivo* by Visible Light. *Photochemistry and Photobiology* **69**(1): 91-98

Sperling, H. 1980. Prolonged Intense Spectral Light Effects on Rhesus Retina in *The Effect of Constant Light on Visual Processes*. Plenum Press. New York, New York. pp. 195-214.

Sperling, H. 1986. Spectral Sensitivity, Intense Spectral Light Studies, and the Colour Receptor Mosaic of Primates. *Vision Research* **26**(9): 1557-1572.

Sperling, H., C. Johnson, and R. Harwerth. 1980. Differential Spectral Photic Damage to Primate Cones. *Vision Research* **20**(12): 1117-1125.

Srinivasan, A., C. Nagineni, and S. Bhat. 1992. αA-Crystallin is Expressed in Non-ocular Tissues. *The Journal of Biological Chemistry* **267**(32): 23337-23341.

Stege, G., K. Renkawek, P. Overkamp, P. Verschuure, A. van Rijk, A. Reijnen-Aalbers, W. Boelens, G. Bosman, and W. de Jong. 1999. The Molecular Chaperone αB-Crystallin Enhances Amyloid β Neurotoxicity. *Biochemical Biophysical Research Communications* **262**(1): 152-156.

Stepczynski, J. 2001. *Master's Thesis: Defining the Molecular Phenotype of the Rat Retina During the Commitment Phase of Light-induced Retinal Degeneration: A Model of Human Retinal Degenerative Disease*. Faculty of Graduate Studies and Research, Department of Biological Sciences, University of Alberta. Edmonton, Alberta.

Stephan, D., E. Gillanders, D. Vanderveen, D. Freas-Lutz, G. Wistow, A. Baxevanis, C. Robbins, A. VanAuken, M. Quesenberry, J. Bailey-Wilson, S. Juo, J. Trent, L. Smith, and M. Brownstein. 1999. Progressive Juvenile-onset Punctate Cataracts Caused by Mutation of the γD-Crystallin Gene. *Proceedings of the National Academy of Sciences, USA* **96**(3): 1008-1012.

Stockton, D., R. Lewis, E. Abboud, A. Al-Rajhi, M. Jabak, K. Anderson, and J. Lupski. 1998. A Novel Locus for Leber Congenital Amaurosis on Chromosome 14q24. *Human Genetics* **103**(3):328-333.

Stone, E., A. Kimura, J. Folk, S. Bennett, B. Nichols, L. Streb, and V. Sheffield. 1992. Genetic Linkage of Autosomal Dominant Neovascular Inflammatory Vitreoretinopathy to Chromosome 11q13. *Human Molecular Genetics* **1**(9): 685-689.

Sung, C.-H., C. Davenport, J. Hennessey, I. Maumenee, S. Jacobson, J. Heckenlively, R. Nowakowski, G. Fishman, P. Gouras, and J. Nathans. 1991. Rhodopsin Mutations in Autosomal Dominant Retinitis Pigmentosa. *Proceedings of the National Academy of Sciences* USA **88**(15): 6481-6485.

Sutcliffe, J., R. Milner, J. Gottesfeld, and W. Reynolds. 1984. Control of Neuronal Gene Expression. *Science* **225**(4668): 1308-1315.

Tan, E., Q. Wang, A. Quiambao, X. Xu, N. Qtaishat, N. Peachey, J. Lem, S. Fliesler, D. Pepperberg, M. Naash, and M. Al-Ubaidi. 2001. The Relationship Between Opsin Overexpression and Photoreceptor Degeneration. *Investigative Ophthalmology and Visual Science* **42**(3): 589-600.

Tanaka, H., Y. Yoshimura, Y. Nishina, M. Nozaki, H. Nojima, and Y. Nishimune. 1994. Isolation and Characterization of cDNA Clones Specifically Expressed in Testicular Germ Cells. *FEBS Letters* **355**(1): 4-10.

Tanito, M., H. Masutani, H. Nakamura, A. Ohira, and J. Yodoi. 2002a. Cytoprotective Effect of Thioredoxin Against Retinal Photic Injury in Mice. *Investigative Ophthalmology and Visual Science* **43**(4): 1162-1167.

Tanito, M., A. Nishiyama, T. Tanaka, H. Masutani, H. Nakamura, J. Yodoi, and A. Ohira. 2002b. Change of Redox Status and Modulation by Thiol Replenishment in Retinal Photooxidative Damage. *Investigative Ophthalmology and Visual Science* **43**(7): 2392-2400.

Tanksale, A., M. Ghatge, and V. Deshpande. 2002. α-Crystallin Binds to the Aggregation-prone Molten-globule State of Alkaline Protease: Implications for Preventing Irreversible Thermal Denaturation. *Protein Science* **11**(7): 1720-1728.

Tatusova, T., T. Madden. 1999. Blast 2 Sequences: A New Tool for Comparing Protein and Nucleotide Sequences. *FEMS Microbiology Letters* **174**(2):247-250.

Thomas, P. 1980. Hybridization of Denatured RNA and Small DNA Fragments Transferred to Nitrocellulose. *Proceedings of the National Academy of Sciences USA* **77**(9): 5201-5205.

Travis, G., J. Sutcliffe, and D. Bok. 1991. The Retinal Degeneration Slow (rds) Gene Product is a Photoreceptor Disc Membrane-associated Glycoprotein. *Neuron* **6**(1): 61-70.

Tycowski, K.; M. Shu, and J. Steitz. 1993. A Small Nucleolar RNA is Processed from an Intron of the Human Gene Encoding Ribosomal Protein S3. Genes and Development **7**(7A): 1176-1190.

Vaughan, D., J. Nemke, S. Fliesler, R. Darrow, and D. Organisciak. 2002. Evidence for a Circadian Rhythm of Susceptibility to Retinal Light Damage. *Photochemistry and Photobiology* **75**(5): 547-553.

Vicart, P., A. Caron, P. Guicheny, Z. Li, M. Prévost, A. Faure, D. Chateau, F. Chapon, F. Tomé, J. Dupret, D. Paulin, and M. Fardeau. 1998. A Missense Mutation in the αB-Crystallin Chaperone Gene Causes a Desmin-related Myopathy. *Nature Genetics* **20**(1): 92-95.

Voet, D., and J. Voet. 1995. *Biochemistry, Second Edition*. John Wiley and Sons, Inc. Toronto, Ontario.

Wagner, B., and J. Margolis. 1995. Age-dependent Association of Isolated Bovine Lens Multicatalytic Proteinase Complex (Proteasome) with Heat-shock Protein 90, an Endogenous Inhibitor. *Archives of Biochemistry and Biophysics* **323**(2): 455-462.

Wang, G.-M., N. Raghavachari, and M. Lou. 1997. Relationship of Protein-Glutathione Mixed Disulfide and Thioltransferase in H_2O_2-Induced Cataract in Cultured Pig Lens. *Experimental Eye Research* **64**(5): 693-700.

Wang, K., and A. Spector. 1995. α-Crystallin Can Act as a Chaperone Under Conditions of Oxidative Stress. *Investigative Ophthalmology and Visual Science*, **36**(2): 311-321.

Wang, K. and A. Spector. 2000. α-Crystallin Prevents Irreversible Protein Denaturation and Acts Cooperatively with Other Heat-shock Proteins to Renature the Stabilized Partially Denatured Protein in an ATP-dependent Manner. *European Journal of Biochemistry* **267**(15): 4705-4712.

Waxler, M., and V. Hitchins, eds. 1986. *Optical Radiation and Visual Health*. CRC Press. Boca Raton, Florida.

Wetlaufer, D. 1984. Nonenzymatic Formation and Isomerization of Protein Disulfides. *Methods in Enzymology* **107**: 301-304.

Wickner, S., M. Maurizi, and S. Gottesman. 1999. Posttranslational Quality Control: Folding, Refolding, and Degrading proteins. *Science* **286**(5446): 1888-1893.

Wilkin, D., S. Kutsunai, and P. Edwards. 1990. Isolation and Sequence of the Human Farnesyl Pyrophosphate Synthetase cDNA. Coordinate Regulation of the mRNAs for Farnesyl Pyrophosphate Synthetase, 3-hydroxy-3-methylglutaryl Coenzyme A Reductase, and 3-hydroxy-3-methylglutaryl Coenzyme A Synthase by Phorbol Ester. *Journal of Biological Chemistry* **265**(8): 4607-4614.

Williams, T., and W. Howell. 1983. Action Spectrum of Retinal Light-damage in Albino rats. *Investigative Ophthalmology and Visual Science* **24**(3): 285-287.

Wimberly, B., D. Brodersen, W. Clemons Jr., R. Morgan-Warren, A. Carter, C. Vonrhein, T. Hartsch, and V. Ramakrishnan. 2000. Structure of the 30S Ribosomal Subunit. *Nature* **407**(6802): 327-339.

Winkler, B., M. Boulton, J. Gottsch, and P. Sternberg. 1999. Oxidative Damage and Age-related Macular Degeneration. *Molecular Vision* **5**:32. (www.molvis.org/)

Wistow, G. and J. Piatigorsky. 1988. Lens Crystallins: The Evolution of Proteins for a Highly Specialized Tissue. *Annual Review of Biochemistry* **57**: 479-504.

Wong, P. 1994. Apoptosis, Retinitis Pigmentosa, and Degeneration. *Biochemistry and Cell Biology* **72**: 489-498.

Wong, P., D. Borst, D. Farber, J. Danciger, M. Tennniswood, and G. Chader. 1994a. Increased TRPM-2/Clusterin mRNA Levels During the Time of Retinal Degeneration in Mouse Models of Retinitis Pigmentosa. *Biochemistry and Cell Biology* **72**(11-12): 439-446.

Wong, P., R. Kutty, R. Darrow, S. Shivaram, G. Kutty, R. Fletcher, B. Wiggert, G. Chader, and D. Organisciak. 1994b. Changes in Clusterin Expression Associated with Light-induced Retinal Damage in Rats. *Biochemistry and Cell Biology* **72**(11-12): 499-503.

Wong, P., T.Ulyanova, D. Organisciak, S. Bennett, J. Lakins, J. Arnold, R. Kutty, M. Tenniswood, T. vanVeen, R. Darrow, and G. Chader. 2001. Expression of Multiple Forms of Clusterin During Light-induced Retinal Degeneration. *Current Eye Research* **23**(3): 157-165.

Wood, L., N. Theriault, and G. Vogeli. 1988. cDNA Clones Completing the Nucleotide and Derived Amino Acid Sequence of the Alpha 1 Chain of Basement Membrane (Type IV) Collagen from Mouse. *FEBS Letters* **227**(1):5-8.

Yamamoto, M., A. Ohira, O. Honda, N. Sato, K. Furuke, J. Yodoi, and Y. Honda. 1997. Analysis of Localization of Adult T-cell Leukemia-derived Factor in the Transient Ischemic Rat Retina After Treatment with OP-1206 α-CD, a Prostaglandin E_1 Analogue. *The Journal of Histochemistry and Cytochemistry* **45**(1): 63-70.

Yi, X., X. Li, and F. Yu. 2000. A Novel Epithelial Wound-related Gene is Abundantly Expressed in Developing Rat Cornea and Skin. *Current Eye Research* **20**(5): 430-440.

Yon, J., R. Palmer, D. Sheer, and M. Fried. 1989. Localization of the Surfeit Gene Cluster Containing the Ribosomal Protein Gene L7a to Chromosome Bands 9q33-34. *Annals of Human Genetics* **53**(2): 149-155.

Yoo, B., S. Kim, N. Cairns, M. Fountoulakis, and G. Lubec. 2001. Deranged Expression of Molecular Chaperones in Brains of Patients with Alzheimer's Disease. *Biochemical Biophysical Research Communications* **280**(1): 249-258.

Young, R. 1971. Shedding of Discs from Rod Outer Segments in the Rhesus Monkey. *Journal of Ultrastructural Research* **34**(1): 190-203.

Young, R. 1972. The Renewal of Diffusely Distributed Protein in the Outer Segments of Rods and Cones. *Vision Research* **12**(2): 161-168.

Young, R. 1978. The Daily Rhythm of Shedding and Degradation of Rod and Cone Outer Segment Membranes in the Chick Retina. *Investigative Ophthalmology and Visual Science* **17**(2): 105-116.

Young, B., and M. Anderson. 1985. Quantitative Analysis of Solution Hybridisation in *Nucleic Acid Hybridisation: A Practical Approach*. IRL Press Limited. Washington, D.C. pp. 47-71.

Zhang, K., M. Kniazeva, M. Han, W. Li, Z. Yu, Z. Yang, Y. Li, M. Metzker, R. Allikmets, D. Zack, L. Kakuk, P. Lagali, P. Wong, I. MacDonald, P. Sieving, D. Figueroa, C. Austin, R. Gould, R. Ayyagari, and Petrukhin. 2001. A 5-bp Deletion in ELOVL4 is Associated with Two Related Forms of Autosomal Dominant Macular Dystrophy. *Nature Genetics* **27**(1): 89-93.

Zhang, S., J. Han, M. Sells, J. Chernoff, U. Knaus, R. Ulevitch, and G. Bokoch GM. 1995. Rho Family Gtpases Regulate P38 Mitogen-activated Protein Kinase Through the Downstream Mediator Pak1. *Journal of Biological Chemistry* **270**(41): 23934-23936.

Ziegler, D. 1985. Role of Reversible Oxidation-Reduction of Enzyme Thiols-disulfides in Metabolic Regulation. *Annual Review of Biochemistry* **54**: 305-329.

Appendix 1. Reagent Recipes

Arranged in the order they appear in Materials and Methods.

Abbreviations

APS = ammonium persulfate
BSA = bovine serum albumin fraction V
DAPI = 4',6-diamidinophenyl-indole
ddH_2O = deionized, distilled water
DEPC = diethylpyrocarbonate
DEPC•H_2O = DEPC-treated water
EDTA = ethylene diamine tetraacetic acid
EtBr = ethidium bromide
EtOH = ethanol
MeOH = methanol
MOPS = 4-morpholine propanesulfonicacid
p-CHO = paraformaldehyde
PBS = phosphate-buffered saline
SDS = sodium dodecyl sulfate
SSC = sodium chloride, sodium citrate buffer
TBS = Tris-buffered saline

DEPC•H_2O
ddH_2O
0.1% (v/v) DEPC
Stir for 12 hours.
Autoclave at 121°C for 20 minutes.
Store at room temperature.

RNA Gel (1%)
1.0 g agarose
72 mL DEPC•H_2O
18 mL formaldehyde
10 mL (10x) MOPS buffer[44]
Boil agarose in DEPC•H_2O.
Cool below boiling.
Add formaldehyde and MOPS buffer in fumehood.
Pour into gel casting tray, add comb, allow to set.
Make fresh.

RNA Gel Loading Mixture
Where [N] = *# samples + # standards + 2:*
[N] x 4 µL (10x) MOPS buffer
[N] x 7 µL formaldehyde
[N] x 20 µL deionized formamide
[N] x 1 µL (1 mg/mL) EtBr
Mix and add to 8 µL of sample (or standard) in DEPC•H_2O.
Heat-denature RNA at 50°C.
Add 5 µL of RNase-free 6x loading dye[45].
Make fresh.

RNA Running Buffer
817 mL DEPC•H_2O
83 mL formaldehyde
100 mL (10x) MOPS buffer
Mix in fumehood.
Make fresh.

20x SSC
3 M NaCl
0.3 M sodium citrate
Dissolve salts in ddH_2O.
Adjust pH to 7.0 with NaOH.
Autoclave at 121°C for 20 minutes.
Store at room temperature.
Related: 2x SSC/0.1% (w/v) SDS, 0.1x SSC/0.1% SDS

Luria-Bertani (LB) Broth
1 L ddH_2O
10.0 g NaCl
10.0 g tryptone
5.0 g yeast extract
Dissolve solids in ddH_2O.
Adjust pH to 7.0 with NaOH.
Autoclave at 121°C for 20 minutes.
Store at room temperature.
Related: LB Top Agar: 1% (w/v) agar, LB Agar: 1.5% agar, 1.0 M $MgSO_4$, 20% maltose (w/v)

[X] Tris•HCl pH [N]
Where [X] = *desired concentration of Tris:*
[X] M Tris
50-100 mL HCl (depending on [X] and [N])
Dissolve Tris in [Y] mL ddH_2O.
[Y] = 75% of final volume of solution.
Adjust pH to [N] with HCl.
Adjust volume to final volume.
Adjust pH to [N] with HCl.
Autoclave at 121°C for 20 minutes.
Store at room temperature.
Required [N]*:* 6.8, 7.5, 8.75, 8.8
Required [X]*:* 1.0, 1.5

[44] 0.5 M MOPS, 10 mM EDTA, pH 7.0
[45] 0.25% Bromophenol Blue (w/v) and 0.25% (w/v) xylene cyanol in 30% (v/v_{H2O}) glycerol

SM buffer
0.01 M $MgSO_4$
0.1 M NaCl
50 mM Tris•HCl (pH 7.5)
0.01% (w/v) gelatin
Dissolve components in ddH_2O.
Autoclave at 121°C for 20 minutes.
Store at room temperature.

10x *Pfu* PCR buffer
0.1 M KCl
0.1 M NH_4SO_4
0.2 M Tris•HCl (pH 8.75)
0.02 M $MgSO_4$
1% (v/v) Triton X-100
Dissolve components in ddH_2O.
Autoclave at 121°C for 20 minutes.
Aliquot into sterile 2 mL tubes and store at -20°C.

50x Tris Acetate EDTA (TAE) Buffer
50 mM EDTA
2.0 M Tris
1 M glacial acetic acid (≅57.1 mL)
Dissolve components in ddH_2O.
Adjust pH to 7.0 with NaOH.
Autoclave at 121°C for 20 minutes.
Store at room temperature.

Alkaline Southern Transfer Buffer

0.5 M NaOH
1.5 M NaCl
Dissolve salts in ddH_2O.
Use extreme caution with NaOH pellets or concentrated NaOH.
Autoclave at 121°C for 20 minutes.
Store at room temperature.

10x Loading Dye
0.25% Bromophenol Blue (w/v)
0.25% xylene cyanol (w/v)
30% glycerol (v/v)
Dissolve components in ddH_2O.
Filter sterilize.
Store at room temperature.

Sodium Acetate/EDTA Buffer
1.5 M sodium acetate
250 mM EDTA
Dissolve components in ddH_2O.
Adjust pH to >8.0 with NaOH.
Autoclave at 121°C for 20 minutes.
Aliquot into sterile 1.5 mL tubes and store at -20°C.

Guanidine•HCl (95% EtOH)
Where [N] = *final volume:*
0.3 M guanidine•HCl
0.05[N] ddH_2O
0.95[N] EtOH
Dissolve all the guanidine•HCl in the ddH_2O, with stirring and *slight* heating.
Heat in fumehood. Guanidine•HCl is explosive.
Cool to room temperature.
Add EtOH with stirring.
Filter sterilize.
Store at room temperature.

Bradford Reagent
5% MeOH (v/v)
9% phosphoric acid (v/v)
0.1% Coomassie Brilliant Blue (w/v)
0.5% sodium lactate (w/v)
Dissolve components in ddH_2O.
Filter sterilize.
Store at room temperature.

Separating Gel
0.375 M Tris•HCl (pH 8.8)
0.1% SDS (w/v)
13% (v/v) [19 acrylamide:1 bisacrylamide]
Dissolve components in ddH_2O.
Stir solution under vacuum to remove oxygen.
Make fresh.
Related: 10% APS (w/v), TEMED[46]

Stacking Gel
0.125 M Tris•HCl (pH 8.8)
0.1% SDS (w/v)
5% (v/v) [19 acrylamide:1 bisacrylamide]
Dissolve components in ddH_2O.
Stir solution under vacuum to remove oxygen.
Make fresh.
Related: 10% APS (w/v), TEMED[46]

5x SDS-PAGE Running Buffer
0.125 M Tris
1.0 M glycine
0.1% SDS (w/v)
Dissolve components in ddH_2O.
Adjust pH to 8.5 with NaOH.
Autoclave at 121°C for 20 minutes.
Store at room temperature.

[46] (N,N,N',N')-tetramethylethylene diamine, Sigma-Aldrich, St. Louis, Missouri

Laemmli Buffer
0.375 M Tris•HCl (pH 6.8)
0.1% SDS (w/v)
0.25% Bromophenol blue (w/v)
13.2% glycerol (v/v)
Dissolve components in ddH_2O.
Filter sterilize.
Store at room temperature.
The buffer is completed fresh each time by mixing 19:1 with β-mercaptoethanol in a separate tube.
Add Laemmli buffer to the protein samples.
The samples are then boiled for 3 minutes.
The samples are then loaded in the wells of the gel.

Western Transfer Buffer
0.025 M Tris
0.2 M glycine
0.05% SDS (w/v)
Dissolve salts in ddH_2O.
Adjust pH to 8.3 with NaOH.
Store at room temperature.

Coomassie Blue Stain
0.1% Coomassie Brilliant Blue (w/v)
45% MeOH (v/v)
10% glacial acetic acid (v/v)
Mix liquid components in ddH_2O.
Add Coomassie Brilliant Blue.
Store at room temperature.
Related: Destaining Solution: 40% MeOH (v/v), 10% glacial acetic acid (v/v)

Ponceau S Stain
0.5% Ponceau S
10% glacial acetic acid (v/v)
Mix acetic acid with ddH_2O.
Add Ponceau S.
Store at room temperature.

Blocking Buffer
10 mM Tris
140 mM NaCl
0.05% (v/v) IGEPAL CA-630 (NP-40)
10% (w/v) BSA
Dissolve components in ddH_2O.
Adjust pH to 7.4 with HCl.
Make fresh.

Antibody Buffer
10 mM Tris
140 mM NaCl
0.03% Tween 20
Dissolve components in ddH_2O.
Adjust pH to 7.4 with HCl.
Make fresh.

PBS
140 mM NaCl
2.7 mM KCl
8 mM Na_2HPO_4
1.5 mM KH_2PO_4
Dissolve salts in ddH_2O.
Adjust pH to 7.4 with NaOH.
Autoclave at 121°C for 20 minutes.
Store at room temperature.
Related: 4% *p*-CHO•PBS, 30% sucrose (w/v) •PBS

Optimal Cutting Temperature (OCT) Compound
Sakura Finetek USA, Torrance, California
For information only.
10.24% polyvinyl alcohol (w/w)
4.26% polyethylene glycol (w/w)
85.50% nonreactive ingredients (w/w)

Citrate Buffer
10 mM citric acid monohydrate
Dissolve citric acid in ddH_2O, note that it is hydrated.
Adjust pH to 6.5 with NaOH.
Autoclave at 121°C for 20 minutes.
Store at room temperature.

TBS
140 mM NaCl
2.7 mM KCl
12.4 mM Tris
Dissolve salts in ddH_2O.
Adjust pH to 7.4 with NaOH.
Autoclave at 121°C for 20 minutes.
Store at room temperature.
Related: TBS/T (0.1% Triton X-100), 5% skim milk (w/v) TBS/T

1000x DAPI
10 mg DAPI
10 mL ddH_2O
Dissolve DAPI in ddH_2O in the dark.
Aliquot into sterile 1.5 mL tubes.
Store at -20°C in the dark.

Appendix 2. Gene Symbols and Names for *Homo sapiens*, *Rattus norvegicus*, and *Mus musculus*

Arranged alphabetically by *R. norvegicus* gene symbol. The correct gene symbol is underlined where alternate gene symbols are given. Gene names are from *H. sapiens* unless otherwise noted. Alternate descriptive names are provided in brackets following the gene name.

Homo sapiens	*Rattus norvegicus*	*Mus musculus*	Gene Name
ABCF1, ABC27, ABC50	Abcf1, Abc50	Abcf1, Abc50	ATP-binding cassette, sub-family F (GCN20), member 1
n/a	AF272892	n/a	Corneal wound healing-related protein
ALDH2	Aldh2	Aldh2, Ahd5	Aldehyde dehydrogenase 2 family (mitochondrial)
ALDOC, ALDC	Aldoc, ALDCAA	Aldo3	Aldolase C, fructose-bisphosphate (*M. musculus*: zebrin II)
AKR1B1, AR, ADR, ALDR1	Aldr1, Alr, ALDRED, Akr1b1, Akr1b3, ALR-P-I	Akr1b3, AR, Ahr1, Aldr1, Akr1b1, Aldor1	Aldo-keto reductase family 1, member B1 (aldose reductase)
ATP1A2	Atp1a2, RATATPA2	Atp1a2, Atpa-3	ATPase, Na^+/K^+ transporting, alpha 2 (+) polypeptide
ATP5G2	Atp5g2	Atp5g2	ATP synthase, H^+ transporting, mitochondrial F0 complex, subunit c (subunit 9), isoform 2
ATP6V0A1, a1, Stv1, VPP1, Vph1, ATP6N1A	Atp6n1a	Atp6v0a1, Vpp1, ATP6a1, Atp6n1a, Atpv0a1	ATPase, H^+ transporting, lysosomal V0 subunit a isoform 1
BAD, BBC2, BCL2L8	Bad	Bad, Bbc2	BCL2-antagonist of cell death
CAPNS1, 30K, CANP, CDPS, CANPS, CAPN4	Capns1, Capn4	Capns1, Capa4, Capn4	Calpain, small subunit 1
CADPS, CAPS	Caps	Cadps, CAPS	Ca^{2+}-dependent activator protein for secretion
CDH1, UVO, CDHE, ECAD, LCAM	Cdh1	Cdh1, Um, UVO, Ecad	Cadherin 1, type 1, E-cadherin (epithelial) (*H. sapiens*: uvomorulin, Arc-1, cell-CAM 120/80; *M. musculus*: E-cadherin; *R. norvegicus*: E-cadherin)
CHST1, C6ST, KS6ST, KSGAL6ST	Chst1	Chst1, C6ST, Gst1, KSGAL6ST	Carbohydrate (keratan sulfate Gal-6) sulfotransferase 1

Appendix 2. Gene Symbols and Names for *Homo sapiens*, *Rattus norvegicus*, and *Mus musculus*

Arranged alphabetically by *R. norvegicus* gene symbol. The correct gene symbol is underlined where alternate gene symbols are given. Gene names are from *H. sapiens* unless otherwise noted. Alternate descriptive names are provided in brackets following the gene name.

Homo sapiens	*Rattus norvegicus*	*Mus musculus*	Gene Name
CNTF	Cntf	Cntf	Ciliary neurotropic factor
COL4A1	Col4a1	Col4a1	Collagen, type IV, alpha 1
CPLX2, CPX2, 921-L	Cplx2	Cplx2, 921-L	Complexin 2 (*H. sapiens*: synaphin 1)
CRY2, PHLL2	Cry2	Cry2	Cryptochrome 2 (photolyase-like)
CRYAA, CRYA1	Cryaa, Crya1, Acry-1	Cryaa, Crya1, lop18, Acry-1	Crystallin, alpha A (*M. musculus*: lens opacity 18)
CRYAB, CRYA2, CTPP2	Cryab, AACRYA	Cryab, Crya2	Crystallin, alpha B (*H. sapiens*: heat-shock 20 kD like-protein)
CRYBA1, CRYB1	Cryba1	Cryba1, Cryb	Crystallin, beta A1
CRYBA2	Cryba2	Cryba2	Crystallin, beta A2
CRYBA4	Cryba4	Cryba4	Crystallin, beta A4
CRYBB1	Crybb1, CRYB1	Crybb1, BB1CRY	Crystallin beta B1
CRYBB2, CCA2, CRYB2, CRYB2A	Crybb2	Crybb2, Aey2, Phil, Cryb-2	Crystallin, beta B2 (*M. musculus*: Philly cataract)
CRYBB3, CRYB3	Crybb3	Crybb3	Crystallin, beta B3
CRYGB, CRYG2	Crygb, Len, Cryg2	Crygb, Nop, Cryg-3, DGcry-3	Crystallin, gamma B (*H. sapiens*: crystallin, gamma 1-2; *M. musculus*: nuclear opacity)
CRYGS, CRYG8	Crygs	Crygs, Opj, rncat	Crystallin, gamma S (*H. sapiens*: crystallin, gamma 8; *M. musculus*: recessive nuclear cataract, opacity due to poor secondary fiber cell junction)
CTBP1	Ctbp1	Ctbp1	C-terminal binding protein 1
CUL4B	Cul4b	Cul4b	Cullin 4B

Appendix 2. Gene Symbols and Names for *Homo sapiens*, *Rattus norvegicus*, and *Mus musculus*

Arranged alphabetically by *R. norvegicus* gene symbol. The correct gene symbol is underlined where alternate gene symbols are given. Gene names are from *H. sapiens* unless otherwise noted. Alternate descriptive names are provided in brackets following the gene name.

Homo sapiens	*Rattus norvegicus*	*Mus musculus*	Gene Name
DDX6, P54, RCK, HLR2	Ddx6, Rck, Hlr2	Ddx6, RCK, P54	DDX6 DEAD/H (Asp-Glu-Ala-Asp/His) box polypeptide 6 (RNA helicase, 54kDa)
ENO1, NNE, PPH, MPB1, ENO1L1	Eno1	Eno1	Enolase 1, (alpha) (*H. sapiens*: tau-crystallin, non-neural enolase, phosphopyruvate hydratase, MYC promoter-binding protein 1, 2-phospho-D-glycerate hydro-lyase; *M. musculus*: alpha-enolase, 2-phospho-D-glycerate hydrolase)
ENO2, NSE	Eno2, NEN3	Eno2, NSE	Enolase 2, (gamma, neuronal) (*H. sapiens*: gamma enolase, neural enolase, neurone-specific enolase, 2-phospho-D-glycerate hydrolyase)
FDPS, FPS	Fdps	Fdps, Fdpsl1	Farnesyl diphosphate synthase (farnesyl pyrophosphate synthetase, dimethylallyltranstransferase, geranyltranstransferase) (*R. norvegicus*: testis-specific farnesyl pyrophosphate synthetase)
FKBP2, PPIase, FKBP-13	Fkbp2	Fkbp2, FKBP13	FK506 binding protein 2, 13kDa (*H. sapiens*: proline isomerase, rapamycin-binding protein, FK506 binding protein 2 (13kD), peptidyl-prolyl cis-trans isomerase
GAPD, G3PD, GAPDH	Gapd, Gapdh	Gapd, Gapdh	Glyceraldehyde-3-phosphate dehydrogenase
GLB1	Glb1	Glb1, Bge, Bgl, Bgs, Bgt, Bgl-e, Bgl-s, Bgl-t	Galactosidase, beta 1 (*M. musculus*: beta-galactosidase temporal, beta-galactosidase electrophoretic, beta-galactosidase systemic regulator)
GNAI2, GIP, GNAI2B	Gnai2	Gnai2 Gia	Guanine nucleotide binding protein (G protein), alpha inhibiting activity polypeptide 2
GNAT1, GBT1, GNATR	Gnat1	Gnat1, Gnat-1, Trα	Guanine nucleotide binding protein (G protein), alpha transducing activity polypeptide 1 (*H. sapiens*: transducin alpha-1 chain, rod-specific transducin; *M. musculus*: transducin)
GPR19	Gpr19	Gpr19	G protein-coupled receptor 19
GSG1	Gsg1	Gsg1	Likely orthologue of mouse germ cell-specific gene 1
HNRPC, C1, C2, SNRPC, hnRNPC	Hnrpc	Hnrpc, Hnrnpc, Hnrpc1, Hnrpc2	Heterogeneous nuclear ribonucleoprotein C (C1/C2)

Appendix 2. Gene Symbols and Names for *Homo sapiens*, *Rattus norvegicus*, and *Mus musculus*

Arranged alphabetically by *R. norvegicus* gene symbol. The correct gene symbol is underlined where alternate gene symbols are given. Gene names are from *H. sapiens* unless otherwise noted. Alternate descriptive names are provided in brackets following the gene name.

Homo sapiens	*Rattus norvegicus*	*Mus musculus*	Gene Name
HNRPU, SAF-A, U21.1, hnRNPU	Hnrpu	Hnrpu, SAFA, hnRNPU	Heterogeneous nuclear ribonucleoprotein U (scaffold attachment factor A) (*H. sapiens*: p120 nuclear protein, scaffold attachment factor A; *M. musculus*: nuclear matrix protein sp120, scaffold attachment factor A)
HSPCA, HSPN, LAP2, HSP86, HSPC1, HSP90A, HSPCAL1	Hspca	Hsp86-1, hsp4, Hsp90	Heat shock 90kDa protein 1, alpha (*M. musculus*: heat shock protein, 86 kDa 1)
HSPC121, B-IND1	Hspc121	Hspc121, B-ind1	Butyrate-induced transcript 1
IL6ST, CD130, GP130	Il6st	Il6st, CD130, gp130	Interleukin 6 signal transducer (gp130, oncostatin M receptor)
ITPR2, IP3R2	Itpr2	Itpr2, Ip3r2	Inositol 1,4,5-triphosphate receptor, type 2
LGALS1, GBP	Lgals1	Lgals1, L14, Galbp	Lectin, galactoside-binding, soluble, 1 (galectin 1)
LZTR1, TCFL2	Lztr1	Lztr1, TCFL2	Leucine-zipper-like transcriptional regulator, 1
MAPT, tau, MSTD, PPND, DDPAC, MAPTL, MTBT1, MTBT2, FTDP-17	Mapt, pTau, Mtapt	Mapt, Tau, Mtapt	Microtubule-associated protein tau (*H. sapiens*: G protein beta1/gamma2 subunit-interacting factor 1)
MEL, RAB8	Mel, Rab8	Mel	Mel transforming oncogene (derived from cell line NK14)-RAB8 homolog (*H. sapiens*: ras-associated protein RAB8)
n/a	Mipp65	n/a	MIPP65 protein
MTCO2, COII	Mtco2	Mtco2	Cytochrome c oxidase II
MTCYB	Mtcyb	Mtcyb	Cytochrome b
NDUFA5, B13, NUFM, UQOR13	Ndufa5, NADHUO	n/a	NADH dehydrogenase (ubiquinone) 1 alpha subcomplex, 5, 13kDa (*H. sapiens*: Complex I-13KD-B, type I dehydrogenase, ubiquinone reductase)

Appendix 2. Gene Symbols and Names for *Homo sapiens*, *Rattus norvegicus*, and *Mus musculus*

Arranged alphabetically by *R. norvegicus* gene symbol. The correct gene symbol is underlined where alternate gene symbols are given. Gene names are from *H. sapiens* unless otherwise noted. Alternate descriptive names are provided in brackets following the gene name.

Homo sapiens	*Rattus norvegicus*	*Mus musculus*	Gene Name
NFKBIA, IKBA, MAD-3, NFKBI	Nfkbia, RL/IF-1	Nfkbia, Nfkbi	Nuclear factor of kappa light polypeptide gene enhancer in B-cells inhibitor, alpha
PAK1, PAKα	Pak1	Pak1	p21/Cdc42/Rac1-activated kinase 1 (STE20 homolog, yeast)
PEA15, PED, MAT1	Pea15	Pea15, Mat1, Pkcs15	Phosphoprotein enriched in astrocytes 15 (*H. sapiens*: homologue of mouse MAT-1 oncogene; *M. musculus*: mammary transforming gene 1)
PKM2, PK3, PKM, OIP3, THBP1	Pkm2, Pk3, PKM12	Pk3, Pk-2	Pyruvate kinase, muscle [*H. sapiens*: Pyruvate kinase-3, thyroid hormone-binding protein, cytosolic (p58); *M. musculus*: pyruvate kinase 3; *R. norvegicus*: pyruvate kinase 3]
PLD3, HU-K4	Pld3	Pld3, Sam-9	Likely orthologue of mouse phospholipase D3 (*H. sapiens*: similar to vaccinia virus *Hin*dIII K4L ORF)
POLR2H, RPB8, RPB17	Polr2h	Polr2h	Polymerase (RNA) II (DNA directed) polypeptide H
PP, SID6-8061	Pp	Pyp	Pyrophosphatase (inorganic)
PRPH, NEF4	Prph, Perf	Prph1	Peripherin [*H. sapiens*: neurofilament 4 (57kD)]
PSMB1, HC5, PSC5, PMSB1	Psmb1	Psmb1, Lmpc5	Proteasome (prosome, macropain) subunit, beta type, 1 (*H. sapiens*: macropain subunit C5, proteasome gamma chain, proteasome component C5, multicatalytic endopeptidase complex subunit C5)
RALA, RAL	Rala	Rala	v-ral simian leukemia viral oncogene homolog A (ras related) (*H. sapiens*: ras-like protein)
RDS, RP7, PRPH, PRPH2	Rds, Prph2, RSRDS	Prph2, Rd2, Rds	Retinal degeneration, slow (retinitis pigmentosa 7) [*H. sapiens*: peripherin 2 (homolog of mouse peripherin, photoreceptor type)]
RHO, RP4, OPN2	Rho	Rho, Ops, RP4, Opn2	Rhodopsin (opsin 2, rod pigment) (retinitis pigmentosa 4, autosomal dominant) (*M. musculus*: L opsin, opsin 2, red Opsin, rod Opsin, long wavelength sensitive opsin)
RNR(#)	Rnr(#)	Rnr(#)	RNA, ribosomal 1-5

Appendix 2. Gene Symbols and Names for *Homo sapiens*, *Rattus norvegicus*, and *Mus musculus*

Arranged alphabetically by *R. norvegicus* gene symbol. The correct gene symbol is underlined where alternate gene symbols are given. Gene names are from *H. sapiens* unless otherwise noted. Alternate descriptive names are provided in brackets following the gene name.

Homo sapiens	*Rattus norvegicus*	*Mus musculus*	Gene Name
RPL7A, TRUP, SURF3	Rpl7a	Rpl7a, Surf3	Ribosomal protein L7a (*H. sapiens*: surfeit 3, PLA-X polypeptide, thyroid hormone receptor uncoupling protein; *M. musculus*: surfeit 3)
RPL10A, NEDD6, Csa-19	Rpl10a	Rpl10a, Nedd6	Ribosomal protein L10a
RPL19	Rpl19	Rpl19	Ribosomal protein L19
RPL34	Rpl34	Rpl34	Ribosomal protein L34
RPL41	Rpl41	Rpl41	Ribosomal protein L41
RPLP1, P1, RPP1	Rplp1	Rplp1, Arpp1	Ribosomal protein, large, P1 (*H. sapiens*: acidic ribosomal phosphoprotein P1; *M. musculus*: acidic ribosomal phosphoprotein P1)
RPS3	Rps3	Rps3	Ribosomal protein S3
FLJ20591, RRP41	Rrp41	Rrp41	Exosome component Rrp41
RTN3, NSPL2	Rtn3	Rtn3	Reticulon 3
SAG	Sag, SAGMR, SANTI	Sag, Irbp	S-antigen; retina and pineal gland (arrestin)
SCHIP1	Schip1	Schip1, Nf2ip	Schwannomin interacting protein 1 (*M. musculus*: neurofibromatosis 2 interacting protein)
SEC3	Sec3	Sec3	Sec3-like (*H. sapiens*: homologue of yeast exocyst protein Sec3p)
SFRS5, HRS, SRP40	Sfrs5, HRS, SRp40	Sfrs5, SRp40, HRS	Splicing factor, arginine/serine-rich 5
n/a	Sharpin, Conneck1	n/a	*R. norvegicus*: Shank-interacting protein
n/a	Sip30	n/a	*R. norvegicus*: SNAP25 interacting protein 30

Appendix 2. Gene Symbols and Names for *Homo sapiens*, *Rattus norvegicus*, and *Mus musculus*

Arranged alphabetically by *R. norvegicus* gene symbol. The correct gene symbol is underlined where alternate gene symbols are given. Gene names are from *H. sapiens* unless otherwise noted. Alternate descriptive names are provided in brackets following the gene name.

Homo sapiens	*Rattus norvegicus*	*Mus musculus*	Gene Name
STMN1, Lag, SMN, OP18, PP17, PP19, PR22, LAP18	Stmn1, Lap18	Lag, 19K, p18, p19, op18, Lap18	Stathmin 1/oncoprotein 18 (*H. sapiens*: prosolin, stathmin, metablastin, oncoprotein 18, phosphoprotein 19, leukemia-associated phosphoprotein p18; *M. musculus*: leukemia-associated gene, prosolin, stathmin; *R. norvegicus*: leukemia-associated gene, Leukemia-associated cytosolic phosphoprotein)
TCEB2, SIII	Tceb2	n/a	Transcription elongation factor B (SIII), polypeptide 2 (18kDa, elongin B)
TCFL4, MLX, MAD7, MXD7	Tcfl4	Tcfl4, Mlx	Transcription factor-like 4 (*H. sapiens*: MAX-like bHLHZIP protein; *M. musculus*: MAX-like bHLHZIP protein)
TLN1, TLN	Tln	TLN1	Talin 1
TLOC1, HTP1, Dtrp1, SEC62	Tloc1	Tloc1	Translocation protein 1 (*H. sapiens*: Dtrp1 protein, 0homologue of yeast membrane protein SEC62)
TUBG1	Tubg	Tubg	Tubulin, gamma 1
UBB	Ubb	Ubb, Ubb2	Ubiquitin B (*H. sapiens*: polyubiquitin B)
UNC119, HRG4	Unc119, RRG4	Unc119h, HRG4, UNC119	Unc-119 homolog (C. elegans) (*H. sapiens*: retinal gene 4; *R. norvegicus*: retinal gene 4)
UPF3B	Upf3b	Upf3b	Similar to yeast Upf3, variant B
VAPB, VAPC	Vapb	Vapb, VAP33b, Vamp33b	VAMP (vesicle-associated membrane protein)-associated protein B and C (*M. musculus*: VAMP-associated protein 33b)
YWHAB, HS1, KCIP-1, 14-3-3β	Ywhab	Ywhab	Tyrosine 3-monooxygenase/tryptophan 5-monooxygenase activation protein, beta polypeptide (*H. sapiens*: Protein 1054, 14-3-3 protein beta/alpha, Protein kinase C inhibitor protein-1; *M. musculus*: 14-3-3 beta; *R. norvegicus*: 14-3-3 beta)
YWHAG, 14-3-3γ	Ywhag	Ywhag	Tyrosine 3-monooxygenase/tryptophan 5-monooxygenase activation protein, gamma polypeptide (*H. sapiens*: 14-3-3 gamma; *M.musculus*: 14-3-3 gamma; *R. norvegicus*: 14-3-3 gamma)

Appendix 3. *Homo sapiens* Gene Expression in Normal Tissues as Determined by Bioinformatics

Source: Unigene database (www.ncbi.nih.nlm.gov/UniGene, 04/10/02). The following genes were not detected and are omitted: AF272892, Cntf, Mipp65, MtCo2, Mtcyb, Rnr(#), Sharpin, and Sip30. Tissues are arranged alphabetically by major organ system, and genes are organized alphabetically by symbol. Descriptive gene names are found in **Appendix 2.**

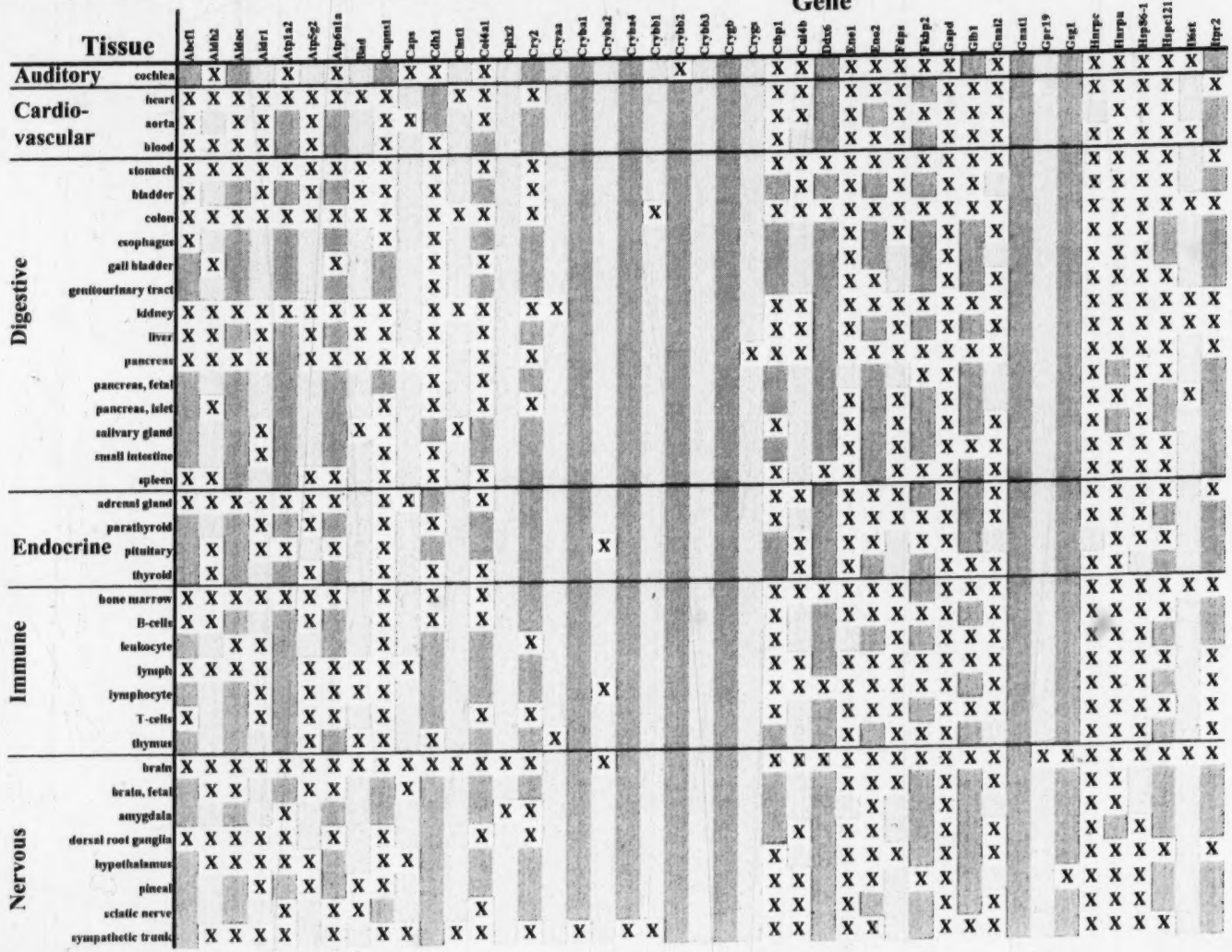

Appendix 3. *Homo sapiens* Gene Expression in Normal Tissues as Determined by Bioinformatics

Source: Unigene database (www.ncbi.nih.nlm.gov/UniGene, 04/10/02). The following genes were not detected and are omitted: AF272892, Cntf, Mipp65, MtCo2, Mtcyb, Rnr(#), Sharpin, and Sip30. Tissues are arranged alphabetically by major organ system, and genes are organized alphabetically by symbol. Descriptive gene names are found in **Appendix 2.**

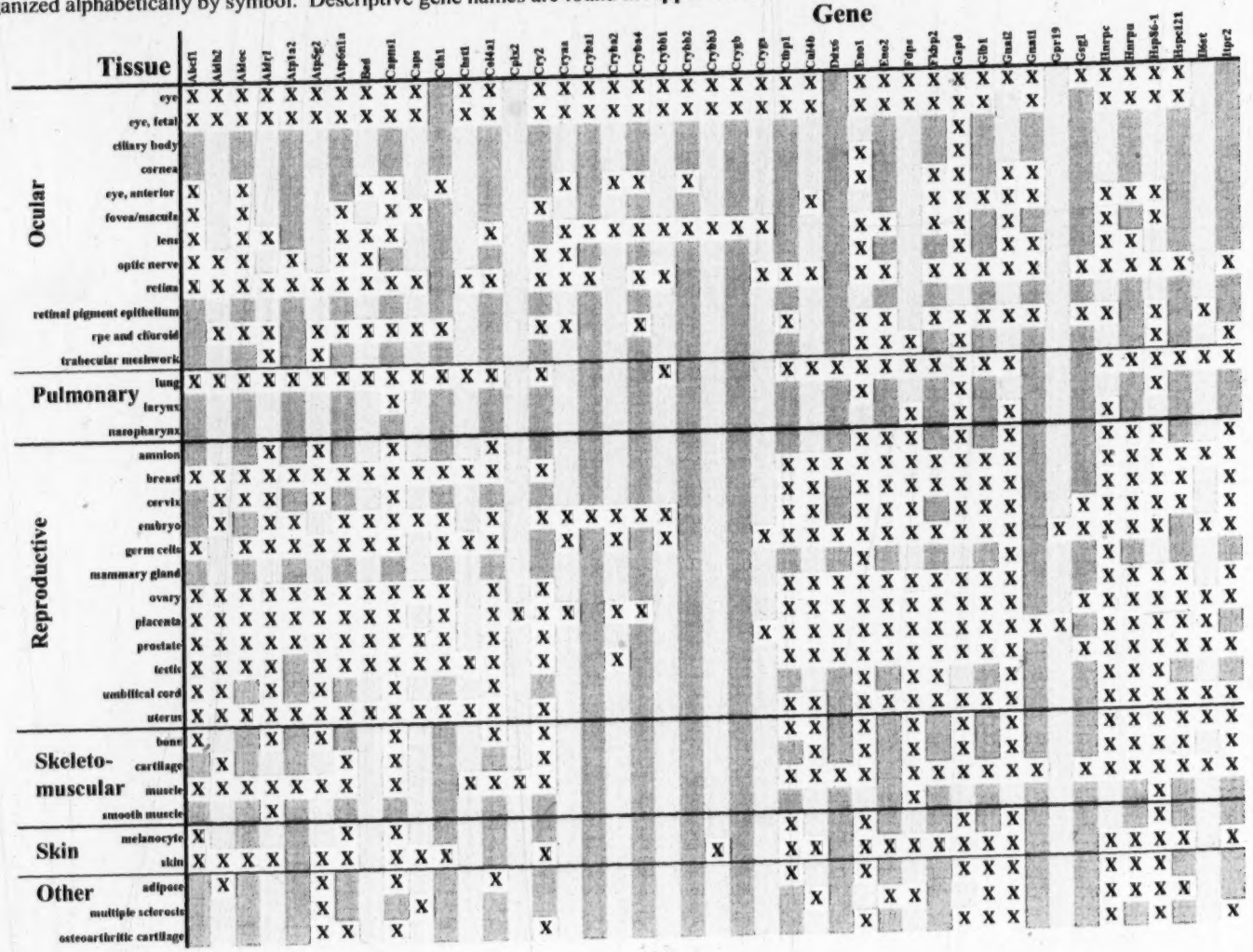

Appendix 3. *Homo sapiens* Gene Expression in Normal Tissues as Determined by Bioinformatics

Source: Unigene database (www.ncbi.nih.nlm.gov/UniGene, 04/10/02). The following genes were not detected and are omitted: AF272892, Cntf, Mipp65, MtCo2, Mtcyb, Rnr(#), Sharpin, and Sip30. Tissues are arranged alphabetically by major organ system, and genes are organized alphabetically.

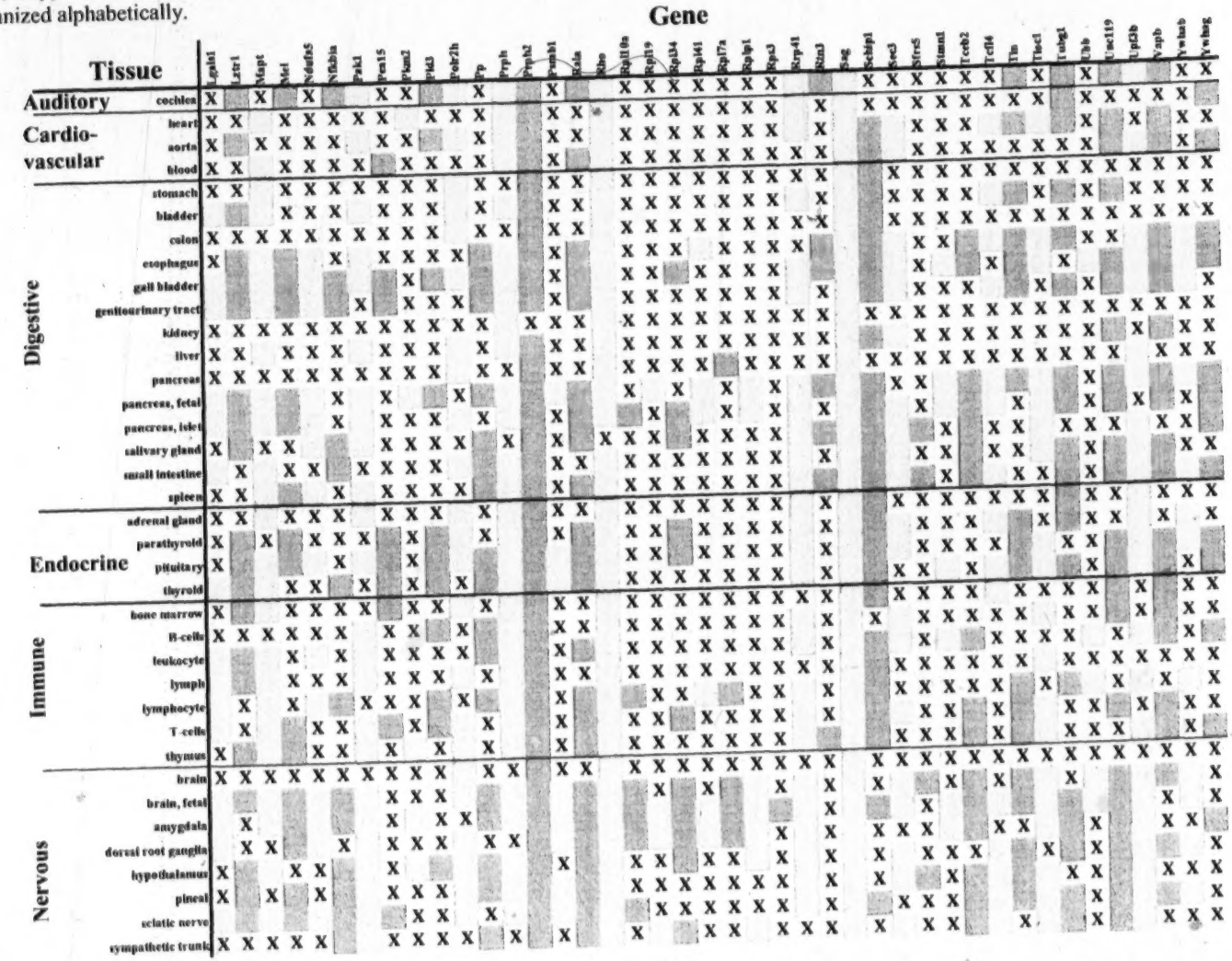

Appendix 3. *Homo sapiens* Gene Expression in Normal Tissues as Determined by Bioinformatics

Source: Unigene database (www.ncbi.nih.nlm.gov/UniGene, 04/10/02). The following genes were not detected and are omitted: AF272892, Cntf, Mipp65, MtCo2, Mtcyb, Rnr(#), Sharpin, and Sip30. Tissues are arranged alphabetically by major organ system, and genes are organized alphabetically by symbol. Descriptive gene names are found in **Appendix 2.**

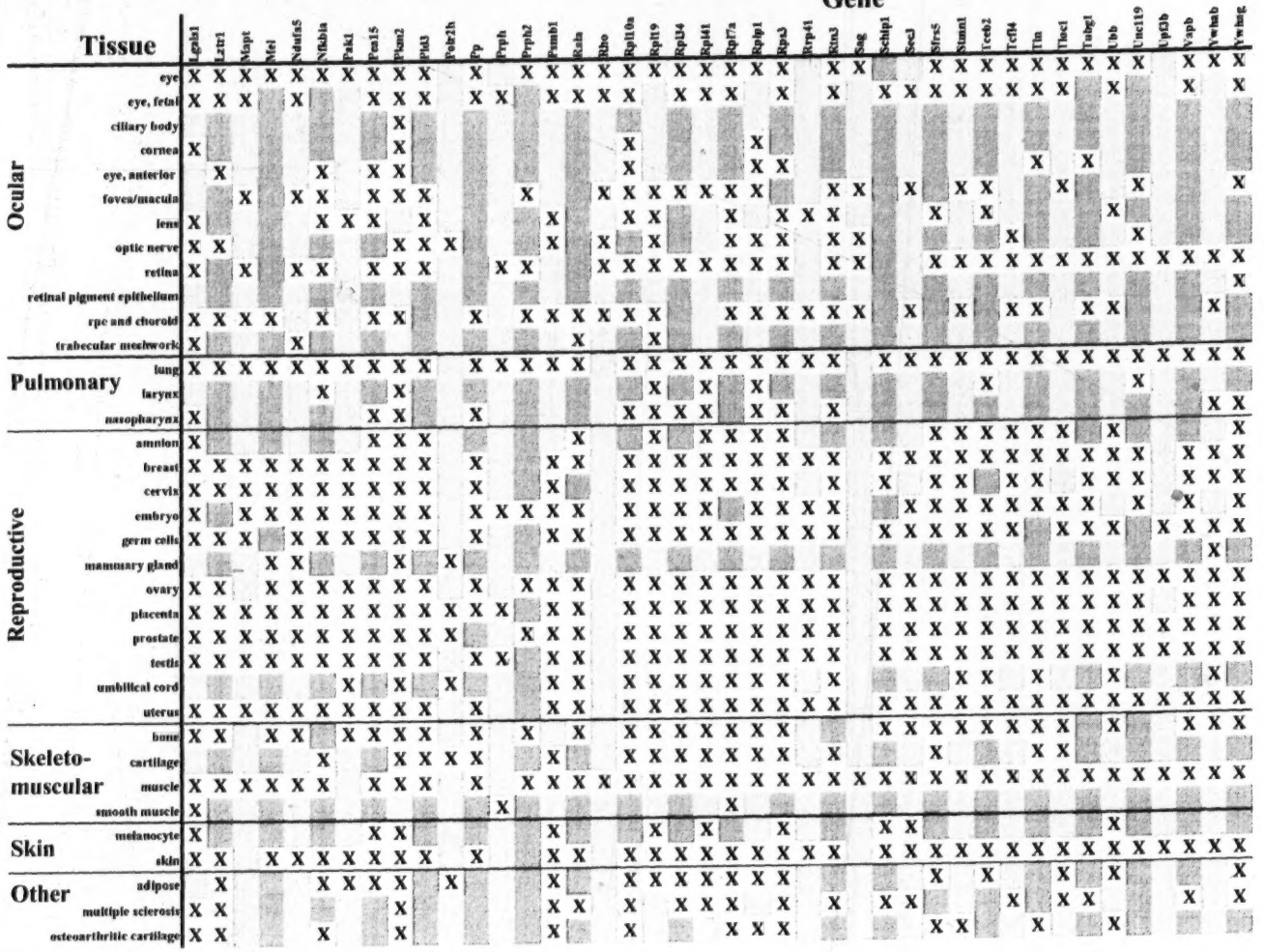

Appendix 4. *Homo sapiens* Gene Expression in Representative Cancerous Tissues as Determined by Bioinformatics, with Accompanying *In Silico* Northern Analysis of Various Genes

Table IIII-1. *Homo sapiens* Gene Expression in Cancerous Tissues

Source: Unigene Database (www.ncbi.hih.nlm.gov/UniGene, 04/10/02). Genes without detected expression are omitted for clarity.

Gene	Burkitt lymphoma B-cells	colon adenocarcinoma	melanoma (MeWo cell line)	T-cells from T-cell leukemia	Tumour, bladder	Tumour, brain	Tumour, kidney	Tumour, lung	Tumour, ovary	Tumour, prostate	Tumour, uterus
	Tissue										
Abcf1					X		X	X			X
Aldh2	X	X			X	X		X		X	
Aldoc					X	X	X				
Aldr1		X		X	X						
Atp5g2		X									X
Atp6n1a		X					X	X	X	X	X
Bad		X									
Capns1		X			X	X	X	X		X	
Caps		X					X				
Cdh1		X			X			X			X
Col4a1		X			X			X		X	X
Cry2		X				X	X	X			
Ctbp1		X						X		X	
Cul4b										X	X
Ddx6										X	X
Eno1	X	X	X	X	X	X	X	X	X	X	X
Eno2				X		X		X		X	X
Fdps		X		X	X			X			X
Fkbp2								X			
Gapd	X			X	X	X	X	X		X	X
Glb1	X	X	X	X					X		
Gnai2	X	X			X		X	X	X	X	X
Gpr19										X	
Hnrpc		X			X		X	X		X	X
Hnrpu		X	X	X	X		X	X			X
Hsp86-1			X		X	X	X	X		X	X
Hspc121	X									X	X
Itpr2	X										X
Lgals1											X
Lztr1			X		X	X					X
Mapt										X	
Mel	X	X						X	X		X
Ndufa5										X	X

Gene	Burkitt lymphoma B-cells	colon adenocarcinoma	melanoma (MeWo cell line)	T-cells from T-cell leukemia	Tumour, bladder	Tumour, brain	Tumour, kidney	Tumour, lung	Tumour, ovary	Tumour, prostate	Tumour, uterus
	Tissue										
Nfkbia					X			X		X	
Pak1					X		X	X			
Pea15		X			X	X		X		X	
Pkm2	X	X	X	X	X	X	X	X	X	X	
Pld3	X	X						X		X	X
Polr2h							X				X
Pp						X					X
Prph						X					
Psmb1									X	X	X
Rala		X			X					X	
Rpl10a						X				X	X
Rpl19	X	X			X		X	X		X	X
Rpl34					X					X	X
Rpl41					X			X		X	X
Rpl7a		X			X		X	X		X	X
Rplp1			X							X	X
Rps3	X	X	X	X	X	X		X		X	
Rrp41		X									
Rtn3		X		X	X		X	X			
Sec3					X					X	
Sfrs5		X			X		X	X		X	X
Sip30				X	X						
Stmnl	X	X	X	X		X		X		X	X
Tcfl4		X									
Tln		X			X	X		X		X	X
Tloc1			X							X	X
Tubg1		X								X	X
Ubb		X			X	X		X		X	X
Unc119		X		X							
Upf3b										X	
Ywhab			X							X	X
Ywhag		X			X		X				X

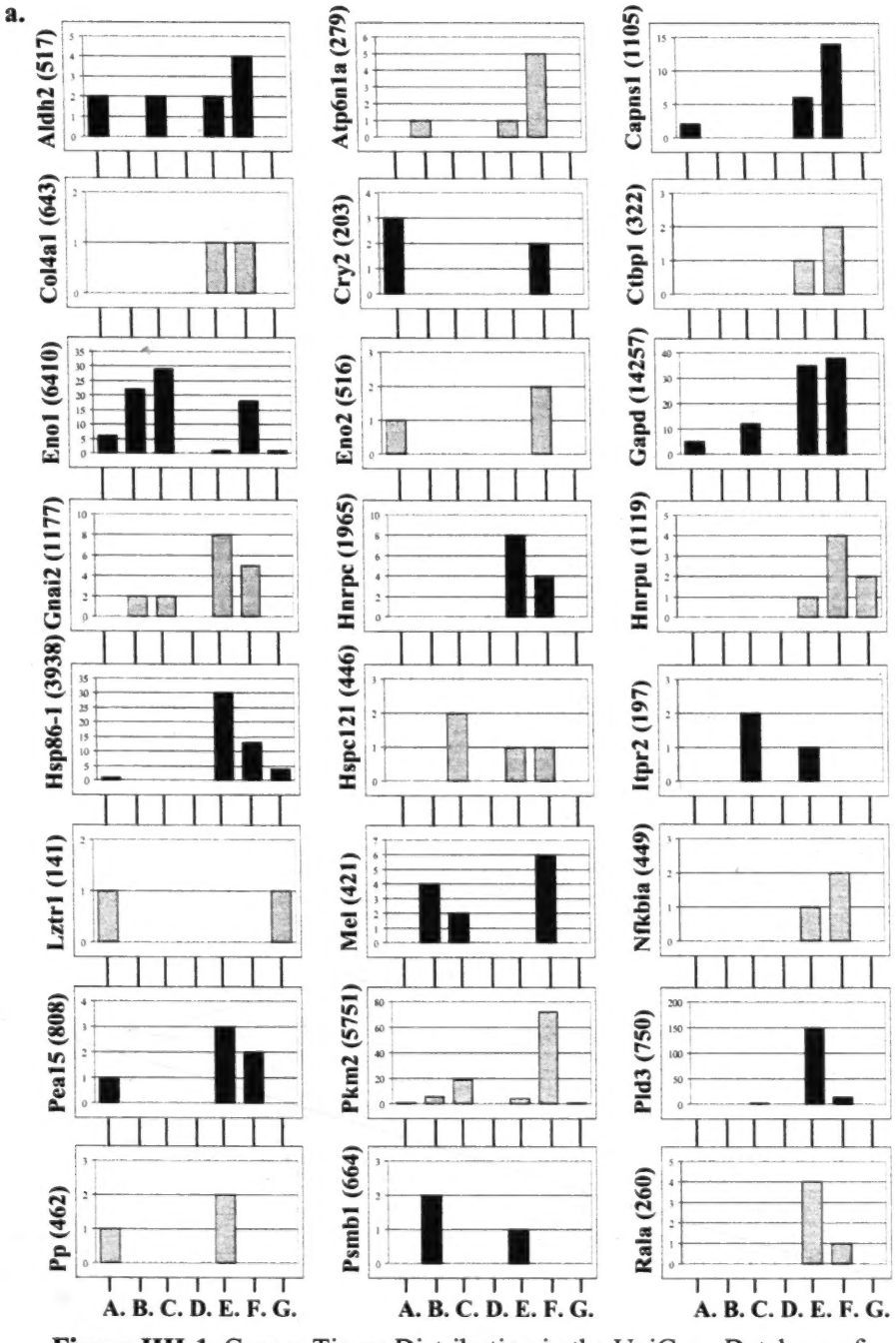

Figure IIII-1. Cancer Tissue Distribution in the UniGene Database of Human Sequences.

Determined by the occurrence of corresponding expressed sequence tags (ESTs) in libraries derived from the tissue.

Source: Unigene Database (www.ncbi.hih.nlm.gov/UniGene, 04/10/02).

Genes without detected expression, or that occur in only one tissue, are omitted for clarity.

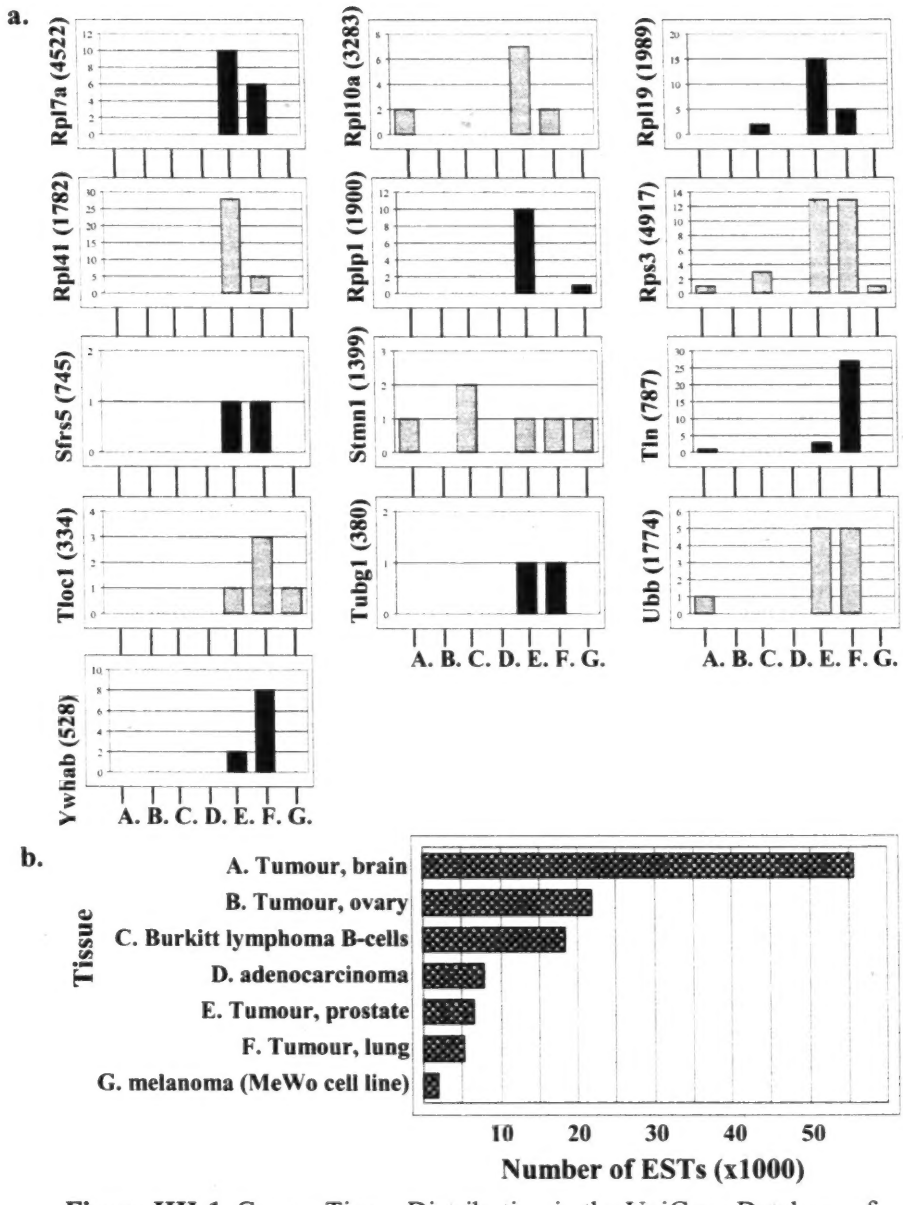

Figure IIII-1. Cancer Tissue Distribution in the UniGene Database of Human Sequences.

Determined by the occurrence of corresponding expressed sequence tags (ESTs) in libraries derived from the tissue.

Source: Unigene Database (www.ncbi.hih.nlm.gov/UniGene/, 04/10/02).

Genes without detected expression, or that occur in only one tissue, are omitted for clarity.

a. EST occurrence for each indicated gene with total Unigene ESTs for that gene given in brackets. A. Tumour, brain; B. Tumour, ovary; C. Burkitt lymphoma B-cells; D. adenocarcinoma; E. Tumour, prostate; F. Tumour, lung; G. melanoma (MeWo cell line).

b. Total number of Unigene ESTs for each tissue.

Appendix 5. Comparison of Mouse and Rat Protein Sequence Identity by Alignment of Sequence

Seven mouse and rat crystallin sequences were aligned using Pair-wise Basic Local Alignment Search Tool (Tatusova and Madden, 1999). The seven proteins showed an average identity of 96%. When conservative amino acid changes (positives) are considered, the average similarity of the seven proteins is 97%.

In the following alignments, the top sequence is mouse, the bottom sequence is rat, the middle sequence is identical or positive (+) sequence of the two proteins. A hyphen (-) indicates that the best alignment between the two proteins occurs if a gap is placed at the position of the hyphen. The "Expect" value is the likelihood that the alignment of the two sequences could have arisen solely by chance. The score is a statistical measurement of the similarity of the two sequences.

Alignment of Mouse (Mm) αA-Crystallin Sequence [Accession (Acc.): XP_128456] with Rat (Rn) αA-Crystallin Sequence (Acc.: NP_036666)

Score = 340 bits (873)
Expect = $8x10^{-93}$

Identities = 173/196 (88%)
Positives = 173/196 (88%)
Gaps = 23/196 (11%)

```
Mm    1 MDVTIQHPWFKRALGPFYPSRLFDQFFGEGLFEYDLLPFLSSTISPYYRQSLFRTVLDSG 60
        MDVTIQHPWFKRALGPFYPSRLFDQFFGEGLFEYDLLPFLSSTISPYYRQSLFRTVLDSG
Rn    1 MDVTIQHPWFKRALGPFYPSRLFDQFFGEGLFEYDLLPFLSSTISPYYRQSLFRTVLDSG 60

Mm   61 ISELMTHMWFVMHQPHAGNPKNNPVKVRSDRDKFVIFLDVKHFSPEDLTVKVLEDFVEIH 120
        ISE                        VRSDRDKFVIFLDVKHFSPEDLTVKVLEDFVEIH
Rn   61 ISE------------------------VRSDRDKFVIFLDVKHFSPEDLTVKVLEDFVEIH 97

Mm  121 GKHNERQDDHGYISREFHRRYRLPSNVDQSALSCSLSADGMLTFSGPKVQSGLDAGHSER 180
        GKHNERQDDHGYISREFHRRYRLPSNVDQSALSCSLSADGMLTFSGPKVQSGLDAGHSER
Rn   98 GKHNERQDDHGYISREFHRRYRLPSNVDQSALSCSLSADGMLTFSGPKVQSGLDAGHSER 157

Mm  181 AIPVSREEKPSSAPSS 196
        AIPVSREEKPSSAPSS
Rn  158 AIPVSREEKPSSAPSS 173
```

Alignment of Mouse (Mm) αB-Crystallin Sequence (Acc.: NP_034094) with Rat (Rn) αB-Crystallin Sequence (Acc.: NP_037067)

Score = 340 bits (873)
Expect = $2x10^{-92}$

Identities = 163/165 (98%)
Positives = 164/165 (98%)

```
Mm    1 MDIAIHHPWIRRPFFPFHSPSRLFDQFFGEHLLESDLFSTATSLSPFYLRPPSFLRAPSW 60
        MDIAIHHPWIRRPFFPFHSPSRLFDQFFGEHLLESDLFSTATSLSPFYLRPPSFLRAPSW
Rn    1 MDIAIHHPWIRRPFFPFHSPSRLFDQFFGEHLLESDLFSTATSLSPFYLRPPSFLRAPSW 60

Mm   61 IDTGLSEMRLEKDRFSVNLDVKHFSPEELKVKVLGDVIEVHGKHEERQDEHGFISREFHR 120
        IDTGLSEMR+EKDRFSVNLDVKHFSPEELKVKVLGDVIEVHGKHEERQDEHGFISREFHR
Rn   61 IDTGLSEMRMEKDRFSVNLDVKHFSPEELKVKVLGDVIEVHGKHEERQDEHGFISREFHR 120

Mm  121 KYRIPADVDPLTITSSLSSDGVLTVNGPRKQVSGPERTIPITREE 165
        KYRIPADVDPLTITSSLSSDGVLTVNGPRKQ SGPERTIPITREE
Rn  121 KYRIPADVDPLTITSSLSSDGVLTVNGPRKQASGPERTIPITREE 165
```

Alignment of Mouse (Mm) βA4-Crystallin Sequence (Acc.: NP_067326) with Rat (Rn) βA4-Crystallin Sequence (Acc.: NP_113877)

Score = 421 bits (1081)
Expect = 10^{-117}

Identities = 192/196 (97%)
Positives = 196/196 (99%)

```
Mm    1 MTLQCTKSAGHWRMVVWDEEGFQGRRHEFTAECPSVLELGFETVRSLKVLSGAWVGFEHA 60
        MTLQCTKSAGHWR+VVWDEEGFQGRRHEFTAECPSVL+LGFETVRSLKVLSGAWVGFEHA
Rn    1 MTLQCTKSAGHWRVVVWDEEGFQGRRHEFTAECPSVLDLGFETVRSLKVLSGAWVGFEHA 60

Mm   61 GFQGQQYVLERGDYPGWDAWGGNTAYPAERLTSFRPVACANHRDSRLTIFEQENFLGRKG 120
        GFQGQQYVLERGDYPGWDAWGGNTAYPAERLTSFRPVACANHRDSRLTIFEQENFLGRKG
Rn   61 GFQGQQYVLERGDYPGWDAWGGNTAYPAERLTSFRPVACANHRDSRLTIFEQENFLGRKG 120

Mm  121 ELNDDYPSLQAMGWDGTEVGSFHVQSGAWVCSQFPGYRGFQYILESDHHSGDYKHFREWG 180
        EL+DDYPSLQAMGWDGTEVGSFHVQSGAWVCSQFPGYRGFQY+LESDHHSGDYKHFREWG
Rn  121 ELSDDYPSLQAMGWDGTEVGSFHVQSGAWVCSQFPGYRGFQYVLESDHHSGDYKHFREWG 180

Mm  181 SHAHTFQVQSVRRIQQ 196
        SHAHTFQVQSVRRIQQ
Rn  181 SHAHTFQVQSVRRIQQ 196
```

Alignment of Mouse (Mm) βB1-Crystallin Sequence (Acc.: NP_076184) with Rat (Rn) βB1-Crystallin Sequence (Acc.: NP_037068)

Score = 510 bits (1314)
Expect = 10^{-143}

Identities = 240/250 (96%)
Positives = 244/250 (97%)
Gaps = 1/250 (0%)

```
Mm   1 MSQAAKASATTAVNPGPDGKGKGAPSTGPAPAPGPTPVPASVPRPAAKVGDLPPGSYRLI 60
       MSQ AKA+ATTAVNPG  GKGKG PSTG APAPGPTPVPASVPRPAAKVG+LPPGSYRL+
Rn   1 MSQVAKAAATTAVNPGY-GKGKGTPSTGTAPAPGPTPVPASVPRPAAKVGELPPGSYRLV 59

Mm  61 VFEQENFQGRRVEFSGECLNLGDRGFDRVRSLIVVSGPWVAFEQSAFRGEMFVLEKGEYP 120
       VFEQENFQGRRVEFSGECLNLGDRGFDRVRSLIV+SGPWVAFEQSAFRGEMFVLEKGEYP
Mm  60 VFEQENFQGRRVEFSGECLNLGDRGFDRVRSLIVLSGPWVAFEQSAFRGEMFVLEKGEYP 119


Mm 121 RWDTWTSSYRSDRLMSFRPIRMDSQEHKICLFEGANFKGNTMEIQEDDVPSLWVYGFCDR 180
       RWDTWTSSYRSDRLMSFRPIRMDSQEHKICLFEGANFKGNTMEIQEDDVPSLWVYGFCDR
Rn 120 RWDTWTSSYRSDRLMSFRPIRMDSQEHKICLFEGANFKGNTMEIQEDDVPSLWVYGFCDR 179

Mm 181 VGSITVSGGTWVGYQYPGYRGYQYLLEPGDFRHWNEWGAFQPQMQAVRRLRDRQWHQEGC 240
       VGSITVS GTWVGYQYPGYRGYQYLLEPGDFRHWNEWGAFQPQMQAVRRLRDRQWHQEGC
Rn 180 VGSITVSSGTWVGYQYPGYRGYQYLLEPGDFRHWNEWGAFQPQMQAVRRLRDRQWHQEGC 239

Mm 241 FPVLTAEPPK 250
       FPVLTAEPPK
Rn 240 FPVLTAEPPK 249
```

Alignment of Mouse (Mm) βB2-Crystallin Sequence (Acc.: NP_031799) with Rat (Rn) βB2-Crystallin Sequence (Acc.: NP_037069)

Score = 436 bits (1122)
Expect = 10^{-121}

Identities = 205/205 (100%)
Positives = 205/205 (100%)

```
Mm   1 MASDHQTQAGKPQPLNPKIIIFEQENFQGHSHELSGPCPNLKETGMEKAGSVLVQAGPWV 60
       MASDHQTQAGKPQPLNPKIIIFEQENFQGHSHELSGPCPNLKETGMEKAGSVLVQAGPWV
Rn   1 MASDHQTQAGKPQPLNPKIIIFEQENFQGHSHELSGPCPNLKETGMEKAGSVLVQAGPWV 60

Mm  61 GYEQANCKGEQFVFEKGEYPRWDSWTSSRRTDSLSSLRPIKVDSQEHKIILYENPNFTGK 120
       GYEQANCKGEQFVFEKGEYPRWDSWTSSRRTDSLSSLRPIKVDSQEHKIILYENPNFTGK
Rn  61 GYEQANCKGEQFVFEKGEYPRWDSWTSSRRTDSLSSLRPIKVDSQEHKIILYENPNFTGK 120

Mm 121 KMEIVDDDVPSFHAHGYQEKVSSVRVQSGTWVGYQYPGYRGLQYLLEKGDYKDNSDFGAP 180
       KMEIVDDDVPSFHAHGYQEKVSSVRVQSGTWVGYQYPGYRGLQYLLEKGDYKDNSDFGAP
Rn 121 KMEIVDDDVPSFHAHGYQEKVSSVRVQSGTWVGYQYPGYRGLQYLLEKGDYKDNSDFGAP 180

Mm 181 HPQVQSVRRIRDMQWHQRGAFHPSS 205
       HPQVQSVRRIRDMQWHQRGAFHPSS
Rn 181 HPQVQSVRRIRDMQWHQRGAFHPSS 205
```

Alignment of Mouse (Mm) βB3-Crystallin Sequence (Acc.: NP_067327) with Rat (Rn) βB3-Crystallin Sequence (Acc.: NP_113878)

Score = 441 bits (1135)
Expect = 10^{-123}

Identities = 207/211 (98%)
Positives = 209/211 (98%)

```
Mm    1 MAEQHGAPEQAAAGKSHGGLGGSYKVTVYELENFQGKRCELSAECPNLTDSLLEKVGSIQ 60
        MAEQHGAPEQAAA KSHGGLGGSYKVTVYELENFQGKRCELSAECPNLT+SLL+KVGSIQ
Rn    1 MAEQHGAPEQAAANKSHGGLGGSYKVTVYELENFQGKRCELSAECPNLTESLLQKVGSIQ 60

Mm   61 VESGPWLAFERRAFRGEQFVLEKGDYPRWDAWSSSRRSDILLSLRPLHIDGPDHKLHLFE 120
        VESGPWLAFERRAFRGEQFVLEKGDYP WDAWSSSRRSDILLSLRPLHIDGPDHKLHLFE
Rn   61 VESGPWLAFERRAFRGEQFVLEKGDYPAWDAWSSSRRSDILLSLRPLHIDGPDHKLHLFE 120

Mm  121 NPAFSGRKMEIVDDDVPSLWAHGFQDRVASIRVINGTWVGYEFPGYRGRQYVFERGEFRH 180
        NPAFSGRKMEIVDDDVPSLWAHGFQDRVASIRVINGTWVGYEFPGYRGRQYVFERGEFRH
Rn  121 NPAFSGRKMEIVDDDVPSLWAHGFQDRVASIRVINGTWVGYEFPGYRGRQYVFERGEFRH 180

Mm  181 WNEWDANQPQLQSVRRIRDQKWHKRGCFLSS 211
        WNEWDANQPQLQSVRRIRDQKWHKRGCFLSS
Rn  181 WNEWDANQPQLQSVRRIRDQKWHKRGCFLSS 211
```

Alignment of Mouse (Mm) γD-Crystallin Sequence (Acc.: NP_031802) with Rat (Rn) γD-Crystallin Sequence (Acc.: NP_149086)

Score = 375 bits (962)
Expect = 10^{-103}

Identities = 167/174 (95%)
Positives = 172/174 (97%)

```
Mm    1 MGKITFYEDRGFQGRHYECSTDHSNLQPYFSHCNSVRVDSGCWMLYEQPNFAGCQYFLRR 60
        MGKITFYEDRGFQGRHYECSTDHSNLQPYFS CNSVRVDSGCWMLYEQPNF GCQYFLRR
Rn    1 MGKITFYEDRGFQGRHYECSTDHSNLQPYFSRCNSVRVDSGCWMLYEQPNFTGCQYFLRR 60

Mm   61 GDYPDYQQWMGFSDSVRSCRLIPHAGSHRIRLYEREEYRGQVIEFTEDCPSLQDRFHFNE 120
        GDYPDYQQWMGFSDSVRSCRLIPHAGSHRIRLYERE+YRGQ++EFTEDCPSLQDRFHFNE
Rn   61 GDYPDYQQWMGFSDSVRSCRLIPHAGSHRIRLYEREDYRGQMVEFTEDCPSLQDRFHFNE 120

Mm  121 IYSLNVLEGCWVLYDMTNYRGRQYLLRPGEYRRYHDWGAMNAKVGSLRRVMDFY 174
        IYSLNVLEGCWVLY+MTNYRGRQYLLRPGEYRRYHDWGAMNA+VGSLRRVMDFY
Rn  121 IYSLNVLEGCWVLYEMTNYRGRQYLLRPGEYRRYHDWGAMNARVGSLRRVMDFY 174
```